D-brane instanton backreaction and a Swampland conjecture

Memoria de Tesis Doctoral realizada por

Eduardo Garcia-Valdecasas Tenreiro

presentada ante el Departamento de Física Teórica
de la Universidad Autónoma de Madrid
para optar al Título de Doctor en Física Teórica

Tesis Doctoral dirigida por **Dr. Ángel M. Uranga**,
Profesor de Investigación del Instituto de Física Teórica

Departamento de Física Teórica
Universidad Autónoma de Madrid

Instituto de Física Teórica UAM/CSIC

Junio de 2019

This work has been financed by the ERC Advanced Grant SPLE under contract ERC-2012-ADG-20120216-320421 and by the "Centro de Excelencia Severo Ochoa" Programme under grants SEV-2012-0249 and SEV-2016-0597.

Esta tesis doctoral está basada en los siguientes artículos:

1. "*On the 3-form formulation of axion potentials from D-brane instantons*"
   Eduardo García-Valdecasas Tenreiro y Angel M. Uranga.
   Publicado en JHEP 1702 (2017) 087 ; arXiv e-Print: 1605.08092 [hep-th].

2. "*Backreacting D-brane instantons on branes at singularities*"
   Eduardo García-Valdecasas Tenreiro y Angel M. Uranga.
   Publicado en JHEP 1708 (2017) 061 ; arXiv e-Print: 1704.05888 [hep-th].

3. "*Bipartite field theories and D-brane instantons*"
   Sebastián Franco, Eduardo García-Valdecasas Tenreiro y Angel M. Uranga.
   Publicado en JHEP 1811 (2018) 098 ; arXiv e-Print: 1805.00011 [hep-th].

4. "*Supersymmetry Breaking Warped Throats and the Weak Gravity Conjecture*"
   Ginevra Buratti, Eduardo García-Valdecasas Tenreiro y Angel M. Uranga.
   Publicado en JHEP 1904 (2019) 111 ; arXiv e-Print: 1810.07673 [hep-th].

A todos aquellos
que tuvieron paciencia.

Agradecimientos

Estando esta tesis dedicada a aquellos que alguna vez tuvieron paciencia, no pueden empezar estos agradecimientos de otra forma que rindiendo honores a Angel, la batuta que dirige esta tesis. Gracias por estar ahí siempre que te he buscado. Gracias por enseñarme física casi sin querer, como sin darte cuenta de la sabiduría que estabas transmitiendo, haciendo que todo parezca natural, sencillo. Gracias por guiar de esa forma sutil, preparando el camino y dejando las piedras justas. Gracias, en definitiva, para haberme enseñado que la grandeza no esta reñida con la humildad sin pretensiones.

Y cómo continuar estos agradecimientos sin hablar de Seba, mi anfitrión en Nueva York y colaborador. Muchas gracias por enseñarme, desde la distancia, y en CUNY, los secretos de las gargantas, los BFTs, los Cluster Algebras, los Brane Brick Models, el Crystal Melting y mil otros temas. Por no mencionar las enseñanzas vitales y alguna charla para levantarme los ánimos. Gracias por acogerme en Nueva York con entusiasmo y generosidad. Un abrazo, fiera! No quiero dejarme a Manuel, por hacer de Nueva York un barrio de mi Madrid natal y hacerme sentir en casa.

Hablando de aquellos que me enseñaron física en estos 4 años, no pueden quedar sin nombrar Ander, Miguel y Gianluca. Ander, gracias por todas las veces que te he pedido ayuda, ya sea en temas de física o alguna cosa más práctica. Contigo y Gianluca pasé un muy buen año en la tercera planta. Ahí queda el póster del Eibar en recuerdo. Y, por supuesto, Miguel, gracias por tus respuestas en forma de audio siempre que te he preguntado desde la distancia. Pero no todo pueden ser halagos, hay algo que nunca os perdonaré: haber dejado el listón demasiado alto.

Una vez Ander y Gianluca abandonaron el despacho 312 me mudé al 412 para compartir despacho con Fede, Sebastian y Paco. Muchísimas gracias a los tres vuestra compañía. Gracias Fede por tu contagiosa pasión por la física. Y por tu paciencia al tener que explicarme 28 veces el Minajan-Nemenmanski y demás cosas demasiado complicadas. Gracias también por tus ideas y por tratar de llevar alguna a buen puerto conmigo. Sebastian, ha sido un placer compartir despacho contigo y, sobre todo, aprender el valor de los detalles. Muchas gracias también por los congresos y, sobre todo por vuestro apoyo en Virginia, Sebastian y Álvaro. Cuando vosotros también me abandonasteis llegaron Alessandro y Ginevra, muchas gracias a los dos, por vuestra colaboración científica y vuestra compañia. Gracias Alessandro por estar trabajando duro en el proyecto estos meses que yo escribo :).

A Luis, Fernando y Angel les tengo que agradecer la gestión del grupo de fenomenología de cuerdas del IFT. Creo que es un ejemplo de buen ambiente y buen trabajo. Un grupo con el que identificarse y al que llamar casa. Aparte de los ya mencionados, en el grupo de cuerdas he conocido a gente magnífica. El resto de estudiantes de doctorado: Aitor, Dagoberto, Álvaro, Edu Junior y la horda del último año, Alessandro, Ginevra, Jose, Joan y Max. Por no mencionar a los Posdocs: Clemens, Pramod, Michael, Florent y, por supuesto, Wieland. Muchas gracias por tu trabajo, no suficientemente reconocido. Sin él, los SPLE's y los congresos no habrían sido lo mismo. Aunque los herederos del SPLE están haciendo un trabajo magnífico. Hablando de cosas magníficas, magnífico fue

el viaje a Crackovia con Irene, Pierre y Florian. Unos grandes. Seguiremos coincidiendo, why not?. Y Pierre, we are exchanging countries, but you will still wonder, who is this guy?

Y... muchas gracias a todos los compis de fuera de cuerdas! Jota, Edu Lattice, Medrano, Javi, Quilez, Jorge, Jose, Gordo, Christian, Martin, Francesca y a todos los que se me quedan en el tintero. Jota, Medrano, Edu, Quilez, Javi, Cristian, Martin, Jorge... Buenos congresos y escuelas hemos pasado juntos, que no se olvidan fácilmente. Especialmente Oviedo, con su cachopo y sus vinos, y Zaragoza, con una piscina y una terraza para el recuerdo. Medrano, nuestros tenis no llegaron muy lejos, pero tus canciones seguro que lo harán. Y bueno, Jota, nuestras worldlines se separan, pero dicen que las líneas paralelas se cruzan en una esfera. Edu, aunque nuestros senderos laborales se separan, seguiremos celebrando la amistad en torno a una buena longaniza!

El IFT no sería lo que es sin sus investigadores, pero lo sería aún menos sin todas esas personas que lo sostienen. Isabel, ha sido un placer ser uno de tus niños. Mónica Vergel, Mónica Encinas, Rebeca, no hace falta que os diga que me habéis salvado el culo en varias ocasiones. Gracias por ayudarme y hacer del IFT un lugar mas humano. Andrés, Emilio, Marcos, gracias por vuestra inestimable ayuda y todas las cosas que os robé, como la pantalla que prometí devolver... Y Susana, ya te daré las gracias (o no) cuando vea los malditos vídeos :).

Y ya de puertas para fuera, gracias a toda la gente que me ayudó en este camino, desde el colegio y pasando por la universidad. Gracias a los que compartieron aula conmigo y crearon un ambiente inolvidable en la UAM: Huerta, Barbudo, Heredia, Vicente, Acero, Beiran, Santiago, David, Ibai, Diego... Y gracias a todos aquellos que alguna vez me enseñaron algo. Gracias por vuestra paciencia.

Y por supuesto gracias a todos mis amigos extra-iefeteros. Jorge, Pedro, Lupo, Lucas, Miguel, David, Alvaro, Alvar, Gago, Carmen, Marta G, Marta B, Celia... Sois todos la hostia. Y si el viento me lleva lejos, nos mantendremos siempre cerca. Anton, Miriam y Mati: primos, y un poco hermanos. Rosamari, gracias por guiarme por estas procelosas aguas.

He mencionado a todos los que, de alguna manera han puesto su granito de arena en este sendero. Esta tesis es de todos vosotros. Y por supuesto, como primeros autores, mis padres. Probablemente debería poneros de coautores, pero ya sabéis, las trabas burocráticas... En compensación os voy a dar las gracias. Gracias por responder a la insistente pregunta “Eto que é” con paciencia. Gracias por cultivar la curiosidad con mimo. Por los libros, por los juegos y por abrirme los ojos a un mundo que no me cansaría ya de explorar. Porque sin los insectos, las piedras o el migoga, yo no sería. Muchas gracias por enseñarme a ser.

Y no puedo acabar de otra forma que agradeciéndote, Raquel, cada sonrisa que me has arrancado en estos años. Gracias por ser aliento y cobijo. Gracias por los mundos descubiertos y las aventuras compartidas. Por las cumbres y los valles. Este camino lo empezamos juntos y lo hemos recorrido juntos. Tú lo has empedrado y cubierto de flores.

Contents

1 Introduction

Since the dawn of time, curiosity has led humankind to wonder about nature and its fundamental underpinnings. Phenomena close to our experience, or in our energy scale, are more easily accessible, while the laws governing the huge and the tiny elude us with greater success. Although the way hasn't been easy, science is ultimately a story of success and today we stand on solid ground. Our knowledge of nature today is summarized in two principles, Quantum Mechanics and General Relativity.

Quantum Mechanics is the principle ruling the small scales. The understanding of ever tinier phenomena has led to the establishing of the Standard Model (SM) of particle physics. It, or a suitable extension of it explains, to date, in a unified framework everything our best microscopes can see. These microscopes are accelerators such as the LHC and they insist that the SM is, if anything, more accurate than we thought. Huge scales, on the contrary, are described by General Relativity (GR). This theory dictates how spacetime is curved in the presence of mass and how trajectories bend in response to this curvature. These two theories, when combined, give us a remarkable understanding of the history of the universe since its first moments. The model describing cosmology is known as ΛCDM, the Λ standing for the cosmological constant and CDM for cold dark matter. It is an astonishing success that brings in itself the prediction of its failure. It is complicated to conceive that quantum matter may move in a classical spacetime. One is led to conclude that gravity needs to be quantized. The biggest indication that this is the case comes from the quantization of the Black Hole(BH) entropy. It implies that the metric of a BH has a quantized area. There are furthermore several loose ends in the ΛCDM story:

- **The CDM:** Cold Dark Matter amounts to around 25% of the energy content of the universe and is required to explain a growing amount of observations ranging from the rotation of galaxies to the formation of large scale structure. It is however missing microscopically and yet to be found. This part of the universe should be describable in similar terms as the SM.
- **The Λ:** Dark Energy is a different beast. A quantum field theory has a zero point energy and the SM famously mispredicts the vacuum energy felt by gravity by 120 orders of magnitude. This mismatch has been refereed to as the biggest disagreement with experiment ever measured. This further hints to problems where gravity meets quantum mechanics. The vacuum energy would naively be set by the UV of the theory, yet its value is extremely tiny. This IR/UV mixing contradicts renormalization group ideas but is a property of Quantum Gravity.
- Some loose ends on the SM also exist, most notably the neutrino mass, but we will not extend here on them.

The obvious question is how to quantize gravity. This turns to be extremely complicated, since it is not renormalizable. Presumably the theory looses predictivity near the Planck Mass M_p, unless a fixed point is reached. A different route must be taken and, as of today, the only consistent theory of Quantum Gravity (QG) is String Theory(ST).

Renormalization issues come from diverging integrals as one approaches higher energies. It is somewhat intuitive that divergences might vanish if pointlike objects are traded by one-dimensional strings. This intuitive idea is proven right by computing string amplitudes, as modular invariance removes dangerous limits from the moduli space. The simple assumption of a one-dimensional object ends up producing gravity as an unavoidable result upon quantization. Once the string in quantized, one must specify how they interact. String Theory is defined as a perturbative expansion summing over topologies of the Worldsheet, describing different string interactions. This game, with the help of supersymmetry, gives rise to five superstring theories that famously unify under a web of dualities. Indeed, the five string theories describe different perturbative limits of a putative M-theory that would not even be a theory of strings. More surprisingly, some string theories turn out to not be theories of strings, as they naturally include dynamical BPS solitons called D-branes.

Building on these ideas, String Theory has been incredibly fruitful in the last decades. There are two directions on which this thesis builds up: string phenomenology and QFT engineering using D-branes. On the one hand, string theory has made contact with phenomenology, being able to accommodate all ingredients in the Standard Model such as non-abelian gauge fields and chiral matter. Amusingly, String Theory is capable of producing viable theories for beyond the standard model physics with no free parameters. Start from 10d, fix 6 of them to be a compact Calabi-Yau (CY) manifold and a low energy effective field theory (EFT) emerges whose parameters are fixed by the internal geometry. The plethora of such EFTs a has been dubbed the Landscape. However, in the same way as Quantum Field Theory (QFT) is an extremely tight framework that severely restricts the consistent theories, ST seems to be quite picky in terms of the EFTs it allows. The set of disallowed EFTs in String Theory and, more widely, Quantum Gravity, are lovingly referred to as the Swampland. Charting the boundaries separating the Landscape from the Swampland is an ongoing feat.

On the other hand, String Theory has been extremely useful as a theoretical tool to better understand supersymmetric QFTs. Indeed String Theory has the ability of geometrizing problems in QFT making them more tractable. Particularly useful for this task are D-branes, in whose worldvolume a QFT lives at low energies. A stack of D-branes in a CY_3 gives rise to $\mathcal{N} = 1$ gauge theory with unitary group. Further placing them in webs or at singularities allows to engineer complicated gauge theories whose properties might be understood geometrically. For instance, Seiberg Duality, a remarkable field theory strong-weak coupling duality can be rephrased as a crossing of branes. Even non-perturbative objects in the field theory are easily understood as D-branes wrapping some cycles. This interplay between Sting Theory and QFT has as its most remarkable achievement the conjecture that $\mathcal{N} = 4$ Super Yang Mills (SYM) in 4 dimensions is dual to type IIB String Theory in $AdS_5 \times \mathbf{S}^5$.

There are many contributions String Theory has made to both mathematics and physics that are not contained in the last two paragraphs. The shadow it casts is so long that we shall not attempt to describe it here. Let us just mention that it goes from describing some strongly coupled condensed matter systems using AdS/CFT to deep

contributions in algebraic geometry, such as mirror symmetry.

In 2014 BICEP2 announced the discovery of B-modes signaling the existence of gravitational waves most likely coming from inflation. This discovery was subsequently found to be a false signal due to dust by the Planck collaboration. Nonetheless it spurred a flurry of activity around large field inflation, needed to explain the experimental results. Large field inflation turns out to be extremely complicated to realize in String Theory because it implies transplanckian field ranges, subsequently forbidden by a modification of the Weak Gravity Conjecture (WGC) applying to axions. The Weak Gravity Conjecture states that gravity should be the weakest force. For a U(1) gauge force, this means that a particle should exist whose charge is bigger, or equal, than its mass, in planck units $q \geq m$. An axionic version exists stating that $fS < M_p$, where f is the axion decay constant setting the periodicity and S the instanton action. If we want the higher order corrections to be under control, the decay constant should not be much bigger than 1, restricting the available field range. As a way out, axion monodromy was introduced. These models have sub-planckian decay constants, in agreement with the WGC but give rise to large field inflation through a multibranched potential. A somewhat more natural description of the multibranch structure arises when considering the 2-form dual to the axion and a 3-form responsible of the potential. In this language, the 2-form is eaten by the 3-form, which encodes the non-perturbative potential from instantons. In the case of stringy instantons, no 3-form is available. This is the starting point of the first part of this thesis, comprising Chapters 3 to 5.

The task of finding the 3-form description of the non-perturbative potential produced by stringy instantons, those with no gauge description, is taken up in Chapter 3, where a D3-brane instanton coupling to an RR axion is considered. The required 3-form is only found once the presence of the D-brane instanton is taken into account as deforming the geometry. In particular, a new 1-form appears in the deformed geometry that may be used when KK reducing the RR 4-form effectively producing the correct Kaloper-Sorbo structure. The result is generalized in Section 3.2.5 using T-duality. Whenever the instanton has a gauge interpretation, backreacting it can be seen as a "holographic" dual to this description, as detailed in Section 3.3.

The change in cohomology induces a change in the topology of the compactification manifold. In particular, the cycle wrapped by the d-dimensional D-brane instanton becomes trivial, being the boundary of a $(d+1)$-chain. Accordingly, the cycle hodge-dual to the cycle wrapped by the instanton develops a boundary. This is used in Chapter 4 to extend the previous discussion to more general settings of (mirrors of) D3-branes probing a CY singularity. In this setup the instanton may intersect gauge (or flavor) D-branes that are cut by the backreaction and recombine, as described in Section 4.2.1. Along the way, we reinterpret the generation of charged operators mediated by Worldsheet (WS) instantons in Section 4.2.2. We see that WS instantons are in fact required for anomaly cancellation. Multi-instantons and the non-abelian case are briefly discussed in Section 4.2.3. In Section 4.3, a recipe is developed to recover directly from the deformed geometry the charged operators induced by the instanton. Illustrative examples are detailed, including non-compact and multiple instantons. Instantons triggering complex deformations are studied in Section 4.4.

In Chapter 5 we focus on the field theories resulting from the backreaction in analogy to the AdS/CFT spirit of warped throats. The resulting theories are generically Bipartite Field Theories (BFTs). This provides the first realization in String Theory of a large class of

BFTs. A recipe for the backreaction directly in the dimer is provided in Section 5.1, where a series of examples are detailed, possibly with non-trivial identifications in the dimer unit cell. BFTs have as moduli space higher dimensional toric Calabi-Yau manifolds. Their relation to the CY_3 of the original theory is investigated in Section 5.2. The interplay with Seiberg Duality is studied in Section 5.3. Multi-instanton processes with instantons in faces corresponding to complex deformation fractional branes are discussed in Section 5.4.

The power of the WGC in constraining models of large field inflation spurred interest on it and possible ways it may be generalized to further constrain the Effective Field Theories reachable from String Theory. The set of EFTs that can be UV completed to Quantum Gravity(QG) is known as the Landscape. Anything else lies in the Swampland. Fast progress followed, as this was understood to be a huge possibility, rather than a liability. String Theory has been criticized as not having predictive power, since the number of EFTs arising in compactifications is huge. The Swampland program opens up the possibility of genuine Quantum Gravity predictions. In the subsequent years an effort, that continues today, of charting the boundaries between the Landscape and the Swampland, followed. Today, several conjectures exist, with varying degrees of support. Of particular interest for us is the AdS-WGC, a spin-off of the original WGC that forbids stable non-supersymmetric AdS vacua in String Theory. This follows from requiring that only BPS states saturate the WGC bound. Then, looking at certain D-brane setups whose near to horizon geometry is AdS, it is argued that, unless supersymmetric, and thus BPS, the setup is either unstable or metastable. The lifetime of metastable vacua is always zero however, as the decay probability is multiplied by an infinite volume factor in AdS[1].

In the second part of this thesis, comprising Chapter 6, we follow this lead by looking at warped throats that are locally AdS, with a dependence on the radius. We argue that this geometries should not be stable whenever SUSY is broken. Unlike in the case of the AdS-WGC, in our case, metastable vacua are not ruled out. A particular throat form the literature is studied in Section 6.3, and a novel decay mechanism is found that makes it unstable. Systems with orientifold planes breaking SUSY are discussed in Section 6.4.

In Chapter 7 we give some concluding remarks and an outlook of the possible avenues of research that one could follow building up on this thesis.

[1] Let us remind that a light-like signal reaches an infinite distance in a finite time in AdS.

Introducción

Desde los albores de la civilización, la curiosidad ha impulsado al género humano a buscar las causas fundamentales de los fenómenos naturales. Los procesos más cercanos a nuestra experiencia, aquellos que ocurren a una escala similar a la nuestra, son más accesibles, mientras que las leyes que rigen lo enorme y lo minúsculo nos han evadido con mayor facilidad. Aunque el camino no ha sido fácil, la ciencia es una historia de éxito y hoy nos alzamos en terreno sólido. Nuestro conocimiento de la naturaleza se puede resumir en dos principios, la Mecánica Cuántica y la Relatividad General.

La Mecánica Cuántica reina en las pequeñas escalas. El estudio de procesos más y más energéticos ha culminado (por el momento) con el Modelo Estándar (SM) de la física de partículas. Él, o una modificación del mismo, explica todo lo que podemos ver con los mayores microscopios que la humanidad haya creado. Estos microscopios, aceleradores de partículas como el LHC, insisten tozudamente en que el modelo estándar es aun más exacto de lo que creíamos. Las grandes escalas se describen, por el contrario, mediante la Relatividad General. Esta teoría establece cómo el espacio se deforma en presencia de cuerpos pesados y cómo las trayectorias de estos cuerpos se curvan según la forma del espacio. Usando estas dos teorías hemos logrado una comprensión increíble de la historia del universo. El paradigma cosmológico actual se denomina ΛCDM, donde Λ representa una constante cosmológica y CDM se refiere a la materia oscura fría, por sus siglas en inglés (Cold Dark Matter). A pesar del impresionante éxito de este paradigma, sabemos que tiene limitaciones. En particular, resulta complicado pensar que la materia, gobernada por la discretitud de la mecánica cuántica se mueva de forma suave por un espacio-tiempo clásico. Si queremos describir la materia y el espacio-tiempo de forma unificada, necesitamos cuantizar la gravedad. Probablemente la mayor indicación en este sentido venga de la cuantización de la entropía de los agujeros negros, que implica la cuantización de su área, en principio descrita por relatividad general! Por otro lado, el modelo ΛCDM presenta otras preguntas:

- **El CDM:** A partir de observaciones indirectas como la curva de rotación de las galaxias o la formación de estructura, sabemos que la materia oscura representa el 25 % del contenido de energía del universo. Conocemos algunas de sus propiedades pero no sabemos su descripción microscópica. No obstante, es de esperar que se pueda describir en términos similares al modelo estándar.

- **La Λ:** La energía oscura es otra historia completamente distinta, puesto que cuestiona los principios más básicos de teoría cuántica de campos. Una teoría cuántica de campos (QFT) tiene energía de punto cero y el modelo estándar falla en 120 órdenes de magnitud al predecir la energía de vacío que siente la gravedad, dando otra muestra de cómo la mecánica cuántica y la gravedad no terminan de encajar. La energía de vacío estaría de forma naif dada por las altas energías de la teoría (UV). Pero el valor observado es muy pequeño. Este mezcla entre las escalas grandes y las escalas pequeñas (mezcla IR/UV) contradice las ideas del grupo de renormalización pero es una propiedad de Gravedad Cuántica.

- Por el lado del Modelo Estándar también hay algún cabo por atar, como las masas de los neutrinos, pero no nos extenderemos aquí.

Intuimos que hay que cuantizar la gravedad, pero ¿cómo?. Resulta que es extremadamente complicado, puesto que no es renormalizable. Presumiblemente, la teoría deja de ser predic-

tiva a la escala de Planck M_p, a no ser que haya un punto fijo no trivial en el ultravioleta. Es necesario seguir otro camino y, a día de hoy, el único camino consistente es el que lleva a la Teoría de Cuerdas.

Los problemas con la renormalización están asociados a integrales que divergen a altas energías, o pequeñas distancias. Resulta intuitivo que, al sustituir las partículas puntuales por cuerdas unidimensionales, estos infinitos desaparezcan. Esta intuición es correcta, como se demuestra al calcular amplitudes de cuerdas, en las que la invariancia modular elimina los límites peligrosos del espacio de integración. Asombrosamente, el simple hecho de asumir un objeto fundamental unidimensional produce, al cuantizarlo, de forma inevitable, gravedad. Así, teoría de cuerdas, es una teoría cuántica de la gravedad por construcción. Desde un punto de vista práctico, se define como una serie perturbativa que suma topologías de la cuerda, correspondiendo con sus distintas interacciones. Esta idea, con la ayuda de supersimetría, da lugar a cinco teorías de cuerdas que están unificadas bajo una red de dualidades. Desde este punto de vista, las cinco teorías serían simplemente cinco límites perturbativos de una "super-teoría" conocida como teoría M. Esta teoría no sería una teoría de cuerdas y sería presumiblemente una formulación no-perturbativa donde las cuerdas serían solo uno de los objetos. De hecho, algunas teorías de cuerdas no son teorías de cuerdas, puesto que incluyen solitones BPS dinámicos llamados D-branas.

Partiendo de estas ideas, teoría de cuerdas ha sido un campo muy activo en las últimas décadas, dando lugar a multitud de aplicaciones y sub-campos. Para esta tesis dos de las direcciones de investigación son particularmente importantes. En primer lugar, fenomenología de cuerdas, el campo que trata de conectar la teoría con nuestro universo. De hecho, la teoría es capaz de producir todos los ingredientes del modelo estándar, como campos gauge no abelianos o materia quiral. Es increíble comprobar que teoría de cuerdas puede reproducir teorías mas allá del modelo estándar sin parametros libres. Empieza en 10 dimensiones, fija 6 de ellas como una variedad Calabi Yau compacta y, a bajas energías, en las cuatro dimensiones restantes, emerge una teoría efectiva de campos cuyos parámetros están fijados por la geometría de la variedad compacta. La multitud de teorías efectivas (EFTs) que se pueden obtener a partir de cuerdas se denomina el Paisaje. No obstante, de la misma forma que QFT es un marco muy rígido que restringe enormemente las posibles teorías consistentes, la teoría de cuerdas es muy selectiva en las EFTs que puede producir. El conjunto de EFTs que no están permitidas por teoría de cuerdas o, de forma más general, por gravedad cuántica (QG), se denominan cariñosamente como la Ciénaga. Dibujar los límites entre el Paisaje y la Ciénaga es un desafío que no ha hecho más que empezar.

La segunda rama de teoría de cuerdas que emplearemos es la que usa la teoría como herramienta teórica para el estudio de Teorías Cuánticas de Campos (QFTs) supersimétricas. Teoría de cuerdas tiene la capacidad de geometrizar problemas de QFT haciendo que sean más accesibles. De particular utilidad son las D-branas, en cuyo interior aparecen teorías de campos a bajas energías si se desacopla la gravedad. Un conjunto de N D3-branas situadas en un CY_3 produce una teoría $\mathcal{N} = 1$ con grupo $SU(N)$, por ejemplo. Colocándolas en singularidades, se obtienen teorías más complejas cuyas propiedades se pueden estudiar de forma geométrica. Por ejemplo, una profunda dualidad como la de Seiberg, se puede describir como un cruce de D-branas y objetos no perturbativos se pueden describir como D-branas enrolladas en ciclos compactos. Esta interacción entre Teoría de Cuerdas y QFT encuentra su máxima expresión en la conjetura de que Super Yang Mills (SYM) $\mathcal{N} = 4$ en 4 dimensiones es dual a teoría de cuerdas tipo IIB en $AdS_5 \times \mathbf{S}^5$.

Hay innumerables contribuciones que Teoría de Cuerdas ha hecho tanto a la física

como a las matemáticas que no están contenidas en los dos párrafos anteriores. No trataremos de describirlas aquí, pero baste mencionar que van desde la descripción de ciertos sistemas de materia condensada en acoplamiento fuerte usando AdS/CFT hasta profundas contribuciones en geometría algebraica tales como la simetría espejo.

En 2014 BICEP2 anunció un descubrimiento que estremeció al mundo (científico), había medido modos B en el fondo cósmico de microondas señalando la existencia de ondas gravitacionales originadas, probablemente, durante inflación. A pesar de que la colaboración Planck demostró al poco tiempo que se trataba de un error provocado por polvo intergaláctico, este descubrimiento generó un gran interés en inflación a muy altas energías, necesaria para explicar los resultados. Conseguir inflación con campos grandes resulta ser muy complicado en Teoría de Cuerdas porque implica campos transplanckianos, que resultan complicados de estabilizar. Posteriormente se ha conjeturado, de hecho, que este tipo de campos estarían prohibidos por la versión axiónica de la Conjetura de Gravedad Débil (WGC). Esta conjetura establece que la fuerza gravitacional ha de ser más débil que el resto de fuerzas de una teoría, siendo la versión original relativa a fuerzas gauge $U(1)$. Esto implica la existencia de una partícula cuya carga sea mayor, o igual, que su masa $q \geq m$, en unidades naturales. La versión axiónica implica que $fS < M_p$, donde f es la constante de decaimiento del axión, que fija la periodicidad del potencial y, por tanto, el rango de valores que puede tomar durante inflación, y S es la acción del instantón que genera el potencial no perturbativo. Si queremos mantener las correcciones instantónicas bajo control, la constante de decaimiento no debería ser mucho mayor que 1, restringiendo el rango del campo a no ser mayor que M_p. Una escapatoria es usar un potencial con $f < 1$, pero con varias ramas, de tal forma que la distancia efectiva que recorre el campo sea transplanckiana, esto se denomina axión con monodromía. Una descripción más clara de este tipo de potenciales se puede hacer en términos de la 2-forma dual al campo escalar y una 3-forma no dinámica encargada de generar el potencial no perturbativo de los instantones. En el caso de instantones gauge, la 3-forma apropiada es la de Chern-Simons, mientras que para instantones cuerdosos, sin análogo gauge, no se conoce la 3-forma que hace el trabajo. En la primera parte de esta tesis, que compone los Capítulos 3, 4 y 5, partimos de este interrogante.

En el Capítulo 3 llevamos a cabo la tarea de encontrar la 3-forma que describe el potencial no-perturbativo para instantones cuerdosos considerando un instantón de D3-brana que se acopla a un axión Ramond-Ramond (RR). La 3-forma solo aparece cuando tenemos en cuenta la presencia del instantón, que deforma la geometría. Esa deformación hace que aparezca una nueva 1-forma que se puede utilizar en la reducción Kaluza-Klein(KK) de la 4-forma RR en 10d para obtener el acoplo correcto con el axión. Este resultado es generalizado en el Capítulo 3.2.5 usando T-dualidad. Además, cuando el instantón tiene una descripción gauge, la deformación en la geometría se puede ver como una interpretación dual, en el sentido holográfico, como se indica en la Sección 3.3.

Este cambio en la cohomología de la variedad induce un cambio en la topología por la dualidad de Poincaré. El ciclo cubierto por el instantón d-dimensional de D-brana se convierte en la frontera de una cadena $(d+1)$-dimensional y desaparece de la homología. De forma análoga, su dual de hodge desarrolla una frontera. En el capítulo 4 utilizamos este efecto para extender la discusión previa al contexto general de (duales espejo) de D3-branas localizadas en una singularidad tórica. En esta configuración los instantones pueden intersecar con D-branas de color o sabor, que son cortadas y recombinadas por la deformación en la geometría, como describimos en la Sección 4.2.1. En la Sección 4.2.2 reinterpreta-

mos la generación de operadores cargados por los instantones de D-brana mediados por instantones de cuerdas. Vemos que estos instantones de cuerdas son, de hecho, requeridos para cancelar anomalías. En la Sección 4.2.3 discutimos el caso de multi-instantones y el caso no abeliano. En la Sección 4.3 introducimos una receta que permite obtener directamente, a partir de la geometría deformada y la recombinación de las branas, el operador generado por el instantón. Discutimos además algunos ejemplos, incluyendo instantones no-compactos y multi-instantones. En algunos casos particulares, el instantón produce una deformación compleja en la geometría, como se muestra en la Sección 4.4.

En el Capítulo 5 nos centramos en las teorías de campos que resultan de deformar la geometría en presencia de un instantón, siguiendo el espíritu AdS/CFT de las gargantas curvadas. Las teorías resultantes son teorías de campos bipartitas (BFTs), proporcionando la primera descripción de un gran subgrupo de estas BFTs en Teoría de Cuerdas. Una receta para encontrar la BFT resultante es expuesta en la Sección 5.1, donde se detallan una serie de ejemplos. Los espacios de moduli de las BFTs son variedades tóricas de dimensión mayor a 3 (la original). En la Sección 5.2 describimos estas variedades y su relación con la geometría original. En la Sección 5.3 estudiamos el uso conjunto de instantones y dualidad de Seiberg. Finalmente, en la Sección 5.4 estudiamos procesos multi-instantónicos correspondientes a deformaciones complejas.

El poder de la WGC para constreñir modelos de inflación de campos grandes, generó un gran interés en posibles generalizaciones que permitiesen imponer requisitos en las teorías efectivas que pueden descender de Teoría de Cuerdas. La Teoría de Cuerdas ha sido criticada por tener un Paisaje demasiado extenso. Según estas críticas, al poder acomodar universos muy variados, no tendría predictividad. Establecer las fronteras entre el Paisaje y la Ciénaga se ha convertido en un tema de investigación muy activo, puesto que permitiría hacer predicciones genéricas de Teoría de Cuerdas e, incluso, de Gravedad Cuántica. El progreso ha sido rápido y, actualmente, hay varias conjeturas, con distinto grado de aceptación y apoyo teórico, sobre qué propiedades tienen las teorías de la Ciénaga. En esta tesis nos vamos a interesar por la conjetura AdS-WGC, surgida a partir de la WGC original y que prohíbe la existencia de vacíos Anti-deSitter no supersimétricos estables. Esta idea surge de endurecer la WGC al establecer que la desigualdad solo está saturada por estados BPS. Aplicando esta idea a unas configuraciones de D-branas particulares, cuyas geometrías cerca del horizonte son AdS, se puede justificar que, a no ser que sean supersimétricas (y, por tanto, BPS), han de ser inestables o metaestables. Además, en el caso de ser metaestables, la vida del vacío sería 0, puesto que la probabilidad de decaer va multiplicada por un factor del volumen que es infinito en el caso de AdS[2].

En la segunda parte de esta tesis, que comprende el Capítulo 6, tomamos este testigo y estudiamos gargantas curvadas que son, localmente, AdS, con una dependencia en el radio. Conjeturamos que estas geometrías no pueden ser estables si supersimetría está rota. No obstante, en este caso, resulta concebible un vacío metaestable con una vida larga, puesto que no hay factor infinito de volumen. En la Sección 6.3 estudiamos un ejemplo de la literatura y encontramos un innovador mecanismo de decaimiento que lo hace inestable. En 6.4 consideramos gargantas con planos orientifold que rompen supersimetría y discutimos los distintos mecanismos que impiden su estabilidad.

En el Capítulo 7 concluimos este trabajo y ofrecemos una perspectiva de los posibles caminos que se pueden emprender a partir de lo estudiado en esta tesis.

[2]Es importante recordar que una señal llega a una distancia infinita en un tiempo finito en AdS.

2

Background Material

2.1 $\mathcal{N} = 1$ gauge dynamics

In this section we review the standard notions of $\mathcal{N} = 1$ QCD, dubbed SQCD. Good introductory references are [1–3]. We discuss the different phases of the theory as a function of the matter content and gauge group, introducing Seiberg Duality along the way. Scale matching and t'Hooft anomaly matching are reviewed in Appendix A. Finally, dynamical breaking of supersymmetry(DSB) is discussed in Section 2.1.5. We rely heavily in these techniques throughout the thesis.

Let us start by stating the one-loop β-function for an $N = 1$ SYM theory, easily derived from the standard QCD result and exact to all orders in perturbation theory,

$$\frac{1}{g^2(\mu)} = \frac{1}{g^2(\mu_0)} + \frac{b}{8\pi^2}\log\frac{\mu}{\mu_0} \tag{2.1}$$

So, the β-function is,

$$\beta(g) = -\frac{g^3}{16\pi^2}b \tag{2.2}$$

Where the coefficient b is,

$$b = \frac{3}{2}T(Adj) - \sum_{i=1}^{N_F} T(R_i) \tag{2.3}$$

Where $T(R) = C(R)/C(F)$ is the Dynkin index of the representation R, and $C(R)\delta^{ab} = \mathrm{tr}(R(t^a)R(t^b))$. For the $SU(N)$ case at hand, the following holds,

$$T(\square) = 1/2, \quad T(Adj) = 2N, \quad T(\square\square) = N - 2 \tag{2.4}$$

We take SQCD to have gauge group $SU(N_C)$ and N_F flavors $(Q, \bar{Q})$, giving a global symmetry group $SU(N_F)_L \times SU(N_F)_R \times U(1)_B \times U(1)_R$, with an anomalous $U(1)_A$. Matter fields transform as,

	$SU(N_F)_L$	$SU(N_F)_R$	$U(1)_B$	$U(1)_R$
Q	$\square$	1	1	$\frac{N_F - N_C}{N_F}$
$\bar{Q}$	1	$\bar{\square}$	-1	$\frac{N_F - N_C}{N_F}$

Using Equation (2.2), the 1-loop β-function for SQCD is,

$$\beta(g) = \frac{-g^3}{16\pi^2}\left(3N_C - N_F\right) \tag{2.5}$$

One may define the dynamical scale as the energy where the gauge coupling blows up. Introducing the complexified holomorphic coupling, the complexified dynamical scale reads,

$$\Lambda(\mu_0) = \mu_0 e^{2\pi i \tau(\mu_0)} \tag{2.6}$$

2.1.1 Pure SYM

The flavorless case $N_F = 0$ or SYM is strongly coupled in the IR, see Equation (2.5). Thankfully for life, in non-SUSY QCD the quark bilinear develops a non-vanishing vev that triggers chiral symmetry breaking. Similarly, in SYM, gauginos become strongly interacting in the IR and condense,

$$\langle \lambda\lambda \rangle = -32\pi^2\Lambda^3, \tag{2.7}$$

giving rise to a non-perturbative superpotential,

$$\mathcal{W}_{SYM} = N_C \Lambda^3 \tag{2.8}$$

This bilinear vev breaks the non-anomalous part of the R-symmetry $\mathbb{Z}_{2N_C}$ to $\mathbb{Z}_2$ giving rise to N_C degenerate vacua that are labeled by phases of the gaugino condensate.

2.1.2 $N_F < N_C$, The ADS Superpotential

For $N_F < N_C$ the classical scalar space has N_F^2 flat directions that can be described by the expectation values of a $N_F \times N_F$ meson matrix,

$$M = Q\bar{Q} \tag{2.9}$$

At a generic point in this moduli space the gauge group is broken down to $SU(N_C - N_F)$ by the meson vev. The theory is strongly coupled in the IR, see Equation (2.5). The strong dynamics generate the Affleck-Dine-Seiberg superpotential [4], the only superpotential invariant under the perturbative symmetries of the theory, with correct dimensionality and compatible with scale matching,

$$\mathcal{W}_{ADS} = (N_C - N_F) \left(\frac{\Lambda^{3N_C - N_F}}{\det M} \right)^{\frac{1}{N_C - N_F}} \tag{2.10}$$

Note that the case of SYM can be viewed as a particular case with $N_F = 0$ by setting $\det M = 1$. Conversely, the ADS superpotential can be understood as the gaugino condensation of the unbroken $SU(N_C - N_F)$ gauge group. The prefix $N_C - N_F$ is standard in the literature but depends on the renormalization scheme.

This superpotential lifts all directions in moduli space and actually leaves the theory unstable with a runaway $\langle M \rangle \to \infty$ to SYM, where supersymmetry is restored. Indeed, if $\langle M \rangle \neq 0$, SUSY is broken for any finite value of the meson vev. Adding masses to the mesons modifies this result.

2.1.3 $N_F \geq N_C$

For $N_F \geq N_C$ the classical moduli space is drastically different. This case was studied in the seminal work by Seiberg [5]. A vev for the quarks $\langle Q \rangle$, $\langle \bar{Q} \rangle$ now generically breaks the whole gauge group $SU(N_C)$. The moduli space can be parametrized in terms of gauge invariant operators: mesons and baryons. Baryons are fully antisymmetric combinations of chiral superfields that couldn't be constructed for $N_F < N_C$,

$$M_{f_2}^{f_1} = Q^{f_1 c} \bar{Q}_{f_2 c} \tag{2.11}$$

$$B^{f_1 \ldots f_{N_C}} = Q^{f_1 c_1} \ldots Q^{f_{N_C} c_{N_C}} \epsilon_{c_1 \ldots c_{N_C}} \tag{2.12}$$

$$\bar{B}_{f_1 \ldots f_{N_C}} = \bar{Q}_{f_1 c_1} \ldots \bar{Q}_{f_{N_C} c_{N_C}} \epsilon^{c_1 \ldots c_{N_C}} \tag{2.13}$$

Where f and c indices are flavor and color indices, respectively. In total, there are N_F^2 mesonic and $\binom{N_F}{N_C}$ baryonic operators, which overspecify the moduli space of dimension $2N_F N_C - (N_C^2 - 1)$ and are thus subject to classical constraints.

For $N_F \geq N_C$, there is no superpotential compatible with all requirements, that could be generated dynamically by strong dynamics. However, as we will see, strong dynamics are still interesting and may modify the moduli space and even give rise to a dual description.

- $\mathbf{N_F = N_C}$: Being N_F equal to N_C implies that $\det(Q) = B$. Thus, the classical constraint on the gauge invariant operators is just $\det(M) = B\bar{B}$. Seiberg argued that it is modified by the strong dynamics to,

  $$\mathrm{M} - B\bar{B} = \Lambda^{2N_C} \tag{2.14}$$

  The quantum dynamics thus modifies the moduli space and actually makes it non-singular!

- $\mathbf{N_F = N_C + 1}$: As pointed out by Seiberg, the classical moduli space is actually quantum exact in this case. The main point is that the classical constraint can be introduced to the Lagrangian through an effective superpotential.

- $\mathbf{N_F > N_C + 1}$: For these cases, it is not possible to write a superpotential encoding the classical constraints. As we will see, there is a weakly-coupled dual theory describing the same IR physics whenever the original theory is strongly coupled.

2.1.4 $N_F > N_C + 1$, Seiberg Duality

A remarkable idea was developed by Seiberg in [6]: the low energy physics of SQCD with $\mathbf{N_F > N_C + 1}$ is conjectured to be described by a dual SQCD theory with different matter content. This is not a full duality, since only the IR physics described by the two theories is equal. In analogy with the electro-magnetic duality, we will refer to the original and dual theories as electric and magnetic, respectively.

The duality goes as follows, introduce dual quarks $q, \bar{q}$ by interpreting the hodge dual (in flavor space) baryons $\tilde{B}$ as composite objects of $\tilde{N}_C = N_F - N_C$ dual quarks. The mesons in the electric theory are identified with a new gauge singlet $\mathcal{T}_{f_2}^{f_1}$ in the magnetic

theory. Finally, mesons in the magnetic theory are set to zero on the moduli space by a suitable superpotential. Summing up,

$$M \to \mathcal{T} \tag{2.15}$$

$$B \to \tilde{B} \tag{2.16}$$

$$\mathcal{W} = q_{f_1} \mathcal{T}^{f_1}_{f_2} \bar{q}^{f_2} \tag{2.17}$$

Where,

$$\tilde{B}^{f_1 \dots f_{\tilde{N}_C}} = q^{f_1 c_1} \dots q^{f_{\tilde{N}_C} c_{\tilde{N}_C}} \epsilon_{c_1 \dots c_{\tilde{N}_C}} \equiv B_{i_1 \dots i_{N_C}} \epsilon^{i_1 \dots i_{N_C} f_1 \dots f_{\tilde{N}_C}} \tag{2.18}$$

Indeed, the global symmetry of the magnetic theory matches the electric one. Gauge symmetries don't need to match, as they are just redundancies in the Lagrangian description[1]. The magnetic theory has thus field content,

	$SU(N_F)_L$	$SU(N_F)_R$	$U(1)_B$	$U(1)_R$
q	$\bar{\square}$	1	$\frac{N_C}{N_F - N_C}$	$\frac{N_C}{N_F}$
$\bar{q}$	1	$\square$	$\frac{-N_C}{N_F - N_C}$	$\frac{N_C}{N_F}$
$\mathcal{T}$	$\square$	$\bar{\square}$	0	$2\frac{N_F - N_C}{N_F}$

Depending on N_F and N_C the electric and magnetic theories will be in different phases in the IR. They can either be free, strongly coupled or flow to a non-trivial fixed point. There are thus three possibilities,

- $\mathbf{N_C + 1 < N_F \leq \frac{3}{2} N_C}$ **: Free Magnetic Phase**. Consider increasing N_F past N_C+1. The electric theory still is strongly coupled in the IR, see Equation (2.5). The magnetic theory however, has $\tilde{N_C} = N_F - N_C$, so for $N_F \leq \frac{3}{2} N_C$, it is asymptotically free. In this range therefore, the magnetic theory describes the IR in terms of free fields!

- $\mathbf{\frac{3}{2} N_C < N_F < 3 N_C}$ **: Conformal Window.** In this range both theories are believed to flow to the same interacting fixed point in the IR. This can be argued for just below $N_F = 3N_C$, where the magnetic theory looses asymptotic freedom, using the exact NSVZ β-function. Below $N_F = \frac{3}{2} N_C$, the scaling dimension of the mesons is $\Delta(M) \frac{3}{2} R(Q\bar{Q}) = 3 \frac{N_F - N_C}{N_F} \leq 1$. Since M lowest component is an scalar field, this would imply a violation of unitarity in a superconformal theory, hence there can be no conformal fixed point. Likewise, for $N_F \geq 3N_C$ the theory becomes IR free.

- $\mathbf{3 N_C \leq N_F}$ **: Free Electric Phase.** The electric theory becomes strongly coupled in the UV but IR free. In this regime the magnetic theory is asymptotically free but strongly coupled in the IR. This is just the opposite as the free magnetic phase. We have taken Figure 2.1 from [1] to illustrate the three possible regimes. The electric theory phase, as a function of N_F is shown in Figure 2.2, likewise borrowed from Bertollini's notes.

[1] Global gauge symmetries do have a physical meaning as boundary conditions or superselection rules.

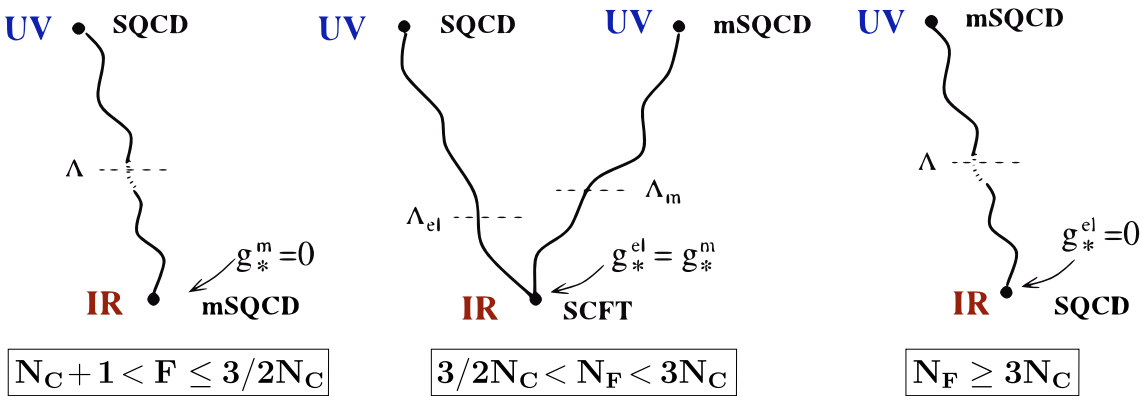

Figure 2.1: Phases of SQCD with $N_F > N_C + 1$. In the free magentic phase (left) the thheory is described in the UV by the electric theory and in the IR by the magnetic one. The opposite is true for the free magnetic phase (right). In the conformal window (center), the two theories differ in the UV but flow to the same superconformal fixed point in the IR. Adapted from [1].

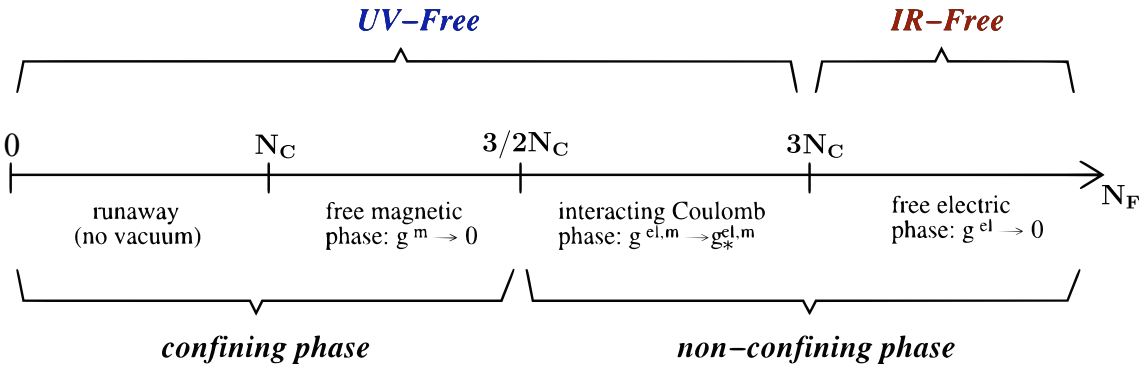

Figure 2.2: Phases of the electric SQCD theory as a function of N_F. Adapted from [1].

2.1.5 Dynamical Supersymmetry Breaking

As usual, most likely in favor of complexity, nature has chosen not to realize exact supersymmetry. It must be broken at some scale and, for some time, it was hoped that the SUSY breaking scale would be much lower than the Planck scale. This could alleviate the hierarchy problem, for instance. A natural way to break supersymmetry without further introducing fine tuning is through non-perturbative effects, thus making the SUSY breaking scale naturally low. This is Dynamical Supersymmetry Breaking (DSB). In this section we review a few indirect arguments for DSB and the $SU(5)$ model, which we shall consider in Section 6.3.

In general, assessing whether SUSY is broken by non-perturbative effects is a complicated problem. Usually one doesn't know neither the superpotential nor the Kahler potential and the only way to argue for DSB is through indirect arguments. In some cases, we are luckier and able to compute the superpotential (non-calculable models) and even the Kahler potential (calculable models). For a classic review see [7].

2.1.5.1 Indirect Criteria for DSB

In non-calculable models one may argue for DSB in several ways.

- **The Witten Index.** A supersymmetric theory has at least one state with zero energy. Thus one can compute the Witten index, which counts the difference between zero energy bosonic and fermionic states: $\mathcal{I} = n_B^0 - n_F^0$. It is furthermore an invariant of the theory, hence can be computed at any point in parameter space. If nonzero, there is one or more zero energy states and SUSY is unbroken. If it is zero it can either be broken or unbroken.

- **Global Symmetries and flat directions.** Consider a theory with no flat directions (no moduli space) and a global symmetry that is broken spontaneously. Then a massless goldstone boson arises. If SUSY was unbroken, this scalar would be part of a chiral superfield where another scalar sits. Being in the same supermultiplet, this scalar partner would have no potential, thus parametrizing a flat direction, in disagreement with our initial assumption. One can conclude that, a theory with no flat directions and a broken global symmetry must break SUSY. Although the criterion is straightforward, it might be complicated to show that a symmetry is broken in a strongly coupled phase. Sometimes one can use t'Hooft anomaly matching conditions, see Appendix 1.2. Another usual argument is looking for superpotential terms acquiring a vev. They have R-charge 2 and break R-symmetry automatically.

2.1.5.2 The $SU(5)$ model

A well-known theory showing DSB is an $SU(5)$ gauge theory with matter in the antifundamental and antisymmetric representations, $\tilde{Q}^i$, A_{ij}. Clearly, no gauge invariants can be formed from these fields and the theory does not admit a superpotential. Not having gauge invariant operators, the theory does not have a moduli space and, classically, there is an isolated supersymmetric vacuum in the origin.

The theory has global symmetry group $G = U(1) \times U(1)_R$ and the vanishing of anomalies fixes the charges of the fields to be $A : (1, 1)$ $Q : (-3, -9)$. In [8], Affleck, Dine and Seiberg studied the t'Hooft anomalies of this theory, looking for a suitable description in the IR. The theory confines, so computations are hard, but t 'Hooft anomalies must match. In particular, if G is unbroken all correlators involving $U(1)$ and $U(1)_R$ must match. They showed that a theory describing this phase needs a rather bizarre combination of fields and charges making it hard to assume. The way out is to propose that G breaks upon confinement. Since the theory does not have flat directions, the breaking of the global symmetry lifts the vacuum and breaks SUSY.

There are alternative ways of providing additional hints towards SUSY breaking, see [9] for an argument based on gaugino condensation.

2.2 Toric Geometry

In this section we review basic notions about toric varieties that will be useful in later chapters. We start by defining toric varieties as compactifications of $(\mathbb{C}^*)^n$ and as a generalization of weighted protective spaces. We then go on to describe how their geometry can be translated into an object called fan that can be further simplified to a toric diagram for the CY case in Section 2.2.2. We then introduce their description as moduli spaces of Gauged Linear Sigma Models (GLSM). We also discuss resolutions and deformations of the singularity in Section 2.2.4. Nice references for physicists include [10–12].

2.2.1 Defining Toric Varieties

Toric varieties can be defined in several ways. A mathematical definition is that a toric variety X of dimension n is an algebraic variety containing the algebraic torus $\mathbb{T} = (\mathbb{C}^*)^n$ as a dense open subset such that the natural action of the torus $\mathbb{T}$ on itself extends to X. Intuitively, a toric variety is a compactification of $(\mathbb{C}^*)^n$. As an example, $\mathbb{CP}^1$ is a toric variety isomorphic to S^2 which is just the compactification of $\mathbb{C}^*$ upon addition of the points at the origin and infinity. In this spirit, different compactifications (and gluings among compactifications) give raise to different toric varieties.

The points added can be though of as the limiting points of the action of $\mathbb{T}$ on itself. Consider focusing on a one parameter subgroup of the full action,

$$(z_1, ..., z_n) \to (\lambda^{\omega_1} z_1, ..., \lambda^{\omega_n} z_n 1) \tag{2.19}$$

The limit point is reached when $\lambda \to 0$. The specific exponents and the way of gluing different patches in their limiting points determines the toric variety.

Another route to defining toric varieties is suggested by the action in Equation (2.19). This looks just like the defining equation of a weighted projective space. Toric varieties are generalizations that admit several $\mathbb{C}^*$ actions and with a set of points Z_Δ removed.

$$X = \frac{\mathbb{C}^n - Z_\Delta}{(\mathbb{C}^*)^p} \tag{2.20}$$

As an example consider the conifold. The set of points is $Z_\Delta : \{z_1 = z_3 = 0\} \cup \{z_2 = z_4 = 0\}$ and the $\mathbb{C}^*$ action is

$$(z_1, z_2, z_3, z_4) \to (\lambda z_1, \lambda^{-1} z_2, \lambda z_3, \lambda^{-1} z_4) \tag{2.21}$$

2.2.2 Fans, Toric Diagrams and Web Diagrams

The information describing a toric variety (exponentials in the action in Equation (2.19) and grouping of limit points) can be encoded in a **"fan"**, which is a collection of cones spanned by vectors in a lattice N such that faces of cones are also cones and intersections of two cones are faces of both. They are, essentially, like pyramids in different dimensions. To obtain the toric variety from a fan:

- Find relations among the vectors spanning the fan. They give rise to the different $\mathbb{C}^*$ actions.
- Find sets of vectors that do not generate a cone $\{v_i\}$. For each of these sets define the locus satisfying $Z_j = \{z_i\} = 0$. Then, $Z_\Delta = \sum Z_j$.

As an example consider the **conifold** whose fan is spanned by vectors,

$$v_1 = (0, 0, 1), \quad v_2 = (1, 0, 1), \quad v_3 = (1, 1, 1), \quad v_4 = (0, 1, 1) \tag{2.22}$$

The only relation among the vectors is $v_1 - v_2 + v_3 - v_4 = 0$, giving rise to an action with vector $(1, -1, 1, -1)$:

$$(z_1, z_2, z_3, z_4) \to (\lambda z_1, \lambda^{-1} z_2, \lambda z_3, \lambda^{-1} z_4) \tag{2.23}$$

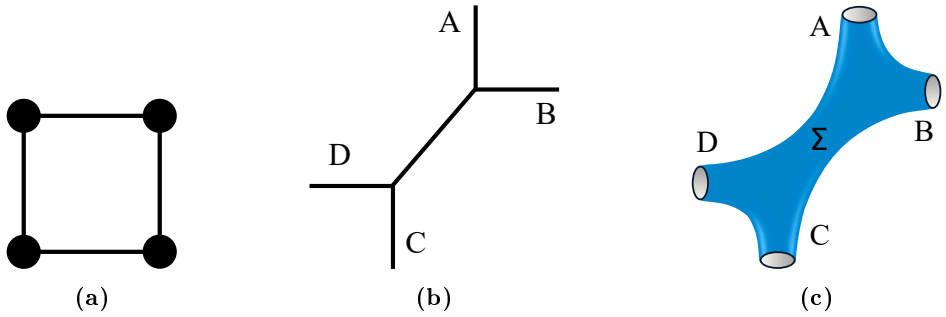

Figure 2.3: Diagrams associated to the conifold geometry. a) Toric Diagram. b) Web Diagram. c) Mirror Riemann surface that can be seen as a thickening off the web diagram.

The only combinations of vectors not giving rise to a cone are $\{v_1, v_3\}, \{v_2, v_4\}$. Thus, the locus of points to be removed is,

$$Z_\Delta : \{z_1 = z_3 = 0\} \cup \{z_2 = z_4 = 0\} \tag{2.24}$$

The resulting space is fully characterized by the invariants,

$$x = z_1 z_2, \quad y = z_1 z_4, \quad w = z_3 z_2, \quad z = z_3 z_4 \tag{2.25}$$

Subject to the condition $xz = yw$, which is a usual description for the conifold.

Through this thesis the toric varieties considered are Calabi-Yau varieties, which preserve a quarter of the supersymmetry. Interestingly for us, a toric variety is Calabi-Yau iff all the vectors in the fan end on the same hyperplane. This allows to simplify the combinatorial description of the geometry by taking the projection of the fan on this hyperplane and using it instead of the fan. This object is named **"toric diagram"** and for the CY_3 case is just a $2d$ diagram in a lattice. See the toric diagram of the conifold in Figure 2.3a.

Another interesting object is the dual to the toric diagram in the following sense. For every edge in the toric diagram, draw a line orthogonal to it. One then finds a **"web diagram"** or "(p,q)-web". See for instance the web diagram for the conifold in Figure 2.3b. The toric diagram and web diagram encode the geometric properties of the variety as follows. For toric CY_3, the variety has a $\mathbb{T}^3$ fibration structure. There are 3 $U(1)$ isometries that may degenerate in particular set of points. This is precisely described by the toric diagram. Each point corresponds to a divisor where one $U(1)$ action degenerates. Lines in the toric diagram are loci where two isometries degenerate, and, in the faces, the 3 isometries degenerate.

The web diagram, being the dual graph to the toric diagram, encodes the same information. Its faces correspong to loci where one action degenerates, legs correspond to 2 actions degenerating and intersections of legs signal 3 actions degenerating. It is at these points where the singularity lies. Vertices with 3 legs are smooth though, since they correspond to flat space $\mathbb{C}^3$. We will return to the web diagram in Section 2.4.3 as it has a physical significance in the mirror geometry.

2.2.3 The GLSM description

Yet another way of discussing toric varieties, and of particular interest for us, is as moduli spaces of Gauged Linear Sigma Models (GLSM). Given a gauge field theory, to

find the moduli space one must find solutions to the D-terms modulo the gauge freedom. It turns out that this is equivalent to modding out by the complexified gauge group. We have seen that toric varieties have a $(\mathbb{C}^*)^p$ action, which is the complexification of $U(1)^p$. Indeed one can find gauge theories with the appropriate $U(1)^p$ symmetry whose moduli space is the toric variety. Consider n quiral superfields Φ_i and gauge group $U(1)^p$. The moduli space is the gauge quotient of the solution to the D-term equations,

$$\sum_{i=0}^{n} q_i^a |\phi_i|^2 = \xi^a \tag{2.26}$$

Where the q_i^a are the charges of the Φ_i chiral fields under the $U(1)_a$ gauge groups and ξ_a are Fayet-Iliopoulos terms. Each D-term equation thus specifies a $\mathbb{C}^*$ action with the corresponding charges.

Consider the conifold, for example. The relevant GLSM has 4 chiral fields charged under a $U(1)$ gauge group with charges (1,-1,1,-1), thus giving the D-term equation,

$$|z_1|^2 - |z_2|^2 + |z_3|^3 - |z_4|^2 = 0 \tag{2.27}$$

Which is indeed the defining equation of the conifold. Let us now describe how the toric diagram is found from the GLSM data with a single $U(1)$.

- Find linear relations between the charges of the chiral fields under the $U(1)$ action.
- Write this relations in matrix form. They specify coordinates of points in the fan.
- Actually, since the variety is CY, one can find a lower dimensional space spanned by this points. This is the toric diagram.

This can be illustrated with the conifold. The charges are as specified by the action in Equation (2.23). The relations are:

$$q_1 + q_2 = 0, \quad q_1 + q_4 = 0, \quad q_1 + q_2 + q_3 + q_4 = 0 \tag{2.28}$$

The resulting matrix is,

$$\begin{pmatrix} 1 & 1 & 0 & 0 \\ 1 & 0 & 0 & 1 \\ 1 & 1 & 1 & 1 \end{pmatrix} \tag{2.29}$$

The last row is trivial, so the diagram is two dimensional, as expected. Indeed it reproduces the conifold toric diagram in Figure 2.3a. In this procedure we are free to choose relations between the charges, which amounts to an $SL(2,\mathbb{Z})$ transformation on the coordinates of the toric diagram. The inverse process of finding the GLSM from the toric diagram is not unique however. This was called toric duality [13] and was eventually understood as Seiberg duality [14, 15].

2.2.4 Resolving and deforming toric singularities

Singularities are typically unwanted in physical theories. A main example are singularities signaling the breakdown of a theory beyond a certain scale, as in some non-renormalizable QFTs. Another example are classical singularities in GR, hopefully cured

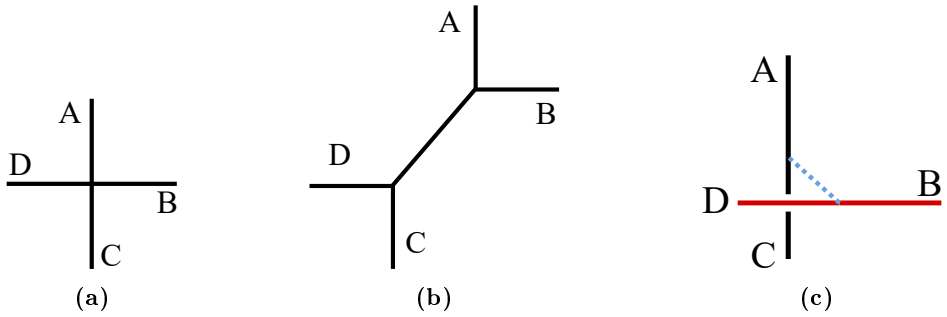

Figure 2.4: a) Web diagram of the singular conifold. b) Web diagram of the resolved conifold. c) Web diagram of the deformed conifold.

by QG. Indeed, there are several examples where String Theory is able to cure singularities such as the conifold one, see for instance [16]. From a mathematical point of view, one can try to slightly deform the singularity and make it smooth. In the following we discuss two such processes, **resolving** and **deforming** singularities. Given the defining polynomials $p(x) = 0$ of an algebraic variety, the singular locus is the set of points such that,

$$p(x) = 0, \quad dp(x) = 0, \tag{2.30}$$

For toric varieties, knowing whether it is singular is straightforward. It is non-singular iff the toric diagram is fully triangulated, such that all triangles have area one. Each of these triangles corresponds to a $\mathbb{C}^3$ factor. In the following we consider the conifold, which is topologically a cone over $\mathbf{S}^2 \times \mathbf{S}^3$, as an example.

2.2.4.1 Resolving the singularity

It is clear that a simple way to de-singularize the variety is by triangulating its toric diagram. From the web diagram point of view, it corresponds to growing intermediate legs in vertices with more than 3 legs. This is illustrated in Figure 2.4b. Consider resolving the singularity in a conifold by turning on a non-zero Fayet-Iliopoulos term,

$$|z_1|^2 - |z_2|^2 + |z_3|^3 - |z_4|^2 = \xi \tag{2.31}$$

The variety is no longer singular, since $p(z_i) \neq 0$. Before the resolution, the web diagram is Figure 2.4a, each face corresponding to a $z_i = 0$ and all meeting at a point. Now, taking ξ positive, it is clear that $z_2 = 0$ and $z_4 = 0$ can't intersect anymore. Furthermore, in the locus $z_1 = z_3 = 0$, only one fiber degenerates. As a result, the web diagram has changed by growing a segment corresponding to this locus and the four faces don't meet anymore. The geometry is now fully non-singular, since the web diagram only has $\mathbb{C}^3$ factors. The line connecting them is an additional $\mathbf{S}^2$ that has been blown up, thus resolving the singularity.

2.2.5 Deforming the singularity

One can also deform the singularity, which implies modifying its complex structure. The resulting variety is not toric anymore but in general is still Calabi-Yau. Let us consider

the example of the conifold again. A complex deformation of the conifold is parametrized as,

$$xz - yw = a \tag{2.32}$$

Where $a \in \mathbb{C}^*$ is the deformation parameter. Since this equation breaks one of the $U(1)$ actions, the variety is non-toric. Using the $U(1)$ actions this equation can be transformed into $|x|^2+|y|^2 = a$. It describes the appearance of a finite $\mathbf{S}^3$. The resulting geometry does not have an associated web-diagram but it can be described by two such diagrams linked by the $\mathbf{S}^3$, as described in [17]. The sub-webs are in equilibrium, meaning that the total charge of their external legs is zero. The set of such decompositions of the web diagram of a given singularity classifies its complex deformations. The conifold example is illustrated in Figure 2.4c. A description also exists for the toric diagram in terms of Minkowski sum decompositions, see [18].

2.3 Warped Throats

Type IIB String Theory on $AdS_5 \times S^5$ is widely believed to be equivalent to $\mathcal{N} = 4$ Super Yang Mills in 4d. This is an striking example of the holographic principle and, arguably, the best controlled theory of quantum gravity we know of. However, the gauge theory has too much symmetry to be applied to any natural phenomena. In particular it has conformal invariance and too much Supersymmetry. It is thus very far from realizing a viable phenomenology model or from allowing us to tackle problems as confinement in QFTs. As we will see, placing D-branes at singularities provides us with a generalization of Maldacena's insight to setups with reduced Supersymmetry and no conformal invariance. This gives rise to multiple applications such as:

- Studying confining gauge theories.
- Producing $N = 1$ gauge theories with several gauge factors and chiral matter, useful for String Phenomenology.
- Producing meta-stable and even stable[2] SUSY-breaking vacua.

In the remaining of this section we will introduce Maldacena's original conjecture and then proceed to more involved examples of AdS/CFT, in particular D3-branes at a conifold singularity. We discuss the Klebanov Strassler solution for fractional D-branes on this setup and the corresponding dual gauge theory. In the next section we generalize our discussion to general toric singularities probed by D3- and D5-fractional branes.

2.3.1 The Maldacena Correspondance

In [19] Juan Maldacena proposed the remarkable duality between Type IIB String Theory on $AdS_5 \times \mathbf{S}^5$ and $\mathcal{N} = 4$ SYM in 4d. We follow [20], for pedagogical purposes. Consider N D3 branes in flat space in type IIB string theory. The string perturbation theory effective coupling is g_sN, where $g_s = e^{\phi}$ is the string coupling. In the limit where the string perturbation theory is under control, that is $g_sN \ll 1$, the closed string excitations

[2] Although in Chapter 6 we argue that stable non-SUSY vacua are not allowed in this kind of throats.

decouple. Thus, the massless theory is $U(N)$ SYM coming from the open strings sourcing the adjoint fields, collective scalar coordinates and fermionic partners.

The supergravity solution for black D3-branes sourcing N units of D3-brane flux is,

$$ds_{10}^2 = Z(r)^{-1/2}\eta_{\mu\nu}dx^\mu dx^\nu + Z(r)^{1/2}h_{mn}dx^m dx^n, Z(r) = 1 + \frac{L^4}{r^4}, \quad r^2 = x^m x^m, \quad h_{mn} = diag(1,1,1,1,1,1) \tag{2.33}$$

Where $L^4 = 4\pi g N \alpha'^2$. Taking the near horizon limit, $r \to 0$, the metric becomes,

$$ds^2 \to \frac{r^2}{L^2}\eta_{\mu\nu}dx^\mu dx^\nu + \frac{L^2}{r^2}dr^2 + L^2 d\Omega_{S^5}^2 \tag{2.34}$$

This metric describes $AdS_5 \times \mathbf{S}^5$, both factors with characteristic radius L. The radius is large for $g_s N \gg 1$, thus the limit where the supergravity approximation is trustworthy. Now, as one approaches the limit $r \to 0$, the excitations are redshifted by the vanishing warp factor. Thus, any massive string excitation will become arbitrarily light near the horizon and needs to be kept at low energies. We arrive to the conclusion that:

- In the limit of weak coupling $g_s N \ll 1$, the low energy theory is $N = 4$ SYM, a gauge theory propagating in $\mathbb{R}^{1,3}$.
- In the limit of strong coupling $g_s N \gg 1$ the theory is described by full fledged type IIB string theory propagating in a classical $AdS_5 \times \mathbf{S}^5$ background.

2.3.2 The Conifold Theory

In [21], Klebanov and Witten studied the field theory dual to String Theory with D3-branes probing conical singularities. Nice reviews for this section and Section 2.3.3 are [22,23]. In the spirit of [19], it is natural to suggest that the field theory will be dual to type IIB string theory probing the near-horizon geometry close to the singularity when a large number of D3-branes sit on it. A conical singularity is a point where the metric of an n-dim manifold $\mathbf{Y}_n$ can be put on the form,

$$h_{mn}dx^m dx^n = dr^2 + r^2 g_{ij}dx^i dx^j. \tag{2.35}$$

Where the metric g_{ij} describes an $n-1$-dimensional manifold $\mathbf{X}_{n-1}$. Then, $\mathbf{Y}_n$ is the cone over $\mathbf{X}_{n-1}$. Crucially, for $\mathbf{Y}_n$ to be Ricci-flat (i.e. CY), the base of the cone $\mathbf{X}_{n-1}$ must be an Einstein manifold (Ricci tensor proportional to the metric) of positive curvature.

Considering N parallel D3-branes near a conical singularity in $\mathbf{Y}_6$ produces a 10-dimensional metric of the form 2.33 with h_{mn} the metric of $\mathbf{Y}_6$ near the singular point. Taking the near horizon limit now yields the metric of $AdS_5 \times \mathbf{X}_5$.

2.3.2.1 The conifold

The simplest CY conical singularity is the conifold $\mathcal{C}$, described by $z_i \in \mathbb{C}$, $i = 1, ..., 4$ satisfying,

$$|z_1|^2 + |z_2|^2 + |z_3|^2 + |z_4|^2 = 0 \tag{2.36}$$

This geometry has an $SO(4) \times U(1)$ symmetry under which the z_i transform in the $(\square)_1$. The $U(1)$ symmetry induces a non-trivial transformation in the holomorphic 3-form and is thus an R-symmetry,

$$\Omega = \frac{dz^2 \wedge dz^3 \wedge dz^4}{z_1} \tag{2.37}$$

To see the topology of the base X_5 let us remove the singular point by intersecting $\mathcal{C}$ with a unit sphere,

$$|z_1|^2 + |z_2|^2 + |z_3|^2 + |z_4|^2 = 1 \tag{2.38}$$

Note that the group $SO(4)$ acts transitively in this space. Furthermore, every point on it is invariant under a $U(1)$ subgroup of $SO(4)$. Thus, the space is described by the group of transitive action modulo the stabilizer group, $U(1)$: $X_5 = SO(4)/U(1) = (SU(2) \times SU(2))/U(1)$, which is also known as $T^{1,1}$.

Let us introduce alternative variables that will be useful when discusing the gauge theory,

$$z_1 = A_1 B_1, \quad z_2 = A_2 B_2, \quad z_3 = A_1 B_2, \quad z_4 = A_2 B_1. \tag{2.39}$$

Where we have the freedom $A_k \to \lambda A_k, \quad B_k \to \lambda^{-1} B_k,$. This freedom allows us to rewrite Eq. 2.38 as,

$$|A_1|^2 + |A_2|^2 = |B_1|^2 + |B_2|^2 = 1 \tag{2.40}$$

Note that there is a remaining $U(1)$ symmetry that needs to be modded out, the phase of λ:

$$A_k \to e^{i\alpha} A_k, \quad B_k \to e^{-i\alpha} B_k \tag{2.41}$$

The exact metric of the supergravity dual is known. The base of the cone has metric:

$$ds^2(T^{1,1}) = \frac{1}{6} \sum_{i=1}^{2} \left(d\theta_i^2 + \sin^2\theta_i d\phi_i^2 \right) + \frac{1}{9} (d\psi - \sum_{i=1}^{2} \cos\theta_i d\phi_i)^2 \tag{2.42}$$

Giving a compactification geometry of the form in Section 2.3.1, but substituting the internal metric by a cone over Equation (2.42),

$$ds_{10}^2 = Z(r)^{-1/2} dx_{3,1}^2 + Z(r)^{1/2} (dr^2 + r^2 ds_{T^{1,1}}^2) \tag{2.43}$$

The 10d geometry in the near horizon limit is then,

$$ds^2 = R^2 (ds_{AdS_5}^2 + ds_{T^{1,1}}^2) \tag{2.44}$$

With N units of F_5 flux in $T^{1,1}$,

$$\frac{1}{4\pi^2 \alpha'} \int_{T^{1,1}} F_5 = N \tag{2.45}$$

2.3.2.2 The gauge theory

The D3-branes probing the conifold singularity are aware of the space they are moving in. In particular, the gauge theory describing their low energy dynamics should reproduce it as its moduli space. Furthermore, the theory shold have $\mathcal{N} = 1$ supersymmetry. Consider first a single D3-brane, whose gauge dual should be abelian. Take $\mathcal{N} = 1$ $U(1) \times U(1)$ gauge theory with chiral superfields A_1, A_2, B_1, B_2 with charges $(1, -1)$ and $(-1, 1)$, respectively. The diagonal $U(1)$ subgroup decouples as no field is charged under it, describing the center of mass of the D3-brane. The D-term of the remaining $U(1)$ is,

$$|A_1|^2 + |A_2|^2 - |B_1|^2 - |B_2|^2 = 0 \tag{2.46}$$

This is the same as 2.40. To find the moduli space we mod out by the gauge $U(1)$, thus recovering the conifold! Indeed the chiral field vevs describe the motion of a D3-brane in

a conifold. This is still the case for more complicated theories arising from branes probing more involved singularities. Remarkably, the mesonic[3] branch of the moduli space of the field theory for a single D3-brane is the CY itself. These vevs are describing the movement of the D3-brane on the probed space.

The non-abelian generalization for N parallel D3-branes is straightforward. It has gauge group $U(N) \times U(N)$ and bifundamentals A_1, A_2, B_1, B_2 transforming as $(\Box, \bar{\Box})$ and $(\bar{\Box}, \Box)$. Without superpotential this theory has global symmetry $SU(2)_A \times SU(2)_B$ acting of fields A_k and B_k, respectively and $U(1)_R$ under which both fields have charge $1/2$. This symmetry must be preserved by the superpotential, since it is present in the dual geometry. The most general superpotential to preserve it and, in fact, the only exactly marginal operator we can add, is,

$$W = \frac{\lambda}{2}\epsilon^{ij}\epsilon^{kl}\mathrm{Tr}A_iB_kA_jB_l = \lambda \mathrm{Det}\mathcal{M} \tag{2.47}$$

Where $M_{ij} = A_iB_j$ are gauge invariant mesons. The moduli space is given by their expectation values upon modding out the gauge group after solving the F-terms,

$$\mathrm{Det}\mathcal{M} = 0 \tag{2.48}$$

Which is indeed the conifold condition 2.36.

2.3.3 The Klabanov-Strassler Theory

The conifold theory discussed in the previous section already has reduced SUSY. The next logical step is to get rid of conformal invariance. This is done introducing fractional branes, which are $D5$-branes wrapping the vanishing 2-cycle. These branes behave as fractional $D3$-branes, changing the rank of a subset of the gauge group. They are stuck in the singularity and can move away only after having recombined with other fractional branes to form a "whole" brane. Addition of this branes modifies the SUGRA solution by making it vary in the radial direction of AdS_5. As we will see, from the field theory side, these fractional branes turn on an RG-flow and, generically, trigger a cascade of Seiberg dualities towards the infrared. The energy scale in the field theory will map to the radial direction in the gravity picture.

In [24], Gubser and Klebanov considered the conifold theory and studied the interpretation of several string theoretic objects in the dual field theory. For instance, D3 branes wrapping the S^3 in $T^{1,1}$ were found to correspond to dibaryon operators of the form,

$$\epsilon_{\alpha_1,\ldots,\alpha_N}\epsilon^{\beta_1,\ldots,\beta_N}A^{\alpha_1}_{\beta_1}\ldots A^{\alpha_N}_{\beta_N} \tag{2.49}$$

Where $SU(2)$ flavor indices are omitted. A single $D3$ not wrapping any cycle is interpreted as a rank changing domain wall: $SU(N) \times SU(N) \to SU(N+1) \times SU(N+1)$. More surprisingly, $D5$-branes wrapping the S^2 behave as domain walls across which one gauge group jumps in rank by one. The argument goes as follows:

- Consider such a domain wall and a $D3$-brane wrapping a 3-cycle and crossing to the other side of the domain wall. In the process a fundamental string is created that

[3] The moduli space described by mesonic operators, which is not the complete moduli space in general, one should add for instance Fayet-Iliopoulos terms.

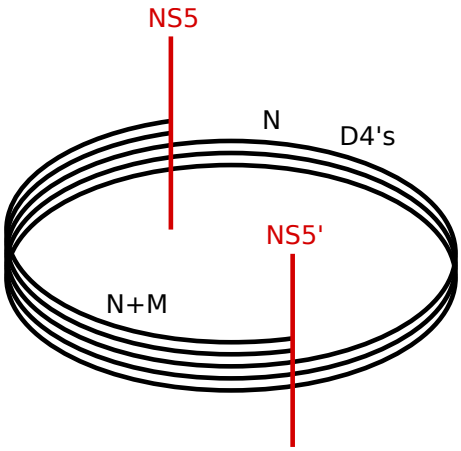

Figure 2.5: T-dual to the conifold with N full branes and M fractional branes.

stretches between the two[4]. The resulting would-be dibaryonic operator will now transform in the fundamental of one of the gauge groups, looking like,

$$\epsilon_{\alpha_1,\ldots,\alpha_N}\epsilon^{\beta_1,\ldots,\beta_N,\beta_{N+1}}A^{\alpha_1}_{\beta_1}\ldots A^{\alpha_N}_{\beta_N} \tag{2.50}$$

Indeed, this corresponds to the gauge group having jumped across the domain wall $SU(N)\times SU(N)\to SU(N)\times SU(N+1)$.

It is instructive to visualize these partially-wraped D-branes in a T-dual picture, as discussed in [27]. In this set-up, see Figure 2.5, the geometry is, effecively, a circle where two inequivalent NS5 branes sit, dividing the S^1 in two segments. Full $D3$-branes map to $D4$-branes wrapping the whole circle, while wraped $D5$-branes map to $D4$-branes covering only one segment of the S^1. Thus the name *factional* $D3$-branes. It is also easy to see in this picture why fractional branes are stuck in the singularity and the fact that, several fractional branes may combine to form a full brane and move away from the singular point. This realization opens up the possibility of studying gauge theories with gauge gruop $SU(N+M)\times SU(N)$, which are non-conformal!. They arise when placing N $D3$-branes and M $D5$-branes wrapping the 2-cycle of $T^{1,1}$ on a conifold singularity. The field theory and dual SUGRA solution is known as Klebanov-Strassler (KS) throat and was first studied in [28], following the initial SUGRA solution in [29] that needed to be IR completed.

In the following we consider then a theory with N $D3$-branes and M fractional branes on the conifold. The $D3$-branes still source F_5 flux on $T_{1,1}$, while the $D5$s source F_3 flux along the S^3,

$$\frac{1}{4\pi^2\alpha'}\int_{S^3}F_3=M,\quad \frac{1}{(4\pi^2\alpha')^2}\int_{T^{1,1}}F_5=N \tag{2.51}$$

2.3.3.1 The Field Theory

As already explained, the field theory gets modified by changing the rank of one gauge group, while the matter content and the classical superpotential stay the same as in the conformal case. The gauge group is $SU(N+M)\times S(N)$ with bifundamentals A_1, A_2

[4]This happens whenever two branes that span 8 dimensions together cross. [25, 26]

in the $(\square, \bar{\square})$ and B_1, B_2 in the $(\bar{\square}, \square)$. The classical superpotential is still 2.47 but, in this case, will be renormalized. The β functions are,

$$\frac{d}{d\ln(\Lambda/\mu)}\frac{8\pi^2}{g_1^2} \sim 3(N+M) - 2N(1-\gamma) \tag{2.52}$$

$$\frac{d}{d\ln(\Lambda/\mu)}\frac{8\pi^2}{g_2^2} \sim 3N - 2(N+M)(1-\gamma) \tag{2.53}$$

And the difference of couplings is,

$$\frac{8\pi^2}{g_1^2} + \frac{8\pi^2}{g_2^2} \sim M\mathrm{Ln}(\Lambda/\mu)\left[3 + 2(1-\gamma)\right] \tag{2.54}$$

While the sum remains invariant, as $\gamma = -1/2 + \mathcal{O}(M/N)^2$. So there is a logarithmic running with the energy. This running matches in the SUGRA description to a radial dependence on the B_2 NSNS form [30]

$$\int_{S^2} B_2 = 6\,\pi\, g_s/, M/, \alpha' \ln\left(\frac{r}{r_0}\right) \tag{2.55}$$

Where r_0 fixes the UV scale. Remarkably, the RG-flow in the field theory matches to a radial dependence in the SUGRA solution, as is usual in AdS/CFT. Equation 2.54 implies that, when flowing to the IR, the gauge coupling g_1 grows enough to become strongly coupled. At this point the theory is not valid anymore and a dual picture must be used. The appropriate microscopic description is the Seiberg dual, which is weakly coupled in this regime. The resulting theory has gauge group $SU(N-M) \times SU(N)$, with the mesons of the original theory $\mathcal{M}_{ij} = A_i B_j$ as fundamental fields, additional magnetic quarks A'_i, B'_j and total superpotential,

$$W = W_0 + \mu \mathrm{Tr}\mathcal{M}_{ij} A'_i B'_j \tag{2.56}$$

Where W_0 is the initial superpotential 2.47. Integrating out the massive meson fields one recovers the original superpotential for the dual bifundamental fields. The game goes on, as the gauge factor with highest rank confines repeatedly when flowing to the IR giving rise to a *duality cascade*:

$$SU(N+M) \times SU(N) \to SU(N-M) \times SU(N) \to SU(N-M) \times SU(N-2M)... \tag{2.57}$$

The flow continues until $N - kM$ becomes zero or smaller than M.

Consider the cascade in the T-dual picture shown in Fig. 2.5. Fractional D4-branes, stretching along half circle, force the NS5s to bend. The full process is shown in Fig. 2.6. One is led to move the NS5 across the $NS5'$. The fractional $D4$s shrink and grow with the opposite orientation, as $N+M$ anti-$D4$s. The other N fractional D4-branes sitting in the segment that grows, now span one and a half circles, so they are effectively $2N$ on one of the segments. Finally the anti-$D4$s are annihilated. And the cascade continues.

2.3.3.2 The bottom of the cascade

Let us focus on the case with $N = kM$, $k \in \mathbb{N}$. The last step of the throat is then $SU(2M) \times SU(M) \to SU(M)$ and only M fractional branes remain. This setup is not useful when trying to IR-complete the SUGRA dual in [29], since the fractional branes are

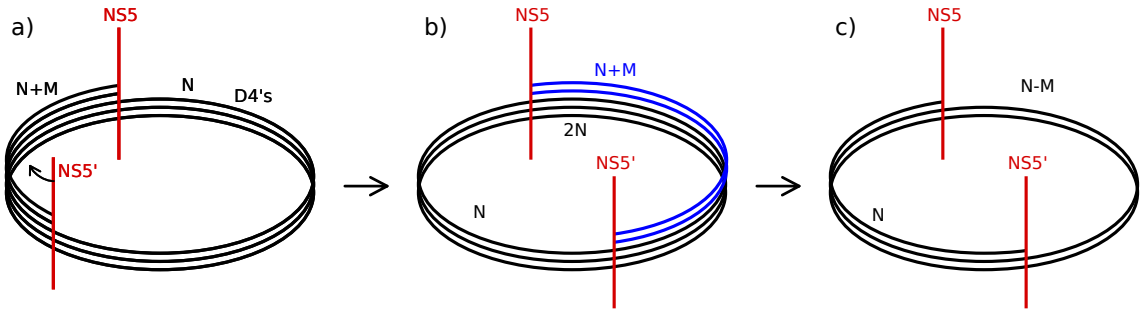

Figure 2.6: Seiberg duality on the T-dual, one step of the cascade. a) the $NS5$ branes cross giving rise to $N+M$ antibranes in b)that annihilate to give the final situation in c).

stuck at the singularity and the gauge theory moduli space is not sensible to the geometry. Klebanov and Strassler instead put a probe $D3$-brane on top of the M fractional branes that may move around the bottom of the cascade. The dual field theory has gauge group $SU(M+1)$ with the usual fields and superpotential $W_0 = \lambda \mathrm{Det}\mathcal{M}$. The classical moduli space is just the conifold, $\mathrm{Det}\mathcal{M} = 0$. This theory, however, develops a non-perturbative Affleck-Dine-Seiberg (ADS) superpotential that modifies the classical moduli space and breaks chiral symmetry,

$$W = \lambda \mathrm{Det}\mathcal{M} + (M-1)\left[\frac{2\Lambda^{3M+1}}{\mathrm{Det}\mathcal{M}}\right]^{\frac{1}{M-1}} \tag{2.58}$$

The quantum moduli space is given by solutions to the F-term,

$$\mathrm{Det}\mathcal{M} = \left[\frac{2\Lambda^{3M+1}}{(2\lambda)^{M-1}}\right]^{1/M} \tag{2.59}$$

This encodes a modification to Eq. 2.48. It is actually describing a deformed conifold, where the S^3 is blown up at the singularity and has a minimal size given by the right hand side of the equation above. Thus, the field theory is resolving the singularity in a non-perturbative way! The interpretation from the SUGRA side is that near the singularity, the geometry is deformed by the strong dynamics of the field theory.

2.3.3.3 The SUGRA solution

In [29] a gravitational dual is proposed which does not include the non-perturbative dynamics of the field theory and blows up in the singularity, failing to capture the IR physics. It is found by imposing Equation (2.51) and solving the BPS equations. The resulting metric has the same form as in Equation (2.43) with a warp factor depending on the radial direction,

$$Z(r) = \frac{L^4}{r^4}\log\frac{r}{r_s},\ L^2 = \frac{9\,g_s\,M\,\alpha'}{2\sqrt{2}} \tag{2.60}$$

Where r_s is the scale where a naked singularity appears, as $Z(r_s) = 0$. There are also the fluxes in Equation (2.51) but modified by the logarithmic running in Equation (2.55) that gives a decreasing F_5 flux towards the infrared:

$$N_{eff}(r) = N + \frac{3}{2\pi}\,g_s\,M^2\log\frac{r}{r_0} \tag{2.61}$$

Where $r = r_0$ sets the UV scale. Note that the metric blows up at $r = r_s$, so it needs to be IR completed. This IR completion should take into account the end of the cascade, where the field theory confines and generates a dynamical scale. The solution was found in [28] and substitutes the conifold by its deformed version, matching the deformation in Equation (2.59),

$$|z_1|^2 + |z_2|^2 + |z_3|^2 + |z_4|^2 = \epsilon^2 \tag{2.62}$$

This parameter should be identified as $r_s = \epsilon^{2/3}$. The metric of the base of the cone is that of the deformed conifold. This deformed conifold removes the singularity, matching this smoothing with the strong dynamics in the field theory. The strong dynamics in the field theory can actually be described by a gaugino condensation,

$$\langle \lambda\lambda \rangle \sim M \frac{\epsilon^2}{(\alpha')^3} \tag{2.63}$$

Precisely matching with the deformation parameter of the conifold.! As we will see later, these deformations generalize to more involved singular geometries probed by D3-branes. Such deformations can be triggered by the so-called *deformation fractional branes* in the general classification of [31]. As described in the next section, branes may probe more involved singularities. In general the SUGRA solution is not known, but the gauge theory is, for so called toric singularities.

2.4 Toric Field Theories, Dimers and Bipartite Field Theories

Placing D3-branes on more complicated toric CY_3 singularities yields more involved theories, but all of them share a particular structure. They are $N = 1$ gauge theories with bifundamental matter and a particularly simple superpotential. This allows us to study their properties using combinatorial objects. The dimer model is a bipartite graph embedded in a torus that encodes all the classical information of the field theory. This easily generalizes to graphs embedded in higher genus Riemann surfaces, which are known as Bipartite Field Theories (BFTs).

2.4.1 Dimer Models

In Section 2.3.2 we have seen that branes probing a conifold singularity give rise to an interesting field theory. More generally, a brane probing a toric CY_3 singularity gives rise to a $\mathcal{N} = 1$ field theory that consists on a bunch of gauge factors, bifundamentals chiral multiplets and a superpotential with a particular structure. Each bifundamental appears in two monomials that have opposite sign. These theories can be referred to as Toric Field Theories. Their content can be encoded in a quiver diagram supplemented by a superpotential, see Figure 2.7a.

Remarkably their particular structure allows us to encode all information in a bipartite graph where nodes come in two flavors and encode superpotential terms whose sign corresponds to the color of the node. A bipartite graph is composed of two sets of nodes (black and white) connected by edges (not connecting nodes of the same color). For the diagram to make sense it is embedded in a torus, whose physical significance will be discussed later. As an example, see the dimer diagram of the conifold in Figure 2.7b. From it one reads the field theory as follows,

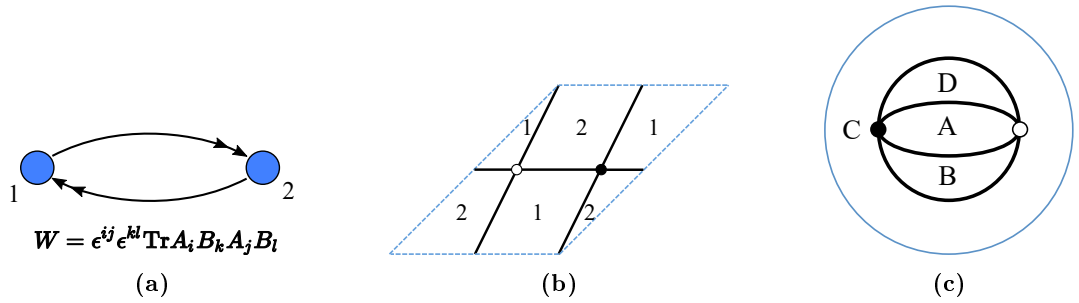

Figure 2.7: Diagrams associated to the conifold geometry. a) Quiver Diagram with superpotential. b) Dimer Diagram. c) Tiling of the sphere corresponding to the mirror Riemann surface.

- Faces correspond to $SU(N_a)$ gauge factors. Not all gauge rank assignments are allowed, as anomalies need to be canceled. In practice, this is assured by imposing the same number of fundamental and antifundamental fields for all gauge groups.
- Edges between the faces represent bifundamental fields charged under the gauge groups associated to the faces it limits with.
- Nodes encode terms in the superpotential with different colors corresponding to different signs. Each node corresponds to a monomial formed by the fields attached to the node and tracing over free gauge indices.
- The bipartite nature of the graph signals an orientation that fixes the bifundamental charges. It also fixes the superpotential. One may draw arrows orthogonal to edges such that they encircle black nodes clockwise and white ones counterclockwise. Edges with an arrow going from face A to face B will transform in the fundamental of B and antifundamental of A. Superpotential terms will be read concatenating arrows, thus ordering the fields in the monomials. Black nodes will correspond to positive terms in the superpotential, and white nodes the opposite.
- We will call consistent dimers those that do not have faces with only two edges.

2.4.2 Combinatorics in the Dimer

At first sight the dimer just looks like a funny way to encode the matter content and superpotential. It has in its guts, however, all the combinatorial power of toric geometries. Here we introduce a couple of ways to recover the geometry from the diagram directly in terms of combinatorial objects.

Zig-Zag paths are oriented paths in the dimer that cross edges through their middle and go parallel to them, turning to the right at black nodes and left at white ones. Remarkably, for a consistent dimer, Zig-Zags are closed paths and don't have self-intersections. One can assign (p,q) charges to them according to their holonomy around the torus where the diagram is embedded. These charges match those of the external legs in the (p, q) web. Hence, from the Zig-Zag paths one finds the (p,q) web very easily. See Figure 2.8a for an example.

Perfect Matchings are subsets of edges in the dimer such that every node only has one edge in it. Using them one can find the toric diagram of the variety in two ways. In

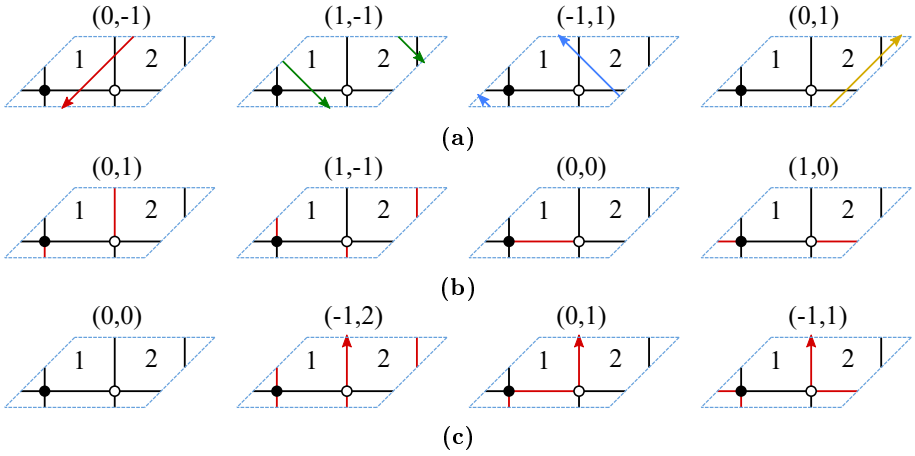

Figure 2.8: 3 ways of finding the CY geometry from the Dimer. a) use Zig-Zag paths to find the web diagram. b) use perfect matchings to find the toric diagram. c) use loops of perfect matchings to find the toric diagram. Note that all give $SL(2,\mathbb{Z})$ transformations of the relevant diagrams.

either case we need to assign an orientation for edges in the dimer, which we take as going from white to black nodes.

- Assign to every perfect matching a two-dimensional charge as follows. Every field that crosses the boundaries of the unit cell adds or subtracts 1 to the charge in that direction, depending on its orientation. Every perfect matching gives a point in the toric diagram. See Figure 2.8b, note that the toric diagram is an $SL(2,\mathbb{Z})$ transformation of the one in Figure 2.3a.

- The second way is by constructing closed loops using perfect matchings and assigning holonomies to them. For this, take a reference perfect matching and subtract the rest to it, concatenating their fields and reversing the orientation of the ones subtracted. Assigning holonomies to these cycles gives the toric diagram of the toric variety. If a subtraction gives several disconnected loops, their charges are added. See Figure 2.8c.

To sum up, given a dimer it is very easy to know what geometry it describes. Finding the dimer (and field theory) for a given geometry is more complicated. The easiest way being to embed the theory in an orbifold of $\mathbb{C}^3$ or the conifold and deform it through partial resolutions. For the shake of simplicity we will refer to theories by the name of the singularity. By this we mean the theory obtained by placing D3-branes at the tip of a complex cone over the singularity. In the examples that follow, we will often use this abbreviated way of referring to the full CY_3 and the corresponding gauge theory.

2.4.3 The Mirror

The set-up of D3-branes probing a toric CY_3 singularity has a nice mirror geometry where D6-branes wrap. Is also helps to better understand some of the objects we have discussed so far and also leads to the introduction of novel ones. This was discussed in [32], which we follow here.

The mirror geometry is a non-compact CY_3 specified by a double fibration over the complex plane $W \in \mathbb{C}$. The first fiber is a $\mathbb{C}^*$ specified by $W = uv$, with $u, v \in \mathbb{C}$. The

second fiber is a Riemann surface satisfying $W = P(z, w)$, where $P(z, w)$ is the Newton polynomial of the toric variety, encoding the toric diagram. The resulting fibration is,

$$\begin{aligned} W &= P(z, w) \\ W &= uv \end{aligned} \tag{2.64}$$

The first equation describes a punctured Riemann surface of genus g, equal to the number of internal points in the toric diagram, fibered over W, Σ_W. Cycles in this surface may shrink and pinch off at points $W = W^*$. At $W = 0$, the S^1 in the other fiber degenerates, as $uv = 0$, being smooth otherwise. This singular points can be used to construct 3-cycles. Consider a segment in W linking a point in W^* to $W = 0$. It has a double S^1 fibration over it such that each fiber degenerates in one endpoint. Clearly this is a 3-cycle with S^3 topology. It is an amusing fact that D3-branes probing a singular CY_3 are mapped under mirror symmetry to D6-branes wrapping these cycles. All the information about the field theory can be read from these branes and their intersections!

Actually, the basic properties of this geometry are captured by the surface Σ_W at the origin $W = 0$, which we denote for convenience simply as Σ. Remarkably this surface can be though of as the thickening of the web diagram, see Figure 2.3. The punctures in Σ map to legs in the (p, q) web, so they are related to Zig-Zags paths in the dimer, as we discuss later. 3-cycles in the geometry intersect this surface in 1-cycles that degenerate in W^* but are smooth in $W = 0$. Looking at these 1-cycles in Σ the whole pattern of intersecting D6-branes is known. Quite nicely, this information is encoded in a bipartite tiling of Σ (We name the tiling of Σ indistinctively as Σ) as follows, see Figure 2.7c, for the tiling of the sphere corresponding to the conifold,

- Depending on the genus of Σ, the global properties of the tiling will change.
- Faces in the tiling of Σ are punctures of the Riemann surface associated to (p, q) legs.
- Zig-Zag paths in Σ describe 1-cycles where the D6-branes may wrap, so are associated to gauge factors.
- Intersections of Zig-Zags paths are physically intersections of D6-branes, where fundamental open strings give rise to bifundamental matter. These intersections are just the edges in the tiling.
- Superpotential terms come from worldsheet instantons living in disks subtended by the intersecting branes. These disks surround the nodes of the diagram.
- In many cases with one internal point in the toric diagram ($g = 1$), the tiling of Σ will just be the dimer diagram. This is true in most cases for the most symmetric Seiberg phase of the theory, but even then counterexamples are known.

One can construct the tiling of Σ from the dimer as follows. Zig-Zag paths in the dimer describe punctures and should map to faces in the mirror. Furthermore, the diagram should really be the same, since it is specified by the matter content and superpotential. So we are looking for a different embedding of the same diagram is a surface with possibly different genus. For us, the simplest way is to take the Zig-Zag paths in the dimer, see their intersection structure, compute the genus of Σ using the euler formula and draw the faces in Σ directly, knowing from the Zig-Zags their adjacent faces. A more systematic

procedure was developed in [32], called untwisting, but the result should is the same. The converse procedure is straightforward, since Zig-Zag paths in Σ correspond to faces in the dimer.

2.4.4 Orientifolds in the dimer

For a system of D-branes at singularities, an orientifold projection is a $\mathbb{Z}_2$ identification of gauge groups, chiral multiplets and superpotential couplings. It should thus act as a $\mathbb{Z}_2$ symmetry on the dimer diagram. This is indeed the case, as discussed in [33], which we follow here. A given theory with a corresponding dimer diagram may admit, or not, one or several geometric actions of this type. Depending on how the $\mathbb{Z}_2$ acts, there are two possibilities,

1. **Involutions with respect to a point.** This transformations shifts the two mesonic directions on the dimer diagram and produce 4 fixed points in it. See an example in Figure 2.9a. The fixed points are interpreted as orientifold planes. Each of them thus needs to be assigned a sign in terms of the projection they give, O^+, O^-. Under the geometric action a series of rules specify the resulting field theory, that can be directly read from the diagram,

   - Faces not mapping to themselves combine with their images to form a $SU(N)$ gauge factor.
   - Faces mapped to themselves give a gauge factor whose group depends on the orientifold projection. It will be $SO(N)$ for O^+ and $USp(N)$ for O^-.
   - Edges that are not on top of an orientifold plane combine with their images to form a bifundamental.
   - Edges on top of an orientifold plane project down to the 2-index antisymmetric representation for O^- and to the symmetric one for the O^+ plane.
   - The superpontial is inherited from the parent theory by removing half the terms as they are identified under the geometric action and replacing the fields as required by the orientifold projection.
   - Some additional matter fields might be necessary for anomaly cancelations.
   - The number of orientifold planes with the same sign is even (resp. odd) for dimers with a number of nodes $4k$ (resp. $4k+2$).

   As an example, in Figure 2.9a, an orientifold of the $\mathbb{C}^3/\mathbb{Z}_3$ orbifold is depicted. There are several possible charge assignments for the orientifold planes. The number of planes with the same charge should be odd, as the dimer has two nodes. Consider, for instance, charge assignment $(+,-,-,-)$ running clockwise in the diagram starting with the star at the origin. The resulting theory has gauge group $USp(N_1)_1 \times SU(N_2)_2$, faces 2 and 3 are identified under the orientifold action. The matter content consists on 2 antisymmetric and 1 symmetric multiplets under $SU(N_1)_1$ and 3 bifundamentals.

2. **Involutions with respect to a line.** These orientifolds reverse a single mesonic direction leaving two or one fixed lines depending on whether the mesonic direction matches a direction in the dimer or not. The rules are identical to the previous case

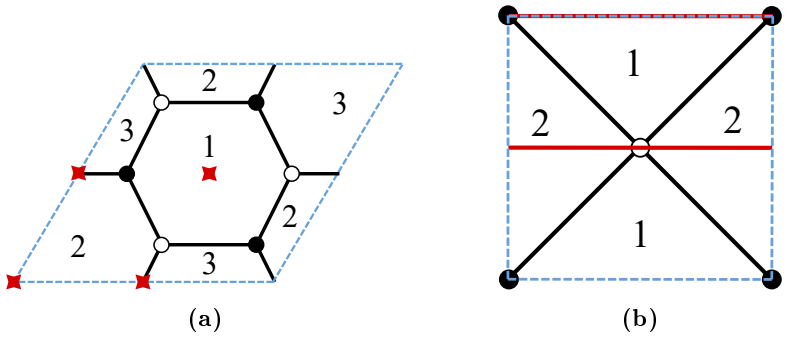

Figure 2.9: Orientifold examples. a) is an orientifold of $\mathbb{C}^3/\mathbb{Z}_3$ with fixed points, while b) is an orientifold of the conifold with fixed lines.).

with the peculiarity that terms in the superpotential may also map to themselves, in which case they are not projected out.
As an example, in Figure 2.9b an orientifold of the conifold is shown. The resulting theory has gauge groups symplectic or orthogonal depending on the sign of the orientifold planes. The matter content is given by bifundamentals $(\square_1, \square_2)$.

2.4.5 Bipartite Field Theories and other beasts

Dimer models are bipartite graphs embedded in a $\mathbb{T}^2$. This construction can be generalized to bipartite graphs in higher genus surfaces, possibly with boundaries. The field theories associated to these diagrams are $\mathcal{N} = 1$ gauge theories called Bipartite Field Theories (BFTs). For a nice discussion the reader may check [34]. These theories have appeared in different physical contexts, such as scattering amplitudes and more recently some classes have been engineered using D-branes in String Theory, see [35,36].

Another direction to generalize is by probing higher dimensional toric Calabi-Yau varieties using D-branes. The case of a CY_4 probed by D1-branes has been discussed in [37,38]. The resulting field theories are described by a 3-dimensional object called Brane Brick Model analogous to the dimer model. Further generalization to CY_5 is discussed in [39]. Finally, the dimer circle has been closed recently by extending the construction to any higher dimer describing the topological B-model probing a CY_n. Remarkably, structures such as perfect matchings generalize nicely, see [40,41].

2.5 Fractional Branes

As already mentioned, rank assignments for the different gauge factors are constrained to cancel non-abelian gauge anomalies, as well as mixed $U(1)$ anomalies. On the String Theory side, this is equivalent to cancellation of RR tadpoles. Practically, this is ensured by having the same number of fundamentals and antifundamentals under all gauge groups. There is always a trivial choice, the one of equal ranks for all gauge groups, since toric quivers have the same number of ingoing and outgoing arrows. As anticipated in Section 2.3.2.2 this choice of ranks corresponds to the case of a single D3-brane probing the singularity. This brane is free to move away from the singularity, as described by the mesonic moduli space of the corresponding field theory, which is just the probed geometry.

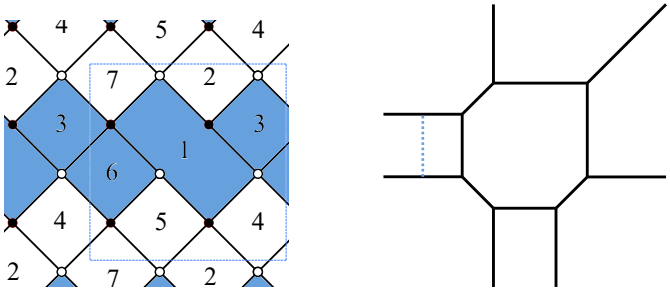

Figure 2.10: a) Dimer diagram showing an $\mathcal{N}=2$ fractional brane in the PdP_4 theory; b) Web diagram, displaying the corresponding mobile $\mathbb{P}_1$ as a blue discontinuous segment.

These branes are refereed to as regular or dynamical branes.

More complicated rank assigments are usually possible and correspond to fractional branes, generalizing the notion in Section 2.3.3. Any complicated rank assigment can be decomposed in a basis of simple fractional branes. In this section we review the different fractional branes that arise and their effect in the field theory.

From the String Theory side, fractional branes can be regarded as D5-branes wraped on 2-cycles vanishing at the singularity such that their dual 4-cycle is non-compact, allowing their RR-flux to escape to infinity. This precisely implies the vanishing of RR-tadpoles and gauge anomalies. Depending on the effect they have in the field theory and the geometry there are three kinds of fractional branes, see [31],

- The so-called $\mathcal{N}=2$ fractional branes correspond to an overall increase of ranks in a subset of faces bounded by zig-zag paths associated to the same (p,q) 1-cycle in the dimer $\mathbb{T}^2$. They are associated to parallel external legs in the web diagram, or equivalently to curves of $\mathbb{C}^2/\mathbb{Z}_k$ singularities sticking out of the singularity at the origin. The gauge theory on these fractional D3-branes has a flat direction, parametrized by the meson obtained by concatenation of bifundamentals joining the faces bounded by the zig-zag paths in the dimer. The flat direction describes the possibility of moving the fractional D-brane off the origin along the curve of singularities, to become a fractional brane of $\mathbb{C}^2/\mathbb{Z}_k$, namely a D5-brane wrapped on one of the collapsed 2-cycles of the orbifold singularity. The gauge theory on this branch is the $\mathcal{N}=2$ A_{k-1} quiver gauge theory [42], hence the name. An example of $\mathcal{N}=2$ fractional brane is shown in Figure 2.10.

- The so-called deformation branes are associated to complex deformations of the CY threefold singularity. They are associated to splittings of the web diagram into sub-webs in equilibrium. The rank assignment corresponds to an overall increase of ranks in the subset of faces bounded by the splitting. Namely, the homological sum of the zig-zag paths associated to the sub-web removed (in a given complex deformation, the two sub-webs give the same result, due to the condition that the total sum of (p,q) charges for external legs is zero). They correspond to checkerboard pictures on the dimer. The complex deformation of the geometry has a field theory counterpart, in which the gauge theory on the fractional branes confines and has a complex deformed moduli space. The resulting gauge theories are associated to the two sub-webs [43,44]. An example of a deformation fractional brane is shown in Figure 2.11. The gauge

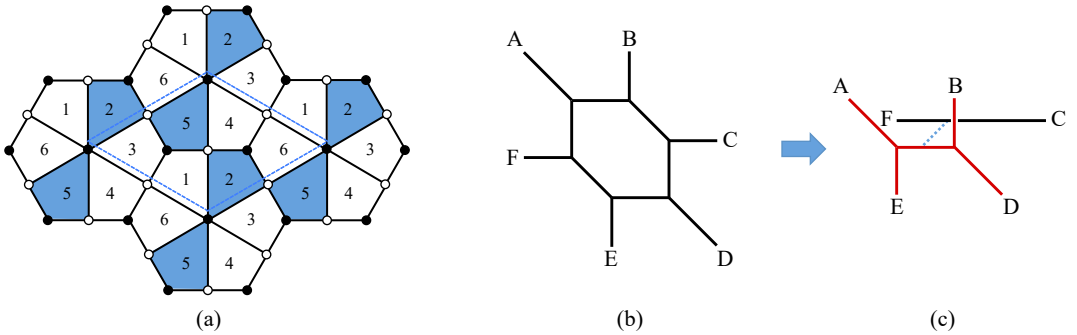

Figure 2.11: a) Dimer diagram showing a deformation fractional brane in the dP_3 theory; b) Web diagram, and (c) its splitting into subwebs in equilibrium, with the finite size $\mathbf{S}^3$ displayed as a blue discontinuous segment suspended between the subwebs.

theory arising from a set of N regular D3-branes and M (deformation) fractional branes, leads to RG flows with a sequence of Seiberg duality cascades, along which the overall number of D3-branes N is reduced in multiples of M, and the number M of D5-branes remains fixed. The gravity dual corresponds to a warped throat supported by RR 3-form fluxes on the 3-cycles associated to the complex deformed singularity, and NSNS flux in the dual (non-compact) 3-cycle. Their combination $G_3 = F_3 - \tau H_3$ is an ISD 3-form of type $(2,1)$, thus preserving supersymmetry [45–47]. The throat is locally similar to $AdS_5 \times \mathbf{X}_5$, but with logarithmic changes in the cosmological constant and the RR 5-form flux along the radial direction.

The simplest example is the conifold, already discussed in Section 2.3.3. The generalization of duality cascades in gauge theories associated with fractional branes in more general singularities has been studied in [43, 48]. We will consider the gravity dual of deformation branes in general singularities in section 6.2.1.

- The last class corresponds to the remaining kind of fractional branes. Their corresponding rank assignments on faces have no correspondence with a set of zig-zag paths defining a sub-web in equilibrium. Therefore, there is no geometric complex deformation of the singularity associated to them. Indeed, contrary to deformation fractional branes, their infrared dynamics involves non-abelian gauge dynamics (even for the minimal such fractional brane) and results in the absence of a supersymmetric vacuum (hence they were dubbed DSB branes in [31], see also [49,50]). On the other hand, similarly to deformation fractional branes, they can trigger duality cascades in the presence of N regular D3-branes, which define some warped throats (albeit with naked singularities in the infrared region) [48]. The discussion of the infrared dynamics, supersymmetry breaking, and its implications for the gravity dual and the deformed AdS-WGC are discussed in section 6.2.1

2.6 A dip in the Swampland

String theory is the only theory of quantum gravity that we have at hand, yet its connection to reality has proven elusive, as stringy phenomena are typically unobservable at low energies. Quite remarkably, String Theory and more generally, Quantum Gravity

seems to be a very constrained framework where many things may just not be possible. In particular some naively correct QFTs might not be UV completable into Quantum Gravity. In this section we review the adventure of finding the borders between what goes and what doesn't. Nice reviews that we follow are [51,52].

String Theory compactifications are known to give rise to a Landscape of vacua, described at low energies by QFTs. However, consistency of Quantum Gravity might not allow certain QFTs to arise from it. Quantum consistency is already very powerful in the QFT framework, forbidding many classically healthy theories to be quantum through the appearance of anomalies. In String Theory this goes even further by fixing the space-time dimension, allowed string theories, types of D-branes, allowed bound states of D-branes... QFTs that may not be UV completed to Quantum Gravity are said to be in the Swampland. A series of swampland criteria or swampland conjectures have been put forward in the last couple of decades that aim at drawing the boundaries between the Landscape and the Swampland. In the following we mention some of these criteria.

- **No global Symmetries.** Probably the better established conjecture is the one stating that a theory with a finite number of states, if coupled to gravity, can't have exact global symmetries. The usual argument states that, if there is a global symmetry, there is an infinite number of stable remnant Black Holes and this might lead to inconsistencies with entropy. A proof in the context of AdS/CFT has been recently proposed in [53].

- **The Weak Gravity Conjecture.** The Weak Gravity Conjecture (WGC) states roughly that gravity should be the weakest force. In particular, a very weakly coupled gauge force would be in contradiction with the previous conjecture, in the limiting case. This conjecture was presented in [54] for a gauge $U(1)$ field and, since then, several forms of it have appeared in the literature, as well as growing evidence. In the original form, it states that:

  - *Electric WGC.* There exists a particle with mass m and charge q such that its mass is smaller than its charge: $m \leq QM_P$.
  - *Magnetic WGC.* The cutoff of the theory is bounded from above by the gauge goupling: $\Lambda \leq gM_p$.

- **Swampland Distance Conjecture**. The original version of the conjecture was stated in [55] and refined in [56,57]. It states that given a point in a moduli space, there is another point whose geodesic distance from the former is infinite. Traveling along this geodesic, as the distance reaches the Planck mass, a tower of states becomes exponentially light,

$$M_f < M_i e^{-\alpha \frac{d_{i,f}}{M_p}} \tag{2.65}$$

  Where $\alpha \sim \mathcal{O}(1)$ and $d_{i,f}$ is the geodesic distance transversed. This equation is further conjectured to hold for scalar fields with a potential. The field theory thus breaks down at some point due to stringy states becoming light. Note these states may come form KK-modes, extended objects and so on.

- **No non-SUSY AdS Conjecture (AdS-WGC).** Non supersymmetric AdS should be unstable in Quantum Gravity. In [58] the WGC was sharpened such that the inequality is saturated only for supersymmetric theories, arguing that only the BPS

property can protect the equality. A remarkable consequence is that non-SUSY AdS_{p+2} supported by fluxes becomes unstable under nucleation of p-brane bubbles that discharge the flux, as the bubble in [59] is always energetically favorable. The conjecture extends this instability to all AdS and concludes that all non-SUSY realizations of AdS in Quantum Gravity are unstable. This conjecture was independently proposed in [60] and received further support in [61], which discusses bubble of nothing decays in non-SUSY AdS. In Chapter 6 we discuss a generalization of this conjecture to warped throats that locally look AdS.

3

Axion potential generation in 3-form language

Axions have become an essential template to describe physics of scalar fields whose potential enjoys special protection properties due to an underlying symmetry principle. Naively, the symmetry corresponds to the perturbative global symmetry shifting the value of the scalar field, which is violated by non-perturbative effects, as originally proposed for the QCD axion [62]. However, it has recently become clear that the most fundamental symmetry structure is that of the dual 2-form. Contributions to the axion potential which spoil the shift symmetry must arise from the existence of a 3-form which eats up the dual 2-form to make it (and so the dual axion) massive. The gauge symmetry of the 3-form constrains the form of these contributions in an advantageous way for many phenomenological applications. The description of the axions in terms of forms and their duals has also been key to the use of the weak gravity conjecture [54] to constrain transplanckian axion model building [56, 63–79].

This formulation has been well understood:

• For the QCD axion, in [80–82], where the 3-form is actually the Chern-Simons composite 3-form built out of the QCD gauge fields.

• In string compactifications producing axion monodromy [83, 84], as described in [85] connecting it to the earlier description in [86, 87] [1]. In these cases, the 3-form is a fundamental field, and its couplings arise from different sources, ranging from Chern-Simons couplings to fluxes in the 10d action [85, 106] (see also [107]), torsion homology [85] (see also [108]) or topological brane-bulk couplings [102].

The two above phenomena, in particular the presence of fluxes and non-perturbative effects on D-brane gauge sectors, play an important role in several scenarios of moduli stabilization (and thus of their axion components), along the lines in [109]. Actually, the gauge non-perturbative effects can be described in string theory as particular cases of D-brane instanton effects wrapping the same cycle as the gauge D-branes in the compact space. In general, in string theory there are other non-perturbative effects from D-brane instantons not wrapping such cycles (sometimes dubbed stringy or exotic D-brane instantons [110–112], see [113, 114] for reviews), and contributing to the stabilization of axions as well. It is therefore natural to wonder about the 3-form description of these latter effects. Interestingly, there is no known description of this kind: since there is no gauge group associated to the cycles, we cannot use any composite Chern-Simons 3-form; on the other hand, for e.g. a D3-brane instanton on a 4-cycle, there is not any obvious corresponding harmonic form able to produce a 3-form in the 4d theory upon compactification.

In this chapter we solve this question and provide the 3-form description for the

[1] For other works related to axion monodromy, see [75, 88–105].

stabilization of an axion by non-gauge D-brane instanton effects. The key idea is to notice that the stabilizaton occurs when the non-perturbative effect is included in the theory, so it is only then that we can hope to find a suitable 3-form. Therefore, the internal form supporting the 4d 3-form must arise only in the geometry backreacted by the presence of the D-brane instanton, in the sense discussed in [115,116]. In general, these correspond to generalized geometries, so the corresponding form need not be harmonic with respect to the underlying CY metric, rather it corresponds to (a piece of) a generalized calibration.

We study this in the particular example of D3-brane instantons on 4-cycles, but the lesson is general (as expected from T-duality/mirror symmetry). Also, we show that the picture is compatible with D-brane instantons corresponding to gauge non-perturbative effects.

This chapter is organized as follows. In Section 3.1 we review the 3-form description of axion stabilization and its interplay with axion monodromy and non-perturbative gauge dynamics. In Section 3.2 we provide the 3-form description of axion potentials induced by non-gauge D-brane instantons: after posing the question in Section 3.2.1, we review the D3-brane instanton backreacted geometry in Section 3.2.2, and obtain the 4d 3-form and its couplings in Section 3.2.3. A simple example is displayed in Section 3.2.4. Section 3.2.5 describes the generalization, in particular the mirror picture of D2-brane instantons in type IIA compactifications. In Section 3.3 we discuss the case of gauge D-brane instantons.

3.1 Review of 3-forms and monodromy

Consider an axion ϕ, regarded just as a scalar taking values in a circle (i.e. with discrete periodicity[2] 2π) and with an (approximate) shift symmetry. In many applications one is interested in generating a non-trivial potential for this axion, violating precisely this shift symmetry. For simplicity we consider the potential expanded at quadratic order around a minimum, as for instance arises in moduli stabilization; the general picture is however more general. Hence we have the lagrangian

$$|d\phi|^2 + \mu^2 \phi^2 \tag{3.1}$$

A potential of this kind is naively not compatible with the axion periodicity, but may be made so by including multivalued branches for the potential, thus inducing axion monodromy. The description of the periodicity properties are automatically implemented by using a dual formulation, in terms of a 3-form c_3 eating up the 4d dual 2-form field b_2 (defined by $*\, db_2 = d\phi$, in 4d). This is described by the following lagrangian[3]

$$|db_2 + nc_3|^2 + |F_4|^2 \tag{3.2}$$

where $F_4 = dc_3$. This theory has the gauge invariance

$$c_3 \to c_3 + d\Lambda_2 \quad , \quad b_2 \to b_2 - n\Lambda_2 \tag{3.3}$$

As emphasized in [85], it is this gauge symmetry that protects the flatness of the axion potential against uncontrolled corrections even in transplanckian field ranges. Dualizing the

[2] For simplicity we set the axion decay constant to $f_\phi = 1$.

[3] We allow for a $\mathbf{Z}_n$ discrete gauge symmetry, see [85, 107, 117] for discussions of such system and the corresponding $\mathbf{Z}_n$ charged domain walls.

2-form back into the axion ϕ, we obtain the Kaloper-Sorbo description of axion monodromy [86,87,94,118]

$$|d\phi|^2 \,+\, n\phi\, F_4 \,+\, |F_4|^2 \tag{3.4}$$

Integrating out the non-dynamical 4-form field strength F_4 one recovers a potential with the structure (3.1).

The idea can be generalized to other potentials by considering corrections, which due to the gauge invariance, (3.3) must be in terms of higher powers in F_4. This leads for instance to the flattening in [119].

At this point we would like to emphasize an important clarification: the description of the massive axion in terms of a 3-form eating up the dual 2-form, or in terms of a coupling between (a function of) the axion and the 4-form field strength, is not necessarily a signature of axion monodromy, but rather of the existence of a non-trivial axion potential. Axion monodromy arises in cases when the potential does not naively satisfy the axion periodicity. On the other hand, the 3-form description should also hold for non-monodromic potentials (i.e. single-valued and consistent with the axion periodicity). Our main interest in this chapter is indeed the 3-form description of single instanton non-perturbative potentials, which indeed are periodic in the axion.

Before entering this discussion, we conclude this review with a brief recap of the 3-form description of axion potentials induced by non-perturbative gauge dynamics. This has been studied in the context of QCD axions in [80–82], but we recast it for pure $\mathcal{N}=1$ $SU(n)$ SYM, which will be useful later on. The axion belongs to a chiral multiplet $\phi = \mathrm{Im}\, T$, and we have a coupling

$$S_{\rm SYM} \,=\, \int d^2\theta d^4x\, T\, W_\alpha W^\alpha \,\sim\, \int_{4d} \phi\ \mathrm{tr}\ F^2 \,+\ldots \tag{3.5}$$

As described in Section 2.1.1, the non-perturbative dynamics produces a gaugino condensate superpotential,

$$W \,=\, \omega^k \Lambda^3 \,=\, \omega^k\, e^{-\frac{T}{n}} \tag{3.6}$$

where $\omega = e^{2\pi i/n}$ and $\Lambda = \exp\left(-\frac{T}{3n}\right)$ is the SYM dynamical scale, regarded as a function of T.

The theory has n gapped vacua, which differ by the value of $\langle\phi\rangle$ (the phase of the gaugino condensate), in the sense that a shift $\phi \to \phi + 2\pi$ changes the k^{th} vacuum to the $(k+1)^{th}$. Therefore the potential has a periodicity of $\phi \sim \phi + 2\pi n$. On the other hand, the axion should actually have a periodicity of 2π; in fact, this is ensured because there is a 3-form description of the above axion potential. This follows from realizing that the coupling (3.5) describes a coupling to a 4-form ϕF_4 structure, with $F_4 = \mathrm{tr}\ F^2$. Namely, the 3-form is the composite Chern-Simons 3-form $c_3 = \omega_3^{\rm CS}$ (defined by $d\omega_3^{\rm CS} = \mathrm{tr}\ F^2$).

In other words, although the potential is periodic with a period $2\pi n$, the periodicity of 2π is achieved via a monodromic structure, but with a finite number n of branches. This is clearly associated with the $\mathbf{Z}_n$ discrete symmetry among the n vacua of $\mathcal{N}=1$ SYM. The structure of domain walls among vacua is naturally described in terms of the (composite) 3-form description [80–82].

3.2 3-forms from D-brane instanton backreaction

3.2.1 The puzzle

In string theory, there are non-perturbative contributions to the superpotential beyond the above non-perturbative gauge dynamics contributions. These come from, for instance, euclidean D-brane instantons which do not correspond to gauge theory instantons. A prototypical example is provided by D3-branes instantons wrapped on 4-cycles in CY compactifications[4], such as those used in moduli stabilization in [109]. In our discussions we will assume the instantons to indeed produce superpotential terms; it would be interesting, but beyond our scope, to develop an understanding of a dual description for instanton effects generating higher F-terms due to extra fermion zero modes [120, 121]. Denoting by T the complex modulus associated to the wrapped 4-cycle, we have a superpotential

$$W_{\rm np} \,=\, A\, e^{-T} \tag{3.7}$$

where A is a prefactor depending on complex structure moduli (and possibly also on open string moduli), whose detailed structure is not essential for our present purposes.

We expect the axion potential induced by these instantons to admit a description in terms of a 3-form eating up the dual 2-form. On the other hand, there is no obvious candidate for such a 3-form in the 4d CY compactification: the only available RR fields are even-degree gauge potentials, so the 3-form should arise from the RR 6-form integrated over a 3-cycle. However, there is no natural pairing between a 3-cycle and a 4-cycle in a CY so as to support the topological coupling ϕF_4 ultimately responsible for the axion potential. Therefore there is no natural candidate for the 3-form coupling to the axion to reproduce its potential.

The solution to this problem is to follow the intuition gained in the discussion of the SYM superpotential. In that case, the 3-form arises only when the existence of non-perturbative sectors in the gauge theory are taken into account; namely, the fact that $F_4 = \text{tr } F^2$ implies that the presence of the instantons is built-in in the coupling ϕF_4. The implementation of a similar concept for non-gauge D-brane instantons requires proposing that the 3-form describing the axion stabilization should be looked for not in the original CY geometry, but rather in the geometry perturbed by the gravitational backreaction of the D-brane instantons. This perturbation of the geometry has been studied in the literature in [115, 116] by exploiting the technology of generalized geometry.

3.2.2 D-brane instanton backreaction

In this section we review ideas in [115, 116] to describe the backreaction of D-brane instantons in terms of generalized geometry. The uninterested reader may wish to jump to Section 3.2.3.

The effect of D-brane instantons can be encoded in the underlying CY geometry by means of a deformation turning the $SU(3)$ holonomy into (in general) an $SU(3) \times SU(3)$ structure, associated to the existence of two spinors (not covariantly constant due to the deformation) corresponding to a 4d $\mathcal{N} = 1$ supersymmetry (possibly in AdS). Here we

[4] In general, these may carry world-volume fluxes, but for simplicity we will restrict to the case of trivial gauge backgrounds.

describe the general setup, while in the remaining of this chapter we will focus on the type IIB case. In Chapter 4, we will instead deal with type IIA. The two spinors are written[5]

$$\epsilon_1 = \zeta_+ \otimes \eta_+^{(1)} + \zeta_- \otimes \eta_-^{(1)} \quad , \quad \epsilon_2 = \zeta_+ \otimes \eta_\mp^{(2)} + \zeta_- \otimes \eta_\pm^{(2)} \tag{3.8}$$

here ζ_+ and η_+ are complex conjugate of ζ_-, η_-, and ζ_+ is the 4d spinor specifying the $\mathcal{N}=1$ supersymmetry, and satisfying $\nabla_\mu \zeta_- = \pm \frac{1}{2} W_0 \gamma_\mu \zeta_+$, where W_0 is the superpotential at the AdS minimum (and for the Minkowski case we just have $W_0 = 0$).

The spinors $\eta^{(1,2)}$ can be used to define two polyforms,

$$\Psi_\pm = -\frac{i}{||\eta^{(1)}||^2} \sum_l \frac{1}{l!} \eta_\pm^{(2)\dagger} \gamma_{m_1 \dots m_l} \eta_+^{(1)} \, dy^{m_l} \wedge \dots \wedge dy^{m_1} \tag{3.9}$$

Noticing the chirality of the spinors in the sandwich, the polyform Ψ_+ contains even degree forms and Ψ_- contains odd degree forms. A common alternative notation is $\Psi_1 = \Psi_\mp$ and $\Psi_2 = \Psi_\pm$ for type IIA and IIB.

The familiar case of $SU(3)$ structure corresponds to $\eta^{(2)} \sim \eta^{(1)}$ and leads to $\Psi_+ \sim e^{iJ}$ and $\Psi_- \sim \Omega$. For $SU(3)$ holonomy the spinors are covariantly constant and the polyforms are closed.

The compactification ansatz is

$$ds^2 \; = \; e^{2A(y)} g_{\mu\nu}(x) \, dx^\mu dx^\nu \; + \; h_{mn}(y) \, dy^m dy^n \tag{3.10}$$

The 10d fields can be organized in two complex quantities, in agreement with the 4d susy structure. One holomorphic quantity is

$$\mathcal{Z} \equiv e^{3A-\Phi} \Psi_2 \tag{3.11}$$

where Φ is the 10d dilaton (not to be confused with the 4d axion). This is motivated because it provides the calibration for BPS domain wall D-branes. More concretely, in type IIA, $\mathcal{Z}$ calibrates even-dimensional cycles, while in IIB it calibrates odd-dimensional ones. In other words, the tension of a D-brane BPS domain wall is obtained by integrating the above form over the wrapped cycle. For instance, for standard CY compactifications, a D5-brane on a supersymmetric 3-cycle Π provides a 4d BPS domain wall, whose tension is given by $\int_\Pi \mathcal{Z}_{(3)} \sim \int_\Pi \Omega$, where the subindex (3) denotes the 3-form part of the polyform

The second quantity is

$$\mathcal{T} \equiv e^{-\Phi} \mathrm{Re}\, \Psi_1 + i \Delta C \tag{3.12}$$

where ΔC describes the RR backgrounds not encoded in the background fluxes $\bar{F}$, i.e. the RR fluxes are split as $F = \bar{F} + d\Delta C$. Again, the above complexification is motivated by the generalized calibration of BPS D-brane instantons. In this case, $\mathcal{T}$ calibrates odd or even-dimensional cycles in type IIA and IIB, respectively. For instance, for standard CY compactifications, a D3-brane wrapped on a holomorphic 4-cycle Σ provides a 4d BPS instanton whose action is given by $\int_\Sigma \mathcal{T}_{(4)} \sim \int_\Sigma e^{iJ} \sim \int_\Sigma J \wedge J$.

[5] In the subscript in $\eta_\mp$, $\eta_\pm$, the upper sign refers to type IIA and the lower to IIB.

3.2.3 The 3-form and its coupling

Let us now focus on the case at hand, D3-brane instantons wrapping an holomorphic 4-cycle Σ. From the supersymmetry conditions recast in terms of the 10d version of the 4d fields $\mathcal{Z}$, $\mathcal{T}$, one can show that, in a weak coupling expansion, we have

$$d_H \mathcal{Z} \,=\, \frac{2i}{n} W_{\rm np}\, \delta_2(\Sigma) \tag{3.13}$$

where $d_H = d + H\wedge$, so the 2-form term above is just $d_H \mathcal{Z}_{(1)} = d\mathcal{Z}_{(1)}$. This encodes the backreaction of the instanton effect on the 10d geometry in terms of the appearance of a 1-form component $\mathcal{Z}_{(1)}$ of $\mathcal{Z}$, which was absent in the CY geometry.

This equation defines an special 1-form $\alpha_1 \equiv \mathcal{Z}_{(1)}$. It is associated to the globally defined supersymmetric spinor, in the presence of the non-perturbative correction to the geometry. Its structure can be obtained by integrating the above equation. For the particular case of a D3-brane instanton ($n = 1$) on a holomorphic 4-cycle defined by the equation $f = 0$, one obtains [115]

$$\mathcal{Z}_{(1)} \,\sim\, df\, \tilde{W}_{\rm np} \tag{3.14}$$

where the tilded superpotential has the dependence on open string degrees of freedom removed.

One intuitive way to understand the above expression is to notice that, in a theory containing gauge D3-branes (i.e. D3-branes sitting at a point in the internal space), the 4d superpotential as a function of the D3-brane position is obtained by considering a 1-chain L joining two different points in the CY and integrating $\mathcal{Z}_{(1)}$ over it. This follows because $\mathcal{Z}_{(1)}$ is the calibrating form for a D3-brane wrapped on the 1-chain L, which defines a domain wall interpolating between the two configurations of the D3-branes at the two (end)points. We thus have

$$\Delta W \,\sim\, \int_L \mathcal{Z}_{(1)} \,=\, f\, \tilde{W}_{\rm np} \tag{3.15}$$

where we regard f as the D3-brane position in the direction normal to the instanton 4-cycle. The result therefore reproduces the familiar dependence on open string moduli, microscopically associated to Ganor strings [122] (see also [123]).

In the following we recast (3.13) as $d\alpha_1 = \beta_2$, and we use both α_1 and β_2 as internal profiles for the KK reduction of higher-dimensional form fields in the backreacted geometry. This is similar to the non-harmonic forms used in KK reduction of massive $U(1)$s, and studied in [108] in compactification spaces with torsion (co)homology.

We may use these forms to perform the KK reduction of the 10d RR 4-form C_4 as

$$C_4 \,=\, \alpha_1(y) \wedge c_3(x) \,+\, \beta_2(y) \wedge b_2(x) \,+\, \ldots \tag{3.16}$$

This produces a 3-form in 4d spacetime, naturally associated to the non-perturbative effect, and a 2-form, dual of ϕ. Moreover, is it clear that the 3-form is eating up the 2-form, by noticing that the field strength F_5 has a term

$$F_5 = (1 + *_{10d}) \left(\beta_2 \wedge (c_3 + db_2) - \alpha_1 \wedge F_4\right) \tag{3.17}$$

where $*_{10d}$ is added to take the self-duality of F_5 into account. This clearly has the gauge invariance

$$c_3 \to c_3 + d\Lambda_2 \quad , \quad b_2 \to b_2 - \Lambda_2 \tag{3.18}$$

This implies that the 3-form is eating up the 2-form to become massive, and correspondingly provides a dual description of the axion ϕ becoming massive, as in Section 3.1.

It is also straightforward to show that this 3-form has a Kaloper-Sorbo coupling to the axion. We focus just on the leading term ϕF_4, where $\phi = \int_\Sigma C_4$, and $F_4 = dc_3$. We simply massage the kinetic term of the (self-dual) 4-form and focus on the components in (3.17) as follows

$$\int_{10d} F_5 \wedge *F_5 \; = \; - \int_{10d} C_4 \wedge d * F_5 \; \to \; \int_{10d} C_4 \wedge \beta_2 \wedge F_4 \; = \; \int_{4d} \phi \, F_4$$

where we used $\beta_2 \sim \delta_2(\Sigma)$.

3.2.4 Some toroidal examples

To flesh out this somewhat abstract description, let us now consider a toroidal compactification $M_4 \times \mathbf{T}^6$, where for simplicity we take a factorizable, $\mathbf{T}^6 = \mathbf{T}^2 \times \mathbf{T}^2 \times \mathbf{T}^2$ with local complex coordinates be z_1, z_2, z_3. Let us study the backreaction caused by a instantonic D3-brane wrapping the 4-cycle Σ_4 defined by $z_3 = 0$. Using the general formulas in [115, 124], the complex structure $\mathcal{Z} = \Omega$ gets corrected, becoming a generalized complex structure with a 1-form piece

$$Z_{(1)} \sim e^{-T} \, dz_3, \tag{3.19}$$

This is the 1-form to be used to produce the 4d 3-form upon compactification of the 10d RR 4-form.

Notice that it actually corresponds to dz_3, a harmonic 1-form already present in the underlying toroidal geometry. Therefore there seems to be essentially no new geometric structure associated to the backreacted geometry, namely, no axion potential due to the instanton effect. This feature is clearly related to the existence of extra harmonic forms in the $\mathbf{T}^6$ geometry, which are not present in generic CYs. However, it nicely dovetails the expectation that D3-brane instantons in toroidal geometries have additional fermion zero modes, and do not produce non-perturbative superpotentials for the corresponding moduli.

In order to actually get non-trivial structure, we can consider orbifolds which remove the extra harmonic forms, and produce genuine CY geometries. Consider for instance $\mathbf{T}^6/(\mathbf{Z}_2 \times \mathbf{Z}_2)$, where the generators of the orbifold group act as $\theta : (z_1, z_2, z_3) \to (-z_1, z_2, -z_3)$, and $\omega : (z_1, z_2, z_3) \to (z_1, -z_2, -z_3)$. To describe the quotient, we introduce local coordinates[6] by building orbifold invariants, $u_i = z_i^2$, $t = z_1 z_2 z_3$, subject to $u_1 u_2 u_3 = t^2$. The instanton wrapped on the second and third torus is defined by $f \equiv u_3 = 0$, so $f = u_3$, and we have

$$\mathcal{Z}_{(1)} \sim du_3 \sim z_3 \, dz_3 \tag{3.20}$$

It is now clear that the 1-form supporting the 3-form in the compactification of the 10d 4-form is non-harmonic with respect to the original CY geometry.

[6] A global construction is easily produced by using Weierstrass equations for the 2-tori, but we will not need this extra complication.

3.2.5 Generalization

Although we have focused on the case of axions with potential arising from D3-brane instantons on 4-cycles, the ideas hold for general RR axions associated to other cycles, and with potentials arising from the corresponding wrapped D-brane instantons. In order to illustrate this, we consider the mirror configuration of type IIA with axions arising from the RR 3-form on a 3-cycle, stabilized by D2-brane instantons.

Let us thus study the mirror dual to the configuration of D3-branes on a 4-cycle, in the setup of a general CY (alternatively the main ideas can already be illustrated in the toroidal examples in Section 3.2.4). Consider the CY in the large complex structure limit, where it can be regarded as a $\mathbf{T}^3$ (parametrized by coordinates y_i, $1,2,3,$) fibered over a 3d base, with local coordinates x_i, $i=1,2,3$. The complex coordinates are locally $z_i = x_i + iy_i$, and we consider a holomorphic 4-cycle given locally by $z_3 = 0$, i.e. spanning x_1, y_1, x_2, y_2.

The mirror dual can be obtained by applying three T-dualities [125], along the coordinates y_i. The D3-brane instanton thus turns into a D2-brane wrapped on the 3-cycles locally spanned by x_1, x_2, y_3' (with the prime denoting the T-dual coordinate). One further sees that the complex structure deformation $Z_{(1)} \sim df = dx_3 + i dy_3$ gives rise to a polyform

$$\delta\mathcal{T} = \mathcal{T}_{(2)} + \mathcal{T}_{(4)}, \tag{3.21}$$

This follows from the fact that $\mathcal{Z}_{(1)}$ is eventually used to expand the RR forms and obtain the 4d 3-form. Hence, these are the 2- and 4-form components of (3.12) produced by the backreaction of the D2-instanton, as we argue later on. Before that, let us conclude that the expansion of the RR polyform $\mathcal{C} = C_1 + C_3 + C_5 + C_7$ along $\delta\mathcal{T}$ produces the 4d 3-form as follows

$$\mathcal{C} \;=\; \delta\mathcal{T} \wedge c_3 \;\rightarrow\; C_7 = \mathcal{T}_{(4)} \wedge c_3 \;,\; C_5 = \mathcal{T}_{(2)} \wedge c_3 \tag{3.22}$$

where the c_3 in the last two expansions is understood to be the same 4d 3-form.

Let us finish by arguing further that the above $\delta\mathcal{T}$ is indeed the backreaction corresponding to the D2-brane instanton. In the original picture in Section 3.2.3 we considered the superpotential in the theory in the presence of a gauge D3-brane, given by the integral of the calibrating form over a 1-chain. Under the mirror transformation we must consider the theory in the presence of a gauge D6-brane wrapped on the 3-cycle Π_3 (i.e. the mirror $\mathbf{T}^3$ fiber, spanned by y_i', $i=1,2,3$). The superpotential is given by the integral of the calibrating form $\mathcal{T}$ over a (generalized) 4-chain Σ interpolating between two (possibly generalized) 3-cycles (see e.g. [126])

$$\Delta W_{D6} = \int_{\Sigma} \delta\mathcal{T} \tag{3.23}$$

We are interested in the superpotential as a function of one D6-brane complex modulus, given by one deformation of the special lagrangian 3-cycle, and the corresponding Wilson line along one 1-cycle in Π_3. The actual components turned on in this $\delta\mathcal{T}$ are $\mathcal{T}_{(4)}$, which will be integrated along the 4-chain produced by the deformation of the 3-cycle Π_3, and a component $\mathcal{T}_{(2)}$ integrated over the 2-chain spanned by the 1-cycle in such deformation. The latter accounts for the contribution to the superpotential of the induced D4-brane charge arising from possible D6-brane worldvolume fluxes on the 2-forms Poincaré dual to the 1-cycle in Π_3.

The resulting variation of the superpotential is

$$\Delta W_{D6} = \int_{\Sigma_4} \mathcal{T}_{(4)} + \int_{\Sigma_4} \mathcal{T}_{(2)} \wedge \mathcal{F} = \int_{\Sigma_4} \mathcal{T}_{(4)} + \int_{\Sigma_2} \mathcal{T}_{(2)}, \tag{3.24}$$

where $\mathcal{F}$ is the magnetic field induced in the D6-brane.

Therefore, the only way to reproduce the D6-brane open string moduli dependence described by the Ganor zeroes is that the instanton backreaction indeed produces the deformation $\delta\mathcal{T}$ with components $\mathcal{T}_{(2)}$ and $\mathcal{T}_{(4)}$.

3.3 Gauge non-perturbative effects

There are D3-brane instantons which admit the interpretation of gauge theory instantons. This happens when the D3-brane instanton wraps precisely the same 4-cycle as a stack of 4d spacetime-filling D7-branes.

The description of stabilization of axions coupling to non-abelian gauge interactions has been recast in terms of coupling to the composite Chern-Simons 3-form in [80–82] c.f. Section 3.1. It is natural to ask about any possible interplay between this and the 3-form discussed in earlier sections.

Actually, the 3-form in earlier sections arises only when the D-brane instantons backreact, in other words when the gauge dynamics is geometrized. This implies that we must consider the geometry that results when the D7-branes, together with the euclidean D3-brane instantons, are backreacted on the geometry. The resulting configuration no longer contains open string degrees of freedom, as everything is encoded in the backreacted geometry. Therefore the relation between the 3-forms is essentially holographic: on one side there are open string degrees of freedom, and the axion stabilization mechanism is described as in [80–82] in terms of a 3-form constructed out of the open string sector gauge fields; on the other side, there is a backreacted geometry, and no open string degrees of freedom, and the axion stabilization arises from a 3-form supported by the distorted geometry.

To flesh out the latter claim, let us consider the description of the backreaction of D7-branes and their euclidean D3-brane instanton effects. We concentrate in the case $\mathcal{N} = 1$ SYM, where the instantons contribute to the superpotential, and therefore to the axion stabilization.

To describe the backreacted geometry, we borrow results from [124]. The backreaction of the D7-branes, at the perturbative level (i.e not including the euclidean D3-brane instantons) is defined by

$$\mathcal{Z} = \Omega \quad , \quad \mathcal{T} = e^{-\Phi} \exp(ie^{\Phi/2} J) \tag{3.25}$$

(where here Φ is the dilaton).

To this order there is no deformation of $\mathcal{Z}$, and moreover no 1-form that can support the 3-form. The latter is however generated when the non-perturbative gaugino condensate (which is described by (fractional) euclidean D3-branes) is included. The gaugino condensate $\langle S \rangle = \langle \lambda\lambda \rangle = e^{2\pi i k/n} \Lambda^3$ is a non-zero vev for the gaugino bilinear. In [124] it was found that

$$d\mathcal{Z} = i\ell_s^4 \langle S \rangle \delta_2(\Sigma) \tag{3.26}$$

This is exactly as in (3.13), thereby confirming the anticipation that the backreacted D7/D3 system can support a 3-form in agreement with the mechanism in earlier sections.

4

Instanton Backreaction on Toric Singularities

Non-perturbative effects in string theory are at the core of a fascinating interplay between formal developments (see e.g. [127–130]) and phenomenological applications, e.g. in moduli stabilization [109, 131].

These non-perturbative effects include field theoretical gauge instantons, as well as genuinely stringy ones such as D-brane instantons. In the previous chapter we succeeded in reformulating the non-perturbative potentials from the latter in the language of 3-forms. As we have seen, this follows from considering the modification of the geometry due to the instanton backreaction in the spirit of [115, 116]. Specifically, the backreaction modifies the topology of the compactification space, producing additional 3-forms, whose coupling to the corresponding axion produces the non-perturbative potential.

In string compactifications with 4d gauge sectors arising from D-branes, some of these axions are gauged by the $U(1)$ symmetries. In those cases, the D-brane instantons produce 4d effective couplings violating the (perturbatively exact global) $U(1)$ symmetries. In the language of type IIA D2-brane instantons in compactifications with 4d gauge sectors from D6-branes, this can be understood microscopically as follows. The insertions corresponding to the 4d charged fields in the effective operator induced by the instanton amplitude, arise form the saturation of charged instanton fermion zero modes arising from open strings at intersections between the D2-brane instanton and the 4d gauge D6-branes [110–112], see [113,114] for reviews. The required coupling of fermion zero modes to 4d charged fields is mediated by a world sheet instanton bounded by the D2- and D6-branes.

There is a large set of scenarios exploiting this mechanism (or its dual versions). For instance, they can generate neutrino masses [110, 111] (see also [132]), Yukawa couplings [133], the μ-term in SUSY extensions of the Standard Model [134, 135], or be crucial in SUSY breaking [136–138] or its mediation [139], as well as in rare processes [140–143] (see [113, 114] for reviews of these and other applications). Achieving these effects typically requires introducing orientifold projections to remove additional fermion zero modes associated to the otherwise underlying $\mathcal{N} = 2$ supersymmetry, see [132, 144, 145] and [113,114] for reviews.

A natural question is thus the description of the backreaction of D-brane instantons in these systems with 4d gauge D-branes, and the mechanism by which the backreacted geometry manages to produce the corresponding charged field theory operators in the 4d effective action. This is the the subject of the present chapter.

In short, in type IIA language, the instanton backreaction produces a change in the topology of the compactification space, in which the instanton cycle becomes trivial, and any cycles intersecting it acquire a boundary. In particular, the gauge D6-branes formerly

intersecting the D2-brane instanton acquire a boundary, and must necessarily recombine among themselves to form actual wrapped D6-branes in the backreacted geometry. In this process, the intersections between the gauge D6-branes and the D2-brane instanton disappear, and so do the charged instanton fermion zero modes. Finally, the original worldsheet instantons supported by the gauge and instanton D-branes, and mediating the coupling of charged fermion zero modes and 4d charged fields, become worldsheet instantons supported, in the backreacted geometry, by just gauge D6-branes, yet producing the same 4d charged field operators in the effective action.

We consider this proposal in the large class of models corresponding to (type IIA mirrors of) D3-branes at toric singularities, and provide a simple combinatoric recipe to obtain the backreacted geometry and recombined gauge D-branes. This provides a new kind of geometric transition for systems of branes at singularities, which reduces to the familiar Klebanov-Strassler type gauge/gravity dualities for brane systems admitting complex deformations of the underlying geometry. Other geometric transitions relate to non-CY geometries, which still seem to admit a simple combinatoric description.

The chapter is organized as follows. In Section 4.1 we review D-brane instantons, both from the open string perspective in Section 4.1.1 and from the backreaction viewpoint in Section 4.1.2. In Section 4.2 we describe the backreaction description of instantons charged under 4d gauge symmetries: in Section 4.2.1 we show that the non-perturbative backreaction forces the recombination of the gauge branes formerly intersecting the instanton. In Section 4.2.2 we provide a topological derivation, based on the Freed-Witten conditions, of the appearance of worldsheet instantons dressing the D2-brane instanton intersected by D6-branes, and show it also explains the appearance of charged field theory operators in the backreaction picture. In Section 4.2.3 we study several generalizations, including non-abelian gauge symmetries, and argue that the backreaction picture implies a sum over brane recombination geometries.

In Section 4.3 we turn to presenting explicit realizations in terms of systems of D3-branes at singularities, or rather their type IIA mirrors, described using dimer diagrams. These are reviewed in Section 2.4.1. In Section 4.3.1 we introduce the D-brane instantons we consider and their properties and in Section 4.3.2 we provide the graphical recipe to describe the backreacted geometry, the D6-brane recombination and the 4d charged field theory operator produced. In Section 4.3.3 we present some illustrative examples of this technique, for single instantons, and generalize to non-compact instantons in Section 4.3.4, and to multi-instanton effects in Section 4.3.5. In Section 4.4 we consider instantons whose backreaction corresponds to complex deformations of the toric singularity and relate them to the deformation fractional branes producing duality cascades generalizing the Klebanov-Strassler conifold. Some generalities are discussed in Section 4.4.1, and concrete examples are provided in Section 4.4.2.

4.1 Review of instantons

4.1.1 The open string story

In string theory, euclidean p-branes wrapped on $(p+1)$-cycles lead to non-perturbative instanton effects. The best understood set of such effects corresponds to wrapped D-brane instantons, for which a microscopic description can be obtained in terms of open string

sectors. In the following we sketch their structure, and their role in the induced terms in the 4d effective action, in 4d $\mathcal{N}=1$ type IIA CY compactifications with D6-branes on intersecting 3-cycles [146,147], see [114] for a review.

Recall that before the introduction of the instantons, each stack of N_a D6-branes wrapped on a 3-cycle Π_a leads to a gauge factor $U(N_a)$, and the D6$_a$-D6$_b$ open sectors produce I_{ab} chiral fields in the bifundamentals $(\,\square_a,\,\overline{\square}_b)$, for all a,b, with $I_{ab}=[\Pi_a]\cdot[\Pi_b]$ being the topological intersection number. Although O6-planes are often present (and in fact, are necessary for globally preserved supersymmetry), we omit the corresponding refinement of the discussion, as it will not be ultimately needed for our later purposes.

Upon introduction of a D2-brane instanton on a 3-cycle Π_3, there are D2-D2 and D2-D6$_a$ open string sectors, which in particular produce the instanton zero modes over which we should integrate. In the D2-D2 sector, the most relevant is a universal set of four bosonic zero modes x^μ, defining the instanton position in 4d, and two goldstinos θ^α of the 4d supersymmetries broken by the instanton. Integration over these produces the superspace measure for the 4d term in the effective action.

$$\int d^4x\, d^2\theta\, A\, e^{-Z}\,(...)_{\text{neutral}}\,\mathcal{O}_{\text{charged}} \tag{4.1}$$

where A is a (Kahler moduli dependent) prefactor, and $Z=\frac{V_3}{g_s}+i\int_{\Pi_3}C_3$ is the instanton action. Finally, $(...)_{\text{neutral}}$ and $\mathcal{O}_{\text{charged}}$ denote additional extra structures from additional zero modes, to be discussed next.

In the absence of additional fermion zero modes, the instanton produces superpotential terms, as suggested above. However, in general, the D2-D2 open sector can lead to additional[1] fermion zero modes, whose saturation introduces the extra structure $(...)_{\text{neutral}}$ and implies that the 4d term is actually a higher F-term, see [120,121], also [148]. These extra fermion zero modes can be lifted by a variety of effects, including orientifold projection [132], fluxes [148–150], overlapping gauge branes [151], etc.

Our work is however more focused on the structure of the operator $\mathcal{O}_{\text{charged}}$, due to charged fermion zero modes from the D2-D6 open string sectors, and which is present both for superpotentials or for higher F-terms.In the D2-D6$_a$ sector, there are I_{a,Π_3} net fermion zero modes in the fundamental or antifundamental representation of the 4d gauge factor $U(N_a)$, according to the sign of the topological intersection number $I_{a,\Pi_3}=[\Pi_a]\cdot[\Pi_3]$. Integration over these fermion zero modes typically leads to insertion of 4d charged chiral multiplets in the instanton amplitude [110–112], see [113,114] for reviews. Let us illustrate this in a simple example. Consider a type IIA compactification with two stacks of N D6-branes wrapping 3-cycles Π_a, Π_b and a D2-brane instanton wrapping a 3-cycle Π_3 such that the intersection numbers are $I_{a,\Pi_3}=1$, $I_{b,\Pi_3}=-1$, $I_{ab}=1$. The intersections between the D2-instanton and the D6-branes produce fermion zero modes λ_a in the $\square_a$, and $\tilde{\lambda}_b$ in the $\overline{\square}_b$. There is also a bi-fundamental chiral multiplet Φ_{ab} from strings stretching between the D6 stacks. These ingredients are coupled through a worldsheet instanton supported (and actually required for consistency, see section 4.2.2) in a disk bounded by these cycles, see Figure 4.1, contributing to the instanton worldvolume action as

$$S_{\text{z.m.}}\sim\lambda_a\Phi_{ab}\tilde{\lambda}_b \tag{4.2}$$

In this setup the amplitude of the D2-instantons contains a piece,

[1] Additional bosonic zero modes may also be present, but they are simply integrated over yielding some numerical prefactor.

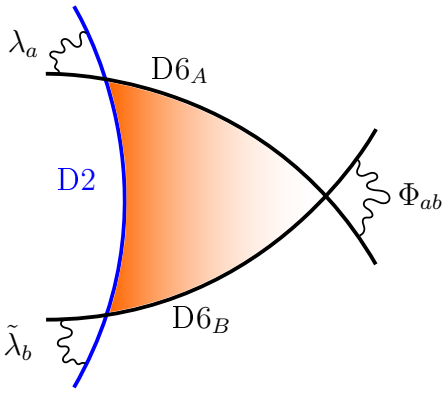

Figure 4.1: A D2-brane instanton intersects two D6-brane stacks. The fermion zero modes λ_a, $\tilde{\lambda}_b$ and bifundamental matter Φ_{ab} live at the intersections. There is a worldsheet instanton in the disk bounded by the cycles, shaded in orange.

$$\mathcal{O}_{\text{charged}} \sim \int \mathrm{d}\lambda_a \, \mathrm{d}\tilde{\lambda}_b \, e^{S_{z.m.}} = \det(\Phi_{ab}), \tag{4.3}$$

This operator breaks the anti-diagonal $U(1)$ subgroup of the group $U(N)_a \times U(N)_b$. In fact, this is the mechanism by which string theory manages to break perturbatively exact $U(1)$ global symmetries from gauge $U(1)$ made massive by Stuckelberg couplings [110–112].

As anticipated, the focus of this chapter is the derivation of $\mathcal{O}_{\text{charged}}$ in the description of D-brane instantons by backreacted geometries [115, 116, 152].

4.1.2 Backreacting instantons

As discussed in Section 3.2.2, the backreaction of the D-brane instanton is encoded in a modification of the exterior derivative of the quantities $\mathcal{Z}$ or $\mathcal{T}$, in type IIB or type IIA respectively. In this section we review this discussion adapting the basic points to D2-brane instantons in type IIA CY compactifications. Inclusion of D6-brane sectors and the corresponding fermion zero modes will provide new results in later sections.

Consider type IIA compactified on a CY $\mathbf{X}_6$, and an instanton given by a D2-brane wrapped on a 3-cycle Π_3. For convenience we consider its dual 3-cycle $\tilde{\Pi}_3$, and denote their Poincare dual classes by $\beta_3 = \delta_3(\Pi_3)$ and its dual $\tilde{\beta}_3 = \delta_3(\tilde{\Pi}_3)$.

The equation determining the backreaction effect of the D2-brane instanton is [115, 116]

$$d\mathcal{T}_2 = W_{\text{np}} \delta_3(\Pi_3) \tag{4.4}$$

where W_{np} is the non-perturbative superpotential. For clarity we reabsorb it into a suitable 2-form $\alpha_2 \sim \mathcal{T}_2$, and write

$$d\alpha_2 = \beta_3 \tag{4.5}$$

This equation encodes a change in the topology of the compactification manifold, see Figure 4.2. In particular, the fact that β_3 is exact implies that the 3-cycle Π_3 has become trivial, i.e. the boundary of a 4-chain which is associated to the non-closed form α_2. Conversely, the dual 3-form $\tilde{\beta}_3$ is now non-closed, i.e. it satisfies

$$d\tilde{\beta}_3 = \tilde{\alpha}_4 \tag{4.6}$$

for some $\tilde{\alpha}_4$, which is therefore exact. This implies that the dual 3-cycle $\tilde{\Pi}_3$, which had intersection number one with Π_3 has now become a 3-chain, whose boundary is some 2-cycle Σ_2, which morally corresponds to the exact form $\tilde{\alpha}_4 = \delta_4(\Sigma_2)$.

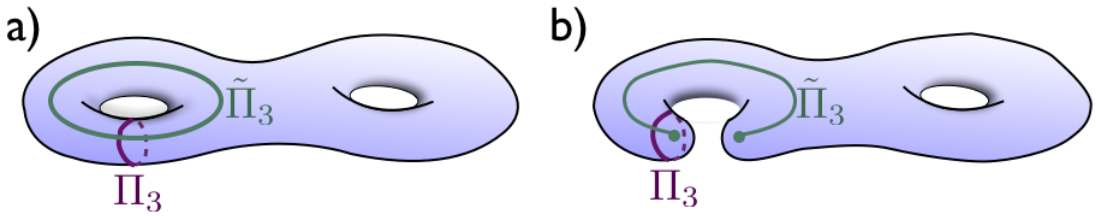

Figure 4.2: In a compactification (a) with a D2-brane instanton on a cycle Π_3, the instanton backreaction modifies the topology (b) such that Π_3 becomes homologically trivial, and its dual $\tilde{\Pi}_3$ turns into a 3-chain.

In the following section we initiate the discussion of the backreaction in the presence of additional ingredients, specifically gauge D-branes.

4.2 Backreacting flavoured instantons

The above description accounts for the generation of non-perturbative terms for isolated instantons. This is interesting for the question of moduli stabilization, as explained in [152]. However, many applications of D-brane instanton involve instantons which intersect non-trivially the sectors of D-branes giving rise to the 4d gauge group. Such instantons generate non-perturbative field theory operators involving 4d charged matter multiplets [110–112], (see [113, 114] for reviews), and have been proposed for the non-perturbative generation of several phenomenologically interesting field theory operators, as mentioned in the introduction.

In the remainder of this chapter we address the geometric description of such instantons in terms of their backreacted geometry. In this section we introduce the basic ingredients, and postpone concrete examples to the coming sections.

Consider a type IIA CY compactification, with stacks of N_a D6-branes wrapped on non-trivial 3-cycles Π_a. For simplicity we consider the theory without O6-planes, so that the RR tadpole condition is

$$\sum_a N_a[\Pi_a] = 0 \tag{4.7}$$

Models with O6-planes can be subsequently considered, but they will not imply any further complication (at least, as long as the O6-planes do not intersect the D2-brane instantons to be introduced shortly). We leave the discussion of O6-plane models for future work[2].

We recall from 4.1.1 that the gauge group of the theory is $\otimes_a U(N_a)$ and there are I_{ab} chiral fields in the bifundamentals $(\ \square_a,\ \overline{\square}_b)$, for all a, b. Here $I_{ab} = [\Pi_a] \cdot [\Pi_b]$

[2]Orientifold planes are also relevant to remove additional fermion zero modes and allow the instanton to generate non-perturbative superpotential terms. As explained before, we are interested just in the field theory operator structures, which are common to superpotential terms and to higher F-terms.

is the topological intersection number (i.e. weighted with ± 1 according to orientation) of the 3-cycles Π_a, Π_b. In supersymmetric intersections, these correspond to chiral multiplets; although compact models without O6-planes are necessarily non-supersymmetric, we keep the supersymmetric terminology in mind, since the ideas apply similarly when supersymmetric models are considered, either by the introduction of O6-planes or in the non-compact setups in later sections.

4.2.1 Brane recombination

Consider a D2-brane instanton wrapped on a non-trivial 3-cycle Π_3. The intersection of the D6-brane 3-cycles with Π_3 leads to fermion zero modes λ in the fundamental representation of the corresponding D6-brane gauge group for positively oriented intersections, and $\tilde{\lambda}$ in the antifundamental for intersections with negatively oriented intersections. Because of the condition (4.7), we obtain

$$\sum_a N_a \, I_{a,\Pi_3} \; = \; 0 \tag{4.8}$$

Namely, there are equal total numbers of fermion zero modes of type λ or $\tilde{\lambda}$ (counted with multiplicity given by the rank N of the corresponding D6-brane groups).

Consider for simplicity only two D6-branes on 3-cycles $[\Pi_+]$, $[\Pi_-]$, respectively, intersecting the D2-brane with $[\Pi_3] \cdot [\Pi_\pm] = \pm 1$. This means that $[\Pi_\pm]$ are essentially given by

$$[\Pi_\pm] \; = \; \pm [\tilde{\Pi}_3] \; + \; \ldots \tag{4.9}$$

where $[\tilde{\Pi}_3]$ is the 3-cycle dual to $[\Pi_3]$, and the dots indicate additional 3-cycle components not intersecting the D2-brane, and which behave as spectators in what follows.

In the backreacted geometry, the D2-brane 3-cycle becomes trivial $[\Pi_3] = 0$, and the dual 3-cycle becomes a chain, whose boundary is a new 2-cycle Σ_2 in the backreacted geometry, $\partial \tilde{\Pi}_3 = \Sigma_2$. Therefore $\partial \Pi_\pm = \pm \Sigma_2$ in homology. This implies that the D6-brane formerly wrapped on Π_+ is no longer consistent, and similarly for the D6-brane wrapped on Π_-; however, their recombination formally corresponds to the class $[\Pi_+] + [\Pi_-]$, which does not have intersection with $[\Pi_3]$, and therefore defines a consistent 3-cycle without boundaries in the backreacted geometry. The effect of the backreaction in the flavour D6-branes is therefore to trigger their recombination. This is depicted in Figure 4.3.

The lesson generalizes easily. Given a general set of N_a D6-branes on 3-cycles Π_a, any 3-cycle having non-zero intersection with Π_3 becomes a 3-chain with boundary $\partial \Pi_a = ([\Pi_a] \cdot [\Pi_3]) \, \Sigma_2$ in homology in the backreacted geometry. The condition (4.8), then implies that the different 3-chains can recombine into a 3-cycle (possibly with several components) without boundary. The effect of the instanton backreaction on the flavour D6-branes is to recombine them into sets defining consistent 3-cycles in the backreacted geometry.

In general, there may be several inequivalent topologically consistent ways to recombine the different D6-brane stacks. This will be discussed in section 4.2.3.

4.2.2 Saturation of charged fermion zero modes revisited

In the following we move on to the next question, namely the appearance of the charged chiral multiplet insertions in the instanton amplitude. In the open string per-

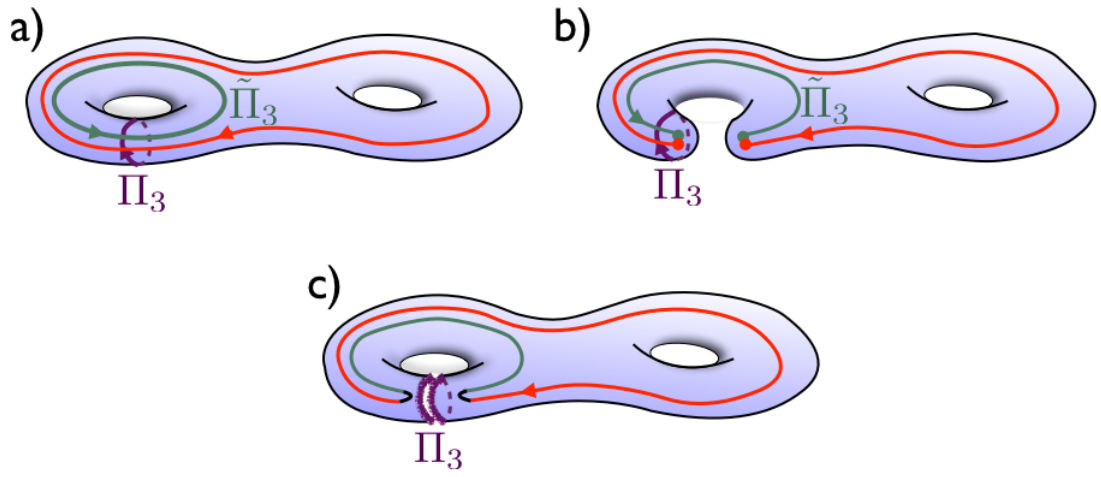

Figure 4.3: Consider (a) a D2-brane instanton on a cycle Π_3, in the presence of gauge D-branes wrapped on cycles (shown as green and red) intersecting Π_3 with opposite intersection numbers. After the instanton backreaction (b) making Π_3 trivial, the red and green cycles become chains, so the corresponding branes must recombine to wrap a consistent combined cycle. In (c) we display a different representation, obtained by excising a local neighbourhood around Π_3 in the original one; the backreacted geometry is obtained by contracting the left-over boundaries to a point.

spective of section 4.1.1, this arises from the saturation of fermion zero modes via couplings arising from worldsheet instantons. As these worldsheet instantons extend away from the instanton locus, we expect them to continue playing a role in the appearance of the field theory operator in the backreacted picture. Indeed we now show that the backreacted configuration necessarily contains euclidean fundamental strings producing the relevant charged field insertions.

For that purpose it is useful to develop a spacetime perspective on the appearance of worldsheet instantons in the presence of the D2-brane instanton. In string compactifications, we are used to think about worldsheet instantons as possible contributions over which one has to sum to obtain a complete quantum amplitude. Namely, we sum contributions from processes with one instanton, two instantons... or none. In other words, the worldsheet instantons may be present or not, and their number is arbitrary, or rather is a quantity over which we should sum. In the presence of a D2-brane instanton, on the other hand, the argument about saturating charged fermion zero modes implies that the presence of the D2-brane requires specific patterns of euclidean worldsheets to be simultaneously present.

There is a simple explanation for this from the spacetime perspective, which to our knowledge has not appeared in the literature. In short, the flux sourced by the presence of the D2-brane produces a Freed-Witten (FW) [3] anomaly on the D6-branes, which forces them to expel a semi-infinite euclidean worldsheet; similarly, the flux sourced by the D6-branes produces a FW anomaly on the D2-brane, forcing them to expel a semi-infinite euclidean worldsheet. Finally, when the D6-branes meet at the intersection point, the

[3] Despite the familiar name coined from the analysis in [153], one actually means the conditions for D-branes in presence of non-torsion NSNS or RR fluxes derived in [154, 155].

euclidean worldsheet can connect with an open string worldsheet escaping to infinity in the 4d spacetime.

In more detail, consider type IIA in flat 10d spacetime and a configuration of an infinite D6-brane along the directions 0123456 and an infinite D2-brane along the directions 789. This choice of directions leads to a non-supersymmetric intersection, but captures the essential topology which holds also in the supersymmetric case, as the interested reader can easily check.

The D6-brane is a source of RR 2-form field strength, with

$$dF_2 = \delta(x^{7,8,9})\, dx^7 dx^8 dx^9 \tag{4.10}$$

where we use the notation $\delta(x^{7,8,9}) = \delta(x^7)\delta(x^8)\delta(x^9)$. Let us consider the integrated flux $\int_{89} F_2$ and its change along the direction x^7. The above equation implies that it jumps from e.g. zero at $x^7 < 0$ to one flux unit at $x^7 > 0$. Since the D2-brane is wrapped on 789, at $x^7 > 0$ there is a non-trivial flux of F_2 over the D2-brane worldvolume. This leads to a Freed-Witten inconsistency, which must be solved by the emission of a semi-infinite fundamental string with worldsheet along a curve on the 89 plane and the semi-infinite direction $x^7 > 0$. This string should not be present at $x^7 < 0$, where no F_2 flux and so no FW anomaly is induced on the D2-brane. This is indeed the case because the worldsheet is forced to end on the D6-brane, by the converse FW effect. Namely, the D2-brane is a source of RR 6-form field strength, with

$$dF_6 = \delta(x^{0,1,2,3,4,5,6})\, dx^0 dx^1 dx^2 dx^3 dx^4 dx^5 dx^6 \tag{4.11}$$

We can argue as above using the flux integral of F_6 along 012356, which jumps as we move from $x^4 < 0$ to $x^4 > 0$, to obtain a FW anomaly forcing the D6-brane to expel a fundamental string with worldsheet along a curve in 012356 and $x^4 = 0$. The worldsheets emitted by the D2- and the D6-brane can nicely combine in a corner near the D2-D6 intersection point, see Figure 4.4. Finally, worldsheets ending on different D6-branes and approaching a D6-D6 intersection escape off to infinity, thus describing the insection of charged 4d matter fields.

This spacetime picture allows to provide a derivation of the structure of worldsheet instantons in the backreacted geometry. The key point is that the instanton backreaction produces not only a change in the geometry, but also produces a (sourceless) RR 6-form F_6 field string flux, which forces the (recombined) D6-branes to emit fundamental string worldsheets, which imply the emission of chiral multiplets supported at D6-brane intersections.

More concretely, in the original geometry the source equation for F_6 is

$$dF_6 = \delta_4(x)\, \delta_3(\Pi_3) \tag{4.12}$$

where $\delta_4(x)$ is a bump 4-form around the location of the instanton in 4d spacetime. Recalling the discussion following (4.4), in the backreacted geometry we have

$$F_6 = \delta_4(x)\, \delta_2(\Sigma_4) \tag{4.13}$$

where Σ_4 is the 4-cycle dual to the 2-cycle Σ_2 defined by $\partial\tilde{\Pi}_3 = \Sigma_2$. For any D6-brane wrapped on a 3-cycle Π intersecting Π_3 in the original geometry, $\Pi = \tilde{\Pi}_3 + \ldots$, and Π acquires a boundary Σ_2 in the backreacted geometry. Focusing on a local neighbourhood

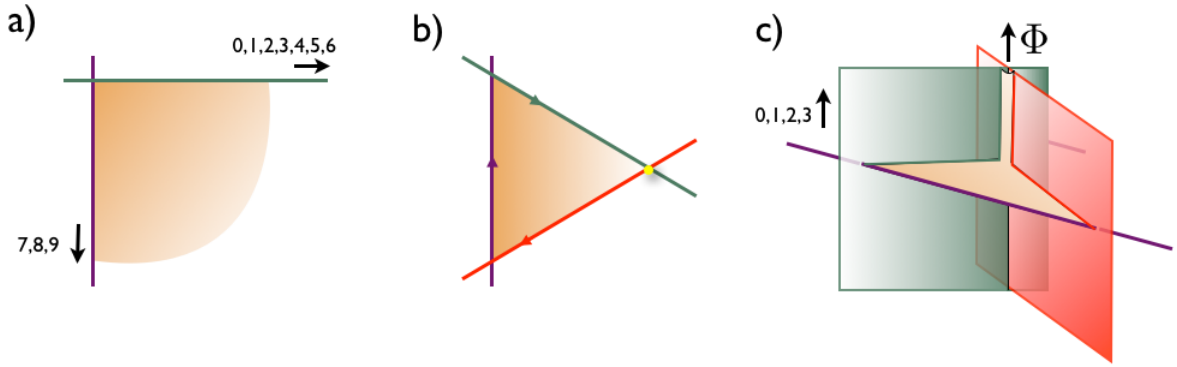

Figure 4.4: (a) Intersecting one D2-brane (violet) and one D6-brane (green) leads to FW anomalies enforcing the appearance of a fundamental string worldsheet bounded by the D2- and the D6-branes. (b) In a configuration of two intersecting D6-branes (red and green), each intersecting the D2-brane (violet), the emitted fundamental string defines a worldsheet instanton spanning the triangle defined by the branes in the internal space, exactly as in the open string argument of saturation of fermion zero modes. (c) Depicting the 4d spacetime dimensions, the boundaries of the fundamental string worldsheet must extend to infinity, implying the emission of the chiral multiplet Φ at the intersection of the D6-branes.

of this boundary, we have $\Pi = \Sigma_2 \times \mathbf{R}^+$. Integrating F_6 over the 4d spacetime times Σ_2 gives

$$\int_{M_4 \times \Sigma_2} F_6 = \int_{\Sigma_2} \delta_2(\Pi_4) = 1 \tag{4.14}$$

This shows that a D6-brane wrapped on Π has a FW anomaly, and must expel a fundamental string. The argument about the structure of worldsheet instantons and emission of charged chiral multiplets at D6-brane intersections follows as in the earlier open string description.

The fact that the D2-brane instanton intersecting the D6-branes is forced by FW to expel charged matter fields in open string sectors fits nicely with the M-theory description of such instantons. The D2-brane instanton lifts to an euclidean M2-brane wrapped on a 3-chain with boundaries; the existence of boundaries is the M-theory version of the FW inconsistency of the D2-brane, and closing the boundaries with M2-branes wrapped on certain 2-cycles is the M-theory version of the emission of massless open strings in type IIA.

4.2.3 Multiple intersections and non-abelian case

Configurations with multiple intersections can be discussed similarly. We sketch their description emphasizing the novel features that may arise.

In this section we consider certain novel features arising when the D2-brane is intersected by multiple D6-branes with intersection numbers $+1$ (and the same number with intersection number -1).

For simplicity we consider the abelian case, in which all the D6-branes intersecting the D2-brane instanton have $N = 1$, i.e. $U(1)$ gauge factor (for which the fundamental or antifundamental translate into ± 1 charges); we comment on the non-abelian case later on.

A preliminary remark is that by the FW arguments, each D6-brane crossing with the D2-brane leads to the emission/absorption of a fundamental string worldsheet, according to the orientation of the intersection. The fact that the number of intersections with positive and negative intersection are equal ensures that all such fundamental string worldsheets close onto each other providing consistent worldsheet instantons (leading to emission of an appropriate set of open string fields at D6-brane intersections). Thus in the presence of the D2-brane instanton, all such worldsheet instantons are necessarily present. In general, the geometry of the worldsheet instanton can lead to insertions of different numbers of charged multiplets. Given that each fundamental string involves two corners at D2-D6 intersections with opposite orientations, it is easy to convince oneself that, after the instanton backreaction and D6-brane recombination, the structure of worldsheet instantons required by the FW consistency conditions reproduces the saturation of fermion zero modes in the open string description.

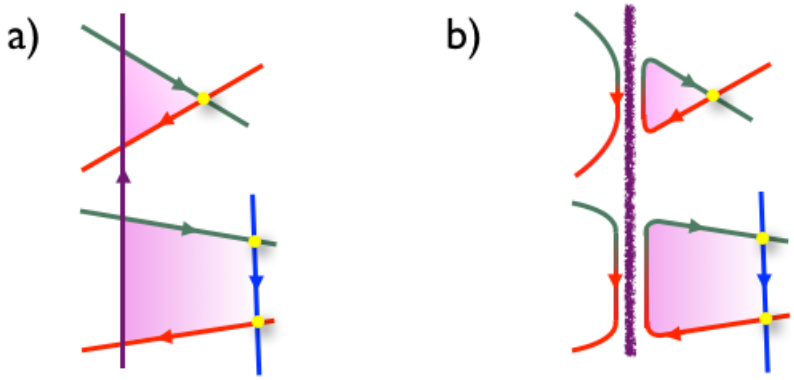

Figure 4.5: Graphical depiction of the worldsheets attached to an instanton process (a) in the open string picture and (b) in the backreacted geometry picture. In the latter, the two pieces of D-branes on both sides of the cut are actually connected on the whole 3-cycle.

For instance, consider the example in Figure 4.5(a). The configuration produces fermion zero modes λ_i, $\tilde{\lambda}_i$, for $i = 1, 2$, and the following couplings in the instanton worldvolume action

$$c_1\, \lambda_1 \Phi_1 \tilde{\lambda}_1 \, + \, c_2\, \lambda_2 \Phi_2 \Phi_3 \tilde{\lambda}_2 \tag{4.15}$$

where the coefficients c_1, c_2 encode the worldsheet instanton amplitude, and the remaining notation is hopefully clear. Saturating fermion zero modes leads to the field theory operator in the D2-brane instanton amplitude

$$(\Phi_1)\,(\Phi_2 \Phi_3) \tag{4.16}$$

Here and in what follows, we introduce the parentheses notation. It is irrelevant in the present abelian case, but is used as a reminder of the index structure relevant in the non-

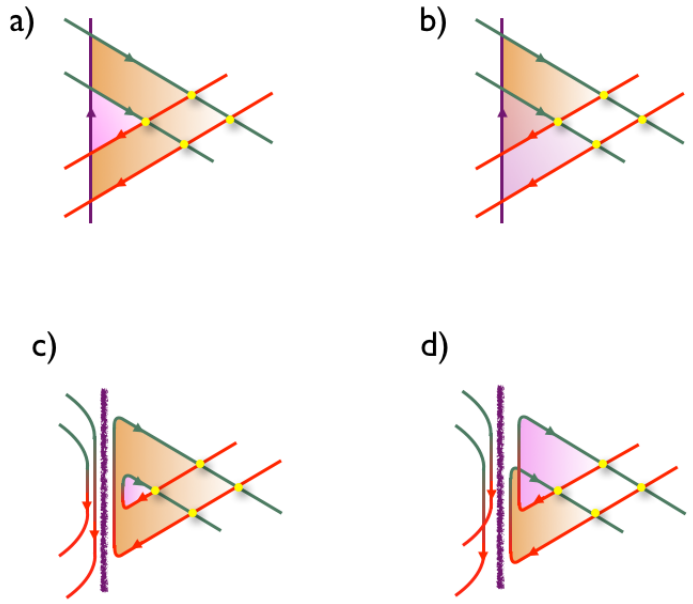

Figure 4.6: D2-brane instanton in the presence of D6-branes, in which the charged fermion zero modes can be saturated in two inequivalent ways, shown as shaded triangles in figures (a) and (b). In the instanton backreaction picture they are described by two possible ways to recombine the D6-branes, sketched in figures (c) and (d). In the latter, the two pieces of D-branes on both sides of the cut are actually connected on the whole 3-cycle.

abelian case (e.g if each D6-brane is promoted to a stack, the field theory operator has the structure $\det \Phi_1 \det(\Phi_2\Phi_3)$, with color index contraction in the operator $\Phi_2\Phi_3$).

The same result is recovered in the backreacted geometry. The operator (4.16) arises from standard worldsheet instanton amplitude, taking into account that the FW consistency due to the flux in the backreacted configuration demands the simultaneous presence of worldsheet instantons on all (recombined) D6-branes. One novelty is the possibility of several inequivalent ways of recombining branes. Consider for instance the example in Figure 4.6. In the open string description, the fermion zero mode couplings on the D2-brane worldvolume action are

$$(\lambda_1, \lambda_2) \begin{pmatrix} \Phi_1 & \Phi_2 \\ \Phi_3 & \Phi_4 \end{pmatrix} \begin{pmatrix} \tilde{\lambda}_1 \\ \tilde{\lambda}_2 \end{pmatrix} \tag{4.17}$$

where we omit the coefficients, and where the notation is hopefully clear. There are two different ways to saturate the fermion zero modes, which are depicted in Figures 4.6 (a) and (b). The resulting field theory operator in the D2-brane instanton amplitude is

$$(\Phi_1)(\Phi_4) - (\Phi_2)(\Phi_3) \tag{4.18}$$

In the backreaction picture, the appearance of two possible terms arises because, in the backreacted geometry there are two inequivalent ways to recombine the flavour D6-branes, so we should sum over both possibilities. Therefore the complete amplitude is a sum over different geometric configurations of D6-branes. On top of the relative coefficients for each amplitude (which we recall have been omitted above), a proper explanation of the relative

sign between the two contributions would require further microscopic understanding about the sum over such geometries. We leave this as an open question, and simply learn the thumb rule that the D6-brane boundaries behave as Grassman objects, such that their exchange in recombination processes leads to extra signs. The generalization to larger numbers of intersections is straightforward.

The above local picture of the recombination of two pairs of half D6-branes is the basic ingredient in other global configurations. For instance, the two incoming half D6-branes may actually belong to the same D6-brane stack, which thus has intersection number 2 with the D2-brane. The above analysis therefore provides the description of setups with multiple intersection numbers.

Also, it encodes the description of the non-abelian case. For instance, consider the configuration when the two incoming D6-branes are coincident and so are the two outgoing D6-branes. We have two $U(2)$ stacks of D6-branes intersecting the D2-brane with intersection number ± 1 respectively. Each pair of fermion zero modes forms a doublet under the corresponding $U(2)$, and the four different charged chiral multiplets $\Phi_1, \ldots, \Phi_4$ form a bi-fundamental Φ_{ab}. The matrix structure in (4.17) encapsulates the $U(2)^2$ indices, and (taking into account that the coefficients of the worldsheet instantons are equal for coincident branes) the expression (4.18) becomes $\det(\Phi_{ab})$. The above argument instructs us that, in the geometric description by the instanton backreaction, the non-abelian case requires a sum over possible recombination patterns, weighted by the relative sign upon exchange of boundaries.

We put these ideas to work in a large class of explicit models in the next section.

4.3 Instanton backreaction and geometric transitions in the mirror

In this section we present a large number of explicit examples of the above ideas, in the setup of local models related to systems of D3-branes at toric singularities, or rather, their type IIA mirror duals. The set of supersymmetric D-branes, the structure of the chiral multiplets in open string sectors, and the worldsheet superpotential couplings are nicely encoded in a graph, the dimer diagram, reviewed in Section 2.4.1. The same diagram can be used to encode the set of fermion zero modes and the instanton worldvolume couplings on D-brane instantons. Moreover, there is a systematic way to construct the type IIA mirror in which we recover a picture of D6-branes and D2-brane instantons, in which we can flesh out the proposal of instanton backreaction in the previous sections. The reader may use Section 2.4 as a handy reference for the dimer diagrams, the mirror and their combinatorial properties.

4.3.1 Instantons at singularities and dimer diagrams

Dimer diagrams are extraordinary tools to characterize the holomorphic properties of supersymmetric D-branes in local toric CY threefolds, and even closely related non-toric geometries. A particular example of the latter is the description of geometric transitions by complex deformations in [43, 44], which we revisit in Section 4.4.

Dimer diagrams can be exploited to describe systems of D-brane instantons in configurations with gauge D-branes. As already noticed in e.g. [33] (see also [144] for related analysis in orbifold singularities), the dimer diagram diagram encodes the content of instanton charged fermion zero modes and their couplings to the 4d chiral multiplets in the gauge D-branes[4]. In short, instantons are associated to faces in the dimer, whose edges correspond to fermion zero modes charged under neighbouring objects, and nodes involving those edges describe the fermion zero mode couplings. This picture again becomes more physical in the mirror configuration: as the gauge D-branes in the dimer turn into D6-branes wrapped on 3-cycles (characterized in terms of 1-cycles in the mirror Riemann surface Σ), the D-brane instantons turn into D2-branes wrapped on the 3-cycles associated to the corresponding faces (and defined in terms of 1-cycles in Σ). Disks defining worldsheet instantons bounded by D6- and D2-branes now define fermion zero mode couplings, while those bounded by D6-branes only still define superpotential terms. The open string description of the system is thus encoded in a set of gauge and instanton 1-cycles on Σ.

In this section, we take one further step and describe the backreaction of these D2-brane instantons, in terms of simple graph operations in the mirror picture. This provides a fairly explicit description of the system after the backreaction, as described in previous sections. In particular, including the explicit D6-brane recombination, and the appearance of the 4d superpotential in terms of purely worldsheet instanton effects in the backreacted geometry. The results nicely agree with the open string analysis, as we show in several explicit examples.

Before describing the detailed recipe and the examples, we would like to note certain points:

• We are considering non-compact intersecting D6-brane systems [160], in which cancellation of charges whose fluxlines can escape to infinity should not be required. However, one should still impose cancellation of RR tadpoles in local homolog; this amounts to requiring that the total homology class of the gauge D-branes should have zero intersection with any compact 3-cycle in the geometry. As is familiar, the condition is equivalent to the cancellation of gauge anomalies for all nodes in the quiver, including the empty ones. For nodes actually occupied by instantons, this condition corresponds to matching the number of fermion zero modes of type λ with the number of those of type $\tilde{\lambda}$, as in the compact case.

• Since we have no orientifold planes, there are additional neutral fermion zero modes and the instantons in general do not contribute to the superpotential. We are however focusing our attention to the generation of charged field theory operators, which occurs even for instantons that generate higher F-terms. In any event, the lessons learnt in this case will apply in any setup in which the extra fermion zero modes are absent, either by removal by orientifold projection, or by other lifting mechanisms.

• For simplicity we consider the case where there are no gauge D-branes on top of the cycle wrapped by the D-brane instantons. Similar conclusions hold in the alternative case, in which the D-brane instantons are related to gauge instantons. One particular instance is related to the discussion of complex deformations in section 4.4, where the D2-brane instantons whose backreaction produces a complex deformation of the geometry are of the same kind as the gauge instantons on deformation fractional branes in the sense of [31,43].

[4] See also e.g. [156–159] for physics of D-brane instantons in systems of branes at singularities in a variety of contexts.

We start our analysis with compact D2-brane instantons, in the presence of compact D6-branes. The analysis with non-compact D6-branes (mirror to D7-branes) is similar and we do not include it explicitly in the present work. Finally we discuss non-compact D2-brane instantons (mirror to non-compact D3-brane instantons).

4.3.2 The recipe for backreaction

In this section we present our prescription to find the geometry after the backreaction of an instanton placed in a dimer model. As described above, the configuration is encoded in a tiling of the mirror Riemann surface Σ, whose zig-zag paths (i.e. faces in the original dimer diagram) correspond to either D2-brane instantons or gauge D6-branes.

For simplicity, we consider starting with the case of a single instanton, namely one 1-cycle, which defines the instanton 3-cycle Π_3. We also consider the abelian case, and introduce precisely one D6-brane in the remaining cycles. The backreacted configuration can be generated with very simple steps on this graph:

- **Step 1. Cut:** Since the 3-cycle Π_3 wrapped by the instanton should disappear from the geometry, we cut Σ by removing a small string around the instanton 1-cycle. After cutting off the strip, each of the two boundaries of Σ should be identified to a point. Any 1-cycle intersecting the cut is split, and turns into a chain with boundary points, weighted by signs according to the orientation of the original intersection; this reproduces the fact that any 3-cycle intersecting Π_3 turns into a 3-chain in the backreacted geometry. These 1-chains will be glued in the next step.

- **Step 2. Recombine:** Since Π_3 is compact in the original geometry, there is an equal number of positive and negative orientation intersections with the whole set of D6-branes. At the level of Σ, this implies that on each side of the cut, there is an equal number of incoming and outgoing 1-chains. The recipe amounts to matching opposite orientation pieces to define recombined 1-cycles. Most importantly, the recombination should be carried out without crossing edges of the underlying tiling of Σ, see examples later on. Remarkably, such matchings are unambiguous as a consequence of the bipartite nature of the dimer diagram, as manifest in the examples below.

- **Step 3. Field theory operators:** The above two steps already define the backreacted geometry. This last step merely establishes that the 4d non-perturbative field theory operator induced by the original D2-brane instanton is easily readable as a worldsheet instanton in the backreacted geometry, bounded by the recombined D6-branes. These are easily found by picking out disks bounded by recombined 1-cycles (and the cut, which recall is regarded as shrunk to a point); the coupling involves the chiral multiplets associated to possible D6-brane intersections still present after recombination.

The general structure of the process is shown in Figure 4.7 for an instanton on a $2k$-sided face of the dimer. Similar recipes apply to the case of multiple instantons, see Section 4.3.5. A similar recipe can be found directly on the dimer diagram, see Section 5.1.

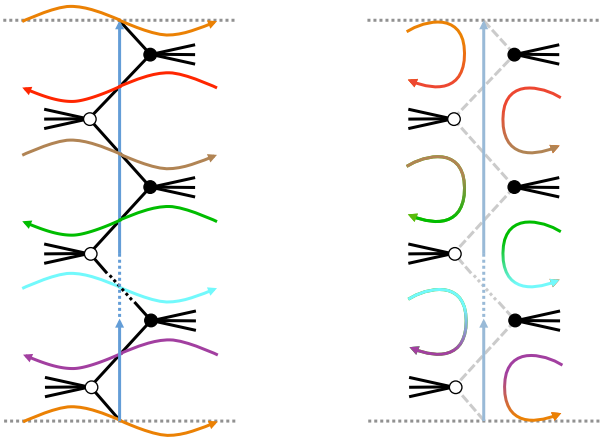

Figure 4.7: Left: Local piece of the mirror Riemann surface around the 1-cycle wrapped by a D2-brane instanton (blue), consisting of $2k$ edges. The top and bottom dotted lines are identified. The collections of half edges sticking out of each node represent general superpotential couplings. The orange, brown and cyan, and the red, green and purple arrowed lines are pieces of additional zig-zag paths that correspond to D6-branes intersecting the D2-brane instanton, with positive or negative intersection numbers, respectively. **Right:** The D2-brane instanton has backreacted, so the blue line has disappeared. D6-brane paths have been cut at their intersection with the former D2-brane instanton cycle, and recombined. The black nodes and the white nodes should be regarded as recombined into a single black and a single white node, respectively.

4.3.3 Explicit examples

We now turn to consider several examples of D-brane instanton backreactions. We point out that they can be classified in two broad classes.

• The first corresponds to cases in which the resulting geometric transition is (the mirror of) the complex deformation of the initial toric singularity. This occurs precisely when the D-brane instanton wraps the same nodes as the deformation fractional branes in the sense of [31, 43], namely the fractional branes triggering duality cascades ending in smooth complex deformed geometries, generalizing the Klebanov-Strassler throat [28]. The complex deformations are associated to splittings of the web diagram into subwebs in equilibrium (i.e. whose external legs have (p, q) labels adding up to zero); therefore, the 1-cycle defined by the instantons (or deformation fractional branes) are homologically trivial in Σ, which ends up split in several components.

• The second class correspond to the more generic situation in which the backreacted geometry does not correspond to a complex deformation of the original configuration. Nevertheless, the proposed recipe to obtain the backreacted geometry applies to more general cases, as we show in explicit examples as well. In these cases, the 1-cycle corresponding to the instanton surrounds a set of punctures corresponding to web diagram external legs whose (p, q) labels do not add up to zero; in these circumstances the topology does not admit a consistent split, which signals that the 1-cycle is homologically non-trivial in Σ. This agrees with the fact that there is no complex deformation associated to the backreaction. An implication is that the resulting geometries are non-CY (since in the IIB language we are growing 3-cycles despite the absence of CY complex deformation). We recall that this poses no problem with supersymmetry, since the framework is that of generalized geomet-

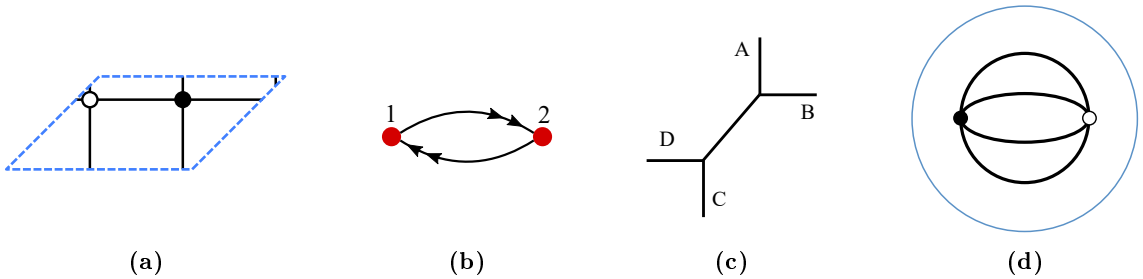

(a) (b) (c) (d)

Figure 4.8: Conifold diagrams. a) The dimer diagram, b) the quiver diagram, c) the web diagram and d) the mirror Riemann surface Σ, is a sphere with 4 punctures, which we depict as a complex plane (with the point at infinity added).

ries, as described in section 4.1.2. We will revisit these theories in Chapter 5 and see that they actually have a higher dimensional Calabi-Yau as moduli space. They are actually described by BFTs.

4.3.3.1 The conifold

We now describe a simple example, which illustrates mainly steps 1 and 2. Consider a system of D-branes at a conifold singularity. In Figures 4.8a, 4.8b, 4.8c and 4.8d we display the dimer diagram, the quiver diagram, the web diagram and the mirror Riemann surface, a sphere with four punctures, respectively. As explained, the cycles corresponding to the two nodes of the quiver (faces of the dimer diagram) are given by zig-zag paths of the tiling of Σ, as shown in blue and red in Figure 4.9a.

Let us put one D6-brane in the red 1-cycle (abusing language, as it actually denotes a 3-cycle) and a D2-brane instanton on the blue 1-cycle. In the open string description, the arrows in the quiver (edges in the dimer) correspond to two fermion zero modes of type λ and two $\tilde{\lambda}$, with quartic couplings (essentially, as in the conifold superpotential), which allow to saturate them. The instanton amplitude therefore reduces to the instanton exponential, with no field theory operator (as expected, since there are no charged chiral multiplets in the theory). Let us turn to the description of the system in terms of the instanton backreaction, and let us describe it using our recipe for the Riemann surface picture. According to step 1, we cut the sphere along the blue line, splitting the red 1-cycle at four points (two with each orientation). We recombine such pieces according to step 2, resulting in the picture in Figure 4.9b.

Concerning step 3, there are two worldsheet instantons, which are obtained by certain recombination of the original disks. They however do not involve any chiral multiplets (as there is none left). This is actually the required result, since the non-perturbative contribution by the original D-brane instanton should include no field-theoretical operator, just the instanton exponential.

In Figure 4.9d we see that, in fact, the deformed geometry corresponds to the complex deformation of the conifold [28], agreeing with the fact that the two punctures in each daughter Riemann surface correspond to sub-webs in equilibrium [43]. In the next section we will see that this is only the case whenever the D-brane instantons introduced match the corresponding fractional brane triggering the complex deformation. In other cases, the backreacted geometry does not correspond to a CY deformation.

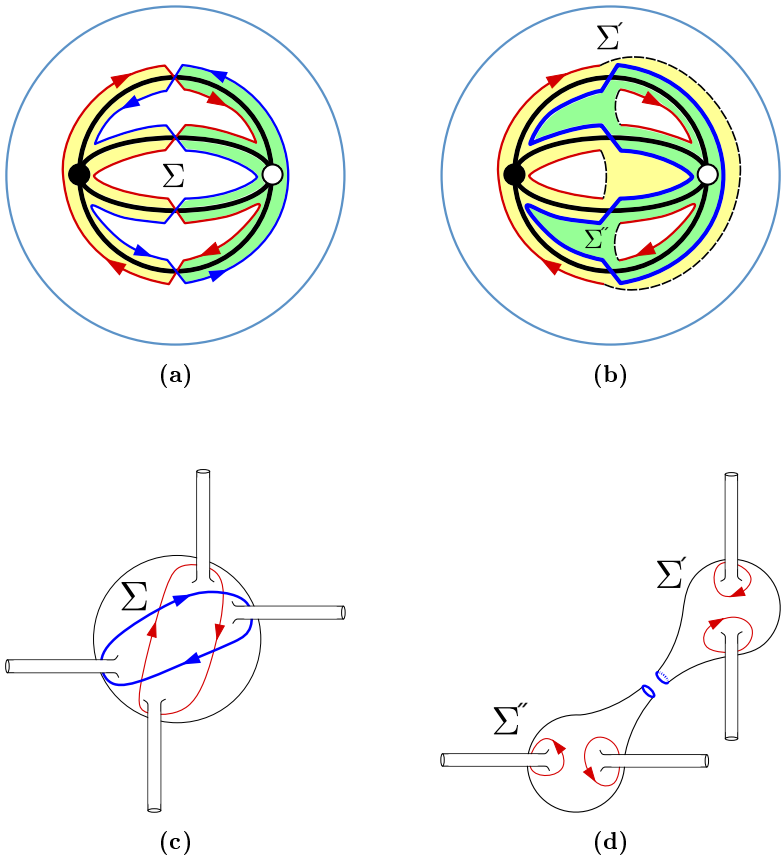

Figure 4.9: Instanton backreaction on a conifold. a) Σ and its zig-zag paths. The red one is wrapped by a D6-brane and the blue one by a D2-brane instanton. b) the Riemann surface is cut along the blue strip wrapped by the D2-brane instanton, cutting the red 1-cycle at four points; the corresponding open endpoints are duly recombined to form four recombined 1-cycles, each surrounding a puncture. c) and d) provide alternative graphical views of the process. Disks supporting Worldsheet instantons generating superpotential terms are shaded in light colors.

Finally let us mention one feature of our recipe. Since it is based on the graphical properties of the tiling of the mirror Riemann surface, with all 1-cycles present, the recipe provides an accurate description of instantons in the presence of D-branes in all nodes (at least, all nodes other than those occupied by the instanton). This will become more clear in richer examples in the next sections.

4.3.3.2 Double Conifold

Let us now turn to a slightly more involved example, to illustrate in more detail step 3, since we will obtain a non-trivial superpotential. Consider a system of branes in a double conifold singularity. The dimer diagram, quiver diagram, web diagram and mirror Riemann surface are shown in Figures 4.10a, 4.10b, 4.10c, 4.10d, respectively. The four cycles in Σ corresponding to the quiver nodes are shown in Figure 4.11b. Let us put 3 D6-branes, one in each cycle but the blue one, and a D2-brane instanton in the blue cycle. The bifundamental matter fields charged under the "would-be-D6-brane" of node 1 become now fermion zero modes $\lambda_{12}, \lambda_{13}, \tilde{\lambda}_{21}, \tilde{\lambda}_{31}$, see Figure 4.11a. These have couplings given by the worldsheet instantons stretching from the D2-instanton to the D6s. As shown in

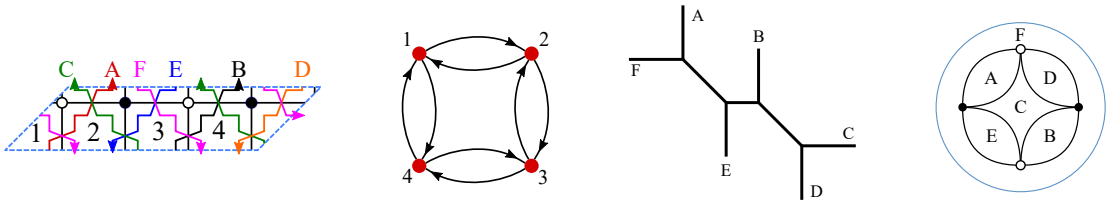

(a) (b) (c) (d)

Figure 4.10: Diagrams for the double conifold, a) shows the dimer diagram, b) the quiver diagram, c) the web diagram and d) the mirror Riemann surface Σ as a complex plane with the point at infinity added.

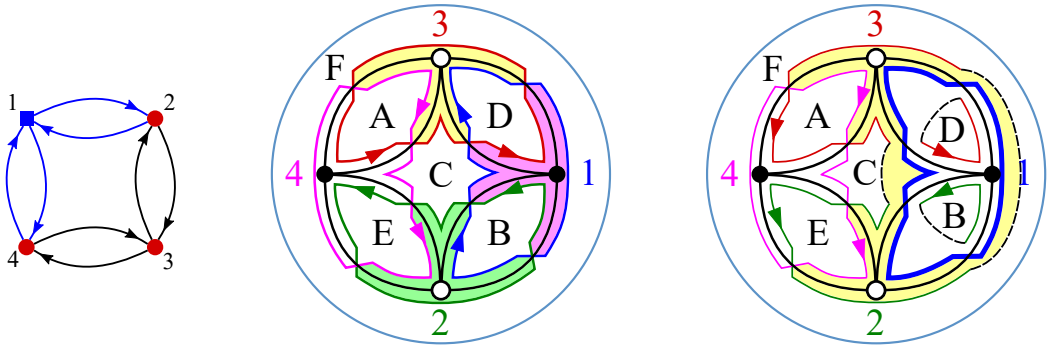

(a) (b) (c)

Figure 4.11: Double conifold backreaction. a) Quiver diagram with a D-brane instanton in node 1 (blue square) and gauge D-branes on the remaining nodes (red circles); blue arrows denote instanton charged fermion zero modes, while black arrows denote 4d charged chiral multiplets. Figure b) shows Σ before the backreaction, where the D-brane instanton (resp. gauge D-branes) is the blue (resp. red) zig-zag path and there are three worldsheet instantons shaded in light colors. In c) Σ after the backreaction is shown. The D-brane instanton has torn Σ apart and the gauge D-branes have recombined.

Figure 4.11b, these couplings are :

$$\sim \lambda_{13} X_{34} X_{43} \tilde{\lambda}_{31} + \lambda_{12} X_{24} X_{42} \tilde{\lambda}_{21}, \tag{4.19}$$

where the $\sim$ indicates that we are omitting coefficients for these couplings.

These couplings can be used to saturate the zero modes, and there is only one way of doing so, yielding the following 4d non-perturbative field theory operator,

$$\mathcal{O}_{\text{charged}} \sim (X_{34} X_{43})(X_{24} X_{42}) \tag{4.20}$$

where recall, that parenthesis indicate determinants when promoting to the non-abelian case.

Let us now consider the description of the instanton in the backreaction picture. According to **step 1** of our recipe, the cycle wrapped by the instanton shrinks to a point. This splits Σ into two pieces and breaks the D6-brane 1-cycles. In **step 2**, the latter are recombined, as shown in Figure 4.11c. Finally, **step 3** instructs us to use worldsheet instantons on disks in the backreacted geometry, shaded in Figure 4.11, to obtain the 4d field theory operator, which indeed reproduces (4.20).

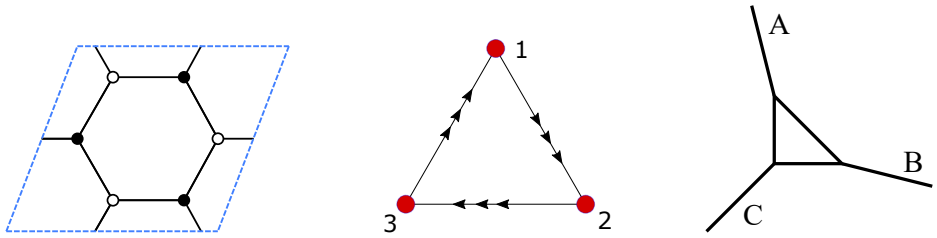

Figure 4.12: Diagrams for dP0 singularity, a) shows the dimer diagram, b) the quiver diagram and c) the web diagram. The mirror riemann surface tiling Σ coincides with the dimer diagram.

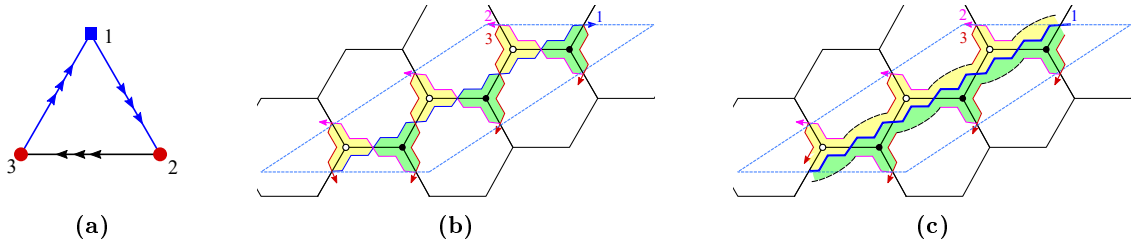

Figure 4.13: dP0 backreaction. a) The quiver diagram with a D-brane instanton in node 1. Blue arrows denote fermion zero modes. b) Shows Σ before the backreaction, where the D-brane instanton is the blue zig-zag path and there are two WS instantons shaded in light colors. In c) Σ after the backreaction is shown. The D-instanton has dissapeared from Σ and the branes have recombined. Two WS instantons remain.

Incidentally, we note that the remaining geometry is just the conifold. Indeed this coincides with the removal of punctures D and B, which corresponds to a subweb in equilibrium and, thus, to a complex deformation. This agrees with the fact that node 1, in which the instanton sits, actually corresponds to a deformation fractional brane in the sense of [31, 43], as reviewed in Section 2.5. We further develop this issue in section 4.4.

4.3.3.3 A dP_0 example

So far all examples have secretly been related to complex deformations, in that the instanton occupies the node of deformation fractional branes, in the sense of [31, 43] (namely, the total 1-cycle class surrounds the punctures associated to a subweb in equilibrium in the web diagram), as we discuss in more detail in Section 4.4. However, our recipe applies to arbitrary instantons, and to illustrate this more generic situation, we now study the case of the $\mathbf{C}^3/\mathbf{Z}_3$ orbifold, also known as the dP_0 quiver theory. The dimer diagram of this theory, its quiver diagram and its web diagram are shown in Figure 4.12. Consider putting one D6-brane in each of the dimer diagram faces 2 and 3, and a D-brane instanton in 1. The quiver diagram is shown in Figure 4.13a, while the mirror picture is depicted in Figure 4.13b. There are charged fermion zero modes $\lambda^i_{12}, \tilde{\lambda}^i_{31}$, $i = 1, 2, 3$, with couplings

$$\sim \epsilon_{ijk}\, \lambda^i_{12}\, X^j_{23}\, \tilde{\lambda}^k_{31}, \quad i, j, k = 1, 2, 3 \tag{4.21}$$

The resulting field theory operator has the structure $\mathcal{O}_{\text{charged}} = (X^1_{23})(X^2_{23})(X^3_{23})$.

Let us now turn to the backreaction description. Note that we have chosen a basis for the unit cell that shows the instanton cycle and worldsheet instantons more easily.

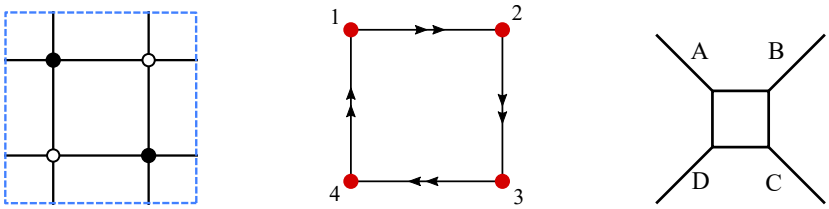

Figure 4.14: Diagrams for F0 singularity, a) shows the unit cell of the dimer diagram, b) the quiver diagram and c) the web diagram. The mirror Riemann surface tiling Σ coincides with the dimer diagram.

Applying steps 1 and 2 one finds that the Riemann surface tiling after the backreaction looks as shown in Figure 4.13c. Unlike in the previous examples, the surface is not split, but merely changed by decreasing its genus by 1, in a fashion similar to Figure 4.3. This is a general feature in backreaction of instantons not associated to complex deformations, as explained in Section 4.4.

Concerning step 3, as the branes recombine, the sets of three original worldsheet instantons of each kind merge to one, thus giving rise to the following operator,

$$\mathcal{O}_{\text{charged}} \sim (X^1_{23})(X^2_{23})(X^3_{23}), \tag{4.22}$$

which indeed coincides with the superpotential obtained by saturating the fermion zero modes of the D-brane instanton. Again, the D-brane instanton disappears but the geometry and the worldsheet instantons reproduce the same field theory operator.

4.3.3.4 An F_0 example

Let us give one further simple example, based on D-branes at a complex cone over F_0. In Figure 4.14 we provide the dimer diagram for the F_0 theory, together with the quiver diagram and the web diagram. Incidentally, the tiling of the mirror Riemann surface coincides with the dimer diagram[5]. From the web diagram one sees that this geometry admits a complex deformation by the removal of the legs A and C, which form a subweb in equilibrium. As we will see in the next section, to reproduce this complex deformation, which implies the removal of two faces in Σ, two instantons are needed.

Let us instead study the system with a single D-brane instanton in node 1, and one gauge D-brane in each of the nodes 2, 3 and 4. The quiver diagram for this configuration is shown in Figure 4.15a. There are four chiral matter multiplets and 4 fermion zero modes $\lambda^i_{12}, \tilde{\lambda}^i_{41}$, $i = 1, 2$ that are saturated using, as usual, the couplings from the worldsheet instantons, see Figure 4.15b,

$$\sim \epsilon_{ij}\epsilon_{kl}\lambda^i_{12}X^k_{23}X^j_{34}\tilde{\lambda}^l_{41}. \tag{4.23}$$

The resulting field theory operator has the structure

$$\mathcal{O}_{\text{charged}} \sim (X^1_{23}X^1_{34})(X^2_{23}X^2_{34}) - (X^1_{23}X^2_{34})(X^2_{23}X^1_{34}) \tag{4.24}$$

[5]This particular theory is special in that the mirror is identical to the original dimer, see e.g. [32] While this behavior is not generic, it is certainly common for simple toric phases (namely those with the smallest number of chiral fields) for geometries for which Σ is a punctured 2-torus, i.e. when the toric diagram has a single internal point. We expect the original dimer and the tiling of the mirror are not confused and that the distinction between them becomes clear from the context.

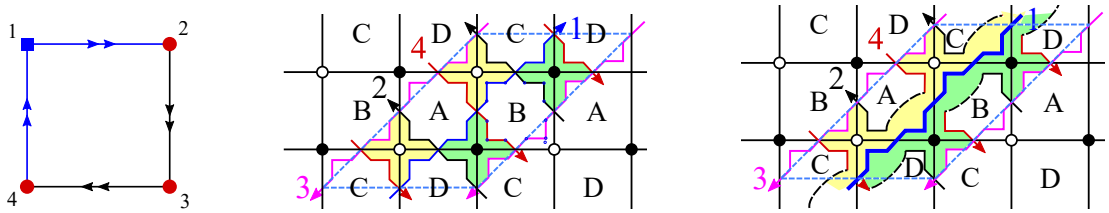

Figure 4.15: F0 backreaction with a single instanton. a) The quiver diagram with a D-brane instanton in node 1. Blue arrows denote fermion zero modes. b) Shows Σ before the backreaction, where the D-brane instanton is the blue zig-zag path and there are two WS instantons shaded in light colors. In c) Σ after the backreaction is shown. The D-instanton has dissapeared from Σ and the branes have recombined. Two WS instantons remain.

with, as usual, parenthesis denoting determinants when promoting to the non-abelian case. Let us now turn to the description from the backreaction perspective. Following steps 1 and 2, the Riemann surface Σ is cut, and the gauge D-brane 1-cycle recombine as shown in Figure 4.15c. Finally, step 3 tells us that the field theory operator can be read off from the remaining worldsheet instantons, which give a contribution in agreement with Section 4.3.3.4. Notice that the complete amplitude contains the sum over two worldsheet instantons, located on either side of the instanton line, which differ in orientation (hence the relative sign) and in the pairing of fields by recombination bridges (hence the change in parenthesis structures). Fields living in intersections connected by a brane, rather than a recombined brane (black dashed line), yield a determinant in the non-abelian case (arising from a sum over recombination possibilities, as discussed in Section 4.2.3).

Note that, like in the dP_0 case, the backreaction has not split Σ in two, but rather reduced its genus, in agreement with our earlier spoiler about instantons not describing complex deformations, see 4.4 for additional details and Chapter 5 for a general discussion.

4.3.4 Non-compact instantons

Let us make one small aside to point out that the description provided can be exploited also for instantons wrapped on non-compact cycles, namely D3-brane instantons on non-compact 4-cycles passing through the singular point in the type IIB picture [161]. Following [35] in the type IIA mirror, we have D2-brane instantons on non-compact 3-cycles, which on the mirror Riemann surface, correspond to 1-cycles stretching between two punctures. As discussed in the references, there is one such non-compact cycle for each bi-fundamental chiral multiplet X_{ab} in the gauge theory, such that the $D2_a$-D6 and D6-$D2_b$ open string sectors give fermion zero modes λ_a and $\tilde{\lambda}_b$, with couplings

$$\lambda_a X_{ab} \tilde{\lambda}_b \tag{4.25}$$

This arises from worldsheet instantons, see Figure 4.16a. Integration over these fermion zero modes gives 4d field theory operators with the structure $\det(X_{ab})$. This structure is easily reproduced in terms of the backreaction picture, by the same steps as in earlier sections: The Riemann surface is cut along the (non-compact) D2-brane instanton 1-cycle, and the D6-brane 1-cycles are duly recombined, and define the necessary worldsheet instantons to produce the field theory operators. The result is shown in Figure 4.16b

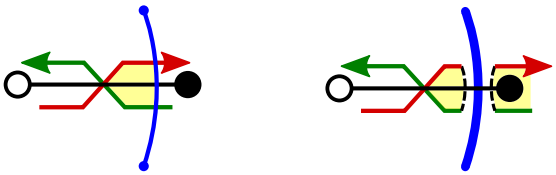

Figure 4.16: Backreaction of a non-compact instanton. In a) two zig-zag paths corresonding to branes are shown in red and green, with a non-compact D2-brane instanton in blue. In b) the instanton has backreacted and the branes recombined; worldsheet instantons are shown shaded in yellow.

4.3.5 Multiple instantons

All the examples given in the previous section correspond to systems with the D-brane instanton in a single node. In this section we consider the more general possibility of effects of multiple instantons occupying several nodes in the quiver diagram.

To be precise, we consider the effects of the simultaneous presence of various instantons; this can be regarded as the effect of an instanton on the combined class, but it is better described as a multi-instanton effect, in the sense of [121, 162]. We will show that, although the system contains novel features in the open string description, like the presence of fermion zero modes stretching between pairs of instantons, the final result is nicely captured by the backreaction picture using the same recipe as in earlier examples.

The novel features in the open string description are the appearance of sectors of open string with both endpoints on the D2-brane instantons, which yield zero modes of the multi-instanton configuration. In these sectors, the 4d Minkowski dimensions yield NN boundary conditions, while the compactification space dimensions are similar to intersecting D6-branes (to which they are related by nominal T-duality along the 4d Minkowski directions). There is one complex bosonic zero mode, and two real fermion zero modes, all in the bi-fundamental of the worldvolume groups on the D2-brane instantons. This is the equivalent to a 4d $\mathcal{N}=1$ chiral multiplet (namely, that in the T-dual D6-brane system). The couplings of this chiral multiplet of zero modes to the standard charged fermion zero modes and the actual 4d chiral multiplet can be read from the dimer diagram (or worldsheet instantons in the mirror Riemann surface), see later for explicit examples.

Finally, recall that the instanton amplitude is obtained upon integration over fermion zero modes (both in D2-D6 and D2-D2 sectors) and over bosonic zero modes. Integration over bosonic zero modes in the D2-D2 sectors effectively drags us into regimes in which the instantons are bound and act as a recombined D2-brane. This will be nicely recovered in the backreacted picture, to be discussed next.

4.3.5.1 An F_0 example

Consider the F_0 theory of Section 4.3.3.4, with instantons in the quiver nodes 1 and 2, as shown in Figure 4.17a, with charged fermion zero modes $\lambda^i_{23}, \tilde{\lambda}^i_{41}$ $i=1,2$, a chiral multiplet worth of D2-D2 zero modes Φ^i_{12} and 4d chiral multiplets X^i_{34}.

The couplings among these fields are

$$\sim \epsilon_{ij}\epsilon_{kl}\lambda^i_{23}X^k_{34}\tilde{\lambda}^j_{41}\Phi^l_{12}. \tag{4.26}$$

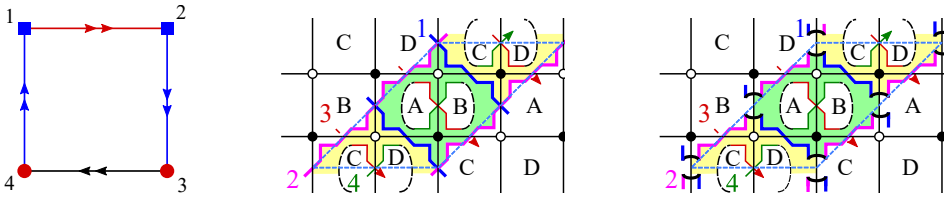

Figure 4.17: Backreaction due to a 2-instanton process in the F_0 theory. Figure a) shows the quiver, with black arrows denoting 4d chiral multiplets, blue arrows denoting charged D2-D6 fermion zero modes, and blue arrows denoting chiral multiplets of D2-D2 zero modes. Figure b) shows the mirror Riemann surface Σ after the backreaction and c) shows it with the instantons recombined.

Note that in addition there are couplings e.g. between the bosonic zero modes determining the D2-brane positions in 4d spacetime and the zero modes in the D2-D2 sector, so that the latter become "massive" upon separation of the instantons. As discussed in [121, 162], the interesting multi-instanton physics arises when the two instantons are coincident and such couplings can be safely ignored. The analysis is most simply carried out by first integrating over the bosonic D2-D2 zero modes, which effectively bind the two instantons. The combined instanton inherits the D2-D6 charged zero modes, which moreover inherit the couplings from the original ones, by simply regarding the D2-D2 chiral multiplet zero modes as a numerical factor, omitted in the following.

In total, we obtain a field theory operator with the structure

$$\mathcal{O}_{\text{charged}} \sim (X^1_{34})(X^2_{34}) \tag{4.27}$$

where brackets signal the structure of determinants in the non-abelian case, as usual. Let us turn to the description of the multi-instanton effect in the backreaction picture. The recipe is a simple generalization of earlier ones. We take the Riemann surface and highlight the 1-cycles wrapped by the instantons, as in Figure 4.17b. One novelty is that in order to account for the integration over D2-D2 bosonic zero modes, the intersections between the instanton must be considered as slightly recombined, see Figure 4.17b. We must cut the Riemann surface along the corresponding cycle, and recombine any D6-brane 1-cycle formerly intersecting it. As in Section 4.3.3.4, the Riemann surface splits in two daughter surfaces, each of them with two punctures. This time, however, the punctures removed do not coincide with the complex deformation.

Step 3 provides the field theory operator produced from the worldsheet instantons after the backreaction. It is straightforward to see that the operator coincides with (4.27), as expected.

4.3.5.2 Two-instanton effect in dP_3

Let us now consider a 2-instanton example in a configuration of branes at a complex cone over dP_3. The dimer diagram, quiver diagram, web diagram and toric diagram for the dP_3 theory are shown in Figures 4.18a, 4.18b, 4.18c, 4.18d, respectively. As we will see in Section 4.4.2, this theory admits several complex deformations, which can be triggered by backreaction of certain multi-instantons; in this section we however focus on a multi-instanton effect whose backreaction does not correspond to a complex deformation.

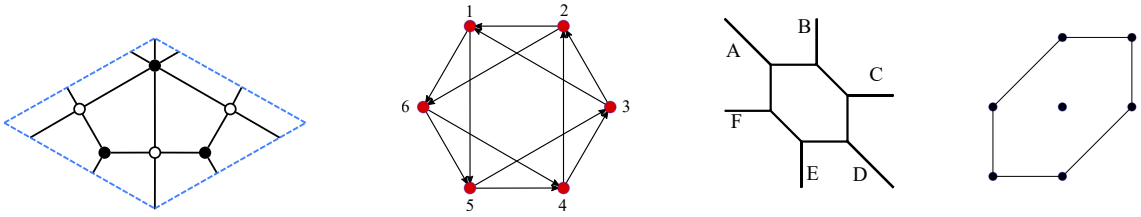

(a) (b) (c) (d)

Figure 4.18: Diagrams for dP_3 theory, a) shows the dimer diagram, b) the quiver diagram, c) the web diagram and d) the toric diagram. The tiling of Σ coincides with the dimer diagram.

We consider introducing one D2-brane instanton in each of the nodes 4 and 5. The quiver diagram, see Fig. 4.19a, shows fermion zero modes $\lambda_{42}, \lambda_{43}, \lambda_{42}, \tilde{\lambda}_{15}, \tilde{\lambda}_{64}, \tilde{\lambda}_{65}$, a chiral multiplet worth of zero modes Φ_{54} and matter fields $X_{16}, X_{21}, X_{32}, X_{26}, X_{31}$. The fermion zero modes have the following couplings

$$\begin{aligned} &\Phi_{54}\lambda_{43}X_{32}X_{21}X_{16}\tilde{\lambda}_{65} + \lambda_{42}X_{26}\tilde{\lambda}_{64} + \lambda_{53}X_{31}\tilde{\lambda}_{15} - \\ &- \lambda_{53}X_{32}X_{26}\tilde{\lambda}_{65} - \lambda_{43}X_{31}X_{16}\tilde{\lambda}_{64} - \Phi_{54}\lambda_{42}X_{21}\tilde{\lambda}_{15} \end{aligned} \tag{4.28}$$

Repeating the arguments of the previous examples about the treatment of D2-D2 zero modes, and saturating the charged D2-D6 fermion zero modes, we obtain the following 4d field theory operator structure

$$\mathcal{O}_{\text{charged}} = (X_{32}X_{26})(X_{31}X_{16})(X_{21}) + (X_{26})(X_{32}X_{21}X_{16})(X_{31}) \tag{4.29}$$

where brackets indicate sets promoting to determinants in the non-abelian case, as usual.

This structure is easily recovered in the backreaction picture, see Figures 4.19c and 4.19e. Note that in order to enforce that the total homology class becomes trivial (rather than both individual classes, we have recombined the instantons at their intersections (in the only way consistent with their orientation), yielding a combined 1-cycle along which to cut Σ. This effectively reproduces the integration over the D2-D2 bosonic zero mode.

4.4 Relation to complex deformations

4.4.1 Generalities

Some toric geometries admit complex deformations, the canonical example being the complex deformation of the conifold, discussed in Section 2.3.3. The complex deformations a given toric geometry admits can be seen from its web diagram. They are defined by the removal of a collection of legs whose (p, q) labels sums to zero, also dubbed subweb in equilibrium [43], as described in Section 2.2.5. Concrete examples are the complex deformations of the conifold and the double conifold. There are richer situations, in which a given singularity admits several (incompatible) complex deformations. For instance, the complex cone over dP_3 admits two complex deformation, as shown in Fig. 4.22.

Geometric transitions corresponding to complex deformations have appeared in the context of warped throats triggered by deformation fractional branes, in the sense of [31,43]. These correspond to anomaly-free rank assignments in the quiver diagram, which have the property that the total 1-cycle they define in the mirror Riemann surface surrounds

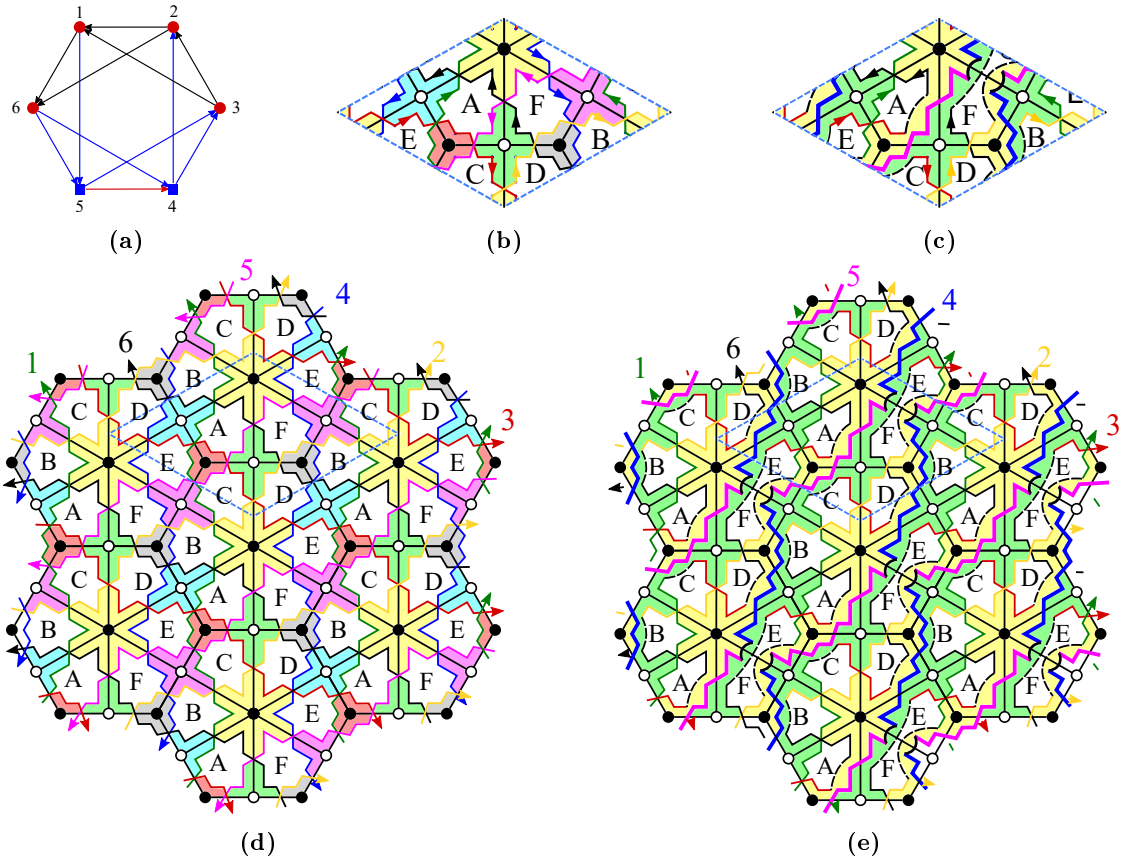

Figure 4.19: dP3 backreaction with two instantons. a) is the quiver diagram with D2-brane instantons in nodes 4 and 5. Blue arrows denote charged D2-D6 fermion zero modes and red arrows denote a chiral multiplet worth of D2-D2 zero modes. Figure b) shows the unit cell of Σ before the backreaction. In Figure c) we show the unit cell of Σ after the backreaction. Note that the integration over the D2-D2 bosonic zero mode induces the recombination of instantons, shown as a thick black curved segment. Also the D6-brane 1-cycles cut by the instanton 1-cycles are duly recombined (sometimes taking advantage of the passages open due to the instanton recombination). In Figures d) and e) we provide the same pictures in the covering space description of Σ.

the punctures corresponding to the sub-web in equilibrium. The geometric transition removes the corresponding cycle and seals the Riemann surface, in a combinatorial dimer prescription described in [44].

It is natural to wonder what happens if we consider D2-brane instantons on the same cycle that corresponds to a given deformation fractional brane, i.e. a complex deformation. In fact this already occurred in the examples in Sections 4.3.3.1 and 4.3.3.2, with the result that the backreacted geometry is the (mirror of the) complex deformation of the initial geometry. In this section we provide further examples showing that this is a general behaviour.

4.4.2 Examples

As just explained, some of the examples already considered provide realizations that instantons on classes corresponding to deformation fractional branes produce backreacted

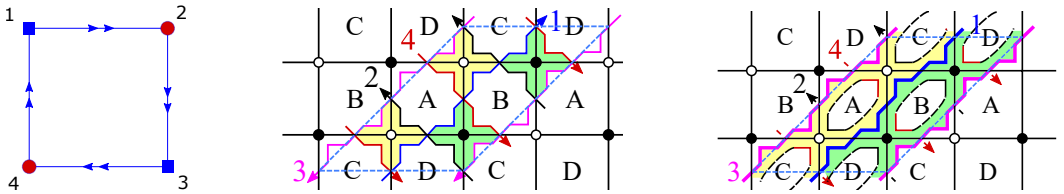

Figure 4.20: F0 complex deformation. a) is the quiver diagram with D2-brane instantons in nodes 1 and 3. Blue arrows denote fermion zero modes. b) shows Σ before the backreaction. In c) Σ after the backreaction is shown. The D-instanton have dissapeared from Σ, splitting it into two daughter surfaces.

geometries given by the complex deformation of the original space. We now provide further examples, based on chiral quivers.

4.4.2.1 Complex Deformation of cone over F_0

Let us start with F_0, whose dimer diagram unit cell, quiver diagram and web diagram are shown in Figure 4.14. This geometry admits a complex deformation given by the splitting of the web diagram into two subwebs in equilibrium, one with external legs A, B and the other with C and D, see Figure 4.21. At the level of deformation fractional branes, this complex deformation is triggered by increasing the rank of the quiver nodes 1 and 3 simultaneously (equivalently, recalling that the sum of all nodes is topologically trivial in compact homology, of nodes 2 and 4).

Let us consider the backreaction effect of D2-brane instantons on the corresponding class. Consider introducing one D2-brane instanton in each of the nodes 1 and 3 in the quiver, see Figure 4.20a. These correspond to the blue and pink 1-cycles in the mirror Riemann surface in Figure 4.20b.

From the open string perspective, there are charged fermion zero modes λ^i_{12}, $\tilde{\lambda}^i_{41}$, λ^i_{34}, $\tilde{\lambda}^i_{23}$, for $i = 1, 2$, and there are no matter fields. Note also that in the present case there are no D2-D2 zero modes of the kind introduced in Section 4.3.5. Saturation of fermion zero modes produces no charged field theory operator, like in the conifold case. Consider now the effect of backreacting these instantons. Following step 1 in our procedure, we cut the Riemann surface along the 1-cycles defined by the D2-brane instantons, and recombine cycles following step 2. The resulting mirror Riemann surface is Figure 4.20c. Unlike in section 4.3.3.4, Σ splits in two surfaces, one with punctures A, C and the other with B, D, precisely in accordance with the complex deformation shown in Fig. 4.21b. We thus derive the result that the backreacted geometry is the (mirror of the) complex deformation of the original singularity. In this case, step 3 gives no operators induced in the field theory, as the worldsheet instantons after the backreaction do not touch any brane intersection with matter. This agrees with the prediction from saturating fermion zero modes. Although we obtain agreement, it is rather trivial as no charged operator is generated; we turn to a more interesting example in the following section.

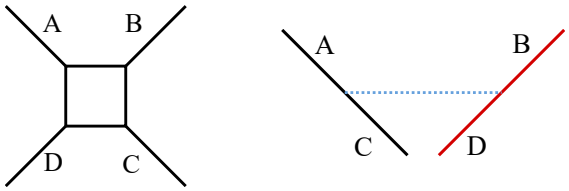

Figure 4.21: Web diagrams of F0 a) before and b) after the complex deformation.

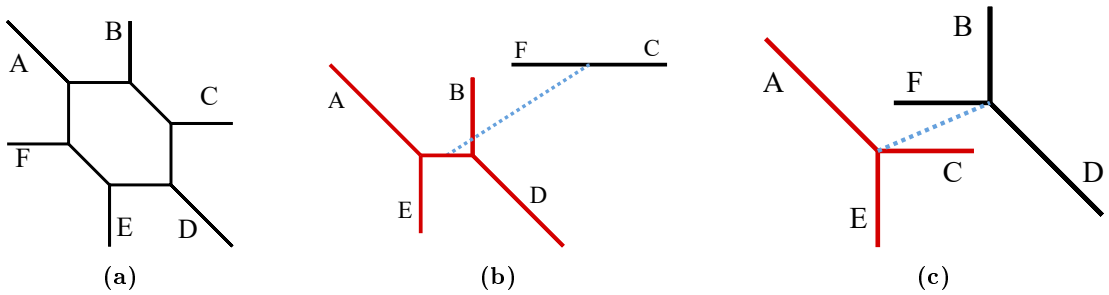

Figure 4.22: Web diagrams of the two possible complex deformations of dP3, corresponding to the removal of a subweb in equilibrium.

4.4.3 Complex deformation of dP_3 into a conifold

There are several different complex deformations for the complex cone over dP_3. In this section we focus on that defined by the web diagrams splitting in Figure 4.22b, by removal of the external legs C and F.

At the level of deformation fractional branes, this corresponds to locating extra branes on the nodes 2 and 5 in the quiver/dimer. This is easily shown by checking that the corresponding 1-cycle in Σ precisely surrounds the relevant punctures. We would now like to consider the backreaction effect of D2-brane instantons on those nodes 2 and 5. The quiver diagram of this setup is shown in Figure 4.23b. There are fermion zero modes $\tilde{\lambda}_{15}$, $\tilde{\lambda}_{32}$, $\tilde{\lambda}_{42}$, $\tilde{\lambda}_{65}$, λ_{21}, λ_{26}, λ_{53}, λ_{54}, and 4d chiral multiplets X_{16}, X_{21}, X_{43} and X_{64}. The couplings are

$$\begin{aligned}&\lambda_{54}X_{43}\tilde{\lambda}_{32}\lambda_{21}X_{16}\tilde{\lambda}_{65} + \lambda_{53}X_{31}\tilde{\lambda}_{15} + \lambda_{26}X_{64}\tilde{\lambda}_{42} - \\ &- \lambda_{54}\tilde{\lambda}_{42}\lambda_{21}\tilde{\lambda}_{15} - \lambda_{53}\tilde{\lambda}_{32}\lambda_{26}\tilde{\lambda}_{65} - X_{43}X_{31}X_{16}X_{64}\end{aligned} \tag{4.30}$$

where the last term is actually a 4d coupling among chiral multiplets, which we include for completeness. Saturation of fermion zero modes produces the structure

$$\mathcal{O}_{\text{charged}} \sim (X_{43})(X_{16})(X_{31})(X_{64}) + \text{const} \tag{4.31}$$

Consider now the description in terms of the instanton backreaction see Figure 4.24b. Following steps 1 and 2 in our prescription, we cut along the pink and blue 1-cycles, and duly recombine the D6-brane 1-cycles. The mirror Σ splits in two Riemann surfaces, one containing the punctures C and F, and the other containing the punctures A, B, D and E. Thus it reproduces the (mirror of the) complex deformation of the original singularity. Following step 3, we consider the worldsheet instantons in the resulting geometry, shown as shaded green and yellow in the Figure. The green one does not produce any charged

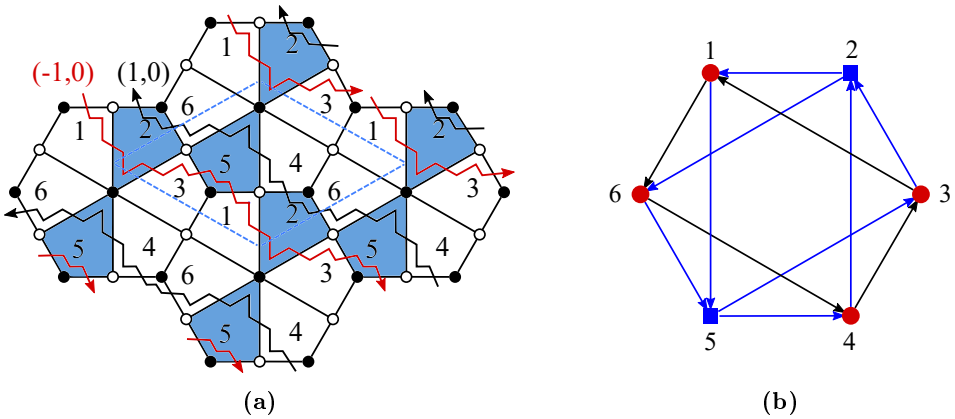

Figure 4.23: dP3 Complex Deformation with two instantons. a) shows the zig-zag paths to be removed from the dimer diagram and the corresponding faces are shaded in blue. In b) the corresponding quiver diagram is shown.

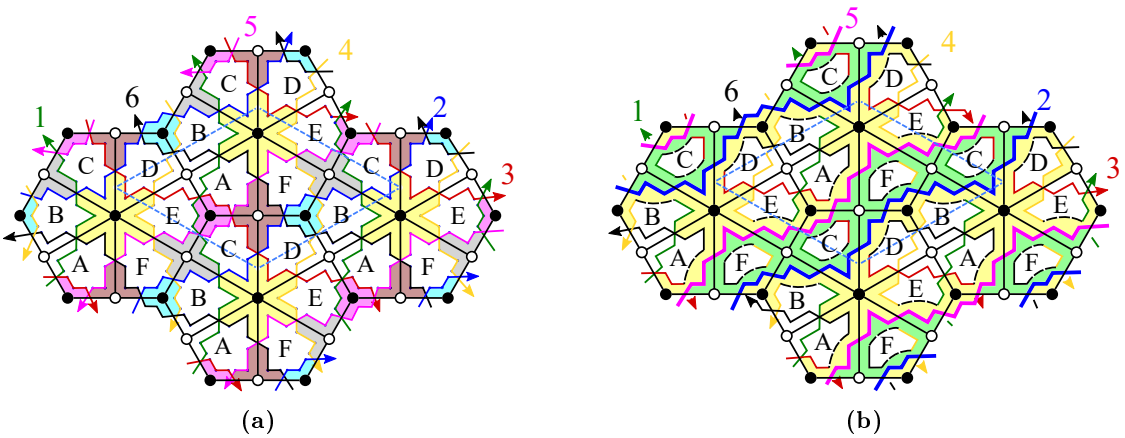

Figure 4.24: dP3 Complex Deformation with two instantons. a) shows Σ before the bacreaction, with D-brane instantons in cycles 2 and 5 and WS instantons shaded in light colors. In b) Σ after the backreaction is shown. D-brane instantons dissapear and branes recombine. Two WS instantons remain, one in each Σ'.

field theory insertion, while the pink one inserts the fields X_{16}, X_{64}, X_{43} and X_{21}; the combination of both reproduces precisely the structure in (4.31).

4.4.3.1 Complex deformation of dP_3 into flat space

In this section we study a second complex deformation, defined by the removal of legs B, D and F, which form a subweb in equilibrium, as shown in Figure 4.22c. This corresponds to the removal of zig-zag paths with weight (-1,0) and (0,1) and (1,-1) in the dimer diagram, as shown in Figure 4.25a. In turn, this implies that faces 2, 4 and 6 must be removed from the dimer (equivalently, for 1,3 and 5). In our description this translates to putting an instanton in the class defined by these three cycles, or faces of the dimer.

We thus consider the configuration with one D2-brane instanton on each of the cycles labelled 2, 4 and 6. The quiver diagram of this setup is shown in Figure 4.25b. We see that there are charged fermion zero modes $\tilde{\lambda}_{54}$, λ_{43}, $\tilde{\lambda}_{32}$, λ_{21}, $\tilde{\lambda}_{16}$, λ_{65}, D2-D2 chiral multiplet

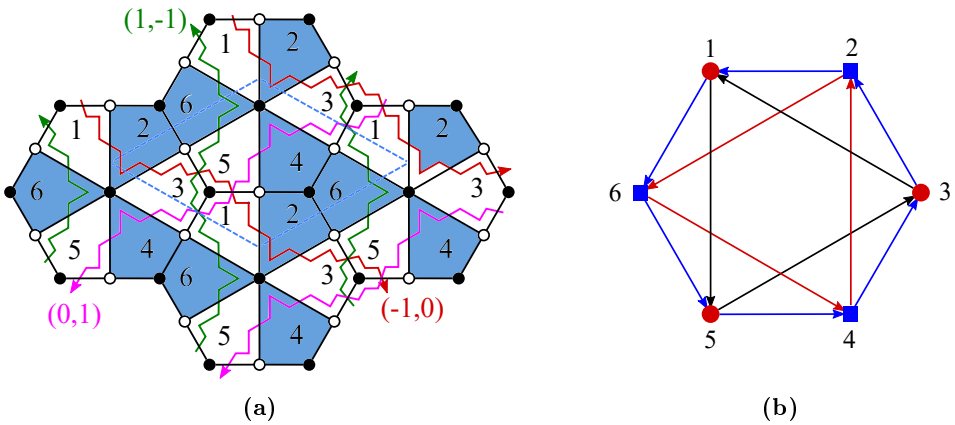

(a) (b)

Figure 4.25: Complex Deformation of the cone over dP_3 triggered by three instantons. Figure a) shows a set of zig-zag paths to be removed from the dimer diagram, and a set of corresponding faces shaded in blue. In b) the corresponding quiver diagram si shown.

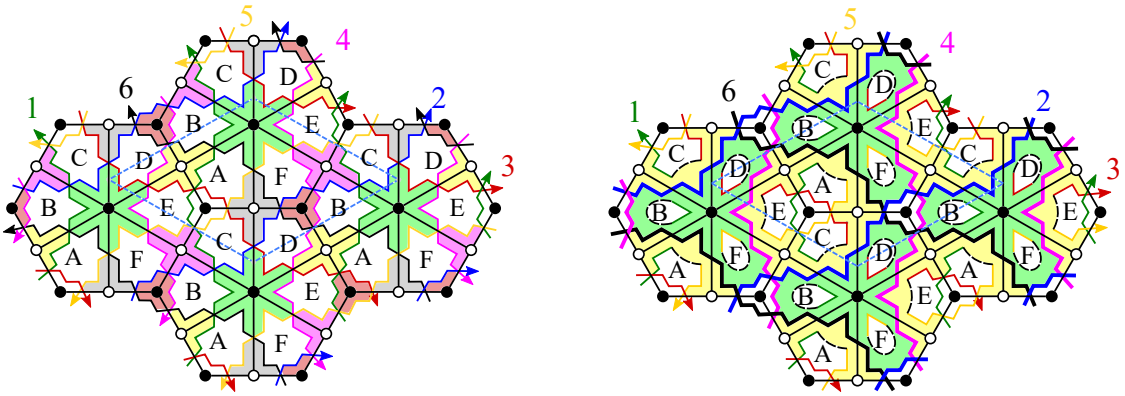

(a) (b)

Figure 4.26: Complex Deformation of the cone over dP_3 triggered by three instantons. Figure a) shows the mirror Riemann surface Σ before the backreaction, with D-brane instantons in cycles 2,4 and 6 and WS instantons shaded in light colors. In Figure b) we show Σ after the backreaction. For clarity the instantons have not been recombined. The surface splits into two, in agreement with the resulting geometry being (the mirror of) a complex deformation.

zero modes Φ_{42}, Φ_{42} and Φ_{64}, and matter fields X_{15}, X_{53}, X_{31}. The worldsheet instantons yield the following couplings among 4d fields and the instantons zero modes

$$\begin{aligned} \sim \quad & \tilde{\lambda}_{54}\lambda_{43}\tilde{\lambda}_{32}\lambda_{21}\tilde{\lambda}_{16}\lambda_{65} - \Phi_{43}\Phi_{26}\Phi_{64} - X_{53}X_{31}X_{15} + \\ & + \Phi_{42}\lambda_{21}X_{15}\tilde{\lambda}_{54} + \Phi_{26}\lambda_{65}X_{53}\tilde{\lambda}_{32} + \Phi_{64}\lambda_{43}X_{31}\tilde{\lambda}_{16} \end{aligned} \tag{4.32}$$

The fermion zero modes can be saturated in two different ways, producing a contribution

$$\mathcal{O}_{\text{charged}} \sim (X_{15})(X_{53})(X_{31}) + \text{constant} \tag{4.33}$$

where brackets indicate determinants in the non-abelian case, as usual.

Let us consider the backreaction description, which is illustrated inFigure 4.26b upon application of steps 1 and 2 of the recipe. The mirror Riemann surface has divided in two: Σ', with punctures A, C and E and Σ'', with punctures B, D and F in agreement with

the complex deformation of the dP_3 singularity to flat space. Step 3 of the recipe allows us to find the field theory operators induced by the WS instantons in each of the new surfaces, and one finds that they indeed agree with the above operator (4.33). Concretely, the worldsheet instanton in Σ' provides the non-trivial operator involving charged fields, while the worldsheet instanton in Σ'' does not produce any charge field insertion.

5

From Instantons on Toric Singularities to Bipartite Field Theories

In this chapter we combine new results in two interesting areas of D-brane physics: non-perturbative D-brane instantons and the realization of Bipartite Field Theories (BFTs) using D-branes.

D-brane instantons have become a centerpiece in the understanding of string theory beyond perturbation theory (see e.g. [127–130]) and in model building applications to moduli stabilization (see e.g. [109,131]) or the generation of charged field theory operators (see e.g. [110–112] and [113,114] for reviews). These field theory operators arise as 't Hooft couplings required by the saturation of fermion zero modes charged under the gauge groups carried by the D-branes [122], coming from the open sector between gauge D-branes and D-brane instantons.

Consider again the case of D3-brane instantons on a CY 3-fold singularity and its mirror, where D2-brane instantons intersect D6-branes. In Chapter 4, we have shown that a dual perspective exists, in which the generation of non-perturbative charged field theory operators can be obtained as a perturbative coupling in a modified geometry, triggered by the backreaction of the D-brane instanton on the mirror CY. In the resulting configuration, the D2-brane instanton is geometrized, along the lines of [115,116,152], and we are left with a set of recombined D6-branes in the modified geometry. The non-perturbative operator can be read as a WS-instanton in the punctured Riemann surface describing the mirror geometry.

In this chapter we show that the resulting gauge theory (and thus the charged field theory operators) can be encoded in a Bipartite Field Theory, albeit in general not defined on a 2-torus (as the original dimer diagram) but on a general (possibly higher-genus) Riemann surface, thus of the kind introduced in [34], see Section 2.4.5. This resulting BFT is related to the original one by a simple operation, which can be regarded as the direct backreaction of the D-brane instanton on the gauge theory. For the simplest case of a D-brane instanton located on a face of the original dimer diagram, it essentially corresponds to the removal of the face and its edges, and the recombination of nodes of the same color. In general, avoiding crossing of edges requires the introduction of handles, so that the new BFT is in general defined in higher genus.

Considered abstractly, this operation can be carried out also by taking a general BFT as starting point. From this perspective, a main result of the present chapter is the definition of a new operation on BFTs, relating theories defined on Riemann surfaces of different genus. This is thus a particularly interesting new insight in the field of BFTs.

As reviewed in Section 2.4.5, BFTs are $4d$ $\mathcal{N}=1$ supersymmetric gauge theories

whose Lagrangians are defined by bipartite graphs embedded into a Riemann surface, possibly with boundaries [34].[1] The special subclass of BFTs defined on a torus without boundaries are the brane tilings or dimer diagrams. Extensive catalogues of explicit BFT examples have been provided in e.g. [34, 165] for general BFTs and [166–168] for higher genus examples without boundaries.

General BFTs and their associated graphs have received several physical interpretations, in particular in connection with the reformulation of $4d$ $\mathcal{N} = 4$ SYM in terms of *on-shell diagrams* [169]. The new approach makes all symmetries of the theory manifest and sheds new light on previous results [169–172]. The connection of on-shell diagrams with bipartite graphs and BFTs has been extensively studied in [34, 35, 165, 173–175].

On the other hand, there has been no direct realization of BFTs in string theory beyond the very restricted subclass of theories associated to graphs with vanishing curvature [35, 164]. Our work provides precisely that link, regarding higher genus BFTs as the result of D-brane instanton backreactions in lower genus theories. We expect that the new operation we have obtained linking BFTs in different genus has interesting implications both for the further study of general BFTs in string theory, and for the complementary physical realizations of the corresponding graphs.

Our work takes first steps in this direction, for instance by computing the toric CYs associated to the new BFTs and establishing how they are connected to the original ones. We expect this to be a very useful tool towards a general dictionary, and the study of dual theories, the inverse problem, etc.

The chapter is organized as follows. In Section 5.1 we derive the description of the D-brane instanton backreaction in the dimer, and its properties. In Section 5.1.1 we prove that in general it leads to a higher genus BFT, and provide illustrative examples in Section 5.1.2.1 and Section 5.1.2.2. In Section 5.1.3 we discuss instances in which the backreaction does not result in an increase of the genus, which correspond to dimers where the global $\mathbb{T}^2$ topology implies certain identifications among faces. In Section 5.1.4 we apply the combinatorial recipe of dimers to general BFTs, thus defining a new operation relating BFTs in different genus Riemann surfaces. In Section 5.1.5 we introduce a useful graphical depiction of the handle attachment surgery which simplifies the discussion of the genus increase. In Section 5.2 we describe the computation of the new toric data corresponding to the backreacted BFTs. The change in perfect matchings between the original and final theories is discussed in Section 5.2.1, yielding the construction of the new toric diagram in Section 5.2.2. A direct construction based on relating new toric coordinates with the bridges identifying formerly different nodes of the original theory is provided in Section 5.2.3. These concepts are illustrated in a detailed example in Section 5.2.4. In Section 5.3 we describe instances of the interplay of instanton backreaction and Seiberg duality: in Section 5.3.1, when they are applied to the same dimer face, and in Section 5.3.2 when applied to neighboring faces. In Section 5.4 we consider the generalization to backreaction of multi-instantons, focusing on cases corresponding to complex deformations of the original CY 3-fold, and recover earlier results in the literature. In Section 5.5 we show the non-uniqueness of the inverse problem of reconstructing initial theories for a given final one.

[1] Closely related theories were introduced in [163] and studied further in [164].

5.1 D-brane Instanton Backreaction on the Dimer

In this section we show that the description of the instanton backreaction can be carried out directly on the dimer diagram, and that it generically turns it into a general BFT. This motivates the definition of a general combinatoric operation, which extends automatically to the whole class of BFTs, and which relates BFTs on different Riemann surfaces.

5.1.1 General Idea

The procedure in Section 4.3.2 to describe the instanton backreaction in the mirror configuration, turns a system of intersecting D6-branes into a different one, which is nevertheless still described in terms of a bipartite graph tiling of the backreacted Riemann surface. The remarkable fact that we obtain a bipartite structure implies that we can reconstruct faces, edges and nodes of a BFT describing the resulting set of D6-branes, including the instanton superpotential.

The fact that, in general, this corresponds not to a 2-torus dimer diagram but rather to a generically different genus BFT is easily derived. Using the recipe for the generic case summarized by Figure 4.7, the change of genus in the corresponding gauge theory is as follows. First, the number of edges is reduced by $\Delta E = -2k$; the number of vertices V changes, since each set of k black/white nodes turns into a single black/white node, hence $\Delta V = -2k+2$; finally, the number of faces in the BFT is determined by the disappearance of the instanton 1-cycle in the mirror, and the recombination of the $2k$ D6-brane 1-cycles into a single one (see Section 5.1.3 for other possibilities in non-generic cases), resulting in $\Delta F = -2k$. Since the Euler formula gives

$$F + V - E = 2 - 2g\,, \tag{5.1}$$

we have a change in the BFT genus

$$\Delta g = \frac{1}{2}\left(\,\Delta E - \Delta F - \Delta V\,\right) \;=\; k - 1\,. \tag{5.2}$$

The above analysis exploits the fact that the gauge theory resulting after the transformation in the mirror discussed in Section 4.3.2 still corresponds to a bipartite graph. In fact, it is easy to check that there is a simple operation that can be carried out in the dimer and which reproduces the different steps in the mirror, and that yields a BFT on a Riemann surface of the appropriate genus.

These steps are:

- **Step 1. Remove:** Remove the face corresponding to the D-brane instanton, and its edges, leaving the adjacent faces open. This reproduces the operation of removing the instanton mirror 1-cycle and cutting the 1-cycles intersecting it.
- **Step 2. Fuse:** Declare that all black nodes of the former instanton face are identified into a single black node, and similarly for all white nodes. The edges ending on the initial nodes remain as edges ending on the final node, and their ordering is preserved (this can be done by performing the identification of nodes sequentially according to their ordering as one circles the original face). In order to avoid edge crossings after

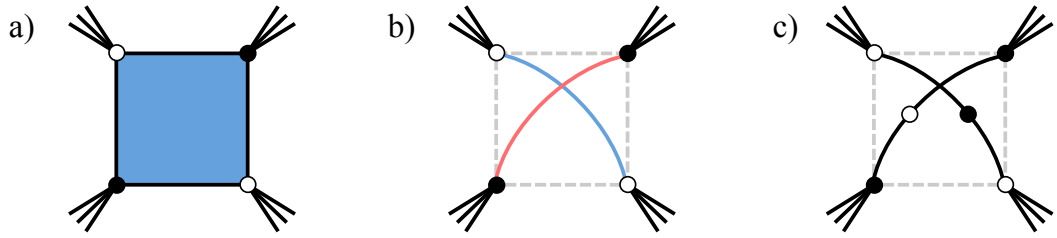

Figure 5.1: a) Local piece of the BFT surface around a face wrapped by the D-brane instanton (blue). The collections of half edges sticking out of each node indicate general superpotential couplings. b) After backreaction, the blue face and its edges disappear. The black and white nodes are recombined into single black and white nodes, respectively; this is indicated by bridges. The crossing of bridges can be avoided by embedding the BFT in a surface with an additional handle, in agreement with $\Delta g = 1$. Generically, the faces around the original instanton recombine into a single one. c) An alternative representation of the backreacted BFT, in which bridges are replaced by pairs of actual edges, joined by 2-valent nodes corresponding to superpotential mass terms.

the identifications of nodes, it is in general necessary to introduce k handles for an original instanton face of $2k$ sides. This provides the required increase in the genus of the resulting BFT. This step closes off the former open faces, in general into a single recombined one.

- **Step 3. Field theory operators:** The above two steps already define the backreacted BFT. This last step merely establishes that the $4d$ non-perturbative field theory operators induced by the original D-brane instanton are simply the superpotential terms corresponding to the combined black and white nodes.

Figures 5.1 and 5.2 illustrate this operation in the case of instantons on 4- and 6-sided faces. The recombination of black and white nodes is indicated by blue (for white nodes) and red (for black nodes) *bridges*. Whenever a bridge connects two nodes of the same color, we understand that there is a 2-valent node of the opposite color in the middle of it, making the graph bipartite. In other words, bridges correspond to massive pairs of chiral fields, which lead to the desired identifications of nodes if they are integrated out. For clarity, we leave such intermediate nodes implicit in the figures that follow.

Clearly, although we have introduced this operation for bipartite graphs defined on 2-tori, the procedure extends to general BFTs, thus defining an operation relating BFTs on Riemann surfaces generically of different genus. In the generic case (see Section 5.1.3 for non-generic situations) the operation corresponds to a local surgery, whose characterization we study in more detail in Section 5.1.5. The application of the operation in general BFTs is discussed in Section 5.1.4. It is easy to check that the above transformation rule on the dimer preserves the structure of zig-zag paths, see Figure 5.3. This dovetails the fact that the instanton backreaction in the mirror preserves the punctures of the Riemann surface.

5.1.2 Examples

Below we present two examples illustrating the ideas introduced in the previous section.

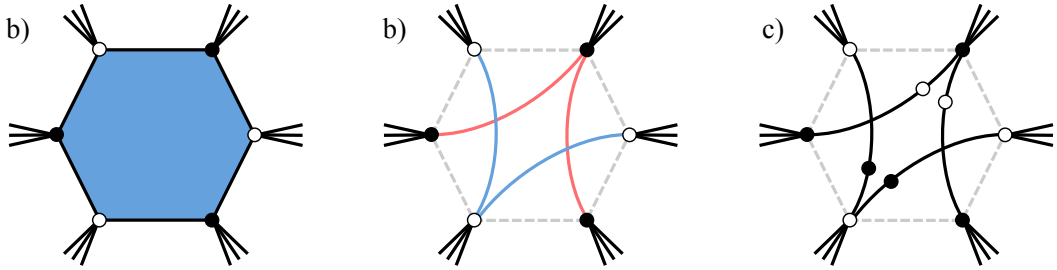

Figure 5.2: Backreaction of a local piece of a BFT surface around a D-brane instanton on a 6-edge face. Similar remarks to Figure 5.1 apply, with the difference that $\Delta g = 2$ in this case.

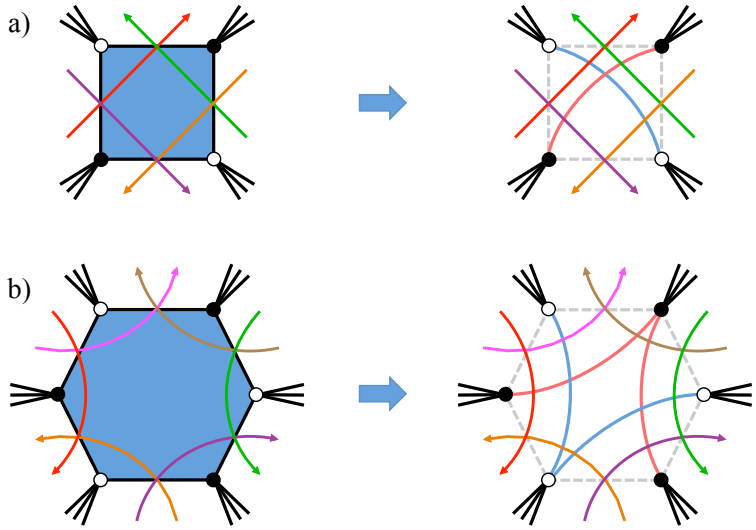

Figure 5.3: Structure of zig-zag paths around faces in a dimer, and in its backreacted version. Zig-zag paths maintain their structure, in agreement with the fact that punctures in the mirror Riemann surface are unchanged by the backreaction process.

5.1.2.1 A PdP_2 Example

Let us consider the pseudo del Pezzo 2 (PdP_2) theory. This geometry, which corresponds to a blowup of $\mathbb{CP}^2$ at two non-generic points, was originally studied in [176], where it was determined that it has a single toric phase. Figure 5.4 shows the toric diagram for PdP_2, the corresponding quiver and the dimer with zig-zag paths.

The mirror surface is presented in Figure 5.5.a. Consider introducing a D-brane instanton on face 4 of the dimer, which corresponds to the zig-zag path 4 on the mirror Riemann surface. Let us first perform the backreaction in the mirror, following the prescription reviewed in Section 4.3.2. The result is shown in Figure 5.5.b. The final theory is described by the recombined 1-cycles, their intersections and worldsheet instanton disks. Interestingly, all the zig-zags in the mirror fuse into a single one, i.e. the corresponding BFT has a single face. We obtain a BFT with $F = 1$, $V = 6$ and $E = 9$, i.e. with 1 gauge group 6 superpotential terms and 9 chiral fields. From the Euler formula (5.1), we conclude that it is a BFT defined on a genus-2 surface. Let us describe the final gauge theory explicitly. The 9 chiral fields transform in the adjoint representation of the single gauge

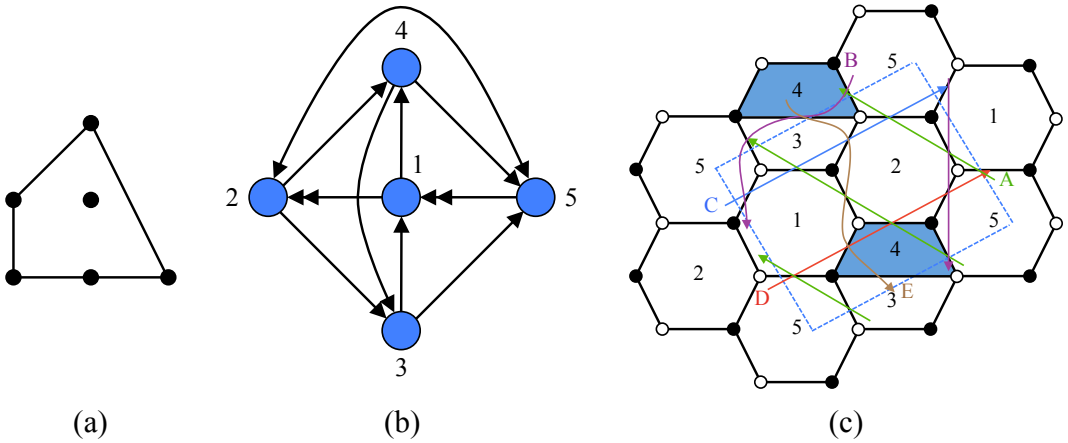

Figure 5.4: Diagrams for PdP_2: a) toric diagram, b) quiver and c) dimer with zig-zag paths.

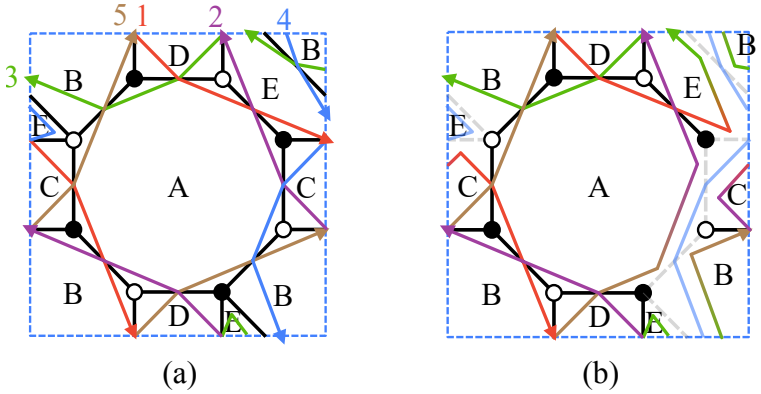

Figure 5.5: a) Mirror surface for PdP_2. b) Backreaction of an instanton on face 4 of the dimer, which maps to the blue zig-zag path. All zig-zags recombine into a single one.

group, as shown in the quiver in Figure 5.6.b. Below we will discuss the superpotential in further detail.

Let us now see how the same theory is recovered by implementing backreaction directly on the dimer, as described in section 5.1.1. Applying this recipe to an instanton on face 4, the edges of the instanton face disappear and the nodes of the same color are identified. The resulting diagram is shown in Figure 5.6.a, where we see that a new handle needs to be introduced for the identification, nicely reproducing the expected genus-2 result. The original face numbers are shown in grey for reference. Integrating out the massive edges associated to the bridges, we obtain a BFT with $V = 6$ and $E = 9$, which combined with the Euler formula imply that $F = 1$. We thus replicate the result of the mirror. As mentioned earlier, the theory has a single gauge group and 9 adjoint chirals as shown in Figure 5.6.b. The superpotential contains 6 terms, which can be read from Figure 5.6.a, where we have labeled the chiral fields associated with the edges, and is given by

$$W = \Phi_1\Phi_2\Phi_9 + \Phi_3\Phi_4\Phi_5 + \Phi_6\Phi_7\Phi_8 - \Phi_2\Phi_3\Phi_5 - \Phi_1\Phi_6\Phi_4 - \Phi_7\Phi_9\Phi_8\,. \tag{5.3}$$

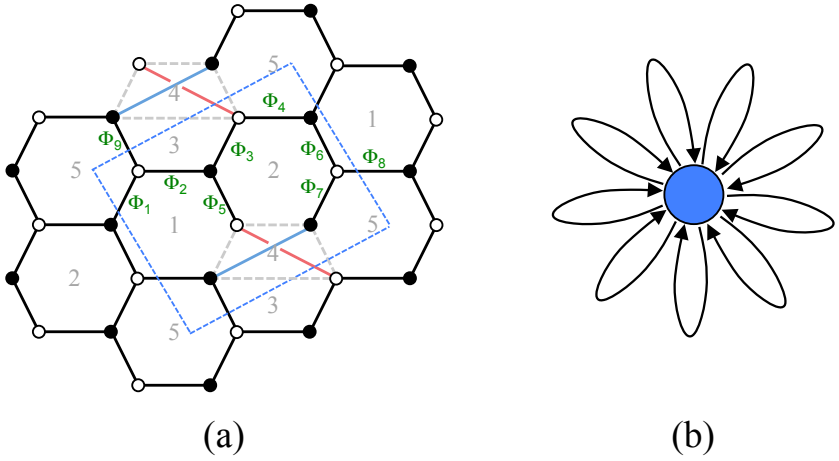

Figure 5.6: a) Backreaction of an instanton on face 4 of the PdP_2 dimer and b) quiver for the resulting BFT.

5.1.2.2 A PdP_4 Example

We now focus on PdP_4, which is a blowup of $\mathbb{CP}^2$ at four non-generic points. This geometry was first considered in [177], where it was established that it has three toric phases. Figure 5.7 shows the toric diagram for PdP_4, and the quiver and dimer for its phase 1, in the classification of [177].

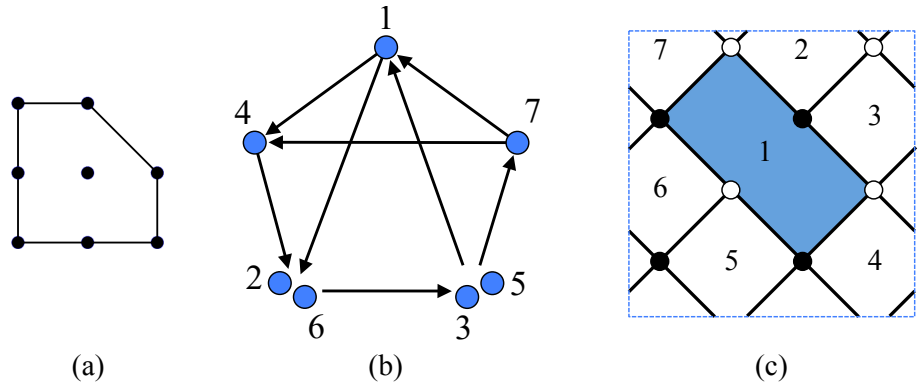

Figure 5.7: a) Toric diagram for PdP_4. b) Quiver and c) dimer for its phase 1.

Let us consider an instanton on the hexagonal face 1 of the dimer, indicated in blue in Figure 5.7. Its backreaction is shown in Figure 5.8.a. Note that it is necessary to add two handles, so the resulting BFT is in genus 3. This theory has $F = 1$, $V = 4$ and $E = 9$. The gauge theory has 1 gauge group with 9 adjoint chiral fields, as illustrated in the quiver in Figure 5.8.b. While this is the same quiver that we obtained for the example in the previous section, shown in Figure 5.6.b, we know that the two BFTs are fundamentally different; in particular the first theory has $g = 2$ and the second one has $g = 3$. The distinction between both theories comes from the superpotential. Instead of the 6 cubic

terms of (5.3), the superpotential of the new theory is given by

$$W = \Phi_5\Phi_4\Phi_3\Phi_8\Phi_7 + \Phi_2\Phi_1\Phi_6\Phi_9 - \Phi_3\Phi_1\Phi_2\Phi_9\Phi_8 - \Phi_4\Phi_5\Phi_7\Phi_6\,. \tag{5.4}$$

In the examples that follow, we will not write the superpotentials explicitly, since it is straightforward to read them from the corresponding bipartite graphs.

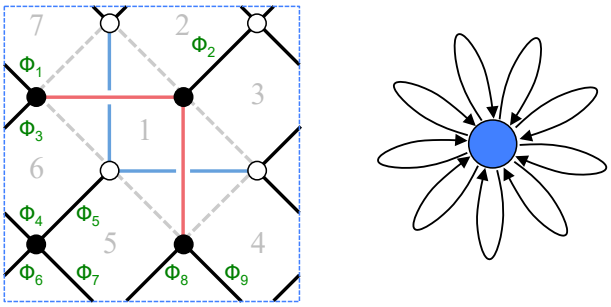

Figure 5.8: a) Backreaction of an instanton on face 1 of the dimer for phase 1 of PdP_4 and b) quiver for the resulting BFT.

5.1.3 Non-Generic Situations: Global Identifications

In the previous discussion we have implicitly assumed that in the dimer diagram all the faces adjacent to the instanton face are different. In terms of the mirror, this implies that any 1-cycle intersects the 1-cycle wrapped by the instanton at most once. Therefore, when the mirror Riemann surface Σ is cut along the instanton 1-cycle, the formerly intersecting 1-cycles become *connected* 1-chains (namely, they do not split into several disjoint pieces). All these 1-chains combine into a single 1-cycle, as accounted for in the change of the number of faces of the BFT that we used in the Euler formula (5.2). If this condition is not satisfied, the genus of the resulting BFT need not be higher than the original one. More generally, it is possible for the change in genus to be in the range

$$0 \leq \Delta g \leq k - 1\,. \tag{5.5}$$

We refer to this situation as cases with *global identifications*, in the sense that faces adjacent to the instanton are identified due to the global topology on the dimer 2-torus.

5.1.3.1 Examples

We now present various examples with global identifications and explain how to implement backreaction at the level of the dimer in such cases.

From F_0 to the Conifold

Let us consider F_0, which admits two toric phases (see e.g. [178]). Figure 5.9 shows the toric diagram for F_0 and the quiver and dimer for its phase 1.

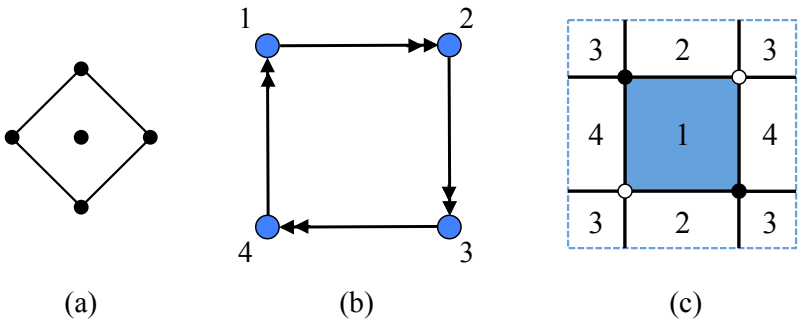

Figure 5.9: a) Toric diagram for F_0. b) Quiver and c) dimer for its phase 1.

Let us consider an instanton on face 1 of the dimer (the symmetry of the theory implies that single instantons on any of the faces are equivalent). We start with the mirror description. The mirror for phase 1 of F_0 is again a square lattice and is given in Figure 5.10.a. Zig-zags have been labeled according to the corresponding faces in the original dimer. An instanton on face 1 of the dimer corresponds to an instanton on the blue 1-cycle in the mirror. The backreaction is shown in Figure 5.10.b. Upon rearranging the diagram and integrating out massive fields associated to some of the 2-valent nodes, we recognize the result (c) as the mirror of the conifold theory. This is a theory that can be defined by a dimer diagram on $\mathbb{T}^2$, so in this case instanton backreaction does not increase the genus of the BFT.

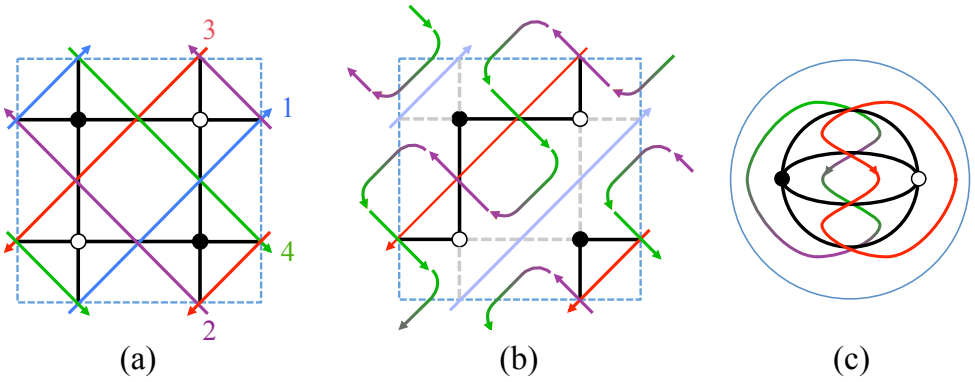

Figure 5.10: Backreaction in the mirror of F_0. The instanton wraps the blue 1-cycle, which corresponds to face 1 of the original dimer. The final result is the mirror of the conifold.

As anticipated, the reason for this behavior is that the original dimer contains faces that intersect the instanton more than once. This implies that some of the 1-cycle pieces in Figure 4.7 are actually not different. In this case, the counting in the Euler formula needs to be modified to take into account that there are two 1-cycles intersecting the instanton, each of them with intersection number ± 2. These 1-cycles recombine into a single one, leading to $\Delta F = -2$ (including the disappearance of the instanton 1-cycle), instead of the generic $\Delta F = -2k = -4$. This implies that $\Delta g = 0$ and the resulting BFT remains defined by a standard dimer on $\mathbb{T}^2$.

Let us now explain how this can be understood directly at the level of the dimer.

The procedure introduced in Section 5.1.1 is still valid, with a minor clarification. The underlying feature of these non-generic cases is that some of the faces intersecting the instanton are globally identified. Therefore, in the process of identifying the black/white corners of the instanton face into a single black/white node, we should not insist in doing so in the local patch given by the instanton face (as implicit in Figures 5.1 and 5.2). Such local procedure would lead to a higher genus BFT. Instead, we should always pick the identifications that minimize Δg. In other words, we should choose bridges such that the number of crossings is minimal. We refer to the original and the new prescriptions as the *local* and *global* recipes, respectively. The global prescription is the correct one and must always be used. The local and global prescriptions agree whenever there are no global identifications.

In Figure 5.11 we illustrate this phenomenon for the F_0 example. (a) shows the instanton. In (b), we removed the corresponding face and added bridges, taking advantage of the periodicity of the $\mathbb{T}^2$ to evade crossings without increasing the genus. We also labeled the new faces in black. In the rest of the chapter, we will apply a similar relabeling in those examples that remain on $\mathbb{T}^2$ after backreaction, for which visualizing the recombined faces is trivial. In (c) we switched to a different (but fully equivalent) unit cell, in order to bring the final theory to a more standard form. Finally, in (d) we condensed the bridges, obtaining the dimer for the conifold. As this example shows, the global properties of the dimer can sometimes lead to $\Delta g < k - 1$, which would be the naive result of the local recipe.

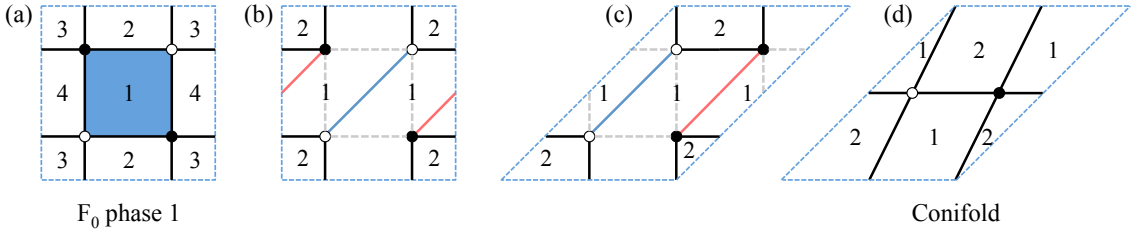

Figure 5.11: Instanton backreaction from phase 1 of F_0 to the conifold.

From dP_0 to $\mathbb{C}^3$

As another example, let us consider dP_0. Its toric diagram, and the quiver and dimer for its only toric phase are presented in Figure 5.12.

Let us consider an instanton on face 1 of the dimer (the two other faces are equivalent by symmetry). The instanton has six edges but they represent intersections with only two gauge factors, since each of them intersects the instanton three times. The number of faces decreases from 3 to 1, i.e. $\Delta F = -2$, instead of the generic $\Delta F = -2k = -6$. This implies that the resulting BFT has $\Delta g = 0$, instead of the generic $\Delta g = k - 1 = 3$, and remains on $\mathbb{T}^2$.

We are now ready to implement the backreaction directly on the dimer, as shown in Figure 5.13. The instanton under consideration is given in (a). (b) shows a choice of bridges that exploits the periodicity of $\mathbb{T}^2$ to avoid crossings. (c) shows a continuous deformation of the diagram, which moves the two middle nodes horizontally. Upon condensation of the

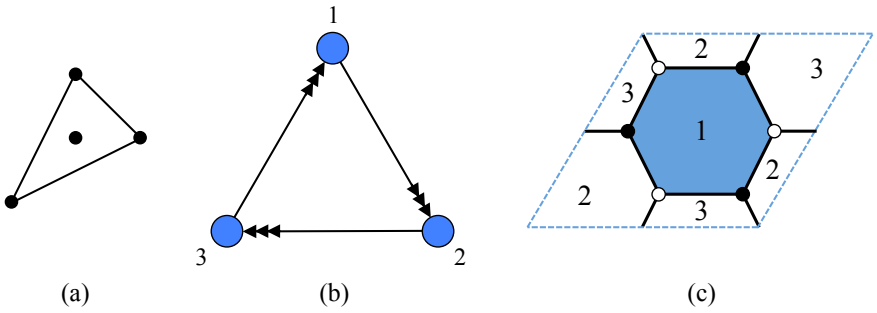

Figure 5.12: Diagrams for dP_0: a) toric diagram, b) quiver and c) dimer.

bridges we obtain the dimer for the $\mathbb{C}^3$ theory, i.e. for $\mathcal{N} = 4$ SYM, as shown in (d). This result is fully reproduced by the mirror, as explicitly worked out in Section 4.3.3.3.

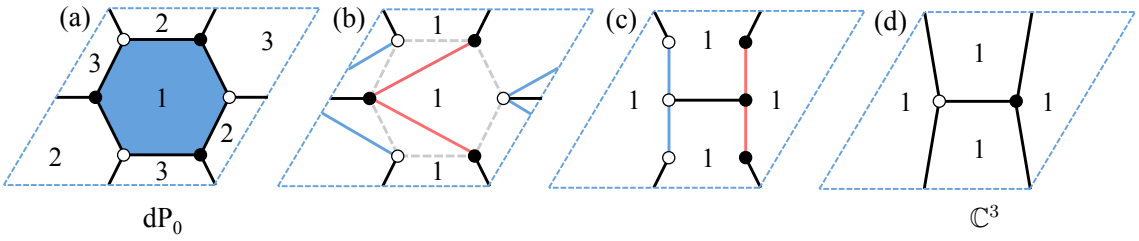

Figure 5.13: Instanton backreaction from dP_0 to $\mathbb{C}^3$.

From dP_1 to $\mathbb{C}^2/\mathbb{Z}_2 \times \mathbb{C}$

Let us finally consider dP_1, whose toric diagram, quiver and dimer are presented in Figure 5.14.

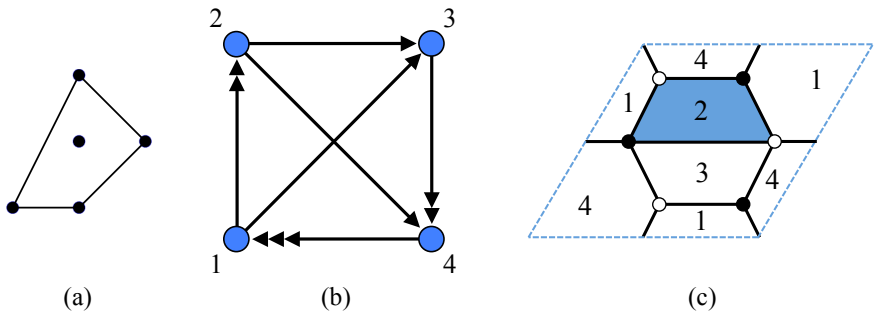

Figure 5.14: Diagrams for dP_1: a) toric diagram, b) quiver and c) dimer.

Let us consider an instanton on face 2. Figure 5.15 shows the backreaction in the dimer. As shown in (b), it is possible to pick bridges such that there are no crossings. The final result is the dimer for $\mathbb{C}^2/\mathbb{Z}_2 \times \mathbb{C}$.

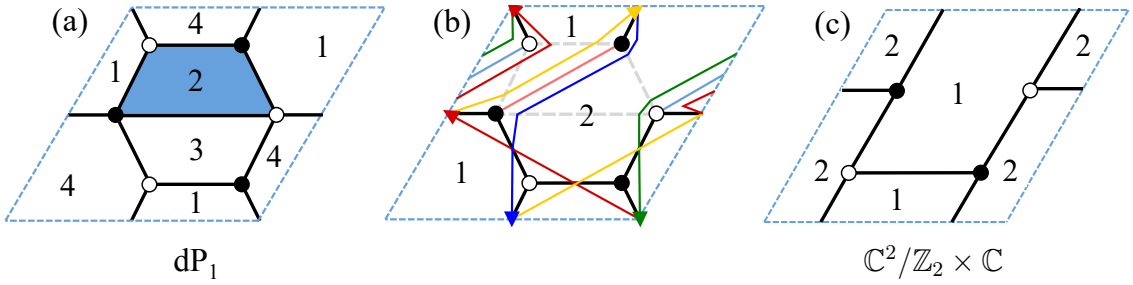

Figure 5.15: Instanton backreaction from dP_1 to $\mathbb{C}^2/\mathbb{Z}_2 \times \mathbb{C}$.

It is interesting to use this example to discuss in further detail how the local recipe for backreaction in the dimer fails when there are global identifications. Figure 5.16 shows the *incorrect* backreaction that would be obtained by naively applying the local recipe. The zig-zag paths in this figure should be compared to the correct ones, which appear in Figure 5.15.b. Note that the local and global backreactions do not change the intersections between the zig-zag paths. They however differ in the topology of their windings around cycles. As we will see in Section 5.1.3.2, the local recipe generates a diagram that is not a consistent tiling.

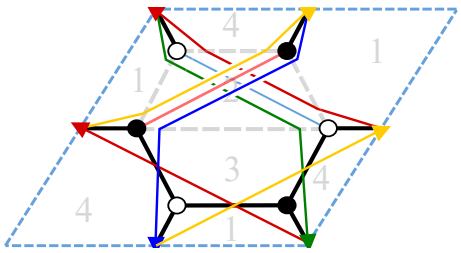

Figure 5.16: Backreaction using the naive local recipe. This figure should be compared with Figure 5.15.b, which correctly exploits global identifications.

5.1.3.2 Fake Tilings

We may provide a deeper insight into why the local recipe fails in cases with global identifications. Since the local recipe preserves the correct intersections of zig-zag paths, e.g. Figures 5.15.b and 5.16, it would naively appear that both pictures correspond to the same mirror. On the other hand, there is a problem with the counting of faces in the configuration obtained with the local recipe, so they cannot agree. The conundrum is solved by noticing that in cases with global identifications the local recipe gives rise to a graph which is not a consistent tiling of the corresponding Riemann surface, so it actually is not a consistent BFT.

Mathematically, a graph embedded in a Riemann surface provides a tiling of it if the Riemann surface is cut into regions which are, topologically, disks bounded by a concatenation of edges. Namely, faces must necessarily have the topology of a disk. It is easy to show that in cases with global identifications, the local recipe produces what we call *fake tilings* of the resulting higher genus Riemann surfaces, in which some of the

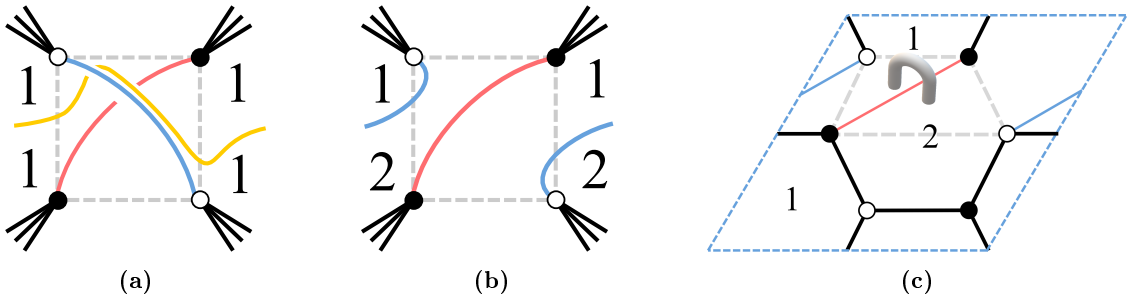

Figure 5.17: a) The local recipe for backreaction leads to a non-contractible cycle, shown in yellow. b) The cycle is not present if the global recipe is used. In both cases, the numbers label the resulting "faces". c) Spurious handle connecting faces 1 and 2 for the example of the backreacted dP_1 theory.

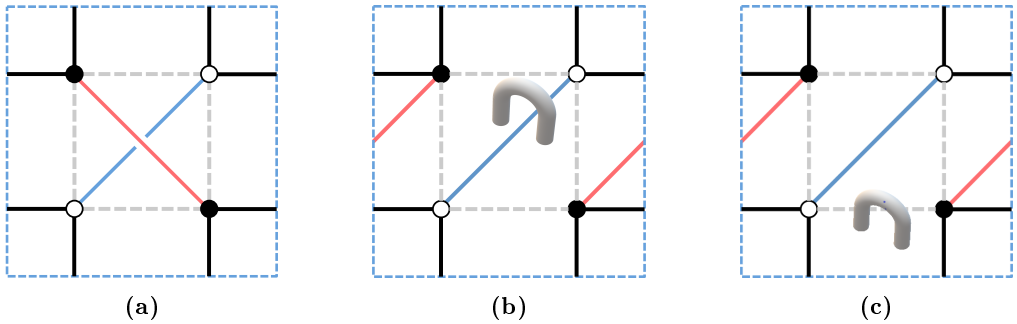

Figure 5.18: a) Application of the local recipe of the backreaction for an instanton on face 1 of F_0. b) It produces a theory identical to the correct (global) backreaction, with an additional spurious handle. c) By a continuous deformation, the spurious handle manifestly connects the face to itself, showing it is not a consistent tiling.

"faces" are not disks but rather correspond to cylinders or other topologies. In particular, they contain non-trivial cycles precisely defined by exploiting the global identifications, as we now show.

As an example, consider an instanon on a square face with opposite edges separating it from a given *same* face and let us apply the instanton backreaction using the local recipe. The local identification leads to a non-contractible cycle along the redundant handle, as shown in Figure 5.17.a. This cycle precisely specifies where the bridge must be, instead of through a spurious handle. Instead, if the correct global prescription is implemented, there is no non-contractible cycle, as shown in Figure 5.17.b.

This non-contractible cycle indicates that two faces are identified by the additional handle. For instance, in the dP_1 example presented in Figure 5.16, the local recipe produces an additional handle as shown in Figure 5.17.c. This handle connects face 1 and 2, supports a non-contractible cycle and spoils the tiling.

Similar comments apply to the case of the F_0 theory, for which the correct global recipe for backreaction was implemented in Figure 5.11. The only subtlety is that the local recipe, shown in Figure 5.18.a would seem to produce the correct theory, but there is still a spurious handle, so it does not define a proper BFT, see Figure 5.18.b. By moving one of the legs off the bridge, the spurious handle manifestly connects the face to itself, as shown in Figure 5.18.c.

We conclude by emphasizing that there is an unambiguous recipe for backreaction on the dimer, described in Section 5.1.1, namely removal of edges and recombination of nodes in the most economic way. In the generic case where the instanton has no repeated neighboring faces, this agrees with the local recipe, which therefore provides a simple surgery prescription for the generic theory. In most of the remainder of this chapter, we focus on this generic situation.

5.1.4 Extension to General BFTs

In the previous section we introduced a graphic implementation of the backreaction of a D-brane instanton on a face of a dimer. It is natural to extend this operation to the case in which the starting point is a general BFT, i.e. with arbitrary genus and number of boundaries. Physically, the initial BFT might be the result of backreacting additional instantons, which would change the genus, with boundaries, if present, generated by flavor D7-branes along the lines of [35]. At this point, it is unknown whether all BFTs can be obtained by this procedure. This is an interesting question that we postpone for future work.

Regardless of whether this operation can always be associated to a D-brane instanton, it is interesting to add it to the list of basic transformations that act on general BFTs, together with the condensation of 2-valent nodes, the square move and bubble reduction (see [34] and references therein for detailed discussions of these operations and their physical interpretation). In particular, it would be interesting to study its effect in the diverse applications of BFTs, e.g. in the context of scattering amplitudes, where the bipartite graphs are interpreted as on-shell diagrams [34, 169, 174, 175, 179–181].

Figure 5.19 illustrates this operation for a BFT on a disk. The initial graph is *reducible*, namely it is possible to decrease the number of internal faces by a combination of square moves and bubble reductions [34, 169]. The resulting non-planarity is reminiscent to the one that is necessary to capture the full matroid stratification of the Grassmannian in terms of on-shell diagrams, as discussed in [174].

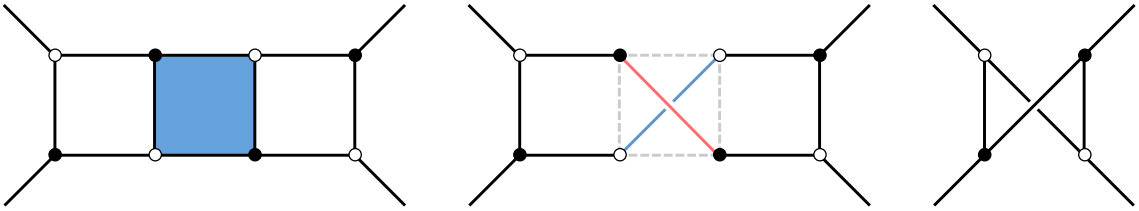

Figure 5.19: Instanton backreaction for a general BFT on a disk, which is left implicit in the figure.

5.1.5 BFT Genus and Instanton Backreaction

Let us try to understand the change in genus on the BFT side in more detail, in the generic case with no global identifications. The discussion below builds on and extends Section 5.1.1. It is phrased in a way that it easily applies to instantons on a $2k$-sided face of the tiling, for general k. For concreteness, we will focus on a $k = 4$ example.

Figure 5.20 shows the backreaction of the instanton on the dimer. This is the $k = 4$ analogue of Figures 5.1 and 5.2. The face disappears and the nodes at its corners are recombined. This can be achieved by introducing $k - 1$ bridges between white nodes (shown in blue) and $k - 1$ bridges between black nodes (shown in red). We label the bridges to facilitate their identification.

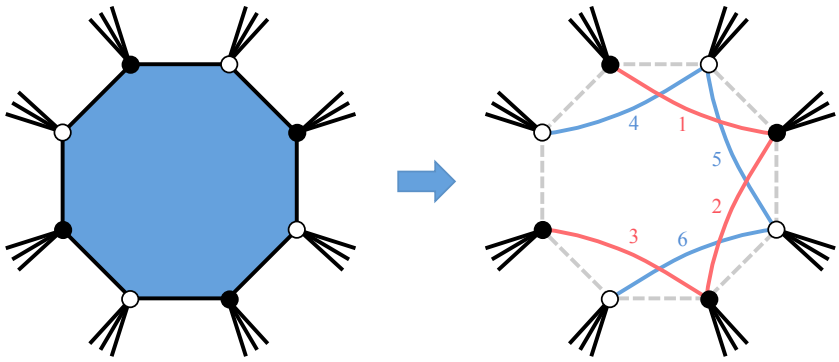

Figure 5.20: Backreaction of an instanton on an octagonal face of the dimer, i.e. $k = 4$.

According to our earlier discussion, in the generic case the genus of the BFT Riemann surface changes by $\Delta g = k-1$. We now device a simple graphical representation that makes the topology of the extra handles manifest.

We can think about the change in the Riemann surface as the result of cutting a hole on the original surface and gluing to it a genus $k-1$ "handle" with an identical hole.[2] The new edges associated with the bridges responsible for recombining the corners of the instanton face are the only ones living on the handle. The rest of the bipartite graph remains on the original Riemann surface.

Figure 5.21 shows the change in the Riemann surface for $k = 4$. Figure 5.21 should be interpreted as follows.

- The green dashed loop indicates the cut at which the handle is glued to the Riemann surface. It is very natural to place this cut at the boundary of the original face.
- A genus g Riemann surface can be represented by a $4g$-gon with pairwise identification of edges. Each of this pairs corresponds to one of the $2g$ fundamental cycles. In Figure 5.21, the handle has genus 3, so it is presented by the 12-sided dashed purple polygon. This handle has a hole, whose boundary is the green loop, along which it is glued to the original Riemann surface.
- As shown in Figure 5.21, each of the fundamental cycles is used exclusively by one of the new bridges. Thus it is natural to label the corresponding pair of sides in the $4g$-gon with the same name of the corresponding bridge. These labels are shown in purple in the figure. It becomes clear how this configuration avoids crossings between bridges and how it is generalized to arbitrary k.
- The fact that each fundamental cycle is used by a single bridge makes the computation of the toric diagram for the new BFT straightforward, as we will explain in the coming section.

[2] For brevity, we will use the term handle even for genus greater than 1.

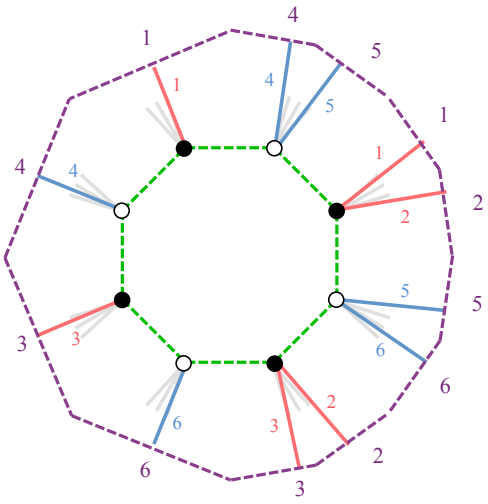

Figure 5.21: Change in the Riemann surface by gluing a $\Delta g = k - 1 = 3$ handle.

Figure 5.22 is identical to Figure 5.21, but shows the original Riemann surface and the handle, both with matching holes, separately.

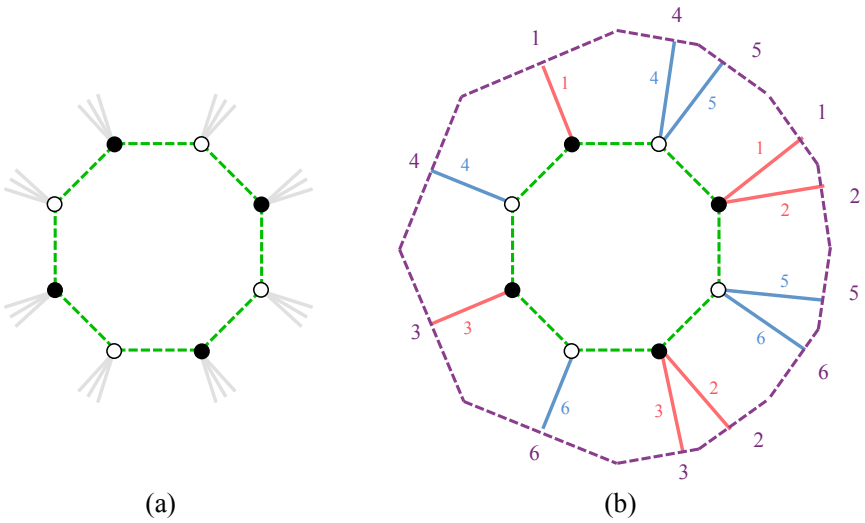

Figure 5.22: a) Part of the dimer that remains on the original Riemann surface. b) The new edges live on the genus $k-1=3$ handle. Both surfaces have matching holes. They are glued along the boundaries, which are shown in green.

5.2 The Toric Geometry of Backreacted Dimers

Since the backreacted theory is a BFT, its moduli space of vacua is a toric CY. This geometry encodes important information about the gauge theory. Following the general discussion in [34], the moduli space of a genus g BFT is a CY $(2g+1)$-fold, which has a

$2g$-dimensional toric diagram.[3] Points in the toric diagram correspond to (collections of) perfect matchings of the bipartite graph.

It is certainly straightforward to directly determine the toric diagram for the resulting BFT (see e.g. [34]). However, it is instructive to understand how the new toric CY relates to the original one. Below we do this in two steps: we first find the perfect matchings of the final theory and then we determine their positions in the toric diagram.

5.2.1 Perfect Matchings

In order to identify the new perfect matchings, it is convenient to condense all the bridges, i.e. the corresponding 2-valent nodes. We will later reintroduce them to determine the final toric diagram.

Let us decompose every perfect matching as $p_\mu = p_\mu^{int} + p_\mu^{ext}$, where p_μ^{int} contains the edges in p_μ that belong to the instanton face, while p_μ^{ext} contains all the other edges. After backreacting the instanton and integrating out bridges, all internal edges disappear and $p_\mu \to p_\mu^{ext}$. Below we will study the conditions under which p_μ^{ext} is a perfect matching of the backreacted dimer. It is important to remark that since only external edges survive backreaction, the p_μ^{ext}'s contain all possible perfect matchings of the final theory.

Removed perfect matchings. We refer to the perfect matchings that do not survive this process as *removed perfect matchings*. It is possible to identify them as follows.

Condensing all bridges, the number of superpotential terms is reduced by $(2k-2)$. Consequently, the number of edges in a perfect matching is reduced by $(k-1)$. Since all surviving edges are external to the instanton face and the exterior content of the perfect matching remains unchanged, we conclude that this change must correspond to internal edges in the perfect matching. Denoting the number of internal edges in p_μ as $E(p_\mu^{int})$, we conclude that iff

$$E(p_\mu^{int}) \neq k-1 \tag{5.6}$$

the perfect matching is removed, i.e. p_μ^{ext} is not a perfect matching after backreaction.

It is straightforward to show that an equivalent condition is that perfect matchings are removed iff p_μ^{ext} contains more than one corner of the instanton face of a given color. In such a case, p_μ^{ext} is not a perfect matching after corner identification, since it contains more than one edge terminating on some of the nodes.

5.2.2 The New Toric Diagram

In order to assign coordinates in the toric diagram to the surviving perfect matchings, it is convenient to reintroduce the bridges, i.e. to integrate in the corresponding massive pairs of edges.[4] Our prescription will generate coordinates in $\mathbb{Z}^{2g}$.

For concreteness, let us assume we start from a dimer, i.e. from a BFT on $\mathbb{T}^2$.[5] By convention, we will identify the first two coordinates with those in the original toric

[3] Here we assume the BFT has no boundaries. It is straightforward to incorporate them to our discussion.

[4] Of course, as already mentioned, it is also possible to directly find these coordinates, without introducing the bridges [34].

[5] In the absence of global identifications, the new BFT has genus $g = 1 + \Delta g = k$, and the toric diagram lives in $\mathbb{Z}^{2k}$.

diagram. They remain unchanged, provided that the instanton face does not intersect the boundaries of the original unit cell. If the parent dimer is sufficiently large, it is always possible to define the unit cell to avoid such crossings. This condition is satisfied in all the explicit examples that we consider below. The remaining $2\Delta g$ coordinates are related to the new cycles introduced with the handle, as discussed in Section 5.1.5.

After reintroducing the bridges, we complete every surviving p_μ^{ext} into a perfect matching. This completion is unique. Given such a completion, there are two standard approaches for establishing its position in the toric diagram, as detailed in Section 2.4.2:

- Method 1: each coordinate is given by the net intersection number between the edges in the perfect matching, counted with orientation, and the corresponding cycle.[6]
- Method 2: perfect matchings are mapped to oriented cycles by subtracting an arbitrary reference perfect matching. Coordinates correspond to winding numbers of the resulting cycles or, equivalently, to the monodromies of the height function.

In the coming section, we will illustrate both of them in an explicit example. In practice, the first approach is typically simpler to implement.

Figure 5.23 shows an example for phase 1 of dP_3. The instanton is located at the top-left face, which is a square, so it has $k = 2$. In Figure 5.23.a, we show the original perfect matching under consideration. It survives in the final BFT because it satisfies the condition that the number of edges in p_μ^{int} is equal to $k - 1 = 1$. In Figure 5.23.b we add the bridges and the corresponding edges to form a perfect matching. In Figure 5.23.c, we implement the backreaction of the Riemann surface using the approach outlined in Section 5.1.5, introducing the genus $k - 1 = 1$ handle.[7] We determine the corresponding coordinates in the toric diagram from the intersections between the perfect matching and the various fundamental cycles.

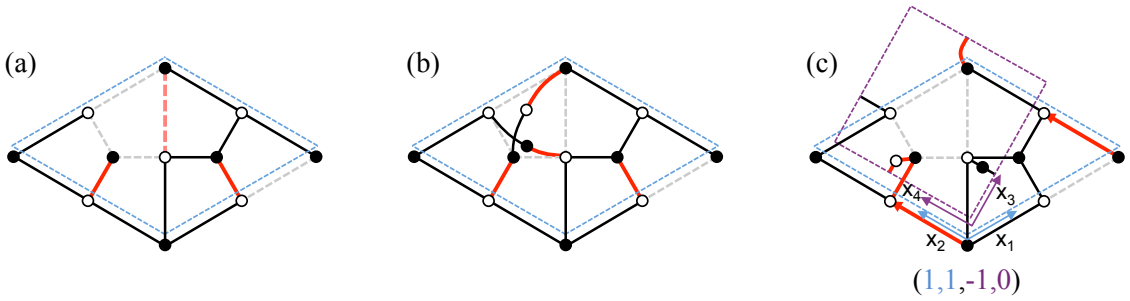

Figure 5.23: An example in phase 1 of dP_3. a) The original perfect matching. b) Backreaction including bridges. c) Explicit introduction of the corresponding genus 1 handle.

5.2.3 Coordinates from Bridges

We discussed a detailed visualization of the new genus $(k-1)$ handle in terms of a $4(k-1)$-gon and explained how to use this construction for determining the new coordinates

[6] By convention, we orient edges in the graph from white to black nodes.

[7] For genus 1 handles, we label the boundaries of the handle's fundamental domain according to the transverse axes. For $k > 2$ it is convenient to label them according to the corresponding bridges, as in Figure 5.22.

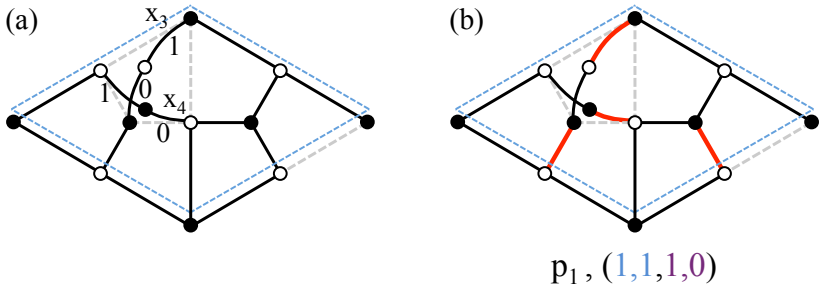

Figure 5.24: a) Prescription for assigning new coordinates to the edges on the bridges. b) The perfect matching of Figure 5.23 and the resulting coordinates.

of perfect matchings. It is however desirable to introduce a simpler prescription in which the coordinates can be directly read from the bridges. This is straightforward, since bridges are in one-to-one correspondence with the new cycles/coordinates. To do so, we draw bridges with the intermediate 2-valent nodes. By convention, we associate 0 and 1 contributions to the corresponding coordinate to the two edges on each bridge. It is always possible to avoid (-1) contributions, which can certainly be generated by the prescription introduced in the previous section, by an appropriate choice of the relative position of the middle point of bridges with respect to the corresponding boundaries of the fundamental domain of the handle. Equivalently, this simply translates into a choice of the positive direction for each of the cycles. In Figure 5.24 we illustrate this rule for the example in Figure 5.23.

The fact that new coordinates can only take values 0 and 1 constraints the BFTs that can be generated by instantons. In particular, we cannot obtain BFTs with toric diagrams that are "too wide" in more than two directions (the ones for the original dimer). This argument applies even for multiple instantons.

5.2.4 Example: dP_3

We now illustrate the ideas introduced in the previous section in an explicit example. Let us consider phase 1 of dP_3. Figure 5.25 presents the perfect matchings for this theory and their positions in the toric diagram, computed from their intersections with the boundaries of the unit cell. We also identify the removed perfect matchings with a cross. In this case, perfect matchings for all points in the original toric diagram survive.[8] However, different perfect matchings for a given point, in this case p_7 and p_8, have different lifts.

[8] Generically, however, there can be cases in which all the perfect matchings for a given point in the original toric diagram disappear.

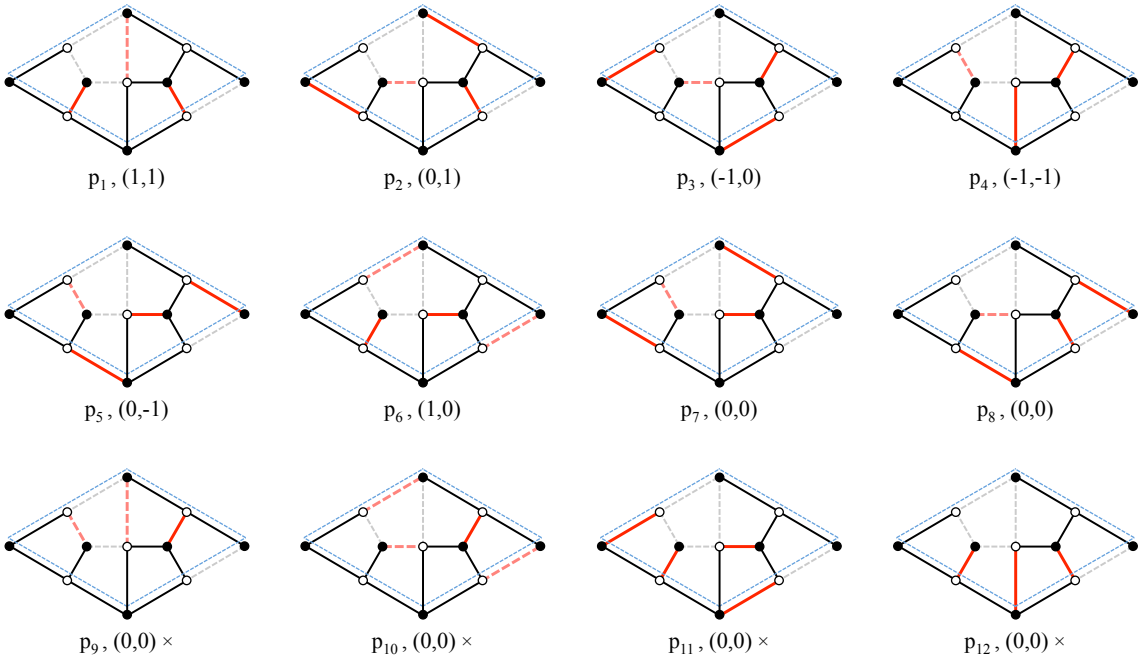

Figure 5.25: The 12 perfect matchings for phase 1 of dP_3.

Figure 5.26 presents the surviving perfect matchings, $p_1, \ldots, p_8$, in the backreacted dimer. This example illustrates how to proceed in general: in order to complete perfect matchings we must include edges on the bridges, which in turn determine the new coordinates in the final toric diagram.

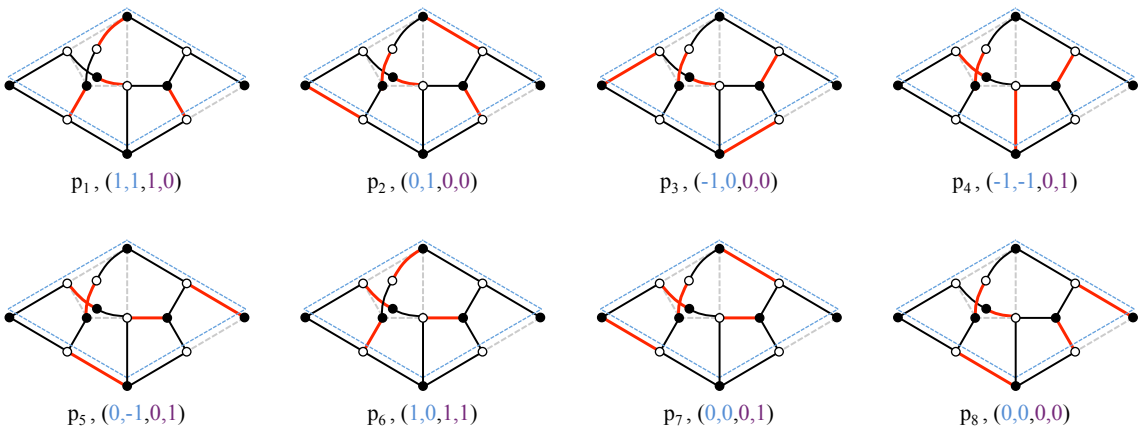

Figure 5.26: Surviving perfect matchings. The new coordinates are determined by the edge content on the bridges, using the convention in Figure 5.24.

The same perfect matchings are presented in Figure 5.27, this time explicitly showing the $k - 1 = 1$ handle in purple.

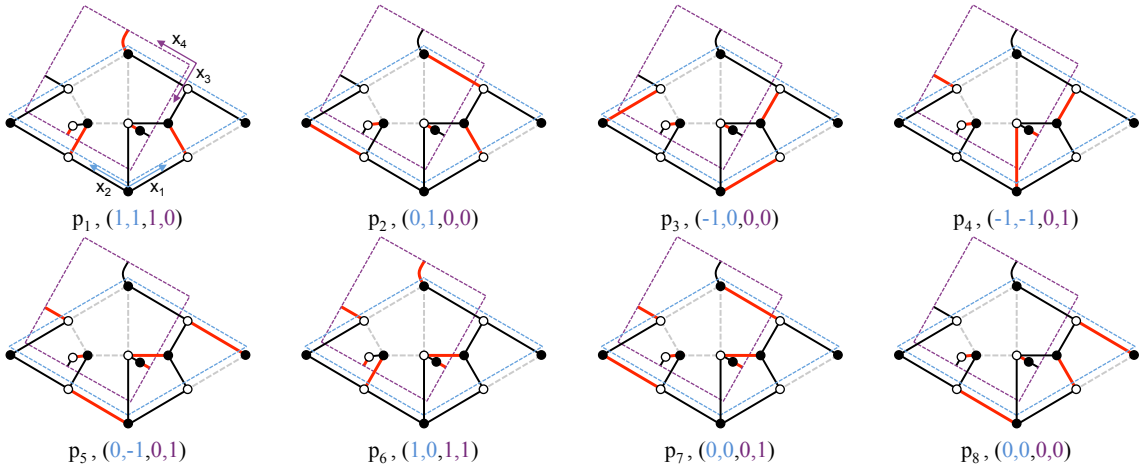

Figure 5.27: Surviving perfect matchings with the bridges and the genus 1 handle.

In Figure 5.28 we map the perfect matchings to cycles, using p_8 as reference. Since the coordinates for p_8 are $(0,0,0,0)$, the winding numbers agree with the coordinates previously computed from the intersection numbers. Otherwise, they would simply differ by a constant shift, given by the coordinates of the reference perfect matching.

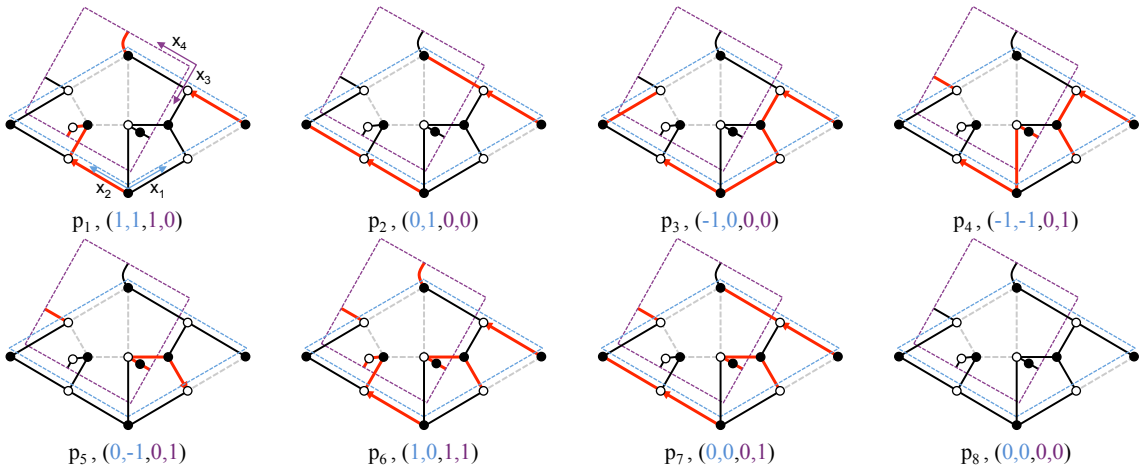

Figure 5.28: Cycles for the surviving perfect matchings using p_8 as reference.

The resulting toric diagram is given by the following matrix

$$\left(\begin{array}{cccccccc} p_1 & p_2 & p_3 & p_4 & p_5 & p_6 & p_7 & p_8 \\ \hline 1 & 0 & -1 & -1 & 0 & 1 & 0 & 0 \\ 1 & 1 & 0 & -1 & -1 & 0 & 0 & 0 \\ 1 & 0 & 0 & 0 & 0 & 1 & 0 & 0 \\ 0 & 0 & 0 & 1 & 1 & 1 & 1 & 0 \end{array}\right) \rightarrow \left(\begin{array}{cccccccc} p_1 & p_2 & p_3 & p_4 & p_5 & p_6 & p_7 & p_8 \\ \hline 1 & 0 & 0 & 0 & 0 & 1 & 0 & 0 \\ 0 & 1 & 0 & 0 & 0 & 0 & 1 & 0 \\ 0 & 0 & 1 & 0 & -1 & -1 & -1 & 0 \\ 0 & 0 & 0 & 1 & 1 & 1 & 1 & 0 \end{array}\right), \tag{5.7}$$

where on the right hand side we have row-reduced it to give it a simpler form and verify that all coordinates are indeed independent. We conclude the toric diagram is $4d$, i.e. it corresponds to a CY 5-fold.

5.3 Seiberg Duality

Seiberg duality, reviewed in Section 2.1.4, admits a simple graphical implementation for BFTs (see [182] for the original discussion for dimers and [34, 163] for general BFTs). More precisely, Seiberg duality acting on a gauge group associated to a 4-sided face of a BFT corresponds to the so-called *square move*, which is shown in Figure 5.29, and generates a new theory which is also of BFT type.[9] It is natural to investigate the interplay between Seiberg duality and instanton backreaction. There are three distinct possibilities, depending on whether Seiberg duality acts on:

a) The instanton face. Since we do not wrap regular D-branes on the face occupied by an instanton, there is no corresponding gauge group. By Seiberg dualizing the instanton face, we mean performing a square move on it.

b) A face that is adjacent to the instanton one, i.e. which have some common edge(s) with it.

c) A non-adjacent face.

Below we discuss the first two possibilities, comparing the results of backreaction in the original and in the Seiberg dual theories. Case (c) is straightforward: since both instanton backreaction and Seiberg duality are local operations in the BFT that at most affect neighboring faces, it is clear that the two operations commute in this case.

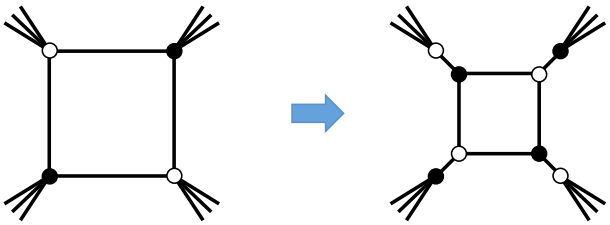

Figure 5.29: Square move implementing Seiberg duality on a 4-sided face of a BFT.

5.3.1 Seiberg Duality on the Instanton Face

Consider a theory with an instanton on a 4-sided face producing a (possibly higher genus) BFT via its backreaction, as illustrated in Figure 5.30. (a) and (b) show the backreaction from the BFT perspective. (c) and (d) show the same process from the mirror viewpoint.

Let us now compare it with the theory obtained by first Seiberg dualizing the node on which the instanton sits and then backreacting the instanton. This process is shown in Figure 5.31. The result is the same as the one obtained by backreacting the instanton on the original theory. From the BFT point of view, we see that Figure 5.31.c is identical to Figure 5.30.b. The field theory analysis is straightforward and can be directly inferred from the bipartite graph, so we skip it.

[9] Acting with Seiberg duality on a face with more than 4 sides leads to a dual theory that is not a BFT, namely that is not described by a bipartite graph. While we will not consider this possibility in this thesis, it is perfectly fine and interesting from a physical standpoint.

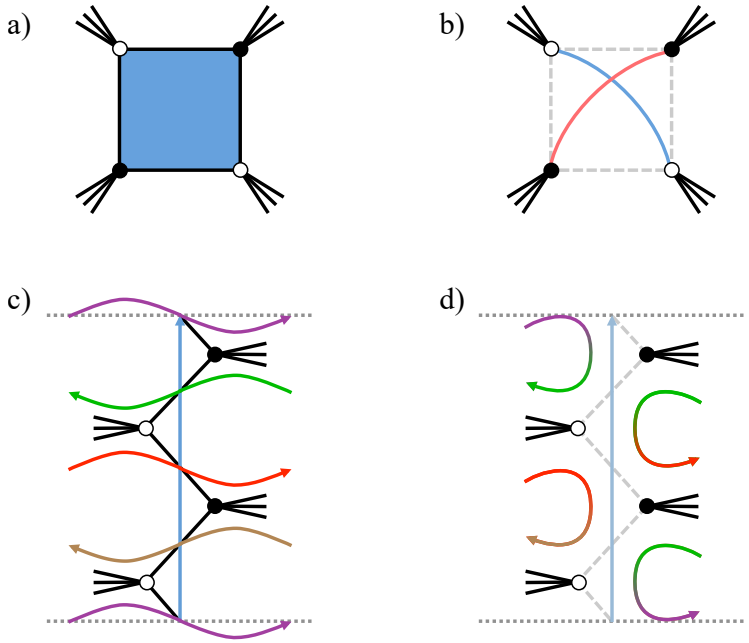

Figure 5.30: a) Local piece of a BFT with an instanton on a 4-sided face. b) Backreacted BFT, with the identification of corner nodes indicated by bridges. c) The initial configuration in the mirror. The instanton wraps the length 4 blue 1-cycle. d) Effect of backreaction in the mirror.

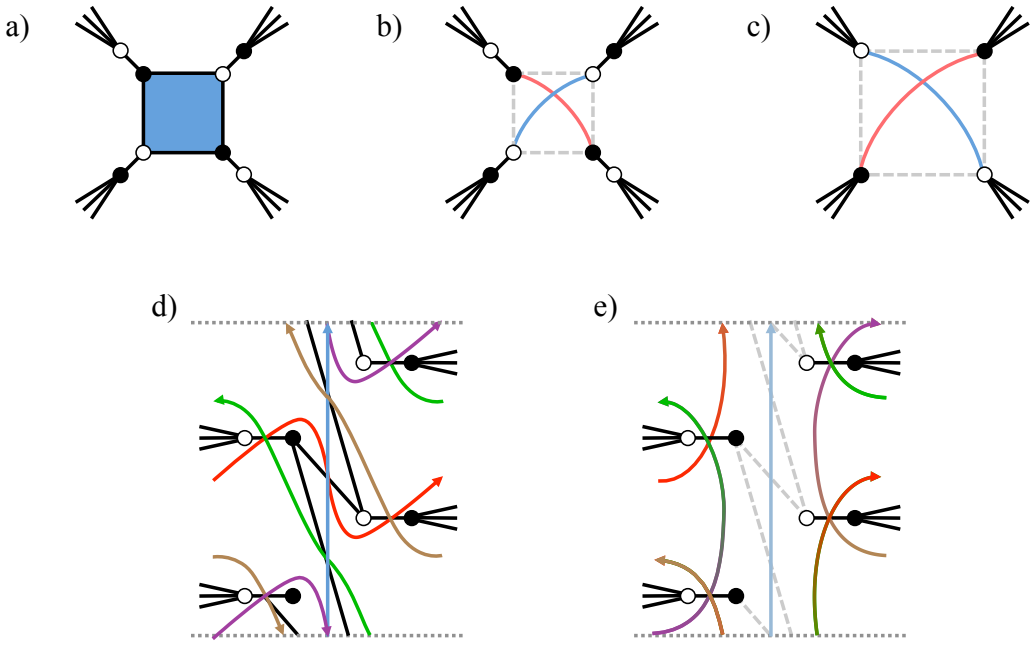

Figure 5.31: a) Seiberg dual of the local configuration in Figure 5.30.a. b) Backreacted BFT, with the identification of corner nodes indicated by bridges. c) After integrating out massive fields we obtain Figure 5.30.b. d) The Seiberg dual configuration in the mirror. The instanton wraps the length 4 blue 1-cycle. e) Effect of backreaction in the mirror.

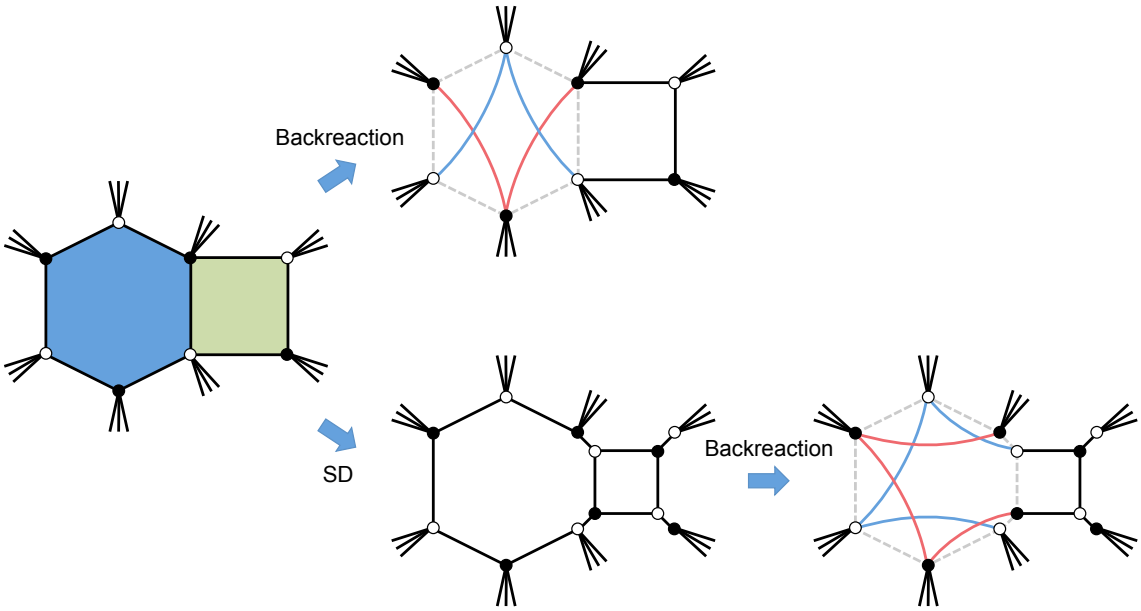

Figure 5.32: Seiberg duality on a face (green) adjacent to a D-brane instanton (blue). On the first row we show the instanton backreaction on the original theory. On the second row, we first apply Seiberg duality and then backreact the face originally occupied by the instanton.

5.3.2 Seiberg Duality on an Adjacent Face

Let us now consider Seiberg dualizing a face that is adjacent to the one with an instanton, as illustrated in Figure 5.32. We indicate the dualized and instanton faces in green and blue, respectively. We restrict the green face to be a square, so that we remain within the BFT class of theories. The instanton face can have an arbitrary number of edges. Without loss of generality, we take it to be an hexagon in this example.

On the first row of Figure 5.32, we backreact the instanton on the original BFT. On the second row, instead, we Seiberg dualize the green face before backreacting the instanton. More specifically, what we mean by this is that in the Seiberg dual we backreact an instanton that occupies the same face as the original one. In Section 5.3.2.3 we will elaborate on the relation between the cycles wrapped by the instantons in both theories. While the details of the final result are example dependent and not so important, a lesson from Figure 5.32 is that these two procedures generically lead to different BFTs. As illustrated below in an example, such BFTs are in general not even Seiberg dual.

5.3.2.1 Different Results: dP_2

We first consider an example in which, as generically expected, the two operations produce different BFTs. Figure 5.33 shows the toric diagram for dP_2 and the quivers for its two toric phases.

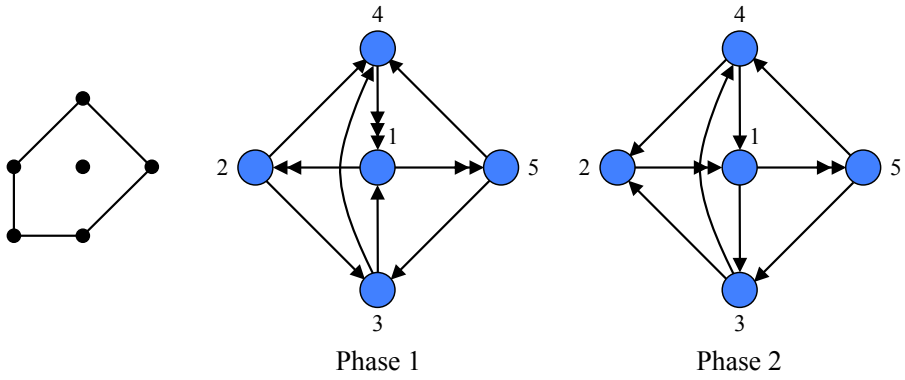

Figure 5.33: Toric diagram for dP_2 and quivers for its two toric phases. The two phases are connected by Seiberg duality on node 2.

Let us start from phase 2, whose dimer is shown in Figure 5.34. We will consider an instanton on node 4 (blue) and Seiberg duality on node 2 (green). Notice that these two faces are adjacent once the periodicity of $\mathbb{T}^2$ is taken into account. Below we study carefully what happens when these two operations are implemented in different orders.

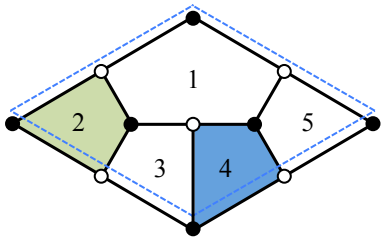

Figure 5.34: Phase 2 of dP_2. We will consider an instanton on face 4 (blue) and Seiberg duality on face 2 (green).

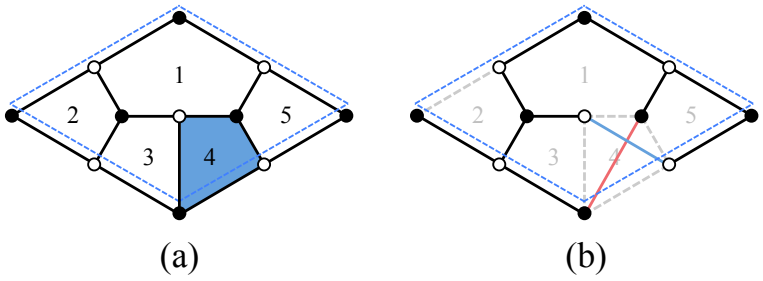

Figure 5.35: Backreaction of an instanton on face 4 of phase 2 of dP_2.

Backreaction First. Let us first backreact the instanton on face 4. The result is shown in Figure 5.35.b

It is impossible to avoid the crossing of bridges and we have $\Delta g = 1$. It is a rather straightforward, albeit tedious, exercise to explicitly embed the final BFT into a genus 2

Riemann surface. This is not very illuminating, so let us exploit the information at hand. After integrating out massive fields in Figure 5.35.b we are left with 4 nodes and 7 edges. Combined with the knowledge that this is a genus 2 BFT, we conclude it has a single face. The 5 faces of the original theory get combined into a single one wrapped over the genus 2 Riemann surface. The corresponding quiver consists of a single gauge group and 7 chirals transforming in the adjoint representation, as shown in Figure 5.36. Its superpotential can be read from the bipartite graph and contains two cubic and two quartic terms. This theory is Model 7.4 in the classification of [167].

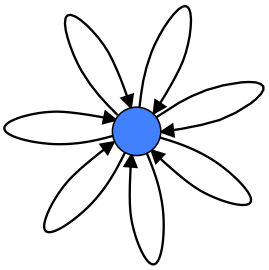

Figure 5.36: Quiver for the genus 2 BFT obtained by backreacting an instanton on face 4 of phase 2 of dP_2.

Seiberg Duality First. Starting from phase 2 of dP_2 and acting with Seiberg duality on node 2 first, we obtain phase 1, whose quiver is shown in Figure 5.33.

The corresponding dimer, with an instanton on face 4, is presented in Figure 5.37 (a). The instanton backreaction is shown in (b). Face 4 has six sides, i.e. $k = 3$, so we would naively expect the genus of the BFT to change by $\Delta g = 2$. Interestingly, as shown in the figure, global identifications make it possible to pick bridges such that there are no crossings. As a result, we obtain a new genus 1 BFT. Integrating out massive chiral fields and rearranging the graph, we obtain (c), which is the dimer model for the suspended pinch point (SPP) [182]. The quiver and toric diagram for the SPP are shown in Figure 5.38.

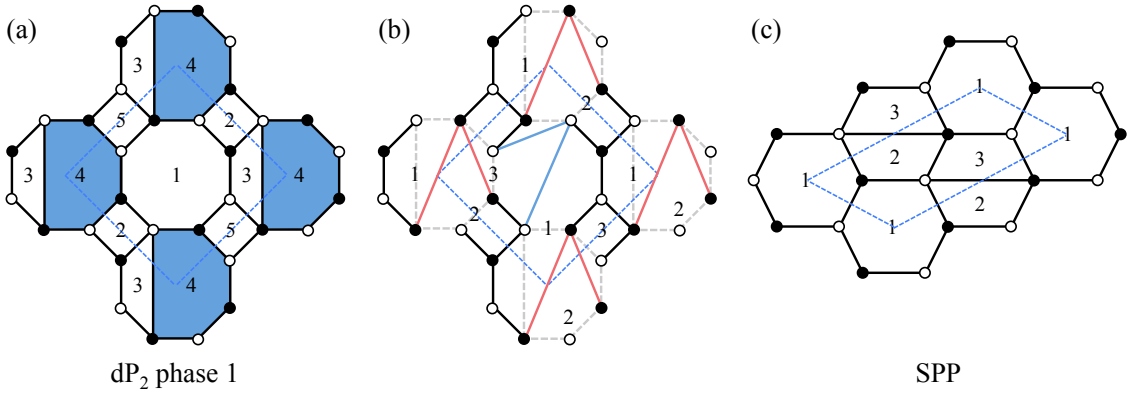

Figure 5.37: Instanton backreaction from phase 1 of dP_2 to SPP.

It is clear that this theory is different from the one obtained by backreacting the

instanton first. In fact it is not even Seiberg dual to it, since the number of gauge groups, BFT genus and moduli space (even its dimension) are different.

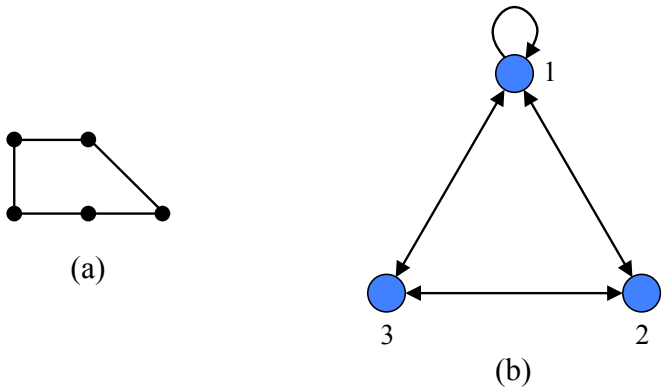

Figure 5.38: a) Toric diagram and b) quiver for the SPP.

5.3.2.2 Same Result: F_0

While generically backreaction in the original and the Seiberg dual theories do not lead to the same BFT, this can occur in simple models. This is the case for F_0, as we now explain. As shown in Figure 5.39, we will start from phase 1 and consider an instanton on face 1 and Seiberg duality on face 4. Backreaction of the instanton leads to the conifold, as discussed in Section 5.1.3.1 and summarized in the top row of the figure. Dualizing face 4 first, we obtain phase 2 of F_0. In this case, backreaction of the instanton on face 1 also leads to the conifold.

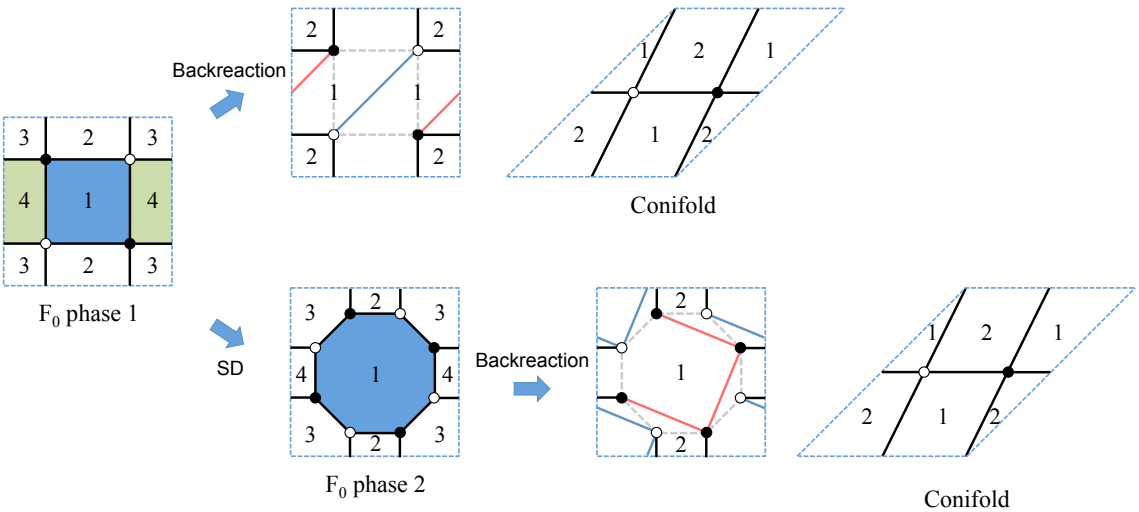

Figure 5.39: Starting from phase 1 of F_0, we compare the backreaction of an instanton on face 1 before and after Seiberg duality on the adjacent face 4.

5.3.2.3 Seiberg Duality and D-brane Charges

We can understand in further detail why instanton backreaction and Seiberg duality on an adjacent face generically do not commute by considering how Seiberg duality transforms the cycles wrapped by different stack of D-branes or, equivalently, their D-brane charges.

Figure 5.40 shows the local configuration we are interested in. Seiberg duality will act on face a. The four adjacent faces are labeled b, c d and e, with the D-brane instanton located on face e. We also explicitly show the arrows representing the bifundamental chiral fields connecting a to the four adjacent faces. Without loss of generality, we assume that the chiral field connecting a and e goes from a to e.[10]

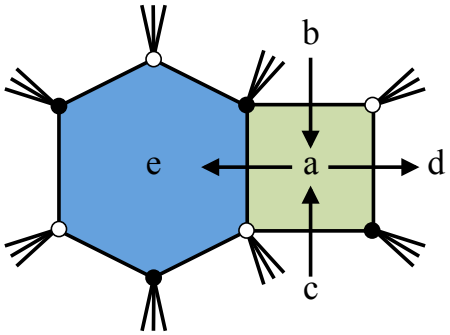

Figure 5.40: Local configuration showing a face to be Seiberg dualized (green) which is adjacent to a D-brane instanton (blue).

The intersection numbers between branes indicate the number of arrows connecting them, with their orientation determined by the sign. In this case, we have

$$\begin{array}{rclcrcl} ([b]\cdot[a]) & = & 1 & & ([d]\cdot[a]) & = & -1 \\ ([c]\cdot[a]) & = & 1 & & ([e]\cdot[a]) & = & -1 \end{array} \tag{5.8}$$

Acting with Seiberg duality on $[a]$, the different branes transform as follows (see e.g. [183, 184]):

$$\begin{array}{rcl} [a'] & = & -[a] \\ [b'] & = & [b] + ([b]\cdot[a])\,[a] = [b] + [a] \\ [c'] & = & [c] + ([c]\cdot[a])\,[a] = [c] + [a] \\ [d'] & = & [d] \\ [e'] & = & [e] \end{array} \tag{5.9}$$

The orientation of the brane for the dualized gauge group is reversed. The branes connected to incoming flavors pick a contribution proportional to $[a]$ and the relative intersection numbers. Finally, the branes connected to outgoing flavors remain unchanged. In particular, the instanton $[e]$ is invariant.[11]

[10] As usual, the orientation of all the arrows can be inverted by flipping the convention for fundamental and antifundamental representations.

[11] In the convention that inverts all the arrows in the quiver, the roles of (b, c) and (d, e) are exchanged. In particular, d and e are transformed while b and c stay the same. The final results are independent of this choice.

Let us now consider the new intersection numbers between the instanton and other D-branes. From (5.9),

$$([e'] \cdot [a']) = -([e] \cdot [a]) \tag{5.10}$$

and

$$\begin{array}{rcccl} ([e'] \cdot [b']) & = & ([e] \cdot [b]) + ([e] \cdot [a]) & = & ([e] \cdot [b]) - 1 \\ ([e'] \cdot [c']) & = & ([e] \cdot [c]) + ([e] \cdot [a]) & = & ([e] \cdot [c]) - 1 \end{array} \tag{5.11}$$

As a consequence of these new intersections, the instanton on the dual theory breaks a different $U(1)$ subgroup of the global symmetry. Hence, as expected, after introducing the instanton generated field theory operator we do not obtain the Seiberg dual of the original theory plus instanton.

5.4 Multi-Instantons and Complex Deformations

Our previous discussion has focused on the case of single instantons, namely those associated to a single face in the original theory. Although the discussion of the richer class of general multiple instantons is left for future work, we would now like to delve into a particularly interesting class, corresponding to (generically) multiple instantons triggering complex deformations of the original geometry.

The effect of backreaction is to pinch off the cycle in the mirror Riemann surface Σ wrapped by the D-brane instanton, which in turn triggers the recombination of the D-branes that intersect it. Interestingly, it is sometimes possible to wrap the instanton on a cycle such that shrinking it to zero size splits Σ into two disconnected components Σ_1 and Σ_2.[12]

Since backreaction preserves the original punctures, whenever such decomposition occurs, the punctures get distributed between Σ_1 and Σ_2. The mirror Riemann surface corresponds to thickening the (p,q)-web dual to the toric diagram. Hence, the $\Sigma \to \Sigma_1 + \Sigma_2$ splitting corresponds to decomposing the web into two subwebs in equilibrium, i.e. webs for which the (p,q) charges of external legs sum up to zero, as described in Section 2.5.

These deformations can be triggered by deformation fractional branes and, as shown in Chapter 4 can also be triggered by wrapping D-brane instantons over the corresponding cycle. Equivalently, this corresponds to locating the instanton on the faces of the dimer associated to the fractional branes. This is perhaps not surprising, since D-brane instanton effects in various CY 3-folds can be understood as the IR dynamics of theories with duality cascades generated by fractional branes [156, 158, 159].

In order to illustrate these ideas, let us again consider the complex deformations of dP_3, already discussed from the mirror perspective in Section 4.4.1. Here we discuss how they are captured by implementing instanton backreaction directly at the level of the dimer. This geometry admits two such deformations, corresponding to the two subwebs in equilibrium in Figure 5.41, which we recover here for convenience.

It would be interesting to investigate whether D-brane instantons that start from BFTs of genus different from 1 can lead to similar deformations of the corresponding toric CYs.

[12] This is the simplest possibility. Splitting Σ into more components is also possible.

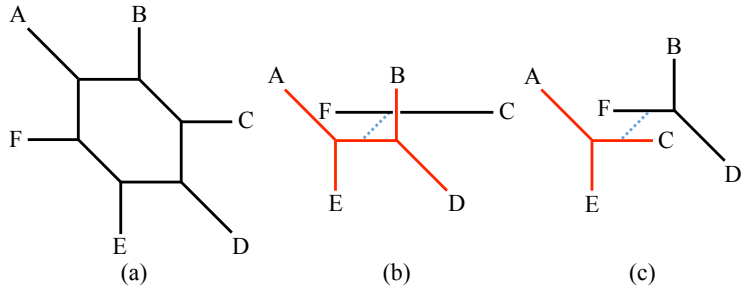

Figure 5.41: Web diagrams of the two possible complex deformations of dP_3. The dashed segments indicate S^3's.

From dP_3 to the Conifold

Let us first consider the deformation in Figure 5.41.b, that goes from dP_3 to the conifold. Figure 5.42 goes through the process step by step. In order to achieve this deformation, the D-brane instanton must wrap a cycle that covers faces 2 and 5 of the dimer, as shown in (a). The instanton backreaction is shown in (b). Interestingly, the blue bridges form a "necklace" that is disconnected from the rest of the graph and that disappears at low energies since it consists entirely of massive fields. Removing the blue bridges we obtain (c). After integrating out the massive fields in the red bridges, we obtain (d), which is the dimer for the conifold.

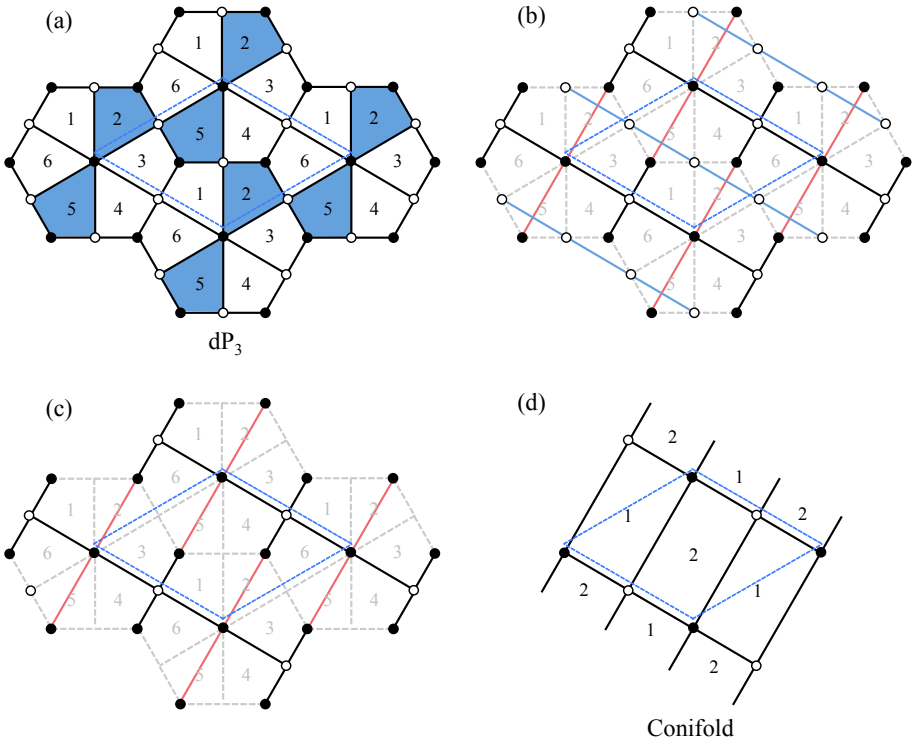

Figure 5.42: Instanton backreaction from phase 1 of dP_3 to the conifold.

From dP_3 to $\mathbb{C}^3$

We now consider the deformation from dP_3 to $\mathbb{C}^3$ of Figure 5.41.c. In this case, the instanton must be placed on faces 2, 4 and 6 as shown in (a). The backreaction is presented in (b). The red bridges form a hexagonal lattice of massive fields, which is decoupled from the rest of the graph and disappears at low energies, leaving the configuration in (c). Blue bridges form triangles that collapse into single white nodes when massive fields are integrated out. The final result (d) is the dimer for $\mathbb{C}^3$.

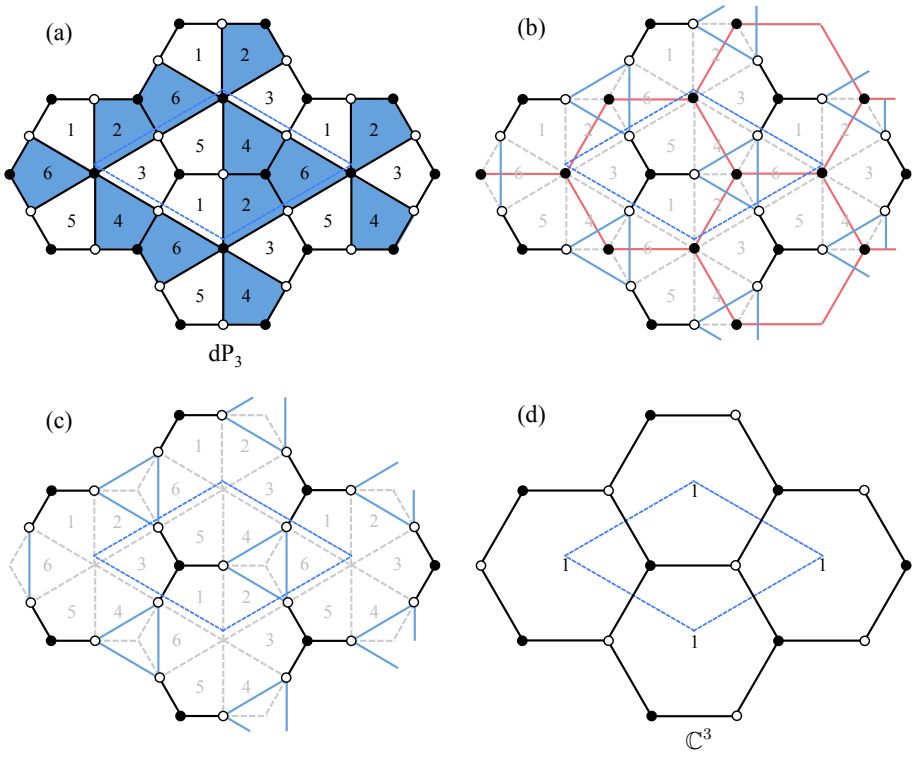

Figure 5.43: Instanton backreaction from phase 1 of dP_3 to $\mathbb{C}^3$.

5.5 The Inverse Problem

We have seen that starting from a BFT and a choice of instanton we generate a second BFT. It is interesting to consider the *inverse problem*, namely: given a BFT and assuming it arises from an instanton backreaction on a parent BFT, can we reconstruct the latter? In general, two different BFTs with two different instantons can produce the same BFT upon backreaction.[13] The underlying toric geometries can be used as a guide, following the transformation of the toric diagrams discussed in Section 5.2. Below we present an explicit example, in which the same BFT is obtained in two different ways.

[13] For simplicity, we restrict to single instantons. Our discussion extends straightforwardly to multi-instantons and even theories with different numbers of instantons.

dP_2 to SPP

Let us first consider phase 2 of dP_2, which we already discussed in the previous section. Its toric diagram and quiver were given in Figure 5.33. Let us now consider an instanton on face 2, as shown in Figure 5.44.a. The backreaction of this instanton is presented in Figure 5.44.b, where we have eliminated the instanton face, added the bridges and given new labels to the resulting faces. Interestingly, as shown in the figure, global identifications in this model make it possible to avoid bridge crossings and remain on genus 1. Integrating out massive chiral fields and rearranging the graph, we obtain Figure 5.44.c, the dimer for the SPP.

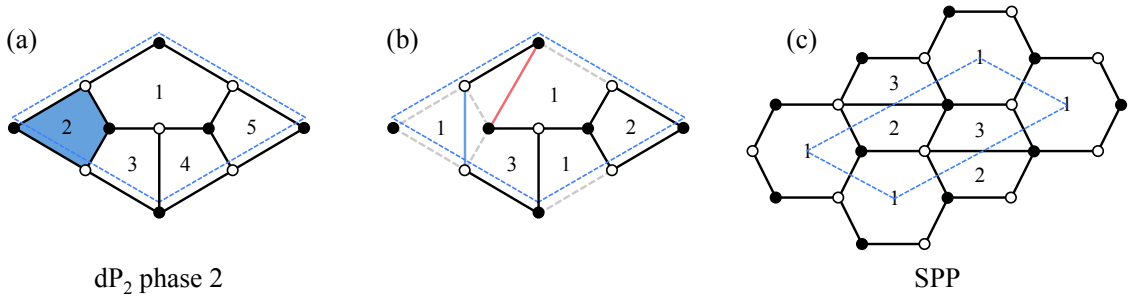

Figure 5.44: Instanton backreaction from phase 2 of dP_2 to SPP.

PdP_2 to SPP

Let us now consider PdP_2, whose toric diagram and quiver were presented in Figure 5.4. Comparing Figures 5.4 and 5.33, we see that the quivers for this theory and for the phase 2 of dP_2 we have just considered are very similar, differing only by a pair of chiral fields associated to a bidirectional arrow connecting nodes 2 and 5. However, the superpotentials are rather different, as encoded in the corresponding dimer models.

In Section 5.1.2.1 we considered the effect of an instanton on face 4. Let us now study, instead, an instanton on face 2, as shown in Figure 5.45. (a) shows the dimer with the instanton. In (b), we show the instanton backreaction and have relabeled the surviving faces of the dimer. Unlike what happens for an instanton on face 4, when the instanton is on face 2 global identifications make it possible to avoid bridge crossing without increasing the genus of the BFT. After integrating out massive fields we obtain (c), which is the dimer for the SPP.

We conclude that, as summarized in Figure 5.46, we can reach the BFT for the SPP by backreacting D-brane instantons on either dP_2 or PdP_2.

We have deliberately made the similarities between phase 2 of dP_2 and PdP_2, and between the instantons we considered, as manifest as possible. However, it is important to emphasize that, in general, instantons on significantly different theories can produce the same BFT.

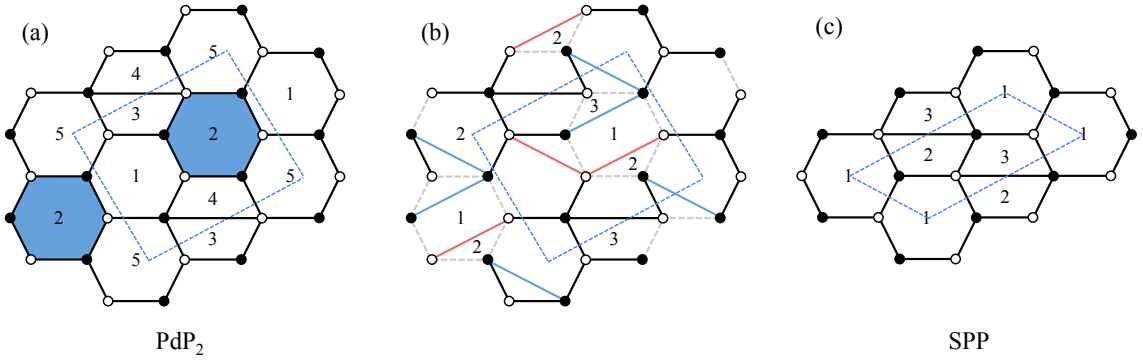

Figure 5.45: Instanton backreaction from PdP_2 to SPP.

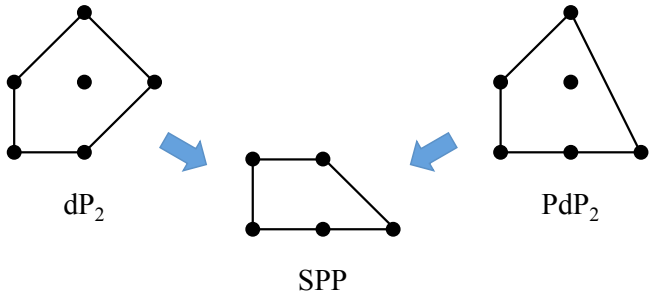

Figure 5.46: The SPP can be obtained from backreaction of instantons on dP_2 and PdP_2.

6

Instabilities in non SUSY warped throats

6.1 Quantum Gravitational String Phenomenology

The recent flurry of activity, largely triggered by [63–65], in constraining phenomenological string model building using Quantum Gravity swampland criteria [53–55, 58, 60, 185–187] (see [51] for a recent review) is giving birth to an emerging field, which can deservedly claim the designation of **Quantum Gravitational String Phenomenology**. An express introduction is provided in Section 2.6.

The application of constraints convincingly argued to hold in any theory of Quantum Gravity is leading to new breakthroughs. In particular, the Weak Gravity Conjecture (WGC) [54] (see [63–71, 75, 76, 188–193] for different formulations and applications) has motivated the remarkable statement that stable non-supersymmetric Anti de Sitter (AdS) vacua are not possible in Quantum Gravity [58, 60]. This AdS-WGC constraint is largely motivated by the application of the refined WGC to systems of branes in the near horizon limit, and has received direct support from the study of decays of non-supersymmetric AdS vacua in string theory via bubbles of nothing [61]. The AdS-WGC has been argued to have far-reaching implications for particle physics and its scales [191–193].

There are also recent proposals of swampland criteria attempting to rule out de Sitter vacua as well [186, 194, 195], possibly in certain regimes under parametric control. This claim clashes with familiar roadmaps for the construction of de Sitter vacua in string theory [109, 131], see [196, 197] for recent discussions. A key ingredient in the parametric control of these scenarios is the presence of warped throats [28, 198] at whose bottom the supersymmetry breaking sectors are localized, so that they undergo a redshift crucial for the tunability of the 4d vacuum energy. Starting from the original proposal of supersymmetry breaking by anti-D3-branes [109], there is a rich variety of proposals, see e.g. [199–201]. Hence, it is interesting to explore the interplay of non-supersymmetric warped throats with constraints from Quantum Gravity.

In this chapter we consider non-compact warped throats and constrain these 5d backgrounds by proposing a new swampland conjecture, the *local AdS-WGC*, which generalizes the AdS-WGC to locally AdS warped throats. The conjecture is motivated by considering the near horizon limit of systems of fractional D-branes at singularities, but should hold more in general. Although it does not constrain metastable non-supersymmetric throats, and hence has no direct implication for e.g. anti-D3-brane models, it can be used to rule out large classes of warped throats with supersymmetry breaking sectors at their bottom. We study this phenomenon in several explicit examples, shedding new light on already known instabilities in supersymmetry breaking D-brane models, such as the dP_1 theory,

and unveiling novel decay channels in AdS or locally AdS backgrounds. For instance, we explicitly discuss warped throats with supersymmetry broken by the introduction of anti-orientifold planes.

A remarkable feature of these examples is that the non-supersymmetric backgrounds are stable at the classical level, and that the pathologies arise at the quantum level, often by nucleation of bubbles hosting interiors of more stable vacua. This is consistent with the interpretation of these constraints as arising from consistency in Quantum Gravity.

In Section 6.2 we propose the local AdS-WGC criterion; we derive it in section 6.2.1, and use it in section 6.2.2 to reinterpret the properties of supersymmetric and non-supersymmetric warped throats dual to fractional D3-branes in toric singularities. In section 6.2.3 we discuss the situation for throats with meta-stable supersymmetry breaking. In Section 6.3 we consider an illustrative example of a system of D3-branes with Dynamical Supersymmetry Breaking due to strong dynamics and consider its embedding into warped throats. The D-brane gauge theory is discussed in section 6.3.1, and in section 6.3.2 we describe the instabilities that arise when embedded into AdS or locally AdS warped throats, in agreement with the (local) AdS-WGC implications for non-supersymmetric throats; in section 6.3.3 we describe the local AdS-WGC statement in an explicit example illustrating how it applies to non-supersymmetric throats from $\mathcal{N} = 2$ fractional branes. Section 6.4 treats warped throats with supersymmetry broken by the presence of anti-orientifold-planes. In section 6.4.1 we discuss generalities about such throats. In section 6.4.2 we focus on anti-O3-planes, describe their different kinds and their interaction with systems of D3-branes. In section 6.4.3 we discuss the corresponding gravitational backgrounds and describe their instabilities, in agreement with the (local) AdS-WGC statement.

6.2 The local AdS-WGC swampland criterion

6.2.1 Derivation

As briefly introduced in Section 2.6, the WGC [54], in its minimal formulation establishes that in any theory including quantum gravity, any $U(1)$ gauge factor should have a super-extremal charged particle, namely $q \geq m$, in natural units. This has been generalized to other p-form gauge fields, requiring the existence of the corresponding branes with tensions bounded by their charges, $Q \geq T$, an extension natural in string theory models via T-duality.

The proposal in [58] of a *refined* WGC establishes that the inequality is saturated only for BPS states in supersymmetric theories. This further motivates the *AdS-WGC* statement that theories of quantum gravity do not have stable non-supersymmetric AdS vacua, which are thus in the swampland, rather than in the string landscape. The AdS-WGC is largely motivated by a particular (but large) class of AdS backgrounds in string theory, which correspond to flux compactifications arising as near horizon limits of systems of D-branes. A prototypical example is the type IIB $\mathrm{AdS}_5 \times \mathbf{S}^5$ solution with N units of RR 5-form flux on the $\mathbf{S}^5$, which arises as the near horizon limit of a system of N D3-branes in flat 10d spacetime, see Section 2.3.1. In short, the $T = Q$ condition is crucial in the structure of these vacua, in which the tension creating the spacetime curvature is balanced against the flux sourced by the brane charge in the underlying picture. This proposal is further supported by the study of instabilities of non-supersymmetric AdS vacua due to bubbles of nothing [61]. The AdS-WGC is a powerful statement, which e.g.

has subsequently been applied to derive novel constraints on particle physics [191–193,202].

In this chapter we propose a generalization of the conjecture, which we dub the *local AdS-WGC*. It states that certain warped throat backgrounds, which are AdS locally in the radial direction but have a slow variation of the local 5d value of the cosmological constant, are not consistent in quantum gravity, except for supersymmetric cases. The precise formulation will be manifest from the derivation below.

The derivation follows the strategy of [58] for AdS fluxed backgrounds, by taking a near horizon limit of D-brane systems. In our case, we apply the near horizon description to systems of regular and fractional D3-branes at singularities, in particular the toric CY singularities of section 2.4.1. We note that the discussion below also applies to throats from $\mathcal{N}=2$ fractional branes, despite the presence of singularities in the near horizon geometry, if one accounts for the additional fields from the twisted sectors, see 6.3.3 for extra details.

The backgrounds correspond to the holographic duals of (the UV regime of) gauge theories with cascading RG flows, like the familiar conifold example. The statements below have well-established translations to the holographic dual gauge theory on the D-branes, but we prefer to emphasize the properties of the gravity side.

Consider a system of N regular and M fractional D3-branes at a toric CY singularity with metric,

$$ds^2_{\bar{\Psi}_6} \,=\, dr^2 \,+\, r^2 ds^2_{\mathbf{X}_5} \tag{6.1}$$

The near horizon geometry is a solution of the kind considered in [29] for the conifold, see Section 2.3.3, and generalized in [47, 48], as a particular class of the supersymmetric warped compactification ansatz in [46, 198],

$$ds^2 \,=\, Z(r)^{-1/2}\,\eta_{\mu\nu}\,dx^\mu\,dx^\nu \,+\, Z(r)^{1/2}\,[\,dr^2 \,+\, r^2 ds^2_{\mathbf{X}_5}\,]. \tag{6.2}$$

One obtains a warped version of the singular manifold, which can be regarded as the 5d horizon $\mathbf{X}_5$ fibered over the 5d space given by 4d Minkowski space and the radial direction r.

There are M units of RR 3-form flux along a non-trivial 3-cycle Σ_3 (topologically an $\mathbf{S}^3$ or a Lens space) in $\mathbf{X}_5$, and a corresponding NSNS 3-form flux, such that the combination (setting the 10d RR axion to zero for simplicity) $G_3 = F_3 - \frac{i}{g_s} H_3$ is a harmonic (2,1)-form, so that the flux is supersymmetric. This H_3 flux can be described as a variation in r of the 5d scalar arising from the axion ϕ given by the component of the NSNS 2-form B_2 along the harmonic 2-form ω_2 Poincaré dual to Σ_3 (equivalently, the period of B_2 over the 2-cycle Σ_2 dual to Σ_3 in $\mathbf{X}_5$),

$$H_3 \,=\, \frac{3\,g_s\,M\,\alpha'}{2}\,\frac{dr}{r}\,\wedge\omega_2(\Sigma_3) \tag{6.3}$$

The combination of fluxes is a source of the RR 5-form $dF_5 = F_3 \wedge H_3$, such that its flux N over $\mathbf{X}_5$ varies logarithmically as in Equation (2.61),

$$N_{eff} \sim g_s\,M^2 \ln(r/r_s) \tag{6.4}$$

where r_s is an IR cutoff distance. The fluxes also backreact on the geometry, via the warp factor, which obeys

$$(\nabla^2_{\bar{\Psi}} Z)\,\mathrm{vol}(\bar{\Psi}_6) \,=\, g_s\,F_3 \wedge H_3 \tag{6.5}$$

leading to

$$Z(r) \;=\; \left(\frac{9\, g_s\, M\, \alpha'}{2\sqrt{2}}\right)^2 r^{-4}\, \ln\frac{r}{r_s}, \tag{6.6}$$

The whole of $\mathbf{X}_5$ shrinks at $r = r_s$, but the F_5 flux has disappeared by then, so there is no topological obstruction to the shrinking from this side. However, the 3-cycle Σ_3 in $\mathbf{X}_5$ also collapses, and it supports the F_3 flux, which is constant. This leads to a naked singularity at the tip of the throat, $r = r_s$.

The 5d part of the above solution describes what we refer to as a *local AdS solution*. It corresponds to a background which locally in r is an AdS_5 background, but whose AdS curvature changes in r, as in (6.6). This variation is controlled by that of a 5d scalar, which in the earlier flux throat is $\phi = \int_{\Sigma_2} B_2$, changing from (6.3). In purely 5d terms, the defining property for this scalar is that (from the 10d topological coupling $F_3 \wedge B_2 \wedge F_5$) it has a 5d topological coupling

$$S_{\rm CS} \;=\; M\, \phi\, F_5 \tag{6.7}$$

This is the 5d version of the topological couplings [80,86], arising in flux compactifications as described in [85,106]. Upon integrating out the non-dynamical F_5, the resulting potential for ϕ controls the local (in r) value of the vacuum energy. The background value for this 5d field, following from (6.3) is

$$d\phi \;=\; \frac{3}{2}\, g_s\, M\, \alpha'\, \frac{dr}{r} \tag{6.8}$$

Alternatively, its boundary condition is fixed by the asymptotic behavior

$$\phi \sim M\, \ln(r/r_0) \tag{6.9}$$

The local AdS solution can thus be described as a (in this case, 5d) AdS solution modified by the backreaction of a (5d) scalar ϕ with topological coupling to a non-dynamical field strength top-form and obeying (6.8). The coupling to the top-form can be replaced by equivalent dual formulations, e.g. the explicit r-dependence of the 5d vacuum energy.

The local AdS backgrounds we have described contain a naked singularity at $r = r_s$, which in fact is known to admit a smooth deformation (preserving supersymmetry) in certain singularities, starting from the celebrated conifold example discussed in Section 2.3.3 and generalized in [43]. Thus, the local AdS solution should be regarded as defining the asymptotics of certain very general class of warped throats, in principle with or without supersymmetry, and imposing swampland constraints on the possible existence of such throats in quantum gravity. This brings us to the precise formulation of a new swampland conjecture.

Local AdS-WGC swampland criterion:
In consistent theory of quantum gravity, there are no stable non-supersymmetric solutions with asymptotics given by local AdS backgrounds, as defined above.

6.2.2 Evidence from deformation and DSB fractional brane systems

Besides the direct derivation in the spirit of the AdS-WGC, we now present additional support for the local AdS-WGC. Although the following results are known in the

literature, their re-interpretation in terms of a swampland constraint is new and provides an interesting insight into the structure of the underlying warped throats and supersymmetry breaking, which we further exploit in later sections.

As mentioned in Section 6.1, there is a large class of local AdS backgrounds arising as holographic duals of (the UV regime of) systems of regular and fractional D3-branes at singularities, specifically, fractional branes of the deformation or DSB kinds ($\mathcal{N} = 2$ fractional branes are discussed in section 6.3.3). We discuss their interplay with the local AdS-WGC in turn.

Toric CY singularities admitting a complex deformation can support deformation branes. The gauge theory on their worldvolumes has an UV RG flow whose holographic dual is given by a supersymmetric local AdS background supported by M units of RR flux on the 3-cycle Σ_3 associated to the complex deformation. Thus the naked singularity at the origin in the local AdS background can be smoothed out by giving this 3-cycle a finite size. The resulting configuration is a smooth supergravity solution described by a warped version of the deformed CY threefold, preserving supersymmetry, and with asymptotics given by a local AdS background; this is thus in agreement with the local AdS-WGC statement. The field theory counterpart of this deformation process was described in [28, 43].

Toric CY singularities can also support DSB fractional branes which are not associated to complex deformations. Still, the gauge theory on their worldvolume has a UV RG flow whose holographic dual is a supersymmetric local AdS background supported by M units of RR flux on a 3-cycle Σ_3. The latter, however, cannot be given a finite size while preserving supersymmetry. Naively, one may think that the infrared region is smoothed out to an alternative configuration breaking supersymmetry, either in the form of a supergravity background beyond the warped CY ansatz (in the spirit of e.g. [203] in the supersymmetric case), or perhaps involving stringy ingredients, such us explicit sources from branes or other singular objects. However, if such re-stabilization would indeed be possible, it would contradict our local AdS-WGC statemetnt.

The actual answer is that the warped throats created by DSB fractional branes actually do not admit any such stable non-supersymmetric smooth version, in agreement with the local AdS-WGC conjecture. This has actually been already studied in the lilerature, from the gauge theory side. The complex cone over dP_1 is the prototypical case of a duality cascade triggered by a DSB brane, and the lack of a supersymmetric vacuum in this dP_1 theory was discussed in [31, 49, 50]. This however does not imply the existence of a non-supersymmetric stable vacuum, rather [31] already established that the theory shows a runaway behaviour, as follows. By keeping the $U(1)$ factors in the description of the gauge theory, the system has a supersymmetry breaking minimum only if the Fayet-Iliopoulos terms are kept fixed, due to the constraints from the D-term potential. However, the FI terms are actually field dependent, and are controlled by the vevs of closed string twisted sectors. When they are taken as dynamical, the D-term potential can relax in new directions leading to the runaway. The same physics was reinterpreted in [204] as a baryonic runaway direction in the gauge theory with the (massive) $U(1)$'s integrated out. In either of these descriptions, the runaway direction corresponds to a dynamical blow-up of the singularity, since FI terms, or baryonic vevs, are related to blow-up modes. The fractional brane remains as a D5-brane wrapped on a 2-cycle in the dP_1 exceptional divisor.

The gravity dual of this runaway has not been determined in the literature, but its structure should correspond to a time-dependent solution, in which the geometry is resolved by growing a finite size dP_1 itself, with M explicit D5-branes wrapped on one of

its 2-cycles. The latter plays the role of sourcing the M units of RR 3-form, peeling it off the 3-cycle and allowing it to shrink to zero size at the bottom of the (disappearing) throat.

It is interesting to point out that this system provides an interesting link between two seemingly unconnected swampland criteria. On one hand, the statement that in theories of quantum gravity all FI terms should be field-dependent, and thus dynamical [205]; on the other hand, our newly proposed local AdS-WGC. We expect other connections of the local AdS-WGC constraint with other swampland criteria.

We thus see that the class of throats obtained from the different kinds of fractional branes provide illustrative examples of the local AdS-WGC constraint. In later sections we illustrate the power of this conjecture to exclude candidates to non-supersymmetric throats proposed in the literature.

6.2.3 Meta-stable throats

It is important to emphasize that the present form of the local AdS-WGC still allows for certain kinds of non-supersymmetric warped throats. For instance,

• The conjecture poses no conflict so far with the existence of supersymmetry breaking meta-stable throats with local AdS asymptotics. For instance the systems of anti-D3-branes at the bottom of conifold-like warped throats (i.e. created by deformation fractional branes), extensively used since [109], are in principle allowed [1]. See also [207], where non-supersymmetric orbifolds are considered and shown to be unstable through nucleation of bubbles of nothing. In contrast with the AdS-WGC, in local AdS throats there is no isometry in the radial direction introducing an infinite volume factor multiplying the decay probability, rather instabilities tend to nucleate near the tip of the throat. Hence, a finite and potentially small decay amplitude is in principle feasible, although this point deserves further study[2].

• Similarly for the nilpotent Goldstino scenario realized in terms of a single anti-D3-brane on top of an O3-plane [200], for which the stability remarks of [208] specially apply.

• Finally, global compactifications including warped throats may contain ingredients in the CY bulk which modify non-trivially the boundary conditions in the UV region of the throat, thus changing its asymptotics, and allowing it to evade the local AdS-WGC constraint. For instance, this may well be the case if one introduces euclidean D3-brane instantons on 4-cycles intersecting the underlying DSB D3-brane system (thus, stretching in the radial direction of the throat) to stop their runaway, as proposed in [112] (see also [110, 132] for related tools). Also, if one includes D7-branes introducing new flavours in DSB D-brane systems, to allow for metastable supersymmetry breaking vacua [209,210] in the ISS spirit [211]. For a recent discussion of orientifolded throats, see [212].

In the following discussions, we consider several large classes of non-supersymmetric warped throats, and reconcile them with the local AdS-WGC by looking for decay channels. Whether these decay channels render the configurations unstable or just meta-stable is not constrained by the conjecture in its present form, hence we loosely refer to them

[1] For discussions on asymptotics and stability of these throats, there is a long-standing debate, see e.g. [206] for a recent work, and references therein.

[2] We thank M. Montero for raising this point.

as instabilities of the configuration, even in cases where they could host meta-stable backgrounds.

6.3 Warped throats with Dynamical Supersymmetry Breaking

In the previous discussion, the system of D3-branes breaking supersymmetry had a fairly manifest runaway behaviour. There are however other systems of D3-branes at singularities which trigger genuine dynamical supersymmetry breaking, rather than runaway. In this section we explore the proposal of embedding such systems in warped throats [201], and how they face the local AdS-WGC.

Again, there are systematic tools for the construction of such theories in terms of D3-branes at toric singularities (possibly in the presence of orientifold quotients), producing $\mathcal{N}=1$ supersymmetric gauge theories with supersymmetry broken only by non-perturbative dynamics. As explained in [201], dimer diagram tools moreover allow to realize them as the theories arising in the infrared of duality cascades of systems of further (deformation) fractional D3-branes at singularities. The gravity dual description of these configurations would correspond to a locally AdS supersymmetric warped throat supported by 3-form fluxes on a 3-cycle associated to a complex deformation, and at whose tip we have the supersymmetry breaking D-brane sector.

If stable, such configurations would lead to a supersymmetry breaking warped throat violating the local AdS-WGC. In this section, we provide a detailed analysis of an illustrative example and show that the configurations are actually unstable. Concretely, although the DSB D3-brane system is consistent in isolation, its embedding into a warped throat contains an instability against bubble nucleation of certain D-brane domain walls. The latter are however more involved than just D3-brane domain walls peeling off the 5-form flux, and provide a novel kind of decay for warped throats. The system also relates to warped throats from (orientifolds of) $\mathcal{N}=2$ fractional branes, which we discuss as well.

6.3.1 The DSB D-brane system

To make the discussion concrete, we consider an illustrative explicit example given by the DSB theory introduced in [33]. We start with the $\mathbb{C}^3/\mathbb{Z}_6'$ geometry, where the $\mathbb{Z}_6'$ generator θ acts as

$$\theta: \quad z_i \to e^{2\pi i v_i} z_i \tag{6.10}$$

with $v=(1,2,-3)/6$. We consider the quotient by an orientifold group $(1+\theta+\ldots+\theta^5)(1+\Omega\alpha(-1)^{F_L})$, where α acts as

$$(z_1,z_2,z_3)\to(e^{2i\pi/12},e^{4i\pi/12},e^{-6i\pi/12}). \tag{6.11}$$

Equivalently, we may introduce invariant coordinates

$$x=z_1^6,\ y=z_2^3,\ z=z_3^2. \tag{6.12}$$

in terms of which the orientifold corresponds to the geometric action

$$x\to -x,\ y\to -y,\ z\to -z. \tag{6.13}$$

We consider sets of D3-branes at this orientifold singularities. The resulting gauge theory can be determined from its dimer diagram, shown in Figure 6.1. As discussed in Section 2.4.4, there are different choices of orientifold signs, which lead to different results of SO or Sp gauge factors and of $\square\!\square$ / $\square\square$ matter fields. For our choice of interest, corresponding to orientifold signs $(a,b,c,d) = (++--)$, the resulting gauge theory is

$$\begin{gathered} SO(n_0) \times U(n_1) \times U(n_2) \times USp(n_3) \\ (\,\square_0,\,\overline{\square}_1) + (\,\square_1,\,\overline{\square}_2) + (\,\square_2,\,\overline{\square}_3) + \\ +(\,\square_0,\,\overline{\square}_2) + (\,\square_1,\,\square_3) + \square\!\square_2 + \overline{\square\!\square}_1 + \\ +[\,(\,\square_0,\,\square_3) + (\,\square_1,\,\square_2) + (\,\overline{\square}_1,\,\overline{\square}_2)\,] \quad . \end{gathered} \tag{6.14}$$

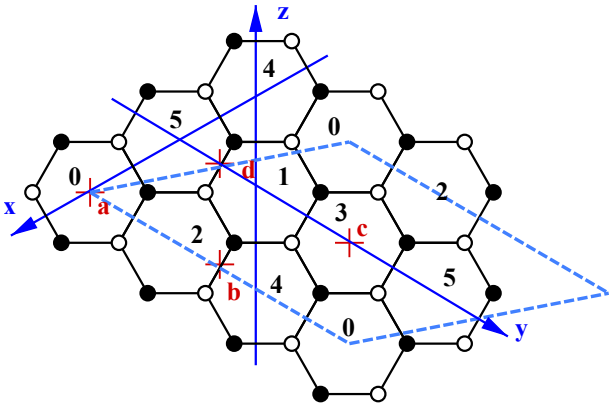

Figure 6.1: Dimer diagram for an orientifold of the $\mathbf{C}^3/\mathbf{Z}_6'$ theory, from [33].

As is familiar [213], cancellation of non-abelian gauge anomalies is equivalent to the requirement of cancellation of compact RR tadpoles, which leads to

$$-n_0 + n_2 + n_3 - n_1 - 4 = 0. \tag{6.15}$$

We consider the solution $n_1 = n_3 = 0$, $n_0 = k$, $n_2 = k+4$, which yields the gauge group $SO(k) \times U(k+4)$ with matter $(\,\square\,,\,\overline{\square}\,) + (1,\,\square\!\square\,)$. The $U(1)$ gauge factor is anomalous, with anomaly canceled by Green-Schwarz couplings, which make it massive and remove it from the massless spectrum. Focusing on $k=1$, we have an $SU(5)$ theory with chiral multiplets in the $10 + \bar{5}$ and no superpotential. This theory has been argued to show dynamical supersymmetry breaking [8, 214] as reviewed in Section 2.1.5.2. Since there is no moduli space, there is an isolated non-supersymmetric vacuum, which however lies at strong coupling and is non-calculable. Nevertheless, the vacuum energy should scale with the strong dynamics scale Λ as

$$V \sim |\Lambda|^4 \tag{6.16}$$

This provides a consistent configuration displaying supersymmetry breaking localized at the tip of the corresponding singularity.

It is natural to consider its embedding into warped throats, as a possible source of tunable uplifting energy to be used in attempts to build de Sitter string vacua. In the following we argue this not to be possible.

6.3.2 The DSB AdS throat

As a warm-up towards such throats, we may consider the simple addition of a large number of dynamical D3-branes to the earlier system, and take the near horizon limit. This corresponds to increasing the rank of all gauge factors in 6.14 by the same amount, namely

$$n_0 = N + 1 \quad , \quad n_1 = n_3 = N \quad , \quad n_2 = N + 5 \tag{6.17}$$

For consistency with the USp factor, N should be taken even, but is otherwise unconstrained.

Since the DSB D-brane system (including the orientifold and the $k = 1$ $SU(5)$ D-brane set) is subleading in $1/N$, standard arguments show that in the large N limit we obtain a gravity dual given by $\mathrm{AdS}_5 \times \mathbf{X}$, where $\mathbf{X}$ corresponds to an orientifold of the $\mathbb{Z}_6'$ orbifold of $\mathbf{S}^5$. Note that since the $\mathbb{Z}_6'$ orbifold contains fixed complex planes in $\mathbb{C}^3$, there are fixed circles in the action on $\mathbf{S}^5$. This leads to circles of $\mathbb{C}^2/\mathbb{Z}_2$ and $\mathbb{C}^2/\mathbb{Z}_3$ singularities, which are however well understood [215,216]. The orientifold action (6.13) has instead the origin as only fixed point, hence it is freely acting on $\mathbf{S}^5$.

At leading order in $1/N$, which corresponds to the classical gravity level, we have a supersymmetric AdS configuration, associated to the near horizon limit of a D-brane system saturating the WGC bound, hence satisfying the AdS-WGC. In the exact configuration, however, the DSB D-brane sector breaks supersymmetry, and implies that at the quantum level the gravitational background becomes non-supersymmetric, hence according to the AdS-WGC, the system should exhibit an instability.

Naively, it would seem that the instability corresponds, as suggested in [58], to the emission of shells of D3-branes peeling off the 5-form flux background from the AdS solution. This would correspond, in the underlying picture of D-branes at singularities, to the DSB D-brane system repelling dynamical D3-brane off the origin towards generic points in the transverse space. This actually turns out to be incorrect, as can be shown using the field theory description, using standard supersymmetric field theory arguments. Expelling the dynamical D3-branes corresponds to the Higgsing down the gauge theory with the rank assignment (6.17) to the original $N = 0$ $SU(5)$ theory, by giving vevs to suitable mesonic operators. To make the point, it suffices to turn on a vev for the gauge invariant operator involving fields in the first line in (6.14)

$$\langle \, (\, \square_0, \, \overline{\square}_1) \cdot (\, \square_1, \, \overline{\square}_2) \cdot (\, \square_2, \, \overline{\square}_3) \, \rangle \equiv \Phi^3 \tag{6.18}$$

Here Φ is the dimension 1 order parameter for this vev. The superpotential involves only triples of fields from the three different lines in (6.14), hence it is an F-flat direction. As follows from the D-brane picture, there are more general choices, allowing for three independent vevs – for similar mesonic operators built from fields in the three different lines in (6.14) — for each of the dynamical D3-branes. But for our present purposes it suffices to consider only this overall position vev Φ.

From the viewpoint of the infrared $SU(5)$ theory this corresponds to a Higgsing of the UV $SU(N + 5)$ theory by the N flavours acquiring vevs involved in Φ. Denoting Λ, and Λ_{UV} the dynamical scales of the $SU(5)$ and $SU(N + 5)$ theories, the potential for Φ would follow from (6.16) from the implicit dependence of the IR scale Λ on Φ. However, taking the $SU(5)$ theory, with a $10 + \overline{5}$ matter content, and the UV $SU(N + 5)$ theory,

with matter content $(3N+1)\,\overline{\square}\,+2N\,\square\,+\,\begin{smallmatrix}\square\\\square\end{smallmatrix}$, the matching relation is just $\Lambda=\Lambda_{\rm UV}$, see Appendix 1.1, with no dependence of Φ. This implies that the DSB D-brane systems does not exert forces on dynamical D3-branes, which are thus not repelled from the origin. The non-supersymmetric AdS configuration is not unstable towards the emission of such D3-brane shells peeling off the 5-form flux.

Actually, the contradiction with the AdS-WGC statement is avoided by a novel mechanism, related to a different kind of instability, which we explain as follows. Let us return to the picture of D3-branes at the orientifold of the $\mathbb{C}^3/\mathbb{Z}_6'$ singularity, i.e. the rank assignment (6.17). The $\mathbb{Z}_6'$ quotient does not actually define an isolated singularity; indeed, the generator (6.10) has the origin as only fixed point, but θ^3 leaves invariant the complex plane parametrized by z_2, and θ^2 leaves z_3 invariant. This implies that there is a complex plane (along z_2) of $\mathbb{C}^2/\mathbb{Z}_2$ singularities, and a complex plane (along z_3) of $\mathbb{C}^2/\mathbb{Z}_3$ singularities. In the field theory, there are flat directions corresponding to splitting some of the dynamical D3-branes into fractional D3-branes (of the $\mathcal{N}=2$ kind, i.e. D5-branes wrapped on the collapsed cycles of the $\mathbb{C}^2/\mathbb{Z}_n$) which can slide off the origin along the corresponding complex plane. Once the non-perturbative supersymmetry breaking kicks in, these flat directions can turn into runaway, providing an instability, bringing back agreement with the AdS-WGC.

The existence of this instability can again be analyzed in terms of the field theory, by Higgsing and scale matching. Consider for concreteness the splitting of dynamical D3-branes into fractional D3-branes of the $\mathbb{C}^2/\mathbb{Z}_2$ singularity associated to θ^3, and moving the latter along z_2. A similar analysis could be performed using the fractional branes of the $\mathbb{C}^2/\mathbb{Z}_3$ curve of singularities. Motion in z_2 corresponds to mesonic vevs for fields in the second line in (6.14). Denoting the fields $(\,\square_{\,0},\,\overline{\square}_{\,2})$ and $\begin{smallmatrix}\square\\\square\end{smallmatrix}_{\,2}$ by ${Q_A}^i$ and A_{ij}, respectively, and $(\,\square_{\,1},\,\square_{\,3})$, $\overline{\square\square}_{\,1}$ by $Q'_{j',B'}$, $S^{i'j'}$, respectively, the vevs for the two kinds of fractional branes have the structure

$$v\,=\,\langle\,\epsilon_{AB}{Q_A}^i{Q_B}^j A_{ij}\,\rangle\quad;\quad v'\,=\,\langle\,S^{i'j'}Q_{i'A}Q_{j'B}\delta^{AB}\,\rangle \tag{6.19}$$

For simplicity we have assumed all fractional D3-branes of the same kind to be located at the same position. The fact that the two different fractional branes are related to vevs of fields Higgsing the combinations of gauge factors (0,2) and (1,3), respectively, is manifest in the dimer diagram in Figure 6.1, where the above combinations correspond to two sets of faces forming two different strips in the z_2 mesonic direction.

Let us compute the scale matching. Considering for instance $v\gg v'$ (eventually shown to be the realistic regime), the Higgsing pattern is

$$\begin{aligned}&SO(N+1)\times SU(N)\times SU(N+5)\times USp(N)\;\xrightarrow{v}\\&\xrightarrow{v}SO(1)\times SU(N)\times SU(5)\times USp(N)\;\xrightarrow{v'}\;SO(1)\times SU(5)\end{aligned} \tag{6.20}$$

where the $SO(1)$ factor is kept for bookkeeping purposes. In the first step, the $SU(N+5)$ is Higgsed down to $SU(5)$. In the second step, the $SU(5)$ theory maintains the number of colors, but $2N$ flavours become massive. The scale matching between the IR and UV scales Λ, $\Lambda_{\rm UV}$ is

$$\Lambda^{13}\;=\;\Lambda_{\rm UV}^{13}\,v'^{2N}\,v^{-2N} \tag{6.21}$$

Replacing in (6.16), the vev v runs away to infinity, while the vev v' is attracted to zero.

Note that, although the two kinds of fractional branes have similar features in isolated $\mathbb{C}^2/\mathbb{Z}_2$, they have a very different behavior in the presence of the orientifold action. This is in fact manifest already in the orientifold projection on the gauge group and matter content.

The resulting configuration is given by a set of D-branes describing the $SO(1) \times SU(N) \times SU(5) \times USp(N)$ gauge theory. The $SU(5)$ gauge factor still has the antisymmetric matter, but it has extra vector-like flavours, and the theory has supersymmetric vacua [214]. This fits nicely with the vacuum energy from (6.16), (6.21) going to zero as $v' \to 0$. Note that the final configuration can be described as a quotient (a $\mathbb{Z}_3$ orbifold of an orientifold of) a set of N $\mathcal{N}=2$ fractional branes at $\mathbb{C}^2/\mathbb{Z}_2$. This configuration has a supersymmetric gravity dual given by a locally AdS throat of the kind studied in [217,218]. These can be regarded as $\mathcal{N}=2$ versions of the $\mathcal{N}=1$ Klebanov-Strassler throats, with the singularity at the origin resolved by a stringy phenomenon, the so-called enhancon configuration [219]. The fact that the final end point is a supersymmetric local AdS background avoids conflicts with the local AdS-WGC.

In the gravity picture of the initial configuration, the instability of the non-susy AdS corresponds to the nucleation of bubbles defined by suitable fractional D3-branes, namely D5-branes wrapped on a collapsed $\mathbb{P}_1$ on the $\mathbf{S}^1$ of $\mathbb{C}^2/\mathbb{Z}_2$ singularities, and with spatial topology $\mathbf{S}^3$ in the non-compact dimensions, expanding outwards with time. In the interior, we are left with a supersymmetric locally AdS throat induced by the N fractional branes stabilized at the origin, and with the singularity at its tip smoothed out presumably by an enhançon configuration. In contrast with other examples in the literature, this is neither a bubble of nothing nor a bubble removing the 5-form flux completely. It thus corresponds to a novel decay channel for non-supersymmetric warped throats.

The $\mathbb{C}^3/\mathbb{Z}_6'$ orientifold singularity can be embedded in a locally AdS warped throat associated to a complex deformation, as discussed in section 6.3. In this setup, supersymmetry breaking on the infrared gauge theory would lead to contradiction with our proposed local AdS-WGC. However, our above analysis of the AdS case shows that the locally AdS throat is already unstable due to D5-brane bubble nucleation (on top of other possible decay channels related to the deformation fractional branes). Hence, the conflict with the local AdS-WGC is solved by the decay channel already solving the potential conflict with the AdS-WGC.

6.3.3 Non-supersymmetric warped throats for $\mathcal{N}=2$ fractional branes

In this section we exploit the previous configuration to obtain a non-trivial example of non-supersymmetric warped throat induced by $\mathcal{N}=2$ fractional branes. The discussion is straightforward and the arguments should be familiar by now.

Consider the previous orientifold singularity, with D-branes corresponding to the rank assignment

$$n_0 = M+1 \quad , \quad n_1 = n_3 = 0 \quad , \quad n_2 = M+5 \tag{6.22}$$

with M even, for consistency of the (hidden) USp factor. This leads to a gauge theory with group $SO(M+1) \times SU(M+5)$, with matter $(\,\square\,,\,\overline{\square}\,) + (1,\,\begin{smallmatrix}\square\\\square\end{smallmatrix})$. In the limit of large M, at leading order we have a gravity dual given by a quotient of the supersymmetric $\mathcal{N}=2$ warped throats in [217,218]. The configuration is of the local AdS kind, hence the local AdS-WGC constraints should apply.

On the other hand, the gauge theory does not have a supersymmetric vacuum. The $SU(N)$ theory with odd N, antisymmetric matter, and no extra flavours, breaks supersymmetry, as shown in [8, 214, 220]. Actually, this reference argued for an isolated supersymmetry breaking vacuum for the theory with Yukawa couplings, which remove the classical flat direction. In our present example, such superpotential couplings are absent, and the classical flat direction can turn into runaway ones. This is precisely the conclusion from matching of scales, as in the previous section, which we skip.

This means that, on the gravity side, the classical background has a decay channel given by nucleation of bubbles of fractional branes, exactly as in the previous section. In this case, however, since there are no fractional branes of the supersymmetry preserving kind, the bubbles completely peel off the 5-form flux background of the configuration leading to a complete decay of the local AdS throat.

This example thus provides an explicit example of the application of the local AdS-WGC constraint to non-supersymmetric warped throats induced by $\mathcal{N} = 2$ fractional branes.

6.4 Supersymmetry breaking orientifolds in warped throats

In the previous sections, we have focused on warped throats whose underlying D-brane configuration is supersymmetric in perturbation theory, with supersymmetry breaking arising from non-perturbative strong dynamics effects. It is interesting to check the behavior of warped throats with more dramatic supersymmetry breaking patterns. In this section, we explore a class of warped throats, where supersymmetry breaking is induced by orientifold planes not preserving the supersymmetry preserved by the CY geometry and the 3-form fluxes. In fact, they correspond to the CPT conjugates of the familiar supersymmetric orientifold planes, so we refer to them as anti-orientifold planes. Systems of anti-orientifold planes in the presence of D-branes are identical to systems of anti-D-branes in the presence of orientifold planes, which have been considered in many non-supersymmetric string constructions, pioneered in [221–226].

6.4.1 Non-supersymmetric throats from anti-O3-planes

We focus on anti-O3-planes in the presence of a large number N of D3-branes, possibly at singularities and with extra M fractional branes. In the underlying D-brane construction, they lead to an explictly non-supersymmetric spectrum, which can be easily determined using open string techniques and (non-supersymmetric projections of) dimer diagrams. For $M = 0$, the systems of anti-O3-planes with N D3-branes behave as "supersymmetric" and conformal in the leading large N approximation, in the sense that the effects of orientifold planes (noticed via crosscaps) are subleading in the large N limit. This implies that the gravity dual description corresponds to AdS backgrounds which behave as supersymmetric in the classical supergravity approximation, but have supersymmetry breaking effects at 1-loop. Similarly, in systems in the presence of M additional deformation branes, we obtain locally AdS warped throats which are supersymmetric in the leading approximation, but break supersymmetry at the 1-loop order. These AdS and locally AdS configurations thus correspond to classically stable backgrounds, which, if stable in the full theory, would violate the AdS-WGC or the local AdS-WGC, respectively. Our purpose is

thus to test the stability of these configurations, providing a check of these conjectures at the quantum level.

Concrete examples are easy to build. For instance, [200] provided tools to embed a single (anti-)O3-plane at the bottom of a warped throat with 3-form fluxes, for instance based on the $xy = z^3w^3$ singularity, a $\mathbb{Z}_3$ orbifold of the conifold. The deformed conifold itself $xy - zw = t^2$ also admits an involution $(x, y, z, w) \to (y, x, -z, -w)$ leading to O3-planes (in fact, two, located at $z = w = 0, x = y = \pm i\, t$) [227]. Considering any of these geometries, we may just replace the O3-planes by anti-O3-planes and obtain explicit locally AdS warped throats with supersymmetry broken by anti-orientifold planes.

6.4.2 Dynamics of D3-branes and anti-O3-planes

It is useful to start considering anti-O3-planes in flat space, in the presence of N D3-branes. In the large N limit, the near horizon limit leads to gravity duals of the form $AdS_5 \times \mathbb{R}P_5$, which behave as supersymmetric at leading order and feel the absence of supersymmetry at order $1/N$. The configuration is the CPT symmetric of O3-planes in the presence of anti-D3-branes (denoted by $\overline{\text{D3}}$'s), which was studied in [224] following the analysis in [155] for the supersymmetric O3-D3 system. We now revisit the main points, in anti-O3-plane language.

An anti-O3-plane is a fixed plane of the $\mathbb{Z}_2$ orientifold action on $\mathbb{R}^6$, preserving the 16 supersymmetries broken by D3-branes. There are four kinds of anti-O3-planes, classified according to the (discretized) values 0, $\frac{1}{2}$ for the NSNS and RR 2-form backgrounds on the $\mathbb{R}P_2$ (twisted) 2-cycles on the $\mathbb{R}P_5 = \mathbf{S}^5/\mathbb{Z}_2$ surrounding the origin in $\mathbf{R}^6$. In short, comparing with [155], the tension of an anti-O3-plane equals that of the corresponding O3-plane, while they have opposite RR charge. The tensions and charges, measured in D3-brane units, for the anti-O3-planes are in the following table.

D-brane description	(θ_{NS}, θ_R)	Tension	RR charge
anti-(O3^-)	$(0,0)$	-1/2	+1/2
anti-(O3^-) + 1 $\overline{\text{D3}}$	$(0,1/2)$	+1/2	−1/2
anti- O3^+	$(1/2,0)$	+1/2	−1/2
anti- $\widetilde{\text{O3}}^+$	$(1/2,1/2)$	+ 1/2	−1/2

Just like for O3-planes, the O3^- is a singlet under the type IIB $SL(2,\mathbb{Z})$ and the three remaining ones transform into each other under it.

The stability of the throats built out using these anti-O3-plane can be heuristically understood by considering the dynamics of D3-branes in the presence of these anti-O3-planes. Namely, we can consider the previous anti-O3-planes with a N D3-branes on top (as counted in the double cover), and study the stability properties of the system.

The corresponding analysis can in fact be borrowed from [224] (in its CPT conjugate version). It is straightforward to obtain the spectrum of the non-supersymmetric gauge theories on D3-branes in the presence of the different anti-O3-planes. The stability properties of the system can be assessed from the open string perspective, by the computation of the Coleman-Weinberg potential. We instead focus on the dynamics in the dual closed string channel, by comparing the interaction between D3-branes and anti-O3-planes due to exchange in the NSNS and RR channels. We consider the different cases in turn:

• Consider $N = 2p$ D3-branes in the presence of the anti-($O3^-$). They have opposite sign tensions and equal sign RR charges, hence the gravitational and Coulomb interactions are both repulsive. Thus, D3-branes are expelled away from the anti-($O3^-$) and the configuration is unstable.

• Take $N = 2p$ D3-branes in the presence of the anti-($O3^-$) + 1 $\overline{\text{D3}}$. The D3-branes are attracted to the origin, but when they reach below sub-stringy distances, a tachyon arises from open strings between the stuck $\overline{\text{D3}}$- and the dynamical D3-branes. The result is a configuration of the anti-($O3^-$) with one stuck D3-brane at the origin, and $(2p-2)$ dynamical D3-branes. The system at the origin has tension $+1/2$ and charge $+3/2$, so the Coulomb repulsion overcomes the gravitational attraction and D3-branes are repelled. The result is a (CPT conjugate) of the nilpotent Goldstino configuration [200].

• Consider $N = 2p$ D3-branes in the presence of the anti-($O3^+$). The gravitational and Coulomb interactions are both attractive, so the D3-branes are driven to the origin. Contrary to the previous case, however, there is no obvious annihilation between the anti-($O3^+$) and the D3-branes. This would suggest that the non-supersymmetric $AdS_5 \times \mathbb{R}P_5$ gravity dual is stable, in conflict with the AdS-WGC. Happily, as we will discuss later on, a non-perturbative instability will come to the rescue.

• For $N = 2p$ D3-branes in the presence of the anti-($\widetilde{O3}^+$) we have a similar situation. The D3-branes are driven to the origin, and no obvious decay channel seems to be available. This perturbatively stable configuration is however again rendered unstable by a non-perturbative process described later on, thus solving the potential conflict with the AdS-WGC and the local AdS-WGC constraints.

6.4.3 Instabilities in throats with anti-O3-planes

The large N limit of the above configurations of D3-branes on top of anti-O3-planes leads to near horizon geometries classically given by $AdS_5 \times \mathbb{R}P_5$, with N units of RR 5-form flux (as counted in the covering space) and the corresponding discrete NSNS and RR 2-form backgrounds on $\mathbb{R}P_2 \subset \mathbb{R}P_5$. Absence of supersymmetry is only detectable at the 1-loop (i.e. $1/N$ order), namely via string diagrams involving crosscaps and thus noticing the underlying non-supersymmetric orientifold. Thus, the AdS-WGC condition implies such AdS backgrounds should have instabilities.

The same statement applies in more general local AdS warped throats with anti-O3-planes. For any local AdS warped throat admitting a supersymmetric orientifold involution introducing O3-planes, it is possible to consider the non-supersymmetric version obtained by the introduction of any of the different anti-O3-planes. The resulting gravitational background remains the same at the level of classical supergravity, but subleading corrections encode the breaking of supersymmetry. Thus, the local AdS-WGC conditions imply such local AdS backgrounds should be unstable.

We now analyze the instabilities in these AdS backgrounds, and the same conclusions clearly apply to local AdS configurations. The analysis follows the discussion in the previous section.

• In the case of the anti-($O3^-$) orientifold projection, the repulsion exerted by the anti-O3-plane on D3-branes translates into a decay channel of the corresponding non-supersymmetric $AdS_5 \times \mathbb{R}P_5$ background, by nucleation of D3-brane bubbles, which discharge the N units of RR 5-form flux, much along the lines suggested in [58].

• In the case of the anti-($O3^-$) with an extra anti-D3-brane, the decay channel of the corresponding non-supersymmetric $AdS_5 \times \mathbb{R}P_5$ background is identical to the previous one, since the two configuration simply differ in the value mod 2 of the RR 5-form flux N. Notice that the decay does not change the values of the NSNS and RR 2-form backgrounds, since the anti-($O3^-$) with either the initial stuck anti-D3-brane or the final stuck D3-brane, both have vanishing NSNS background and non-trivial RR 2-form background.

• In the case of the anti-($O3^+$) projection, the flat space configuration seems stable. However, the S-dual of the anti-($O3^+$) is given by the configuration of an anti-($O3^-$) + 1 $\overline{D3}$ of the previous paragraph. This suggests that the anti-($O3^+$) can turn into an anti-($O3^-$) via strong coupling processes. Indeed, notice that if one considers an NS5-brane (whose core is inherently non-perturbative) stretching along three of the anti-O3 directions and three directions transverse to it, the NS5-brane splits the anti-O3 in two halves, which actually have opposite signs for the orientifold plane charge, with one extra half anti-D3-brane on top of the anti-($O3^-$) half to provide a continuous O3-plane charge across the NS5-brane (see [228] for a review including such brane constructions). This allows to nucleate holes in the anti-($O3^+$), in whose interior the stuck $\overline{D3}$ on the anti-($O3^-$) can annihilate against one of the D3-branes around it, leading to repulsion of the remaining D3-branes, and thus, to instability. This suggests that, in the $AdS_5 \times \mathbb{R}P_5$ gravity dual language, there is a decay channel via the nucleation of bubbles bounded by a domain wall given by an NS5-brane wrapped on a maximal $\mathbb{R}P_2$. From the analysis of topological constraints on wrapped branes in [155] (derived in the supersymmetric setup, but valid in general), this is indeed allowed. The NS5-brane may moreover carry arbitrarily large D3-brane charge, thus discharging dynamically the RR 5-form flux and rendering the AdS unstable.

• Similar conclusions hold in the case of the anti-($\widetilde{O3}^+$) projection, where now the required domain wall involves a bound state of one NS5- and one D5-brane (aka a (1,1)-fivebrane) wrapped on $\mathbb{R}P_2 \subset \mathbb{R}P_5$, thus changing both the NSNS and RR 2-form backgrounds. The fivebrane can carry D3-brane charge, so it can peel off the RR 5-form flux of the AdS compactification triggering its instability.

The instabilities of the above non-supersymmetric orientifolds of AdS backgrounds generalize straightforwardly to non-supersymmetric orientifolds of local AdS warped throats. Hence, in this class of examples, the local AdS-WGC is closely related to the ordinary AdS-WGC constraint.

7 Conclusions

In this thesis two somewhat differentiated topics coexist. The first one, comprising Chapters 3 to 5 is a tale of D-brane instanton backreaction. Motivated by the non-perturbative generation of axion potentials we embark in a journey of describing them in terms of the backreacted geometry that brings us ultimately to BFTs. The second topic, discussed in Chapter 6 revolves around the idea of the Swampland and the no-AdS conjecture which is generalized to locally AdS warped throats. A main unifying tool used in these two endeavours is that of dimer models, useful diagrams that ease the discussion of warped throats probed by D3-branes, the dual gauge theory and, possibly non-perturbative, interesting phenomena.

Axions develop a non-perturbative potential from instanton effects that should be describable in terms of the dual 2-form and a suitable 3-form. This description is available for gauge instantons in terms of the CS 3-form. For Stringy instantons, such as euclidean D-branes the required forms are not available. This is solved in Chapter 3, where we have provided the description of the axion potential from non-gauge D-brane instanton effects in terms of a 3-form eating up the 2-form dual to the axion. The D3-brane instanton backreacts on the geometry by giving rise to a new 1-form. The 3-form arises from the KK reduction of higher-dimensional RR fields in the generalized geometry arising when the D-brane instanton backreaction is taken into account. The mechanism also holds for D-brane instantons corresponding to gauge instantons, in which case the generalized geometry description of the axion couplings can be regarded as holographically related to earlier 3-form descriptions of stabilization of QCD-like axions. It may also be generalized to other branes through T-duality.

This process puts axion potentials from non-perturbative effects in a similar footing to other stabilization mechanisms, like flux compactifications. We hope this can improve the study of the interplay between different stabilization mechanisms in string theory. In another line, given recent results in applying the Weak Gravity Conjecture to axion models in terms of their dual 3-forms [75], we expect our analysis to allow similar analysis for non-perturbative axion potentials from instantons.

Once the phenomenological issue of the axion potential is settled, a natural question is to study D-brane instantons in a more general setting, possibly with intersecting D-branes. This is studied in Chapter 4, where the description of non-perturbative effects from D-brane instantons in 4d string compactifications with gauge D-branes is investigated. Again, from the perspective of the geometry resulting from the instanton backreaction. This extends the former results by including the appearance of 4d charged field operators, which arise from standard perturbative couplings, like worldsheet instantons, in the non-perturbatively backreacted geometry. Along the way we provide a novel interpretation for

the appearance of worldsheet instanton amplitudes in the presence of D2-branes instantons in compactifications with D6-branes.

We have provided a large class of examples of D-brane instanton backreaction based on (type IIA mirrors of) systems of D3-branes at toric singularities. The backreacted configuration is obtained by application of a simple set of rules on the graphs associated to the dimer diagram. This defines an interesting new set of operations relating toric CY singularities with a set of generically non-CY geometries. For D2-branes on nodes associated with deformation fractional branes, the resulting geometry is still CY and corresponds to (the mirror of) complex deformations of the original singularity.

The full description of D-brane instanton backreaction purely in terms of the dimer diagrams is provided in Chapter 5, where a simple description of the effect of D-brane instantons in systems of D3-branes at toric CY_3 singularities is provided. It corresponds to a combinatorial recipe in the corresponding bipartite dimer diagram. Interestingly, the prescription brings generically higher-genus BFTs into the game. In this sense, it provides a new physical interpretation for the latter, which adds to those already in the literature, and in fact the first directly relating BFTs to realizations in string theory.

We have applied this recipe to several examples, also considering multi-instantons associated to complex deformations. We have detailed a "global" recipe that gives rise to consistent tilings and considered combining backreaction and Seiberg Duality. A nice representation of the additional handles in the dimer has been provided that also applies to general BFTs. The moduli space geometry of the resulting theories has been discussed.

There are several interesting directions to pursue following the backreaction of D-brane instantons:

• The backreaction procedure is highly reminiscent of gauge/gravity dualities. It would be interesting to find particular setups where this analogy can be made more concrete (beyond the cases associated to complex deformations).

• Since our recipe is combinatoric at the level of the tiling diagrams, it may not completely capture the dynamics in configurations with arbitrary (anomaly-free) ranks in the D3-brane gauge factors.

• It would be interesting to find concrete examples in global compactifications. A related issue is the description of the backreaction of instantons in the presence of non-trivial orientifold projections.

• The combinatorial recipe in the dimer can be generalized to arbitrary BFTs, and provides a new operation relating BFTs on Riemann surfaces generically of different genus. It would be interesting to explore the implications of this operation in the interpretation of bipartite graphs as describing on-shell scattering amplitudes.

• Study the backreaction effects of non-compact instantons, corresponding to Euclidean D3-branes on non-compact 4-cycles. Their proper understanding should connect with the general considerations in [161].

• A systematic study of instanton effects on the D3-brane systems with flavor D7-branes. Since the latter provide the natural arena for the string theory embedding of (low-genus) BFTs with boundaries [35], the introduction of handles via D-brane instanton backreaction presumably allows the embedding of the general class of BFTs in string theory.

• We have taken first steps towards the discussion of multi-instanton backreaction, recovering and explaining earlier results in the case of complex deformations. We expect

a systematic discussion of general multi-instanton backreaction to reveal other interesting geometric operations.

• The higher-dimensional toric data obtained for the higher-genus BFT resulting from instanton backreaction on a CY 3-fold D-brane gauge theory corresponds to a higher-dimensional geometry, whose physical realization is still lacking. It would be interesting to identify physical objects potentially related to this higher-dimensional variety, and its role in the non-perturbative dynamics of the D-brane system.

In Chapter 6 we have turned our attention to the Swampland program and used warped throats as an arena. We have proposed a new swampland conjecture forbidding stable non-supersymmetric locally AdS warped throats. This *local AdS-WGC* generalizes the analogous statement for stable non-supersymmetric AdS vacua. We have illustrated its application, which allows to reinterpret several known results about warped throats from fractional branes, and to derive new results on the (in)stability of large classes of non-supersymmetric throats, with supersymmetry breaking triggered by strong dynamics in infrared D-brane sectors, or by the presence of stringy sources like anti-O3-planes.

Although the local AdS-WGC forbids stable non-supersymmetric throats, it has no direct bearing on meta-stable non-supersymmetric throats. In contrast with the AdS-WGC, there is no isometry in the radial direction introducing an infinite volume factor multiplying the decay probability, so a finite and potentially small decay amplitude is in principle feasible. The question of whether swampland criteria can impose further restrictions on the meta-stable throats used in dS uplifts is a very interesting one, to which we plan to return in the future.

Several of the instabilities of the non-supersymmetric throats we have discussed are of the runaway kind. In actual 4d compactifications, this corresponds to shortening the throat, thus moderating the hierarchies between the bulk and the throat. Hence, even if the dynamics of the global compactification eventually stabilizes the runaway and renders such configurations more stable, there may remain a question on the tunability of scale hierarchies in the final states. The possibility that swampland criteria directly constrain such hierarchies is a tantalizing direction we hope to explore in the future.

We have made some interesting progress, and provided yet another hint that the body of knowledge on swampland criteria on effective theories is paving the way towards an era of Quantum Gravitational String Phenomenology.

Conclusiones

En esta tesis se tratan dos temas diferenciados. En primer lugar, los Capítulos 3, 4 y 5 son la historia de cómo un instantón de D-brana modifica la geometría. Este viaje comienza reformulando el potencial no perturbativo de los axiones y nos lleva hasta las costas de las teorías de campos bipartitas (BFTs). El segundo tema versa sobre la idea de la Ciénaga y la conjetura de no-AdS, que es generalizada a gargantas "retorcidas", que son AdS de forma local. Como herramienta unificadora del trabajo tenemos los modelos dimer, útiles representaciones de las teorías de campos localizadas en D-branas en singularidades. Nos sirven para estudiar de forma sencilla las propiedades de estas gargantas y describir fenómenos interesantes, posiblemente no perturbativos.

Los axiones desarrollan un potencial no perturbativo debido a su acoplo con instantones. Este potencial debería poderse describir en términos de la 2-forma dual y una 3-forma. Para el caso de instantones gauge esto es así, jugando el papel descrito la 3-forma de Chern-Simons, pero para instantones cuerdosos no hay 3-forma que genere el potencial. En el Capítulo 3 encontramos la 3-forma responsable del potencial. Esta se oculta en la deformación de la geometría generalizada producida por la presencia del instantón cuerdoso. La D3-brana deforma la geometría dando lugar a una 1-forma que se puede utilizar en la reducción Kaluza-Klein para encontrar una 3-forma a partir de los campos de Ramond-Ramond. Este mecanismo también se aplica al caso de instantones gauge, donde la descripción en términos de una geometría deformada se puede ver como una descripción dual (en el sentido holográfico) de la realizada en términos de condensación de gauginos en la teoría de tipo QCD. Haciendo uso de T-dualidad, este proceso se puede aplicar a otras teorías de cuerdas con otros tipos de instantones.

Con esta descripción ponemos el potencial no perturbativo de los axiones al mismo nivel que otros métodos de estabilización de moduli, como compactificación por flujos. Esperamos que esto ayude a comprender mejor la relación entre los distintos mecanismos de estabilización en teoría de cuerdas. Por otro lado, en vista de la reciente aplicación de la conjetura de gravedad débil (WGC) a modelos axiónicos en términos de 2 y 3-formas [75], esperamos que nuestro trabajo permita un tratamiento similar para potenciales no perturbativos producidos por instantones.

Solucionado el misterio del potencial de los axiones, resulta natural estudiar la deformación ocasionada por los instantones en la geometría en un contexto más general y en presencia de otras branas. En el Capítulo 4 se ha hecho precisamente esto. Hemos extendido los resultados, incluyendo la aparición de operadores cargados en 4d generados por instantones de D-brana. Una vez la geometría es deformada, son generados por acoplos perturbativos, mediados por instantones de cuerdas fundamentales. Además proporcionamos una innovadora interpretación de estos instantones de cuerda en presencia de instantones de D2-branas y D6-branas.

Hemos expuesto una amplia clase de ejemplos de instantones deformando la geometría en (los duales espejo IIA) sistemas de D3-branas en singularidades tóricas. La geometría deformada se obtiene aplicando una serie de reglas sencillas que modifican el grafo dual al dimer, que codifica la geometría de forma explícita. Este procedimiento define una nueva operación que relaciona singularidades tóricas con otras geometrías que no necesariamente son CY. En los casos especiales de D2-branas en nodos correspondiendo a deformaciones complejas de la singularidad original, la geometría resultante sigue siendo CY y se corresponde precisamente con la deformación compleja.

La deformación de la geometría causada por los instantones de D-brana se puede describir completamente en términos del diagrama dimer, como se explica en el Capítulo 5. Hemos proporcionado una descripción sencilla en términos de una receta combinatoria directamente en el dimer bipartito. Resulta interesante comprobar que esta receta aumenta, de forma genérica, el número de agujeros (género) de la superficie en la que se embebe el diagrama bipartito. De este modo, la geometrización de instantones de D-brana nos permite generar BFTs usando teoría de cuerdas.

Hemos usado la receta en varios ejemplos, incluyendo multi-instantones asociados con deformaciones complejas. Hemos detallado una receta "global" que da lugar a tilings consistentes, además de discutir el uso conjunto con dualidad de Seiberg. Además hemos descrito una representación sencilla de los "mangos" adicionales que también se puede aplicar a BFTs generales. La geometría del espacio de moduli de las teorías obtenidas ha sido estudiada.

A la luz de estos avances, hay varias direcciones en las que se podría seguir trabajando:

• Describir instantones de D-brana en términos de una geometría deformada recuerda poderosamente a la dualidad holográfica entre teorías gauge y de gravedad. Sería interesante estudiar esta relación de forma más concreta, en casos más allá de las deformaciones complejas.

• Dado que nuestra receta es combinatoria y solo depende de los diagramas, podría ser que no capture de forma correcta la dinámica en configuraciones sin anomalías con rangos arbitrarios en los diferentes factores gauge.

• Sería interesante encontrar ejemplos particulares en compactificaciones globales. De forma relacionada, sería interesante estudiar la deformación de la geometría en presencia de proyecciones de orientación (orientifolds).

• La receta combinatoria en el dimer se puede generalizar para BFTs arbitrarios y da lugar a una nueva operación entre BFTs de distinto género. Sería interesante investigar las implicaciones que esta operación pudiera tener en las distintas interpretaciones físicas que tienen los BFTs, tales como la descripción de amplitudes de scattering on shell.

• Investigar instantones no-compactos. Su comprensión debería conectar con las consideraciones expresadas en [161].

• Relacionado con lo anterior, estudiar de forma sistemática efectos instantónicos en sistemas de D3-branas en presencia de D7-branas de sabor. Dado que estas proporcionan el ambiente natural en el que describir en teoría de cuerdas BFTs con fronteras [35], la introducción de mangos haciendo uso de instantones de D-brana debería permitir la descripción de grandes clases de BFTs en teoría de cuerdas.

• Hemos tomado los primeros pasos en la discusión de multi-instantones, recuperando los resultados conocidos para el caso de deformaciones complejas. Creemos que la discusión sistemática de multi-instantones más generales podría revelar otras interesantes operaciones geométricas.

• Hemos visto que los BFTs de género mayor tienen una geometría tórica asociada a su espacio de modulos. No obstante, desconocemos la realidad física de esta geometría en teoría de cuerdas. Sería interesante identificar objetos físicos que pudieran estar relacionados con esta variedad de mayor dimensión, así como su posible rol en la dinámica no perturbativa en sistemas de D-branas.

En el Capítulo 6, hemos cambiado el foco para prestar atención a la idea de Ciénaga en teoría de cuerdas y hemos utilizado las gargantas curvadas como un caso interesante. Hemos propuesto una nueva conjetura de la ciénaga que prohíbe la existencia de gargantas no supersimétricas que sean localmente AdS, en el sentido descrito en el texto principal. Esta conjetura *local AdS-WGC* generaliza la conjetura que prohíbe vacíos AdS no supersimétricos. Hemos ilustrado la aplicación de esta conjetura reinterpretando varias gargantas que, en presencia de branas fraccionarias, son no supersimétricas. Hemos estudiado su inestabilidad en presencia de la conjetura para casos donde la ruptura de supersimetría viene mediada por sectores de acoplamiento fuerte a bajas energías, o por la presencia de ingredientes cuerdosos como planos anti-O3.

A pesar de que la conjetura local AdS-WGC prohíbe gargantas no supersimétricas estables, no tiene nada que decir sobre las gargantas metaestables. A diferencia de la conjetura AdS-WGC, no hay ninguna isometría radial que pueda introducir un factor infinito que multiplique la probabilidad de un decaimiento, por lo que la existencia de una amplitud de decaimiento finita y potencialmente pequeña es en principio factible. La pregunta sobre si es posible usar criterios de la ciénaga para constreñir gargantas metaestables utilizadas en uplifts a dS es muy interesante y esperamos poder decir algo en el futuro.

Varias de las inestabilidades que hemos discutido son del tipo "runaway". En compactificaciones 4d, esto corresponde al acortamiento de la garganta, y la consecuente moderación de las jerarquías entre fuera y dentro de la garganta. De este modo, incluso si la dinámica de la compactificación global pudiese estabilizar la inestabilidad, aún habría que preguntarse sobre la ajustabilidad de las jerarquías. La posibilidad de que este tipo de criterios puedan constreñir estas jerarquías es una dirección que pretendemos explorar en el futuro.

En esta segunda parte hemos hecho un progreso interesante y proporcionado otra pista más de que el conocimiento relacionado con los criterios de la ciénaga sobre las teorías efectivas está abriendo camino a una era de Fenomenología de Gravedad Cuántica Cuerdosa.

A

Some QFT tools

In this appendix we describe a set of tools, used in the body of this work, to study the behavior of QFT's along their RG-flow.

1.1 Scale Matching

scale matching, is a nice tool relevant for studying Quantum Field Theories that have different descriptions along their RG-flow. At the scale where two descriptions meet, the coupling of the two theories should match. This is particularly powerful in the case of supersymmetric theories, as the holomorphic coupling is easily related to the dynamical scale. Let us illustrate this idea with a particular example. Take SQCD with $SU(N_C)$ gauge group and N_F flavors. Give a vev to a quark $\langle Q_1 \rangle = \langle \bar{Q}_1 \rangle = v$. For energies below this vev, the gauge breaks down to $SU(N'_C) = SU(N_C - 1)$ and the quark is integrated out, decreasing the number of flavors, $N'_F = N_F - 1$.

For energies above v and below it the theory is described in terms of different fields,

$$SU(N_C), N_F \quad \to SU(N'_C), N'_F \tag{A.1}$$

The perturbative holomorphic couplings obey Equation (2.6) and must match at scale v,

$$\tau(v) = \tau'(v) \quad \to \quad \Lambda^b = \Lambda'^{b'} \cdot v^{b-b'} \tag{A.2}$$

Where b, b' are the coefficients of the one-loop β-function in Equation (2.3) and the Λ's are the dynamical scales. Note that this result is general for the RG-flow of SQCD with any field content. We use it in Section 6.3.2. In the above formula we have ignored threshold factors, which depend on the subtraction squeme. This result is correct in the $\overline{DR}$ scheme [229].

1.2 't Hooft anomaly matching conditions

Let us now review on-the-go how anomalies arise as triangle diagrams and how correlators of global currents can be used to match different descriptions along the RG-flow.

An anomalous symmetry is a classical symmetry that fails to be preserved in the quantum theory. It can be seen as arising from 3-point functions between currents, as a

failure of the measure to be left invariant by the symmetry and so on. Perturbatively, it arises from a triangle diagram with a global current and two gauge potentials,

$$\langle j_A V_B V_C \rangle \to \partial_\mu j_A^\mu \sim \mathrm{Tr}(t_A, \{t_B, t_C\}) F_B^{\mu\nu} \tilde{F}_{C,\mu\nu} \tag{A.3}$$

From this formula, one learns several things:

- Only complex representations contribute to the anomaly. Thus, only massless chiral fermions contribute.
- The anomaly is proportional to the instanton number. Thus, even though it is exact at one loop, it is related to non-perturbative effects.
- The anomaly can actually be seen as an explicit breaking of the symmetry by the θ-term in the action.

In the correlator in Equation (A.3), two symmetries are gauged. As noted by 't Hooft, correlators between global currents compute scale independent information that can be used along the RG-flow to match different phases.

Consider a theory with an exact global symmetry generated by current j_A^μ. Call $\langle j_A^\mu j_A^\nu j_A^\rho \rangle \sim A_{UV}$ (this is not an anomaly!). Now gauge the global symmetry and introduce the required fermions to compensate for the gauge anomaly. The fermionic sector then contributes to the anomaly as $A_s = -A_{UV}$. Consider now this theory at a lower scale and decoupling limit $g \to 0$. The theory is still anomaly free so the fermion anomaly must cancel the anomaly in the original theory (really a global current 3-point function, but we added gauge fields), $A_s - A_{IR} = 0$. Thus,

$$A_{IR} = A_{UV} \tag{A.4}$$

We can always play this game of gauging, introducing fremions and so on. The bottom line is that correlators of global currents are RG-flow independent information!

Bibliography

[1] M. Bertolini, *Lectures on supersymmetry*, https://people.sissa.it/ bertmat/susycourse.pdf.

[2] J. Terning, *Modern supersymmetry: Dynamics and duality*. 2006, 10.1093/acprof:oso/9780198567639.001.0001.

[3] J. D. Edelstein, *Notes on Supersymmetry*, http://www-fp.usc.es/ edels/SUSY/aSuSy.pdf.

[4] I. Affleck, M. Dine and N. Seiberg, *Dynamical Supersymmetry Breaking in Supersymmetric QCD*, *Nucl. Phys.* **B241** (1984) 493.

[5] N. Seiberg, *Exact results on the space of vacua of four-dimensional SUSY gauge theories*, *Phys. Rev.* **D49** (1994) 6857 [hep-th/9402044].

[6] N. Seiberg, *Electric - magnetic duality in supersymmetric nonAbelian gauge theories*, *Nucl. Phys.* **B435** (1995) 129 [hep-th/9411149].

[7] Y. Shadmi and Y. Shirman, *Dynamical supersymmetry breaking*, *Rev. Mod. Phys.* **72** (2000) 25 [hep-th/9907225].

[8] I. Affleck, M. Dine and N. Seiberg, *Dynamical Supersymmetry Breaking in Chiral Theories*, *Phys. Lett.* **B137** (1984) 187.

[9] Y. Meurice and G. Veneziano, *Susy vacua versus chiral fermions*, *Phys. Lett.* **141B** (1984) 69.

[10] B. R. Greene, *String theory on Calabi-Yau manifolds*, in *Fields, strings and duality. Proceedings, Summer School, Theoretical Advanced Study Institute in Elementary Particle Physics, TASI'96, Boulder, USA, June 2-28, 1996*, pp. 543–726, 1996, hep-th/9702155.

[11] K. Hori, S. Katz, A. Klemm, R. Pandharipande, R. Thomas, C. Vafa et al., *Mirror symmetry*, vol. 1 of *Clay mathematics monographs*. AMS, Providence, USA, 2003.

[12] C. Closset, *Toric geometry and local Calabi-Yau varieties: An Introduction to toric geometry (for physicists)*, 0901.3695.

[13] B. Feng, A. Hanany and Y.-H. He, *D-brane gauge theories from toric singularities and toric duality*, *Nucl. Phys.* **B595** (2001) 165 [hep-th/0003085].

[14] C. E. Beasley and M. R. Plesser, *Toric duality is Seiberg duality*, *JHEP* **12** (2001) 001 [hep-th/0109053].

[15] B. Feng, A. Hanany, Y.-H. He and A. M. Uranga, *Toric duality as Seiberg duality and brane diamonds*, *JHEP* **12** (2001) 035 [hep-th/0109063].

[16] A. Strominger, *Massless black holes and conifolds in string theory*, *Nucl. Phys.* **B451** (1995) 96 [hep-th/9504090].

[17] M. Aganagic and C. Vafa, *G(2) manifolds, mirror symmetry and geometric engineering*, hep-th/0110171.

[18] K. Altmann, *The versal deformation of an isolated toric Gorenstein singularity*, *Inventiones Mathematicae* **128** (1997) 443.

[19] J. M. Maldacena, *The Large N limit of superconformal field theories and supergravity*, *Int. J. Theor. Phys.* **38** (1999) 1113 [hep-th/9711200].

[20] J. Polchinski, *Introduction to Gauge/Gravity Duality*, in *Proceedings, Theoretical Advanced Study Institute in Elementary Particle Physics (TASI 2010). String Theory and Its Applications: From meV to the Planck Scale: Boulder, Colorado, USA, June 1-25, 2010*, pp. 3–46, 2010, 1010.6134, DOI.

[21] I. R. Klebanov and E. Witten, *Superconformal field theory on three-branes at a Calabi-Yau singularity*, *Nucl. Phys.* **B536** (1998) 199 [hep-th/9807080].

[22] C. P. Herzog, I. R. Klebanov and P. Ouyang, *D-branes on the conifold and N=1 gauge / gravity dualities*, in *Progress in string, field and particle theory: Proceedings, NATO Advanced Study Institute, EC Summer School, Cargese, France, June 25-July 11, 2002*, pp. 189–223, 2002, hep-th/0205100.

[23] F. Benini, *Brief Introduction to AdS/CFT*, .

[24] S. S. Gubser and I. R. Klebanov, *Baryons and domain walls in an N=1 superconformal gauge theory*, *Phys. Rev.* **D58** (1998) 125025 [hep-th/9808075].

[25] C. P. Bachas, M. R. Douglas and M. B. Green, *Anomalous creation of branes*, *JHEP* **07** (1997) 002 [hep-th/9705074].

[26] U. Danielsson, G. Ferretti and I. R. Klebanov, *Creation of fundamental strings by crossing D-branes*, *Phys. Rev. Lett.* **79** (1997) 1984 [hep-th/9705084].

[27] A. M. Uranga, *Brane configurations for branes at conifolds*, *JHEP* **9901** (1999) 022 [hep-th/9811004].

[28] I. R. Klebanov and M. J. Strassler, *Supergravity and a confining gauge theory: Duality cascades and chi SB resolution of naked singularities*, *JHEP* **0008** (2000) 052 [hep-th/0007191].

[29] I. R. Klebanov and A. A. Tseytlin, *Gravity duals of supersymmetric SU(N) x SU(N+M) gauge theories*, *Nucl. Phys.* **B578** (2000) 123 [hep-th/0002159].

[30] I. R. Klebanov and N. A. Nekrasov, *Gravity duals of fractional branes and logarithmic RG flow*, *Nucl. Phys.* **B574** (2000) 263 [hep-th/9911096].

[31] S. Franco, A. Hanany, F. Saad and A. M. Uranga, *Fractional branes and dynamical supersymmetry breaking*, *JHEP* **0601** (2006) 011 [hep-th/0505040].

[32] B. Feng, Y.-H. He, K. D. Kennaway and C. Vafa, *Dimer models from mirror symmetry and quivering amoebae*, *Adv. Theor. Math. Phys.* **12** (2008) 489 [hep-th/0511287].

[33] S. Franco, A. Hanany, D. Krefl, J. Park, A. M. Uranga and D. Vegh, *Dimers and orientifolds*, *JHEP* **0709** (2007) 075 [0707.0298].

[34] S. Franco, *Bipartite Field Theories: from D-Brane Probes to Scattering Amplitudes*, *JHEP* **1211** (2012) 141 [1207.0807].

[35] S. Franco and A. Uranga, *Bipartite Field Theories from D-Branes*, *JHEP* **1404** (2014) 161 [1306.6331].

[36] S. Franco, E. Garcia-Valdecasas and A. M. Uranga, *Bipartite field theories and D-brane instantons*, *JHEP* **11** (2018) 098 [1805.00011].

[37] S. Franco, D. Ghim, S. Lee, R.-K. Seong and D. Yokoyama, *2d (0,2) Quiver Gauge Theories and D-Branes*, *JHEP* **09** (2015) 072 [1506.03818].

[38] S. Franco, S. Lee and R.-K. Seong, *Brane Brick Models, Toric Calabi-Yau 4-Folds and 2d (0,2) Quivers*, *JHEP* **02** (2016) 047 [1510.01744].

[39] S. Franco, S. Lee, R.-K. Seong and C. Vafa, *Quadrality for Supersymmetric Matrix Models*, *JHEP* **07** (2017) 053 [1612.06859].

[40] C. Closset, S. Franco, J. Guo and A. Hasan, *Graded quivers and B-branes at Calabi-Yau singularities*, *JHEP* **03** (2019) 053 [1811.07016].

[41] S. Franco and A. Hasan, *Graded Quivers, Generalized Dimer Models and Toric Geometry*, 1904.07954.

[42] M. R. Douglas and G. W. Moore, *D-branes, quivers, and ALE instantons*, hep-th/9603167.

[43] S. Franco, A. Hanany and A. M. Uranga, *Multi-flux warped throats and cascading gauge theories*, *JHEP* **0509** (2005) 028 [hep-th/0502113].

[44] I. Garcia-Etxebarria, F. Saad and A. M. Uranga, *Quiver gauge theories at resolved and deformed singularities using dimers*, *JHEP* **0606** (2006) 055 [hep-th/0603108].

[45] K. Becker and M. Becker, *M theory on eight manifolds*, *Nucl. Phys.* **B477** (1996) 155 [hep-th/9605053].

[46] K. Dasgupta, G. Rajesh and S. Sethi, *M theory, orientifolds and G - flux*, *JHEP* **08** (1999) 023 [hep-th/9908088].

[47] M. Grana and J. Polchinski, *Supersymmetric three form flux perturbations on AdS(5)*, *Phys. Rev.* **D63** (2001) 026001 [hep-th/0009211].

[48] S. Franco, Y.-H. He, C. Herzog and J. Walcher, *Chaotic duality in string theory*, *Phys.Rev.* **D70** (2004) 046006 [hep-th/0402120].

[49] D. Berenstein, C. P. Herzog, P. Ouyang and S. Pinansky, *Supersymmetry breaking from a Calabi-Yau singularity*, *JHEP* **09** (2005) 084 [hep-th/0505029].

[50] M. Bertolini, F. Bigazzi and A. L. Cotrone, *Supersymmetry breaking at the end of a cascade of Seiberg dualities*, *Phys. Rev.* **D72** (2005) 061902 [hep-th/0505055].

[51] T. D. Brennan, F. Carta and C. Vafa, *The String Landscape, the Swampland, and the Missing Corner*, *PoS* **TASI2017** (2017) 015 [1711.00864].

[52] E. Palti, *The Swampland: Introduction and Review*, 2019, 1903.06239.

[53] D. Harlow and H. Ooguri, *Symmetries in quantum field theory and quantum gravity*, 1810.05338.

[54] N. Arkani-Hamed, L. Motl, A. Nicolis and C. Vafa, *The String landscape, black holes and gravity as the weakest force*, *JHEP* **06** (2007) 060 [hep-th/0601001].

[55] H. Ooguri and C. Vafa, *On the Geometry of the String Landscape and the Swampland*, *Nucl. Phys.* **B766** (2007) 21 [hep-th/0605264].

[56] F. Baume and E. Palti, *Backreacted Axion Field Ranges in String Theory*, *JHEP* **08** (2016) 043 [1602.06517].

[57] D. Klaewer and E. Palti, *Super-Planckian Spatial Field Variations and Quantum Gravity*, *JHEP* **01** (2017) 088 [1610.00010].

[58] H. Ooguri and C. Vafa, *Non-supersymmetric AdS and the Swampland*, *Adv. Theor. Math. Phys.* **21** (2017) 1787 [1610.01533].

[59] J. M. Maldacena, J. Michelson and A. Strominger, *Anti-de Sitter fragmentation*, *JHEP* **02** (1999) 011 [hep-th/9812073].

[60] B. Freivogel and M. Kleban, *Vacua Morghulis*, 1610.04564.

[61] H. Ooguri and L. Spodyneiko, *New Kaluza-Klein instantons and the decay of AdS vacua*, *Phys. Rev.* **D96** (2017) 026016 [1703.03105].

[62] R. D. Peccei and H. R. Quinn, *CP Conservation in the Presence of Instantons*, *Phys. Rev. Lett.* **38** (1977) 1440.

[63] A. de la Fuente, P. Saraswat and R. Sundrum, *Natural Inflation and Quantum Gravity*, *Phys. Rev. Lett.* **114** (2015) 151303 [1412.3457].

[64] T. Rudelius, *Constraints on Axion Inflation from the Weak Gravity Conjecture*, *JCAP* **1509** (2015) 020 [1503.00795].

[65] M. Montero, A. M. Uranga and I. Valenzuela, *Transplanckian axions!?*, *JHEP* **08** (2015) 032 [1503.03886].

[66] J. Brown, W. Cottrell, G. Shiu and P. Soler, *Fencing in the Swampland: Quantum Gravity Constraints on Large Field Inflation*, *JHEP* **10** (2015) 023 [1503.04783].

[67] T. C. Bachlechner, C. Long and L. McAllister, *Planckian Axions and the Weak Gravity Conjecture*, *JHEP* **01** (2016) 091 [1503.07853].

[68] A. Hebecker, P. Mangat, F. Rompineve and L. T. Witkowski, *Winding out of the Swamp: Evading the Weak Gravity Conjecture with F-term Winding Inflation?*, *Phys. Lett.* **B748** (2015) 455 [1503.07912].

[69] J. Brown, W. Cottrell, G. Shiu and P. Soler, *On Axionic Field Ranges, Loopholes and the Weak Gravity Conjecture*, *JHEP* **04** (2016) 017 [1504.00659].

[70] D. Junghans, *Large-Field Inflation with Multiple Axions and the Weak Gravity Conjecture*, *JHEP* **02** (2016) 128 [1504.03566].

[71] B. Heidenreich, M. Reece and T. Rudelius, *Weak Gravity Strongly Constrains Large-Field Axion Inflation*, *JHEP* **12** (2015) 108 [1506.03447].

[72] S. Bielleman, L. E. Ibanez and I. Valenzuela, *Minkowski 3-forms, Flux String Vacua, Axion Stability and Naturalness*, *JHEP* **12** (2015) 119 [1507.06793].

[73] E. Palti, *On Natural Inflation and Moduli Stabilisation in String Theory*, *JHEP* **10** (2015) 188 [1508.00009].

[74] B. Heidenreich, M. Reece and T. Rudelius, *Sharpening the Weak Gravity Conjecture with Dimensional Reduction*, *JHEP* **02** (2016) 140 [1509.06374].

[75] L. E. Ibanez, M. Montero, A. Uranga and I. Valenzuela, *Relaxion Monodromy and the Weak Gravity Conjecture*, *JHEP* **04** (2016) 020 [1512.00025].

[76] A. Hebecker, F. Rompineve and A. Westphal, *Axion Monodromy and the Weak Gravity Conjecture*, *JHEP* **04** (2016) 157 [1512.03768].

[77] A. Hebecker, J. Moritz, A. Westphal and L. T. Witkowski, *Axion Monodromy Inflation with Warped KK-Modes*, *Phys. Lett.* **B754** (2016) 328 [1512.04463].

[78] J. P. Conlon and S. Krippendorf, *Axion decay constants away from the lamppost*, *JHEP* **04** (2016) 085 [1601.00647].

[79] B. Heidenreich, M. Reece and T. Rudelius, *Axion Experiments to Algebraic Geometry: Testing Quantum Gravity via the Weak Gravity Conjecture*, 1605.05311.

[80] G. Dvali, *Three-form gauging of axion symmetries and gravity*, hep-th/0507215.

[81] G. Dvali, R. Jackiw and S.-Y. Pi, *Topological mass generation in four dimensions*, *Phys. Rev. Lett.* **96** (2006) 081602 [hep-th/0511175].

[82] G. Dvali, S. Folkerts and A. Franca, *How neutrino protects the axion*, *Phys. Rev.* **D89** (2014) 105025 [1312.7273].

[83] E. Silverstein and A. Westphal, *Monodromy in the CMB: Gravity Waves and String Inflation*, *Phys. Rev.* **D78** (2008) 106003 [0803.3085].

[84] L. McAllister, E. Silverstein and A. Westphal, *Gravity Waves and Linear Inflation from Axion Monodromy*, *Phys. Rev.* **D82** (2010) 046003 [0808.0706].

[85] F. Marchesano, G. Shiu and A. M. Uranga, *F-term Axion Monodromy Inflation*, *JHEP* **09** (2014) 184 [1404.3040].

[86] N. Kaloper and L. Sorbo, *A Natural Framework for Chaotic Inflation*, *Phys. Rev. Lett.* **102** (2009) 121301 [0811.1989].

[87] N. Kaloper, A. Lawrence and L. Sorbo, *An Ignoble Approach to Large Field Inflation*, *JCAP* **1103** (2011) 023 [1101.0026].

[88] M. Berg, E. Pajer and S. Sjors, *Dante's Inferno*, *Phys. Rev.* **D81** (2010) 103535 [0912.1341].

[89] L. E. Ibáñez and I. Valenzuela, *BICEP2, the Higgs Mass and the SUSY-breaking Scale*, *Phys. Lett.* **B734** (2014) 354 [1403.6081].

[90] E. Palti and T. Weigand, *Towards large r from [p, q]-inflation*, *JHEP* **04** (2014) 155 [1403.7507].

[91] R. Blumenhagen and E. Plauschinn, *Towards Universal Axion Inflation and Reheating in String Theory*, *Phys. Lett.* **B736** (2014) 482 [1404.3542].

[92] L. E. Ibanez and I. Valenzuela, *The inflaton as an MSSM Higgs and open string modulus monodromy inflation*, *Phys. Lett.* **B736** (2014) 226 [1404.5235].

[93] A. Hebecker, S. C. Kraus and L. T. Witkowski, *D7-Brane Chaotic Inflation*, *Phys. Lett.* **B737** (2014) 16 [1404.3711].

[94] N. Kaloper and A. Lawrence, *Natural chaotic inflation and ultraviolet sensitivity*, *Phys. Rev.* **D90** (2014) 023506 [1404.2912].

[95] M. Arends, A. Hebecker, K. Heimpel, S. C. Kraus, D. Lust, C. Mayrhofer et al., *D7-Brane Moduli Space in Axion Monodromy and Fluxbrane Inflation*, *Fortsch. Phys.* **62** (2014) 647 [1405.0283].

[96] S. Franco, D. Galloni, A. Retolaza and A. Uranga, *On axion monodromy inflation in warped throats*, *JHEP* **02** (2015) 086 [1405.7044].

[97] R. Blumenhagen, D. Herschmann and E. Plauschinn, *The Challenge of Realizing F-term Axion Monodromy Inflation in String Theory*, *JHEP* **01** (2015) 007 [1409.7075].

[98] A. Hebecker, P. Mangat, F. Rompineve and L. T. Witkowski, *Tuning and Backreaction in F-term Axion Monodromy Inflation*, *Nucl. Phys.* **B894** (2015) 456 [1411.2032].

[99] L. E. Ibanez, F. Marchesano and I. Valenzuela, *Higgs-otic Inflation and String Theory*, *JHEP* **01** (2015) 128 [1411.5380].

[100] I. Garcia-Etxebarria, T. W. Grimm and I. Valenzuela, *Special Points of Inflation in Flux Compactifications*, *Nucl. Phys.* **B899** (2015) 414 [1412.5537].

[101] R. Blumenhagen, A. Font, M. Fuchs, D. Herschmann, E. Plauschinn, Y. Sekiguchi et al., *A Flux-Scaling Scenario for High-Scale Moduli Stabilization in String Theory*, *Nucl. Phys.* **B897** (2015) 500 [1503.07634].

[102] A. Retolaza, A. M. Uranga and A. Westphal, *Bifid Throats for Axion Monodromy Inflation*, *JHEP* **07** (2015) 099 [1504.02103].

[103] D. Escobar, A. Landete, F. Marchesano and D. Regalado, *Large field inflation from D-branes*, 1505.07871.

[104] S. Bielleman, L. E. Ibáñez, F. G. Pedro and I. Valenzuela, *Multifield Dynamics in Higgs-Otic Inflation*, 1505.00221.

[105] R. Blumenhagen, C. Damian, A. Font, D. Herschmann and R. Sun, *The Flux-Scaling Scenario: De Sitter Uplift and Axion Inflation*, 1510.01522.

[106] L. McAllister, E. Silverstein, A. Westphal and T. Wrase, *The Powers of Monodromy*, *JHEP* **09** (2014) 123 [1405.3652].

[107] M. Berasaluce-Gonzalez, P. G. Camara, F. Marchesano and A. M. Uranga, *Zp charged branes in flux compactifications*, *JHEP* **04** (2013) 138 [1211.5317].

[108] P. G. Camara, L. E. Ibanez and F. Marchesano, *RR photons*, *JHEP* **09** (2011) 110 [1106.0060].

[109] S. Kachru, R. Kallosh, A. D. Linde and S. P. Trivedi, *De Sitter vacua in string theory*, *Phys. Rev.* **D68** (2003) 046005 [hep-th/0301240].

[110] R. Blumenhagen, M. Cvetic and T. Weigand, *Spacetime instanton corrections in 4D string vacua: The Seesaw mechanism for D-Brane models*, *Nucl.Phys.* **B771** (2007) 113 [hep-th/0609191].

[111] L. Ibanez and A. Uranga, *Neutrino Majorana Masses from String Theory Instanton Effects*, *JHEP* **0703** (2007) 052 [hep-th/0609213].

[112] B. Florea, S. Kachru, J. McGreevy and N. Saulina, *Stringy Instantons and Quiver Gauge Theories*, *JHEP* **0705** (2007) 024 [hep-th/0610003].

[113] R. Blumenhagen, M. Cvetic, S. Kachru and T. Weigand, *D-Brane Instantons in Type II Orientifolds*, *Ann.Rev.Nucl.Part.Sci.* **59** (2009) 269 [0902.3251].

[114] L. E. Ibáñez and A. M. Uranga, *String theory and particle physics: An introduction to string phenomenology*. Cambridge University Press, 2012.

[115] P. Koerber and L. Martucci, *From ten to four and back again: How to generalize the geometry*, *JHEP* **08** (2007) 059 [0707.1038].

[116] P. Koerber and L. Martucci, *Warped generalized geometry compactifications, effective theories and non-perturbative effects*, *Fortsch. Phys.* **56** (2008) 862 [0803.3149].

[117] M. Berasaluce-Gonzalez, G. Ramirez and A. M. Uranga, *Antisymmetric tensor Z_p gauge symmetries in field theory and string theory*, *JHEP* **01** (2014) 059 [1310.5582].

[118] S. Dubovsky, A. Lawrence and M. M. Roberts, *Axion monodromy in a model of holographic gluodynamics*, *JHEP* **02** (2012) 053 [1105.3740].

[119] X. Dong, B. Horn, E. Silverstein and A. Westphal, *Simple exercises to flatten your potential*, *Phys. Rev.* **D84** (2011) 026011 [1011.4521].

[120] C. Beasley and E. Witten, *New instanton effects in supersymmetric QCD*, *JHEP* **01** (2005) 056 [hep-th/0409149].

[121] I. Garcia-Etxebarria, F. Marchesano and A. M. Uranga, *Non-perturbative F-terms across lines of BPS stability*, *JHEP* **0807** (2008) 028 [0805.0713].

[122] O. J. Ganor, *A Note on zeros of superpotentials in F theory*, *Nucl. Phys.* **B499** (1997) 55 [hep-th/9612077].

[123] D. Baumann, A. Dymarsky, I. R. Klebanov, J. M. Maldacena, L. P. McAllister and A. Murugan, *On D3-brane Potentials in Compactifications with Fluxes and Wrapped D-branes*, *JHEP* **11** (2006) 031 [hep-th/0607050].

[124] A. Dymarsky and L. Martucci, *D-brane non-perturbative effects and geometric deformations*, *JHEP* **04** (2011) 061 [1012.4018].

[125] A. Strominger, S.-T. Yau and E. Zaslow, *Mirror symmetry is T duality*, *Nucl. Phys.* **B479** (1996) 243 [hep-th/9606040].

[126] F. Marchesano, D. Regalado and G. Zoccarato, *On D-brane moduli stabilisation*, *JHEP* **11** (2014) 097 [1410.0209].

[127] K. Becker, M. Becker and A. Strominger, *Five-branes, membranes and nonperturbative string theory*, *Nucl. Phys.* **B456** (1995) 130 [hep-th/9507158].

[128] E. Witten, *Nonperturbative superpotentials in string theory*, *Nucl. Phys.* **B474** (1996) 343 [hep-th/9604030].

[129] J. A. Harvey and G. W. Moore, *Superpotentials and membrane instantons*, hep-th/9907026.

[130] E. Witten, *World sheet corrections via D instantons*, *JHEP* **02** (2000) 030 [hep-th/9907041].

[131] V. Balasubramanian, P. Berglund, J. P. Conlon and F. Quevedo, *Systematics of moduli stabilisation in Calabi-Yau flux compactifications*, *JHEP* **03** (2005) 007 [hep-th/0502058].

[132] L. Ibanez, A. Schellekens and A. Uranga, *Instanton Induced Neutrino Majorana Masses in CFT Orientifolds with MSSM-like spectra*, *JHEP* **0706** (2007) 011 [0704.1079].

[133] R. Blumenhagen, M. Cvetic, D. Lust, R. Richter and T. Weigand, *Non-perturbative Yukawa Couplings from String Instantons*, *Phys.Rev.Lett.* **100** (2008) 061602 [0707.1871].

[134] M. Cvetic, J. Halverson and P. Langacker, *Singlet Extensions of the MSSM in the Quiver Landscape*, *JHEP* **1009** (2010) 076 [1006.3341].

[135] M. Cvetic, J. Halverson, P. Langacker and R. Richter, *The Weinberg Operator and a Lower String Scale in Orientifold Compactifications*, *JHEP* **1010** (2010) 094 [1001.3148].

[136] R. Argurio, M. Bertolini, S. Franco and S. Kachru, *Gauge/gravity duality and meta-stable dynamical supersymmetry breaking*, *JHEP* **0701** (2007) 083 [hep-th/0610212].

[137] R. Argurio, M. Bertolini, S. Franco and S. Kachru, *Meta-stable vacua and D-branes at the conifold*, *JHEP* **0706** (2007) 017 [hep-th/0703236].

[138] M. Cvetic and T. Weigand, *A String theoretic model of gauge mediated supersymmetry beaking*, 0807.3953.

[139] M. Buican and S. Franco, *SUSY breaking mediation by D-brane instantons*, *JHEP* **0812** (2008) 030 [0806.1964].

[140] R. Blumenhagen, A. Deser and D. Lust, *FCNC Processes from D-brane Instantons*, *JHEP* **1102** (2011) 079 [1007.4770].

[141] A. Addazi and M. Bianchi, *Neutron Majorana mass from exotic instantons*, *JHEP* **1412** (2014) 089 [1407.2897].

[142] A. Addazi and M. Bianchi, *Un-oriented Quiver Theories for Majorana Neutrons*, 1502.01531.

[143] A. Addazi and M. Bianchi, *Neutron Majorana mass from Exotic Instantons in a Pati-Salam model*, 1502.08041.

[144] R. Argurio, M. Bertolini, G. Ferretti, A. Lerda and C. Petersson, *Stringy instantons at orbifold singularities*, *JHEP* **0706** (2007) 067 [0704.0262].

[145] M. Bianchi, F. Fucito and J. F. Morales, *D-brane instantons on the T**6 / Z(3) orientifold*, *JHEP* **0707** (2007) 038 [0704.0784].

[146] G. Aldazabal, S. Franco, L. E. Ibanez, R. Rabadan and A. M. Uranga, *Intersecting brane worlds*, *JHEP* **02** (2001) 047 [hep-ph/0011132].

[147] G. Aldazabal, S. Franco, L. E. Ibanez, R. Rabadan and A. M. Uranga, *D = 4 chiral string compactifications from intersecting branes*, *J. Math. Phys.* **42** (2001) 3103 [hep-th/0011073].

[148] R. Blumenhagen, M. Cvetic, R. Richter and T. Weigand, *Lifting D-Instanton Zero Modes by Recombination and Background Fluxes*, *JHEP* **10** (2007) 098 [0708.0403].

[149] P. K. Tripathy and S. P. Trivedi, *D3 brane action and fermion zero modes in presence of background flux*, *JHEP* **06** (2005) 066 [hep-th/0503072].

[150] E. Bergshoeff, R. Kallosh, A.-K. Kashani-Poor, D. Sorokin and A. Tomasiello, *An Index for the Dirac operator on D3 branes with background fluxes*, *JHEP* **10** (2005) 102 [hep-th/0507069].

[151] C. Petersson, *Superpotentials From Stringy Instantons Without Orientifolds*, *JHEP* **05** (2008) 078 [0711.1837].

[152] E. Garcia-Valdecasas and A. Uranga, *On the 3-form formulation of axion potentials from D-brane instantons*, 1605.08092.

[153] D. S. Freed and E. Witten, *Anomalies in string theory with D-branes*, *Asian J. Math.* **3** (1999) 819 [hep-th/9907189].

[154] J. M. Maldacena, G. W. Moore and N. Seiberg, *D-brane instantons and K theory charges*, *JHEP* **11** (2001) 062 [hep-th/0108100].

[155] E. Witten, *Baryons and branes in anti-de Sitter space*, *JHEP* **07** (1998) 006 [hep-th/9805112].

[156] O. Aharony and S. Kachru, *Stringy Instantons and Cascading Quivers*, *JHEP* **0709** (2007) 060 [0707.3126].

[157] A. Amariti, L. Girardello and A. Mariotti, *Stringy Instantons as Strong Dynamics*, *JHEP* **0811** (2008) 041 [0809.3432].

[158] R. Argurio, D. Forcella, A. Mariotti, D. Musso and C. Petersson, *Field Theory Interpretation of N=2 Stringy Instantons*, *JHEP* **1302** (2013) 002 [1211.1884].

[159] S. Franco, A. Retolaza and A. Uranga, *D-brane Instantons as Gauge Instantons in Orientifolds of Chiral Quiver Theories*, *JHEP* **11** (2015) 165 [1507.05330].

[160] A. M. Uranga, *Local models for intersecting brane worlds*, *JHEP* **12** (2002) 058 [hep-th/0208014].

[161] D. Forcella, I. Garcia-Etxebarria and A. Uranga, *E3-brane instantons and baryonic operators for D3-branes on toric singularities*, *JHEP* **03** (2009) 041 [0806.2291].

[162] I. Garcia-Etxebarria and A. M. Uranga, *Non-perturbative superpotentials across lines of marginal stability*, *JHEP* **0801** (2008) 033 [0711.1430].

[163] D. Xie and M. Yamazaki, *Network and Seiberg Duality*, *JHEP* **09** (2012) 036 [1207.0811].

[164] J. J. Heckman, C. Vafa, D. Xie and M. Yamazaki, *String Theory Origin of Bipartite SCFTs*, *JHEP* **1305** (2013) 148 [1211.4587].

[165] S. Franco, D. Galloni and R.-K. Seong, *New Directions in Bipartite Field Theories*, *JHEP* **1306** (2013) 032 [1211.5139].

[166] A. Hanany and R.-K. Seong, *Brane Tilings and Specular Duality*, *JHEP* **08** (2012) 107 [1206.2386].

[167] S. Cremonesi, A. Hanany and R.-K. Seong, *Double Handled Brane Tilings*, *JHEP* **10** (2013) 001 [1305.3607].

[168] Y.-H. He and M. van Loon, *Gauge Theories, Tessellations & Riemann Surfaces*, *JHEP* **06** (2014) 053 [1402.3846].

[169] N. Arkani-Hamed, J. L. Bourjaily, F. Cachazo, A. B. Goncharov, A. Postnikov and J. Trnka, *Grassmannian Geometry of Scattering Amplitudes*. Cambridge University Press, 2016, [1212.5605].

[170] N. Arkani-Hamed, J. L. Bourjaily, F. Cachazo, S. Caron-Huot and J. Trnka, *The All-Loop Integrand For Scattering Amplitudes in Planar N=4 SYM*, *JHEP* **01** (2011) 041 [1008.2958].

[171] R. Britto, F. Cachazo and B. Feng, *New recursion relations for tree amplitudes of gluons*, *Nucl. Phys.* **B715** (2005) 499 [hep-th/0412308].

[172] R. Britto, F. Cachazo, B. Feng and E. Witten, *Direct proof of tree-level recursion relation in Yang-Mills theory*, *Phys. Rev. Lett.* **94** (2005) 181602 [hep-th/0501052].

[173] S. Franco, *Cluster Transformations from Bipartite Field Theories*, *Phys.Rev.* **D88** (2013) 105010 [1301.0316].

[174] S. Franco, D. Galloni and A. Mariotti, *The Geometry of On-Shell Diagrams*, *JHEP* **1408** (2014) 038 [1310.3820].

[175] S. Franco, D. Galloni and A. Mariotti, *Bipartite Field Theories, Cluster Algebras and the Grassmannian*, *J.Phys.* **A47** (2014) 474004 [1404.3752].

[176] B. Feng, Y.-H. He and F. Lam, *On correspondences between toric singularities and (p,q) webs*, *Nucl. Phys.* **B701** (2004) 334 [hep-th/0403133].

[177] B. Feng, S. Franco, A. Hanany and Y.-H. He, *UnHiggsing the del Pezzo*, *JHEP* **08** (2003) 058 [hep-th/0209228].

[178] B. Feng, A. Hanany and Y.-H. He, *Phase structure of D-brane gauge theories and toric duality*, *JHEP* **08** (2001) 040 [hep-th/0104259].

[179] N. Arkani-Hamed, J. L. Bourjaily, F. Cachazo, A. Postnikov and J. Trnka, *On-Shell Structures of MHV Amplitudes Beyond the Planar Limit*, *JHEP* **06** (2015) 179 [1412.8475].

[180] S. Franco, D. Galloni, B. Penante and C. Wen, *Non-Planar On-Shell Diagrams*, *JHEP* **06** (2015) 199 [1502.02034].

[181] J. L. Bourjaily, S. Franco, D. Galloni and C. Wen, *Stratifying On-Shell Cluster Varieties: the Geometry of Non-Planar On-Shell Diagrams*, *JHEP* **10** (2016) 003 [1607.01781].

[182] S. Franco, A. Hanany, K. D. Kennaway, D. Vegh and B. Wecht, *Brane dimers and quiver gauge theories*, *JHEP* **0601** (2006) 096 [hep-th/0504110].

[183] F. Cachazo, B. Fiol, K. A. Intriligator, S. Katz and C. Vafa, *A Geometric unification of dualities*, *Nucl. Phys.* **B628** (2002) 3 [hep-th/0110028].

[184] B. Feng, A. Hanany, Y. H. He and A. Iqbal, *Quiver theories, soliton spectra and Picard-Lefschetz transformations*, *JHEP* **02** (2003) 056 [hep-th/0206152].

[185] C. Vafa, *The String landscape and the swampland*, hep-th/0509212.

[186] G. Obied, H. Ooguri, L. Spodyneiko and C. Vafa, *De Sitter Space and the Swampland*, 1806.08362.

[187] D. Harlow and H. Ooguri, *Constraints on symmetry from holography*, 1810.05337.

[188] C. Cheung and G. N. Remmen, *Naturalness and the Weak Gravity Conjecture*, *Phys. Rev. Lett.* **113** (2014) 051601 [1402.2287].

[189] B. Heidenreich, M. Reece and T. Rudelius, *Evidence for a sublattice weak gravity conjecture*, *JHEP* **08** (2017) 025 [1606.08437].

[190] M. Montero, G. Shiu and P. Soler, *The Weak Gravity Conjecture in three dimensions*, *JHEP* **10** (2016) 159 [1606.08438].

[191] L. E. Ibanez, V. Martin-Lozano and I. Valenzuela, *Constraining the EW Hierarchy from the Weak Gravity Conjecture*, 1707.05811.

[192] E. Gonzalo, A. Herraez and L. E. Ibanez, *AdS-phobia, the WGC, the Standard Model and Supersymmetry*, *JHEP* **06** (2018) 051 [1803.08455].

[193] E. Gonzalo and L. E. Ibanez, *The Fundamental Need for a SM Higgs and the Weak Gravity Conjecture*, 1806.09647.

[194] S. K. Garg and C. Krishnan, *Bounds on Slow Roll and the de Sitter Swampland*, 1807.05193.

[195] H. Ooguri, E. Palti, G. Shiu and C. Vafa, *Distance and de Sitter Conjectures on the Swampland*, 1810.05506.

[196] M. Cicoli, S. De Alwis, A. Maharana, F. Muia and F. Quevedo, *De Sitter vs Quintessence in String Theory*, 1808.08967.

[197] S. Kachru and S. P. Trivedi, *A comment on effective field theories of flux vacua*, 1808.08971.

[198] S. B. Giddings, S. Kachru and J. Polchinski, *Hierarchies from fluxes in string compactifications*, *Phys. Rev.* **D66** (2002) 106006 [hep-th/0105097].

[199] C. P. Burgess, R. Kallosh and F. Quevedo, *De Sitter string vacua from supersymmetric D terms*, *JHEP* **10** (2003) 056 [hep-th/0309187].

[200] R. Kallosh, F. Quevedo and A. M. Uranga, *String Theory Realizations of the Nilpotent Goldstino*, *JHEP* **12** (2015) 039 [1507.07556].

[201] A. Retolaza and A. Uranga, *De Sitter Uplift with Dynamical Susy Breaking*, *JHEP* **04** (2016) 137 [1512.06363].

[202] L. E. Ibanez, V. Martin-Lozano and I. Valenzuela, *Constraining Neutrino Masses, the Cosmological Constant and BSM Physics from the Weak Gravity Conjecture*, *JHEP* **11** (2017) 066 [1706.05392].

[203] A. Butti, M. Grana, R. Minasian, M. Petrini and A. Zaffaroni, *The Baryonic branch of Klebanov-Strassler solution: A supersymmetric family of SU(3) structure backgrounds*, *JHEP* **03** (2005) 069 [hep-th/0412187].

[204] K. A. Intriligator and N. Seiberg, *The Runaway quiver*, *JHEP* **02** (2006) 031 [hep-th/0512347].

[205] Z. Komargodski and N. Seiberg, *Comments on the Fayet-Iliopoulos Term in Field Theory and Supergravity*, *JHEP* **06** (2009) 007 [0904.1159].

[206] I. Bena, E. Dudas, M. Grana and S. Lust, *Uplifting Runaways*, 1809.06861.

[207] S. Kachru, D. Simic and S. P. Trivedi, *Stable Non-Supersymmetric Throats in String Theory*, *JHEP* **05** (2010) 067 [0905.2970].

[208] J. Polchinski, *Brane/antibrane dynamics and KKLT stability*, 1509.05710.

[209] S. Franco and A. M. . Uranga, *Dynamical SUSY breaking at meta-stable minima from D-branes at obstructed geometries*, *JHEP* **06** (2006) 031 [hep-th/0604136].

[210] I. Garcia-Etxebarria, F. Saad and A. M. Uranga, *Supersymmetry breaking metastable vacua in runaway quiver gauge theories*, *JHEP* **05** (2007) 047 [0704.0166].

[211] K. A. Intriligator, N. Seiberg and D. Shih, *Dynamical SUSY breaking in meta-stable vacua*, *JHEP* **04** (2006) 021 [hep-th/0602239].

[212] R. Argurio and M. Bertolini, *Orientifolds and duality cascades: confinement before the wall*, *JHEP* **02** (2018) 149 [1711.08983].

[213] L. E. Ibanez, R. Rabadan and A. Uranga, *Anomalous U(1)'s in type I and type IIB D = 4, N=1 string vacua*, *Nucl.Phys.* **B542** (1999) 112 [hep-th/9808139].

[214] E. Poppitz and S. P. Trivedi, *Some examples of chiral moduli spaces and dynamical supersymmetry breaking*, *Phys. Lett.* **B365** (1996) 125 [hep-th/9507169].

[215] A. Hanany and A. M. Uranga, *Brane boxes and branes on singularities*, *JHEP* **05** (1998) 013 [hep-th/9805139].

[216] S. Gukov, *Comments on N=2 AdS orbifolds*, *Phys. Lett.* **B439** (1998) 23 [hep-th/9806180].

[217] M. Bertolini, P. Di Vecchia, M. Frau, A. Lerda, R. Marotta and I. Pesando, *Fractional D-branes and their gauge duals*, *JHEP* **02** (2001) 014 [hep-th/0011077].

[218] J. Polchinski, *N=2 Gauge / gravity duals*, *Int. J. Mod. Phys.* **A16** (2001) 707 [hep-th/0011193].

[219] C. V. Johnson, A. W. Peet and J. Polchinski, *Gauge theory and the excision of repulson singularities*, *Phys.Rev.* **D61** (2000) 086001 [hep-th/9911161].

[220] I. Affleck, M. Dine and N. Seiberg, *Dynamical Supersymmetry Breaking in Four-Dimensions and Its Phenomenological Implications*, *Nucl. Phys.* **B256** (1985) 557.

[221] S. Sugimoto, *Anomaly cancellations in type I D-9 - anti-D-9 system and the USp(32) string theory*, *Prog. Theor. Phys.* **102** (1999) 685 [hep-th/9905159].

[222] G. Aldazabal and A. M. Uranga, *Tachyon free nonsupersymmetric type IIB orientifolds via Brane - anti-brane systems*, *JHEP* **10** (1999) 024 [hep-th/9908072].

[223] I. Antoniadis, E. Dudas and A. Sagnotti, *Brane supersymmetry breaking*, *Phys. Lett.* **B464** (1999) 38 [hep-th/9908023].

[224] A. M. Uranga, *Comments on nonsupersymmetric orientifolds at strong coupling*, *JHEP* **02** (2000) 041 [hep-th/9912145].

[225] C. Angelantonj, R. Blumenhagen and M. R. Gaberdiel, *Asymmetric orientifolds, brane supersymmetry breaking and nonBPS branes*, *Nucl. Phys.* **B589** (2000) 545 [hep-th/0006033].

[226] R. Rabadan and A. M. Uranga, *Type IIB orientifolds without untwisted tadpoles, and nonBPS D-branes*, *JHEP* **01** (2001) 029 [hep-th/0009135].

[227] I. Garcia-Etxebarria, F. Quevedo and R. Valandro, *Global String Embeddings for the Nilpotent Goldstino*, *JHEP* **02** (2016) 148 [1512.06926].

[228] S. Elitzur, A. Giveon, D. Kutasov, E. Rabinovici and A. Schwimmer, *Brane dynamics and N=1 supersymmetric gauge theory*, *Nucl. Phys.* **B505** (1997) 202 [hep-th/9704104].

[229] W. Siegel, *Supersymmetric Dimensional Regularization via Dimensional Reduction*, *Phys. Lett.* **84B** (1979) 193.